TESIS DE LA UNIVERSIDAD DE ZARAGOZA

2012

36

Juan Miguel Lujano Rojas

Análisis y gestión óptima de la demanda en sistemas eléctricos conectados a la red y en sistemas aislados basados en fuentes renovables

Departamento
Ingeniería Eléctrica

Director/es
Bernal Agustín, José Luis
Dufo López, Rodolfo

ISSN 2254-7606

Prensas de la Universidad
Universidad Zaragoza

Universidad Zaragoza
1542

Tesis Doctoral

ANÁLISIS Y GESTIÓN ÓPTIMA DE LA DEMANDA EN SISTEMAS ELÉCTRICOS CONECTADOS A LA RED Y EN SISTEMAS AISLADOS BASADOS EN FUENTES RENOVABLES

Autor

Juan Miguel Lujano Rojas

Director/es

Bernal Agustín, José Luis
Dufo López, Rodolfo

UNIVERSIDAD DE ZARAGOZA

Ingeniería Eléctrica

2012

Universidad Zaragoza
1542

Tesis Doctoral

Análisis y Gestión Óptima de la Demanda en Sistemas Eléctricos Conectados a la Red y en Sistemas Aislados Basados en Fuentes Renovables

Autor

Juan Miguel Lujano Rojas

Directores

José Luis Bernal Agustín

Rodolfo Dufo López

Departamento de Ingeniería Eléctrica

2012

Esta tesis se presenta en la modalidad de compendio de publicaciones.

Artículos en revistas con índice de impacto SCI:

1. Lujano-Rojas JM, Dufo-López R, Bernal-Agustín JL. Optimal sizing of small wind/battery systems considering the DC bus voltage stability effect on energy capture, wind speed variability, and load uncertainty. **Applied Energy** 2012;93:404-412.

2. Lujano-Rojas JM, Monteiro C, Dufo-López R, Bernal-Agustín JL. Optimum load management strategy for wind/diesel/battery hybrid power systems. **Renewable Energy** 2012;44:288-295.

3. Lujano-Rojas JM, Monteiro C, Dufo-López R, Bernal-Agustín JL. Optimum residential load management strategy for real time pricing (RTP) demand response programs. **Energy Policy** 2012;45:671-679.

Artículos en congresos internacionales:

4. Lujano-Rojas JM, Dufo-López R, Bernal-Agustín JL. Optimal design of PV/Wind/Battery systems by genetic algorithms considering the effect of charge regulation. International Conference on Mechanical and Electronic Engineering (ICMEE 2012). **Se publicará en Lecture Notes in Electrical Engineering.**

5. Lujano-Rojas JM, Dufo-López R, Bernal-Agustín JL. A qualitative evaluation of operational conditions in PV/Wind/Battery systems. Asia-Pacific Power and Energy Engineering Conference (APPEEC 2012). **Disponible en IEEEXplore.**

6. Lujano-Rojas JM, Bernal-Agustín JL, Dufo-López R, Domínguez-Navarro JA. Forecast of hourly average wind speed using ARMA model with discrete probability transformation. **Lecture Notes in Electrical Engineering 98**. Springer-Verlag; 2011. p. 1003-1010.

Los directores de la tesis, el Dr. José Luis Bernal Agustín y el Dr. Rodolfo Dufo López, Profesores del Departamento de Ingeniería Eléctrica de la Universidad de Zaragoza,

Hacen constar:

Que D. Juan Miguel Lujano Rojas, Ingeniero Electricista por la Universidad Simón Bolívar de Venezuela, ha realizado bajo su dirección y supervisión la presente tesis Doctoral que lleva por título:

"Análisis y gestión óptima de la demanda en sistemas eléctricos conectados a la red y en sistemas aislados basados en fuentes renovables",

y autorizamos su presentación en la modalidad de compendio de publicaciones. Y para que así conste a los efectos oportunos, firmamos la presente autorización.

Zaragoza, 28 de mayo de 2012

Fdo.: Dr. José Luis Bernal Agustín	Fdo.: Dr. Rodolfo Dufo López

INFORME MOTIVADO DEL ÓRGANO RESPONSABLE:

Tras revisar la documentación aportada sobre la tesis de título "Análisis y Gestión Óptima de la Demanda en Sistemas Eléctricos Conectados a la Red y en Sistemas Aislados Basados en Fuentes Renovables", realizada por D. Juan Miguel Lujano Rojas, se aprueba por parte del Departamento de Ingeniería Eléctrica su presentación en la modalidad de Compendio de Publicaciones.

Motivos por los que se ha tomado esta decisión:

- En la introducción del documento de la tesis se justifica claramente la unidad temática de los trabajos que han dado lugar a las publicaciones del compendio.

- El número de publicaciones es mayor que el requerido por la normativa de la Universidad de Zaragoza, correspondiendo tres de ellos a artículos en revistas con índice de impacto JCR.

- El índice de impacto de las revistas en las que se ha publicado es elevado, y las publicaciones en congresos internacionales se encuentran indexadas en las bases de datos más relevantes.

Zaragoza, a de mayo de 2012

El Director del órgano responsable

Sello

Fdo.: José Antonio Domínguez Navarro

Agradecimientos

Agradezco a los profesores Rodolfo Dufo López, José Luis Bernal Agustín, Cláudio Monteiro, José Antonio Domínguez Navarro y José María Justa Loyo por el importante aporte que hicieron a este trabajo y en general por el continuo apoyo que me dieron durante el desarrollo del mismo.

Este trabajo es un homenaje a la memoria del Profesor Hernán Lorenzo Díaz de la Universidad Simón Bolívar de Venezuela.

Expreso mi gratitud al Ministerio de Economía y Competitividad del Gobierno de España, el cual, a través de las becas de Formación de Personal Investigador, financió económicamente la realización de este doctorado. A Fernando Palacios del Servicio de Gestión de la Investigación, a Cristina Traid del Centro EURAXESS en Aragón del Vicerrectorado de Investigación, a Esther Labad de Ayudas Predoctorales Personal Investigador en Formación, al personal de la Secretaría de Ingeniería Eléctrica y Mecánica, al Profesor Manuel Matos y a Paula Castro de INESC Porto, al personal de Seguridad del Centro Politécnico Superior, a los revisores de los artículos aquí presentados y a mis compañeros de Doctorado por su continua ayuda.

Índice

1. Introducción

La energía es un instrumento fundamental en el desarrollo social y productivo de cualquier región del mundo. Durante mucho tiempo el consumo de energía a nivel mundial se ha mantenido en constante crecimiento. Según la Administración de Información Energética de Estados Unidos (*EIA, U.S. Energy Information Administration*) [1], se espera que el consumo mundial de energía alcance 770 cuatrillones de BTU en el año 2035, lo cual representa un aumento del 53% desde el año 2008. Este aumento se debe al robusto crecimiento económico y expansión poblacional de algunos países en vías de desarrollo, mientras que en aquellos países con economías más avanzadas, como por ejemplo los pertenecientes a la Organización para la Cooperación y Desarrollo Económicos (OCDE), la recesión económica mundial ha dado lugar a un crecimiento más lento en el consumo energético. Como puede observarse en la Figura 1, se estima que la demanda de energía en países pertenecientes a la OCDE puede crecer según una tasa promedio del 0,6% anual, mientras que el crecimiento en el consumo de energía en los países que no pertenecen a la OCDE se estima que puede ser de un 2,3% anual [1].

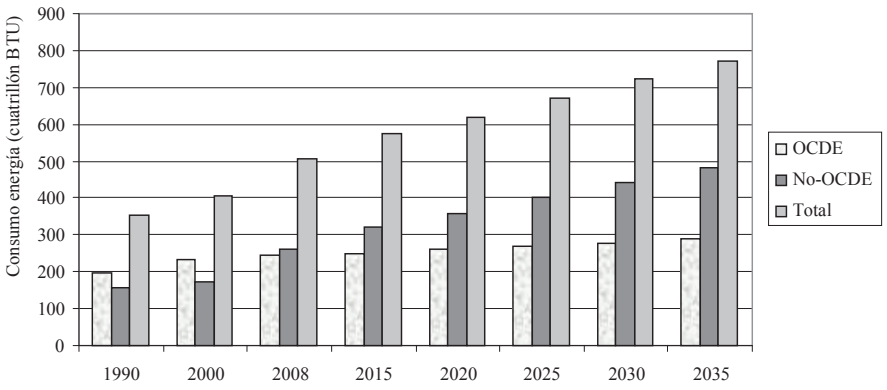

Figura 1. Consumo de energía mundial entre 1990 y 2035 [1]

En la situación actual, de recesión económica mundial, China e India mantienen un crecimiento económico acompañado de un aumento significativo en sus consumos de energía. En 2008 el consumo de energía conjunto de ambos países representó el 21% del consumo energético mundial, mientras que para 2035 se estima que ambas naciones consumirán el 31%. Por otra parte, en 2009 Estados Unidos no lograba superar la recesión económica, mientras que China e India alcanzaban crecimientos económicos

del 12,4% y 6,9%, respectivamente. Como puede observarse en la Figura 2, esto trajo como consecuencia que, por primera vez, el consumo energético de China fuera superior al consumo energético de los Estados Unidos. Se estima que para 2035 el consumo de energía en China será un 68% mayor que el consumo energético de los Estados Unidos [1].

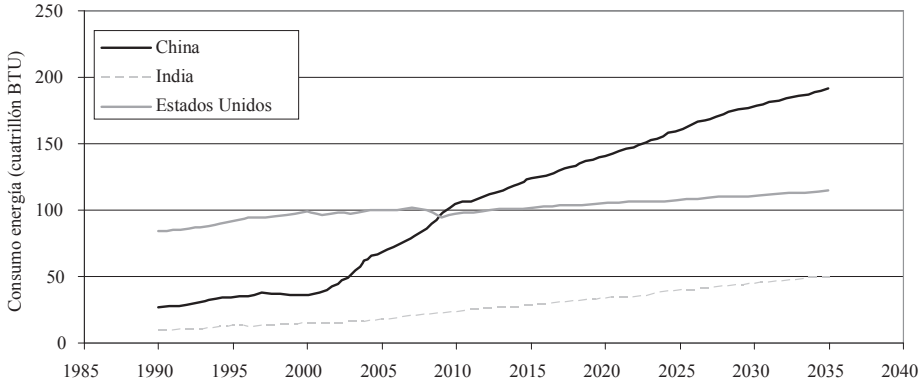

Figura 2. Consumo de energía en Estados Unidos, China e India [1]

De acuerdo a las futuras tendencias (Figura 3), se estima que el consumo de combustibles líquidos se incremente, en promedio, un 1% anual, debido a que probablemente los precios del petróleo y otros combustibles líquidos se mantengan relativamente altos.

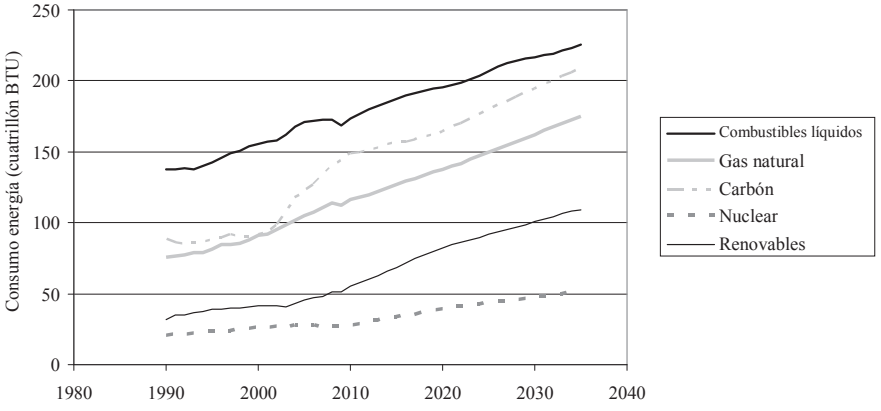

Figura 3. Consumo de energía mundial por tipo de combustible [1]

El consumo mundial de gas natural se espera que aumente, en promedio, un 1,6% anual a causa de su uso en procesos industriales y en la generación de energía eléctrica. El consumo de carbón se espera que aumente, en promedio, un 1,5% anual a causa del

acelerado ritmo en el crecimiento de las economías de los países ubicados en Asia y que no pertenecen a la OCDE. En cuanto al crecimiento de la energía nuclear, todavía existe una elevada incertidumbre, relacionada con la seguridad de las plantas y el tratamiento de los residuos radiactivos, que podría dificultar la instalación de nuevas centrales. Las energías renovables son las fuentes de energía con mayor crecimiento, estimándose que la energía que proporcionan aumentará un 2,8% anual. Esta previsión de aumento se basa en considerar que los precios de los combustibles fósiles se van a mantener relativamente altos, en el impacto medioambiental producido por el uso de combustibles fósiles y en los incentivos ofrecidos por algunos países [1].

Dentro del conjunto de las energías renovables, la energía eólica ha experimentado, durante los últimos años, un importante desarrollo. En la Figura 4 se muestra la evolución de la potencia eólica instalada a nivel mundial, estimándose que puede alcanzar 425 GW para el año 2015 [2].

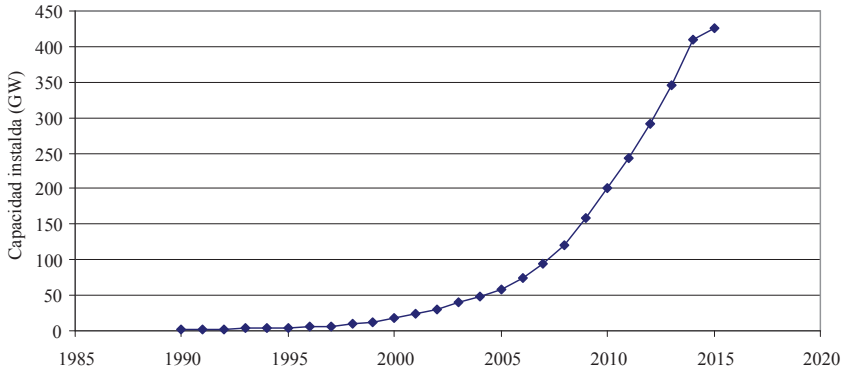

Figura 4. Capacidad instalada mundial de energía eólica [3]

Los cinco países con mayor potencia instalada son China, Estados Unidos, Alemania, España e India. China es el mercado de energía eólica más grande del mundo, con una potencia instalada de 42,3 GW en 2010. Debido a su gran potencial eólico, se espera que para 2015 alcance los 90 GW, y para 2020 los 200 GW de potencia instalada. En 2011 Estados Unidos alcanzó los 40,2 GW, suministrando alrededor del 2% de su consumo de energía eléctrica, y se espera que para el año 2030 la potencia instalada aumente y sea capaz de suministrar el 20% de la demanda. Alemania y España son los principales productores de energía eólica de Europa. En 2010 Alemania alcanzó los 27,2 GW de potencia instalada, suministrando el 6,2% de la demanda eléctrica nacional,

y se espera que para 2020 la potencia instalada de parques eólicos en tierra ascienda a 45GW, mientras que la potencia instalada de parques eólicos en el mar se espera que ascienda a 10 GW. En 2010 España alcanzó 20,7 GW de potencia instalada, suministrando el 16,6% de la demanda eléctrica nacional. Para 2020 se espera que la potencia instalada de parques eólicos en tierra alcance 40 GW, mientras que en el mar se estima que puede llegar a 5 GW. En 2010 la India alcanzó 13,1 GW de potencia instalada [2].

Como puede observarse en la Figura 5, la energía solar fotovoltaica ha crecido significativamente en los últimos años. Este crecimiento se ha debido a la reducción de sus costes y a los incentivos gubernamentales ofrecidos en algunos países con el fin de fomentar su uso y desarrollo, alcanzando 40 GW de potencia instalada en 2010, de los que el 85% corresponde a sistemas conectados a la red [4].

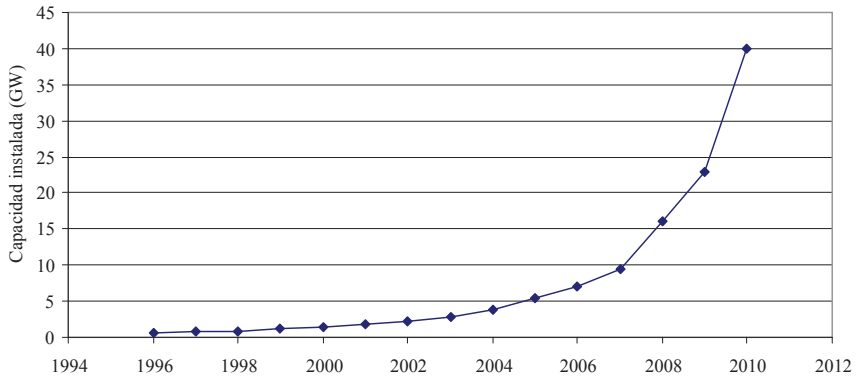

Figura 5. Potencia instalada mundial de energía solar fotovoltaica [4]

En la Figura 6 se muestran los principales productores de energía solar fotovoltaica.

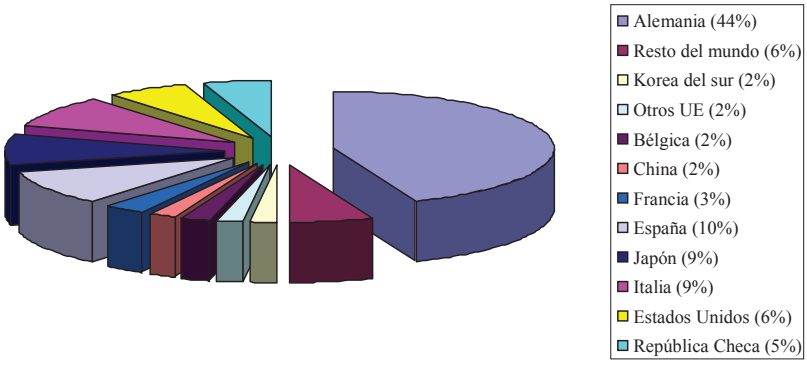

Figura 6. Potencia instalada de energía solar fotovoltaica por país [5]

La República Checa ha elevado su potencia instalada desde casi un valor nulo en 2008 hasta 2 GW en 2010, mientras que la India ha acumulado 102 MW, y China 893 MW. Los países con mayor potencia instalada de energía solar fotovoltaica son Alemania, Italia, España y Estados Unidos. Muchos de los sistemas fotovoltaicos conectados a la red se encuentran ubicados en países pertenecientes a la OCDE, mientras que algunos de los países en vías de desarrollo, liderados por China e India, presentan un mayor desarrollo de sistemas aislados de la red, a causa de sus extensas zonas rurales [5].

De acuerdo con lo expuesto anteriormente, la situación energética actual se caracteriza por un constante aumento de la demanda de energía como consecuencia del crecimiento económico de algunos de los países en vías de desarrollo, lo que a su vez trae como consecuencia un incremento significativo en la capacidad de generación, siendo así posible satisfacer de forma segura y fiable esta creciente necesidad de energía. En este aumento de la capacidad de generación de electricidad intervienen diferentes fuentes de energía, como el gas natural, el carbón, la energía nuclear, los derivados del petróleo y las energías renovables. Respecto a estas últimas, se espera que tengan un acelerado desarrollo, impulsado principalmente por aspectos medioambientales, el agotamiento de las reservas de petróleo y gas, y los avances tecnológicos que han permitido una reducción significativa en sus costes. Tal y como se ha indicado anteriormente, la energía eólica y la energía solar fotovoltaica tienen un gran interés en todo el mundo. En el caso específico de la energía eólica, que de acuerdo a las Figuras 4 y 5 supera en potencia instalada a la energía solar a nivel mundial, tiene un efecto importante sobre el sistema eléctrico por dos motivos: el nivel de penetración y el grado de flexibilidad del sistema [6]. Por un lado, si se incrementa el nivel de penetración, el impacto sobre el sistema eléctrico será mayor, es decir, el uso de la energía eólica trae consigo un grado de incertidumbre, relacionado con su naturaleza aleatoria, que puede incrementar de manera significativa los costes de producción cuando el nivel de penetración es elevado. Las fluctuaciones de la potencia generada por los parques eólicos afectan a otras unidades del sistema de potencia que pueden ser despachadas y controladas. Esta intermitencia de la potencia proveniente de los parques eólicos puede obligar a las centrales de generación convencional a operar en un punto subóptimo. Por otro lado, cuanta mayor flexibilidad tenga el sistema, se puede alcanzar un mayor grado de integración de energía eólica, ya que durante los periodos de baja demanda y abundante

recurso eólico es posible reducir la potencia proveniente de los parques eólicos para que el sistema eléctrico funcione de forma estable y fiable. La decisión de reducir la potencia proveniente de los parques eólicos depende del nivel de penetración de la energía eólica en el sistema y del grado de flexibilidad que ofrezca el mismo [6]. Además, los problemas derivados de las restricciones impuestas a los precios de la energía, tales como el uso de tarifas fijas y la imposición de límites superiores a los precios de la energía, han dado lugar a una significativa diferencia entre los costes de generación y el precio que deben abonar los consumidores. Esta diferencia ha provocado que en muchos países la tasa de crecimiento de la demanda sea mayor a la tasa a la cual crece la potencia instalada de generación de electricidad, es decir, el crecimiento en la capacidad de generación se ve afectado por el hecho de que las tarifas de electricidad no reflejan el verdadero coste de generación. Mientras que el desarrollo de la población y el crecimiento económico requieren del consumo de grandes cantidades de energía, la liberalización del sector de la energía es vista como una política arriesgada que podría dar lugar a la pérdida del beneficio por parte de los consumidores a corto plazo, lo que a su vez pone en peligro la continuidad del desarrollo debido a que los procesos de reestructuración se ven inhibidos [7].

Como solución a los problemas derivados de la creciente penetración de la energía eólica en la red y del aumento constante de la demanda, algunos autores han propuesto el uso de almacenamiento masivo de energía como una opción que permitiría convertir a las fuentes de energía con naturaleza aleatoria en centrales de generación controlables. Anagnostopoulos *et al.* [8] y Varkani *et al.* [9] han propuesto un sistema basado en energía eólica e hidráulica que está diseñado para recuperar y aprovechar la energía eléctrica excedente que proviene de los parques eólicos. Con esta idea se pretende incrementar la potencia instalada de energía eólica y los beneficios económicos provenientes de la misma. Recientemente, Fertig *et al.* [10] han planteado utilizar un sistema de almacenamiento de energía mediante aire comprimido. Bernal-Agustín *et al.* [11] proponen almacenar la energía que excede de los parques eólicos en un tanque de hidrógeno y utilizarla para satisfacer la demanda máxima. Dufo-López *et al.* [12] han propuesto una idea similar pero utilizando diferentes tipos de baterías. Por otro lado, el grado de flexibilidad del sistema puede aumentarse mediante la Gestión de la Demanda (*DSM, Demand Side Management*) o mediante la implementación de programas que

incentiven a los usuarios a utilizar la energía eléctrica durante los momentos en los cuales esta es abundante [6], lo que permitiría utilizar la energía excedente proveniente de centrales eólicas. Este tipo de programas se conocen como Programas de Adaptación de la Demanda (*Demand Response Programs*).

En esta tesis doctoral se propone un análisis profundo del funcionamiento de los sistemas eléctricos residenciales aislados y conectados a la red eléctrica basados en fuentes renovables, así como el desarrollo de estrategias de gestión de la demanda que ayuden al usuario a encontrar la manera óptima en la que sus electrodomésticos podrían ser utilizados. Los principales resultados y aportaciones obtenidos en este trabajo se presentan de forma clara y concisa en los artículos científicos que se encuentran a continuación.

Publicaciones que forman el compendio

Applied Energy 93 (2012) 404–412

Contents lists available at SciVerse ScienceDirect

Applied Energy

journal homepage: www.elsevier.com/locate/apenergy

Optimal sizing of small wind/battery systems considering the DC bus voltage stability effect on energy capture, wind speed variability, and load uncertainty

Juan M. Lujano-Rojas, Rodolfo Dufo-López, José L. Bernal-Agustín *

Department of Electrical Engineering, Universidad de Zaragoza, Calle María de Luna 3, 50018 Zaragoza, Spain

ARTICLE INFO

Article history:
Received 24 August 2011
Received in revised form 9 December 2011
Accepted 12 December 2011
Available online 29 December 2011

Keywords:
Wind energy systems
Optimal sizing
Charge controller
Coulombic efficiency

ABSTRACT

In this paper, a mathematical model for stochastic simulation and optimization of small wind energy systems is presented. This model is able to consider the operation of the charge controller, the coulombic efficiency during charge and discharge processes, the influence of temperature on the battery bank capacity, the wind speed variability, and load uncertainty. The joint effect of charge controller operation, ambient temperature, and coulombic efficiency is analyzed in a system installed in Zaragoza (Spain), concluding that if the analysis without considering these factors is carried out, the reliability level of the physical system could be lower than expected, and an increment of 25% in the battery bank capacity would be required to reach a reliability level of 90% in the analyzed case. Also, the effect of the wind speed variability and load uncertainty in the system reliability is analyzed.

Finally, the uncertainty in the battery bank lifetime and its effect on the net present cost are discussed. The results showed that, considering uncertainty of 17.5% in the battery bank lifetime calculated using the *Ah* throughput model, about 12% of uncertainty in the net present cost is expected. The model presented in this research could be a useful stochastic simulation and optimization tool that allows the consideration of important uncertainty factors in techno-economic analysis.

1. Introduction

Many studies have shown the importance of renewable energy systems in rural electrification and reduction of the emission of greenhouse gases. The main benefits of rural electrification are lighting, access to television, improvements in health, and education [1]. In this sense, several studies about rural electrification have been carried out in places such as India [2], where 72 million households do not have electricity. Another benefit of small wind energy systems is that they can reduce greenhouse gas emissions by 93% compared to diesel systems [3]. The modelling and design are important aspects of the analysis of these types of systems. Bagul et al. [4] developed a methodology for sizing a wind–photovoltaic system in which a fixed wind turbine power and a determined number of photovoltaic panels, weather data, and manufacturer's specifications are used to calculate the probability density function for the daily energy flow (surplus or deficit) into the battery bank. Considering the loss of load probability requirements, the optimal number of batteries is determined. Karaki et al. [5] proposed a methodology for sizing the energy system with wind turbine and battery bank storage based on an estimation of the joint probability distribution function of total wind power and total expected energy to recharge the battery bank. The optimal configuration of wind turbine and battery bank is determined by analyzing the capital cost and energy index of reliability. Celik [6] used experimental measurements to determine the relationship between loss-of-load probability, the monthly produced wind energy, the total load demand during the month, and battery capacity to design the wind energy systems. This technique claims to eliminate the need to use detailed simulation models and wind speed time series. Hybrid2 [7] is a hybrid system simulation model developed by the University of Massachusetts and the US National Renewable Energy Laboratory that simulates and analyzes economically hybrid power systems with a diesel generator, distribution systems, loads, renewable power sources, energy storage, power converters, and dump loads. HOMER [8] is a computer program developed by the US National Renewable Energy Laboratory that simulates and optimizes, including sensitivity analysis, hybrid systems with photovoltaic panels, wind turbines, small hydro, biomass power, diesel generators, fuel cells, lead acid batteries, and hydrogen storage. The optimization of this program is based on minimizing the net present cost over the lifetime of the hybrid system, testing all possible configurations. HOGA [9] is a computer program developed in the University of Zaragoza for the optimization of the configuration and control strategy using Genetic Algorithms. The optimization can be mono or multi-objective depending on net present cost, energy not supplied, and CO_2 emissions in hybrid power systems with

* Corresponding author.
E-mail address: jlbernal@unizar.es (J.L. Bernal-Agustín).

0306-2619/$ - see front matter © 2011 Elsevier Ltd. All rights reserved.
doi:10.1016/j.apenergy.2011.12.035

photovoltaic panels, wind turbines, small hydro, diesel generator, lead acid batteries, fuel cells, and hydrogen storage. Morgan et al. [10] presented a simulation program (ARES) for analyzing autonomous renewable energy systems that uses weather and load profiles to calculate the loss of load probability. The model considers the charge controller effects using the state of voltage and the temperature effects on the battery bank. Roy et al. [11] proposed a methodology for optimum sizing of wind battery systems in which the set of feasible design options are identified and the optimum configuration is selected based in the minimum cost of energy. In [12], the authors improved the design space methodology, incorporating wind speed variability by means of the Weibull probability distribution function. Távora et al. [13] presented a study about optimal sizing of stand-alone photovoltaic systems in which deterministic and stochastic methodologies are compared. The authors concluded that the stochastic model presents more realistic results.

Models such as those presented in [7–9] do not consider the influence of the charge controller and ambient temperature on the hybrid system performance. However, the model presented in [10] considers these factors, using a lead acid battery model that requires empirical data to estimate its parameters. In many of the aforementioned studies, the stochastic analysis using only the Weibull probability distribution function is proposed, and this simple model may create important errors in the performance analysis. The positive correlation between consecutive wind speed observations, diurnal profiles, and the dynamic of the hybrid power system cannot be determined using analytical methods [14]. However, these characteristics of wind speed time series can be incorporated using the Monte Carlo Simulation approach (Billinton et al. discussion [5]).

This paper proposes, for the first time, a mathematical model for the stochastic simulation and optimal sizing of small wind energy systems, considering the loss of energy due to voltage stability, coulombic efficiency in charge and discharge processes, ambient temperature effects on the battery bank capacity, wind speed variability, and load uncertainty.

The effect of wind speed variability and load uncertainty on the reliability of system, and the effect of the battery bank lifetime uncertainty in the total net present cost are also analyzed. To our best of knowledge, no other previous work carried out by other authors, has considered all the aspects included in the research work presented in this paper.

The development of this work is presented as follows:

- The wind/battery system model.
- The wind speed simulation model.
- The optimization criteria.
- The case of study.
- Conclusions.

2. The wind/battery system model

Fig. 1 shows the system under study. The wind turbine, battery bank, and load are coupled at the DC bus. The next sections describe the mathematical model for each system component.

2.1. The wind turbine model

Generally, in low power wind turbines with horizontal axes, the start-up wind speed is between 3 and 4 m/s, and the rated power is reached for wind speeds between 14 and 15 m/s. When the wind speed is higher than 14–18 m/s, the power production falls to between 30% and 70% of the rated power [15]. Fig. 2 shows the typical power curve.

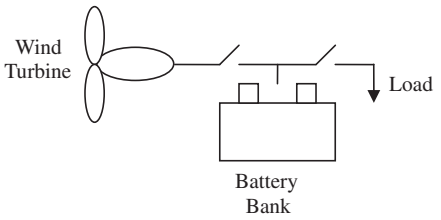

Fig. 1. Small wind/battery system.

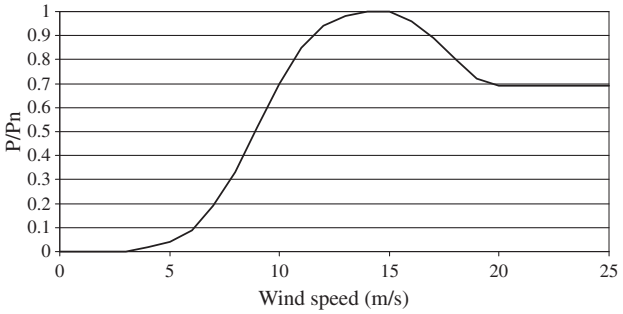

Fig. 2. Small capacity wind turbine power curve.

2.2. The lead acid battery and charge controller model

The lead acid battery model proposed by Manwell and McGowan [16] is used in many simulation and optimization models such as those presented in [7–9]. This approach considers the influence of current on battery capacity based on the interpretation of chemical kinetics as two storage tanks. One tank represents the energy immediately available, and the other represents the energy that is chemically bound. This model can be used jointly with the model proposed by Shepherd [17] to calculate the voltage of the battery. Protogeropoulos et al. [18] proposed a model that estimates the state of voltage considering the battery capacity as a function of the charge and discharge currents, which has been implemented in [10]. Ross et al. [19] presented a simplification of the electrochemical model in which the cell is made up of a number of subcells connected in parallel, and the impedance and concentration of the acid determines the flow of acid between them. The voltage at the terminal is linearly related to the open circuit voltage, the polarization voltage, and the voltage drop across the effective internal resistance. An exponential relationship between the total polarization voltage and the current for each sub-cell is assumed. Schiffer et al. [20] developed a model in which the battery voltage is calculated using a modified version of Shepherd's [17] equation, and the state of the charge is calculated by integrating the difference between the total current and the gassing current. The voltage and state of charge values previously estimated are used to calculate the corrosion and degradation parameters, and then the remaining capacity of the battery is determined.

An important aspect of the models presented in [16–19] is that experimental data is required to fit the model parameters. However, the model presented in [20] can be adapted to different battery types using data normally provided by the manufacturers. This model is based on a detailed analysis of the aging processes in the lead acid battery, and for this reason, it has a complexity level that would not be appropriate for a hybrid system model based on Monte Carlo Simulation. Copetti and Chenlo [21] and Copetti et al. [22] proposed a general model that only requires the rated capacity. This model presents a good performance to represent the complex battery behavior, but its mathematical formulation

is complex because it requires solving a nonlinear equation system for each hour of simulation to obtain the voltage and state of charge of the battery bank. In this paper, a simplified version of Copetti's model [21,22] is used.

Copetti's model [21,22] is normalized with respect to the total ampere-hours that may be charged or discharged in 10 h at 25 °C (C_{10} capacity). The expressions for the battery capacity [21,22] are:

$$C_T = 1.67C_{10}(1 + 0.005\Delta T_a) \tag{1}$$

$$C = \frac{C_T}{1 + 0.67\left(\frac{I}{I_{10}}\right)^{0.9}} \tag{2}$$

where $\Delta T_a = T_a - 25$ is the temperature variation from the reference of 25 °C; T_a is the ambient temperature in °C; C_T is the maximum capacity of the battery; C is the ampere-hours capacity at the charge or discharge constant current I; and I_{10} is the charge or discharge current in 10 h at 25 °C.

The coulombic efficiency (η_b) during the discharge ($I < 0$) and charge ($I > 0$) process is calculated using Eq. (3) [22]:

$$\eta_b = \begin{cases} 1 - \exp\left[\left(\frac{20.73}{I/I_{10}+0.55}\right)(SOC - 1)\right] & I > 0 \\ 1 & I < 0 \end{cases} \tag{3}$$

The state of charge (SOC) of the battery is calculated using Eq. (4) [22]:

$$SOC = \begin{cases} \frac{Q}{C}\eta_b & I > 0 \\ 1 - \frac{Q}{C}\eta_b & I < 0 \end{cases} \tag{4}$$

where $Q = |I|t$ is the charge supplied by the battery (discharge) or to the battery (charge) during time t.

An important component in stand-alone power systems with renewable energy sources and lead acid battery banks is the charge controller. The charge controller protects the battery bank against overcharge or over-discharge conditions using the voltage on its terminals as an indicator. When the battery bank reaches a high voltage set-point, the charge controller disconnects the wind turbine, and when the low voltage set-point is reached, the charge controller disconnects the load. Based on experimental measurements, Corbus et al. [23] showed the relationship between the battery/wind capacity ratio (battery capacity divided by charge current at rated wind power) and high voltage set-point of the charge controller. In systems with a low battery/wind capacity ratio (between 3 and 10 h), the high voltage set-point of the charge controller is reached prematurely due to voltage rises on the DC bus, resulting in low values (60% or less) of the battery bank state of charge.

The battery voltage at which the charge controller disconnects the wind turbine is between 2.40 and 2.55 V per cell [24]. During the charge process, the battery voltage per cell (V) may be approximated by Eq. (5) [21]:

$$V = \left(2 + 0.16\frac{Q}{C}\right) + \frac{I}{C_{10}}\left(\frac{6}{1 + I^{0.6}} + \frac{0.48}{(1 - Q/C_T)^{1.2}} + 0.036\right) \times (1 - 0.025\Delta T_a) \tag{5}$$

For example, if the charge controller setpoint is 2.50 V per cell, Eq. (5) could be used to estimate the Q value at which the battery voltage is 2.50 V per cell, and consequently the state of charge of the battery bank is limited at this value. In the simplified approach used in this work, the Q value obtained using Eq. (5) is used to calculate the upper limit of the SOC due operation of the charge controller. This simplification eliminates the need to calculate in detail the battery voltage in each time step, which would not be appropriate for a model based on Monte Carlo Simulation because the solution of a nonlinear system in each time step is required. During the discharge process, the lower limit of the SOC is the minimum value specified by the battery manufacturer. When this lower limit is reached, the charge controller disconnects the load of the battery bank to prevent over-discharge.

Many efforts have been made to predict the lead acid battery lifetime. Three main types of lifetime models have been developed: a physico-chemical aging model, a weighted Ah aging model, and an event-oriented aging model [25]. The physico-chemical aging model is based on detailed knowledge of the chemical and physical process related to aging of the electrochemical system. This model determines with high precision the relationship between variables related to operating conditions such as temperature, current, state of charge, electrolyte concentration, and the aging processes. The weighted Ah throughput aging model assumes that the lifetime is proportional to the total Ah throughput. The actual Ah throughput is multiplied by a weight factor fitted to the actual operating conditions, and then the end of the lifetime is reached when the total Ah throughput exceeds a limit value determined from nominal conditions. The event-oriented aging model estimates the loss of lifetime by identifying extreme operating conditions using the pattern recognition approach. The implementation of these aging models requires in many cases experimental information obtained through laboratory tests and expert expertise [26].

The Ah throughput aging model without considering the weighting factors has been implemented in many simulation and optimization tools. In [27], an experimental validation of this aging model was carried out considering hybrid systems with flat plate OGi and tubular OPzS lead acid battery types under wind and photovoltaic generation profiles. Under wind generation conditions, results showed 16.7% error on the estimation of the lifetime of flat plate OGi battery, and 17.5% error on the estimation of the lifetime of a tubular OPzS battery.

Based on these results, in this paper, the Ah throughput model (without considering the weighting factors) is incorporated into the Monte Carlo Simulation approach, considering 17.5% error. The Ah throughput model [27] estimates the lifetime of the battery, assuming that the amount of energy that can be cycled through the battery is fixed, independently of the depth of the individual cycles or any other parameters. The estimated throughput is calculated using the depth of discharge versus the cycles to failure curve provided by the manufacturer. Eq. (6) shows the calculation of the throughput (Q_t):

$$Q_t = \frac{1}{N_p}\sum_{i=1}^{N_p} C_{10}(DOD_i)(CF_i) \tag{6}$$

where DOD_i and CF_i are points of the depth of discharge versus the cycles to failure curve, and N_p is the total number of points considered. The estimation of the lifetime is determined by adding the ampere hours cycled by the battery. When this value reaches the expected throughput, the battery has reached its lifetime.

The IEEE Std 1187-2002 [28] proposed a methodology to estimate the effect of temperature on expected battery lifetime. This methodology is based on a 50% reduction in the lifetime for every 8.3 °C increase in temperature. Based in this criterion and the data provided in [28], Eq. (7) was created.

$$LR_{(T_a)} = 2^{\left[\frac{-(T_a-25)}{8.3}\right]} \tag{7}$$

where LR is the battery percentage lifetime, expressed as a fractional value, for each temperature. The corrected expected lifetime (CEL) in years is calculated by the following equation:

$$CEL = \frac{FL}{\sum \frac{1}{LR_{(T_i)}} \times months\ @\ T_i} \tag{8}$$

where FL is the rated life at 25 °C expressed in months, and $months\ @\ T_i$ is the number of months of the year at temperature T_i.

3. The wind speed simulation model

The consideration of the wind speed variability using the Monte Carlo method requires the stochastic wind speed simulation. A model frequently used is the autoregressive moving average (ARMA) model.

3.1. ARMA model

The mathematical formulation of the autoregressive moving average (ARMA) model is:

$$\widehat{W}_{(t)} = \varphi_1 \widehat{W}_{(t-1)} + \cdots + \varphi_p \widehat{W}_{(t-p)} + \varepsilon_{(t)} - \theta_1 \varepsilon_{(t-1)} - \cdots - \theta_q \varepsilon_{(t-q)} \tag{9}$$

where $\widehat{W}_{(t)}$ is the transformed and standardized wind speed of hour t; $\varphi_1,\ldots,\varphi_p$ are the autoregressive parameters; $\theta_1,\ldots,\theta_q$ are the moving average parameters; and $\varepsilon_{(t)},\varepsilon_{(t-1)},\ldots,\varepsilon_{(t-q)}$ are random variables with a mean of zero and standard deviation of σ. The calculation of autoregressive and moving average parameters to the wind speed time series of interest requires the transformation, standardization, estimation, and diagnostic checking processes.

3.1.1. Transformation and standardization

Because the frequency of the probability density function (PDF) used in the wind speed time series is the Weibull distribution, it is necessary to transform the observed series to another that has a Gaussian PDF. This transformation [29] is as follows:

$$U_{T(t)} = U_{(t)}^{m} \quad \text{with} \quad t = 1,\ldots,n \tag{10}$$

where $U_{(t)}$ is the wind speed time series with n observations; $U_{T(t)}$ is the transformed time series with Gaussian PDF; and m is the power transformation. With k as the Weibull shape factor, Dubey [30] showed that for shape factors between 3.26 and 3.60, the Weibull PDF is similar to the Gaussian PDF. Thus, with m between k/3.60 and k/3.26, the series of Eq. (10) adequately describes the Gaussian PDF. The selected value of this range is the m value, for which the coefficient of skewness (SK) is closest to zero. The coefficient of skewness is calculated by Eq. (11) [31].

$$SK = \frac{Q_3 + Q_1 - 2Q_2}{Q_3 - Q_1} \tag{11}$$

where $Q_1 = A^{-1}(0.25)$, $Q_2 = A^{-1}(0.5)$, and $Q_3 = A^{-1}(0.75)$ are the first, second, and third quartiles, respectively. $A^{-1}(.)$ is the inverse of the Cumulative Distribution Function (CDF), calculated by the algorithm of Fig. 5 (Section 3.1.4).

The transformed time series of Eq. (10) is not stationary because that would require subtraction of the hourly average and division by the hourly standard deviations. If $\mu_h(h)$ and $\sigma_h(h)$ with h = 1,2,...,24 are the hourly average and standard deviation of transformed wind speed series, respectively, these functions are periodic: $\mu_h(h = 25) = \mu_h(h = 1)$ and $\sigma_h(h = 25) = \sigma_h(h = 1)$ [29]. The transformed and standardized series ($W_{(t)}$) is as follows:

$$W_{(t)} = \frac{U_{T(t)} - \mu_{h(t)}}{\sigma_{h(t)}}. \tag{12}$$

3.1.2. Estimation of the order of ARMA

The order of the ARMA model (p,q) (see Eq. (9)) can be estimated using the plots of the autocorrelation function (ACF) and the partial autocorrelation function (PACF). For example, in a pure autoregressive process of order p, the ACF tails off, while PACF has a cut-off value after lag p [32]. Other approaches use the Bayesian Information Criterion (BIC) [33] and the Akaike Information Criterion (AIC) [34]. The p and q values are selected, minimizing the respective criteria, BIC or AIC, of:

$$BIC(p,q) = n\log\left(\sigma^2_{(p,q)}\right) + (p+q)\log(n) \tag{13}$$

$$AIC(p,q) = n\log\left(\sigma^2_{(p,q)}\right) + 2(p+q) \tag{14}$$

$$\sigma^2_{(p,q)} = \frac{\sum_{t=1}^{n}\left(W_{(t)} - \widehat{W}_{(t)}\right)^2}{n-(p+q)} \tag{15}$$

where $\sigma^2_{(p,q)}$ is the variance of the residual and $\widehat{W}_{(t)}$ is the value calculated by the ARMA model. The autoregressive and moving average parameters are calculated by minimizing the quadratic prediction error criterion [35].

3.1.3. Diagnostic checking

According to the Ljung-Box test [36], statistical checking requires comparing the chi-square distribution χ^2_α with L–p–q degrees of freedom and signification level α with the statistical S, calculated by:

$$S = n(n+2)\sum_{\beta=1}^{L}\frac{r^2_\beta}{(n-\beta)} \tag{16}$$

where L is a number of lags considered and r_β is the correlation coefficient of the residuals corresponding to lag β. The null hypothesis is rejected if the statistics S is higher than $\chi^2_\alpha(L–p–q)$.

3.1.4. Simulation of hourly average wind speed with ARMA model

The simulation process begins by evaluating expressions (9) and (17).

$$\widehat{U}_{T(t)} = \mu_{h(t)} + \sigma_{h(t)}\widehat{W}_{(t)} \quad \text{with} \quad t = 1,\ldots,n \tag{17}$$

Fig. 3 shows the probability transformation in discrete form that is used to undo the transformation process. Using this transformation process, the PDF of Eq. (17) will be the PDF of the

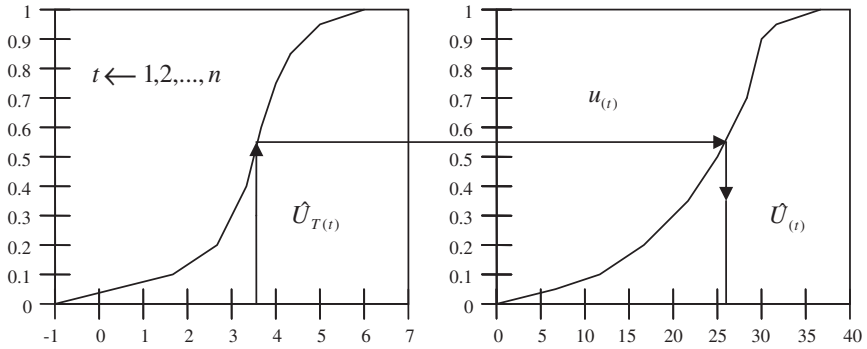

Fig. 3. Probability transformation.

original wind speed time series. This probability transformation is based on Eq. (18) [37], and the simulating values $\hat{U}_{(t)}$ are calculated by Eq. (19).

$$A\left(\hat{U}_{(t)}\right) = u_{(t)} = \hat{A}_T\left(\hat{U}_{T(t)}\right) \tag{18}$$

$$\hat{U}_{(t)} = A^{-1}\left(\hat{A}_T\left(\hat{U}_{T(t)}\right)\right) \tag{19}$$

where A is the CDF in discrete form of the original wind speed time series $U_{(t)}$; $\hat{A}_T$ is the CDF of the series from Eq. (17); and $u_{(t)}$ is a variable with uniform density function in the interval [0,1].

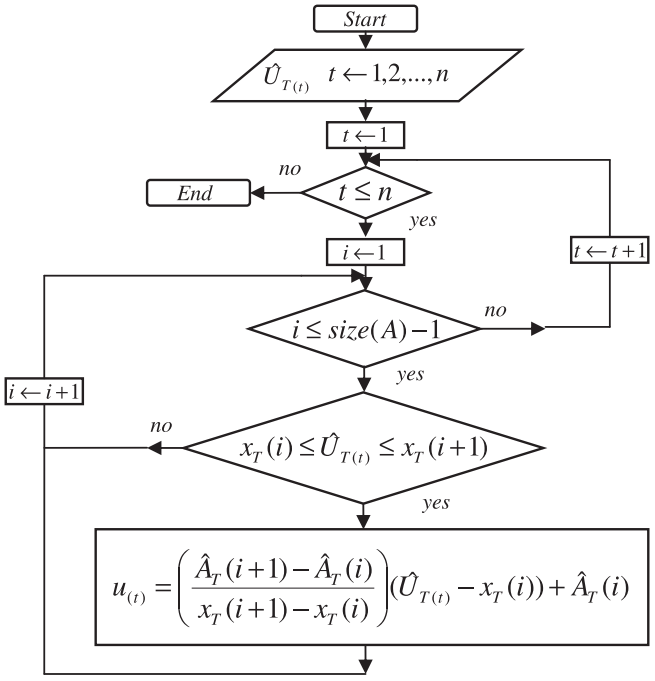

Fig. 4. Algorithm to evaluate the CDF expressed in discrete form.

Let $\hat{A}_T$ be the CDF in discrete form of the series from Eq. (17). For each hour t, it is necessary to calculate the $u_{(t)}$ value. The first step is to build the vector x_T; the elements of this vector are zero until $ceil(\max(U_{T(t)}))$ with $t = 1,2,\ldots,n$ in step Δx_T. The next step is to build the vector $\hat{A}_T$; the elements of this vector are the CDF of each element of vector x_T. The value of $u_{(t)}$ is calculated using the algorithm of Fig. 4, where the function $size(\hat{A}_T)$ calculates the number of rows of vector $\hat{A}_T$.

Let A be the CDF in discrete form of the original time series; for each hour t, it is necessary to calculate the $\hat{U}_{(t)}$ value. The first step is to build vector x. The elements of this vector are zero until $ceil(\max(U_{(t)}))$ in step Δx. The next step is to build vector A. The elements of this vector are the CDF of each element of vector x. Finally, the simulated value of wind speed $\hat{U}_{(t)}$ is calculated by the algorithm shown in Fig. 5, where the function $size(A)$ calculates the number of rows of vector A.

4. The optimization criteria

The main variables considered for the optimization are the net present cost (*NPC*) and the energy index of unreliability (*EIU*). The *NPC* is the cost throughout the operative lifetime of the system, comprised of the annualized capital cost (*ACC*), the annualized replacement cost (*ARC*), and the annualized maintenance cost (*AMC*). *NPC* is calculated by Eq. (20) [8,38].

$$NPC = \frac{(ACC + ARC + AMC)}{CRF(i,j)} \tag{20}$$

$$CRF(i,j) = \frac{i(1+i)^j}{(1+i)^j - 1} \tag{21}$$

where i is the annual real interest rate; j is the project lifetime; and $CRF(i,j)$ is the capital recovery factor.

The *EIU* is the energy index of unreliability defined according to:

$$EIU = \frac{ENS}{E_0} \tag{22}$$

where *ENS* is the energy not supplied and E_0 is the total energy demanded.

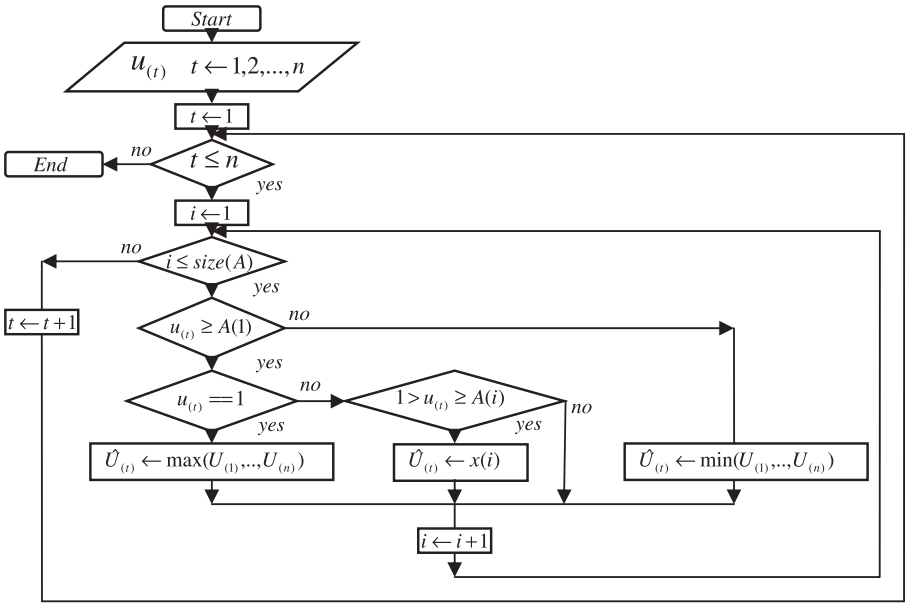

Fig. 5. Algorithm to calculate the inverse of the CDF in discrete form.

5. The case of study

The effect of the charge controller on the performance of small wind energy systems was analyzed using as a study case a system installed in Zaragoza, Spain. The wind speed and temperature time series of 2005 and the load profile of Fig. 6 were considered.

The model of the system, which considers the charge controller, the effect of temperature in the battery bank capacity and the coulombic efficiency during charge and discharge processes (model presented in Section 2), and the HOMER model [8], which does not consider the charge controller nor the influence of temperature in the battery bank capacity, and which considers the square root of the battery roundtrip efficiency instead of the coulombic efficiency, were compared. The system under study consists of a wind turbine of 1000 W and a battery bank of 12 V with minimum state of charge of 0.3. Battery bank capacities between C_{10} = 100 A h and C_{10} = 1000 A h have been considered; its capacity curves have been obtained by evaluating Eqs. (1) and (2). These curves are presented in Fig. 7.

By analyzing the system configuration of C_{10} = 100 A h, which has a very low battery/wind capacity ratio (1.2 h), the probability distribution function of the *SOC*, shown in Fig. 8, was obtained. The simulations showed that the HOMER model estimates high values of the state of charge (including *SOC* = 1) and low values of the energy not supplied (*ENS* = 210 kW h/year). The model described in Section 2 (which is a more accurate and realistic model than the HOMER model) estimates an energy not supplied value that is considerably higher (*ENS* = 318 kW h/year). These results align with those found by [23], which recorded that high charge current produces premature disconnection of the wind turbine, low state of charge of the battery bank, and high energy not supplied.

The coulombic efficiency has an important effect in the acceptance of coulombs during the charge process because the efficiency

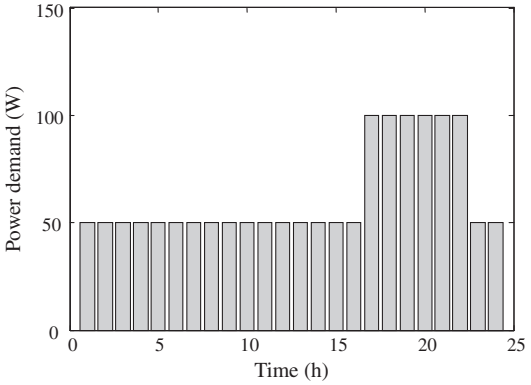

Fig. 6. Typical load curve.

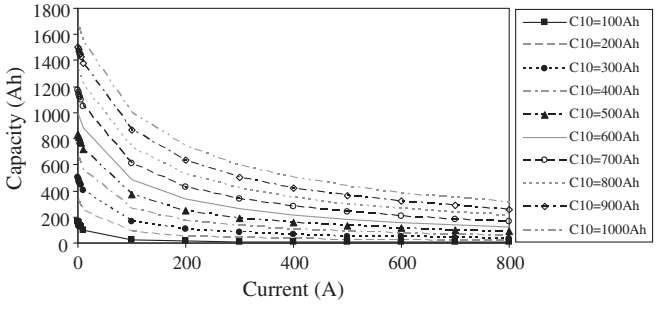

Fig. 7. Capacity curves for different batteries considered.

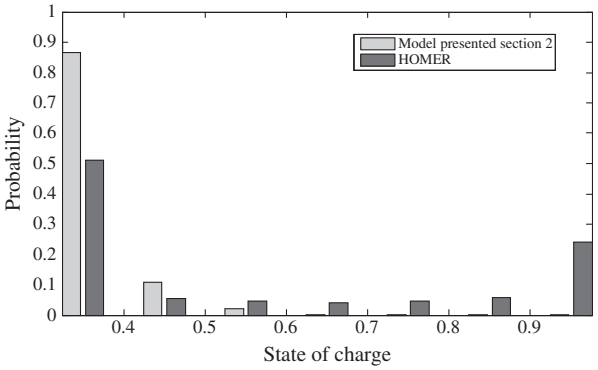

Fig. 8. Comparison of PDF of *SOC* (C_{10} = 100 A h).

is high (above 95%) at low states of charge and drops off near full charge [39]. This loss of efficiency is mainly related with gassing reactions during the charge of the battery [40], and therefore, it is difficult for the states of charge to reach high values. Otherwise, as mentioned previously, the charge controller operation could limit considerably the acceptance of charge of the battery in systems with high charge currents [23]. This factor explains the results presented in Fig. 8 that were obtained from the model presented in Section 2, for which the probability of low states of charges is high. However, results obtained using HOMER model suggest high probability of high state of charge, because a constant efficiency defined as the square root of the battery roundtrip efficiency is used and the charge controller operation is not considered.

Fig. 9 shows comparative results of the *EIU* obtained for the different battery bank capacities shown previously in Fig. 7. According to these results, the charge controller operation, temperature, and coulombic efficiency have an important effect on the ability of the battery bank to store energy. For example, if an *EIU* of 0.1 is required and the charge controller operation, temperature effect in the battery capacity, and coulombic efficiency are not considered, a battery bank of C_{10} = 800 A h is recommended. However, if those factors are considered, a battery bank of C_{10} = 1000 A h is needed. The reliability level obtained in the operation of the physical system could be lower than that obtained in the analysis using the HOMER model (without considering the charge controller operation, the influence of temperature in battery bank, and the coulombic efficiency). If a system optimized by HOMER is installed and is working physically, the reliability level will be lower than expected. Consequently, an increment in the battery bank capacity would be required during the operation of the physical system; in this specific case, an increment of 25% would be needed to reach a reliability level of 90% (unreliability of 10%).

Fig. 10 shows the evolution of average temperature for the location under study, which reached 25 °C only in July. According to Eq.

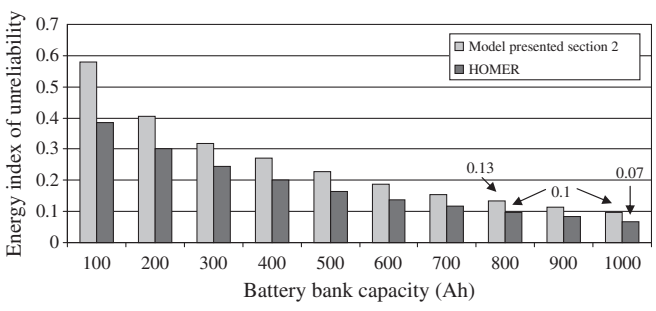

Fig. 9. *EIU* for different battery bank capacities.

(8), the reduction of the battery lifetime due to changes in the temperature is only about 2.2%. This result suggests that in some cases, the influence of ambient temperature on battery lifetime could be neglected.

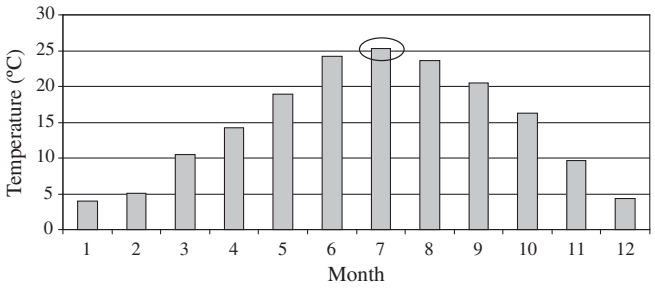

Fig. 10. Monthly average temperature in Zaragoza.

Table 1
Characteristics and diagnostic checking of the ARMA model.

Season	p	q	$L–p–q$	$\chi^2(\alpha = 0.05)$	S	m
Winter	9	0	207	241.5657	239.1245	0.3724
Spring	9	0	212	246.968	212.4908	0.4533
Summer	7	0	214	249.1275	242.3096	0.542
Autumn	8	0	211	245.8879	208.6985	0.4597

To illustrate the methodology for the stochastic optimization using the wind/battery model presented in this paper, another case study is analyzed. The wind turbines have a power between 100 W and 600 W, 12 V, a lifetime of 20 years, and are installed at 10 m. The cost of this type of wind turbine (including the charge controller) is between 720 € and 3045 €. The replacement is assumed to be 70% of capital cost. The battery bank capacities are between C_{10} = 100 A h and C_{10} = 1000 A h, with 300 cycles at 70% depth of discharge, floating lifetime of 9 years, 12 V, and cost of 250 €/kW h. The operation and maintenance costs for the wind turbines and lead acid batteries were negligible. The economic analysis included an inflation rate of 3% and a nominal interest rate of 4.5% for a project lifetime of 35 years.

The variability of the wind speed and load uncertainty were considered using the Monte Carlo simulation method. The hourly temperature time series of 2005 was used, but the ambient temperature variability was not considered. The wind speed simulation model explained in Section 3 was used to generate 100 wind speed time series synthetically (i.e., 100 years). Similarly, 100 load time series with 10% error on the load profile of Fig. 6 was used. As mentioned in Section 2.2, 17.5% of error in the *Ah* throughput model was considered.

Table 2
ARMA model parameters.

Season	φ_1	φ_2	φ_3	φ_4	φ_5	φ_6	φ_7	φ_8	φ_9	σ
Winter	0.6563	0.0786	0.1581	−0.0501	0.0105	0.031	0.0275	−0.0215	0.0655	0.4184
Spring	0.6422	0.1336	0.0818	0.011	−0.0109	0.0187	0.0168	−0.0326	0.0562	0.5312
Summer	0.7049	0.1039	0.0907	−0.0055	−0.0405	0.0893	−0.0305	–	–	0.509
Autumn	0.6429	0.1435	0.0567	−0.0249	0.0368	0.0156	0.0133	0.0428	–	0.5171

Table 3
Comparison of observed and simulated values.

Season	Average wind speed		Standard deviation		k		c	
	Observed	Simulated	Observed	Simulated	Observed	Simulated	Observed	Simulated
Winter	4.9067	4.9159	4.0393	4.05	1.3408	1.3391	5.8463	5.8531
Spring	4.5329	4.5412	3.0464	3.0569	1.6321	1.6286	5.1951	5.2015
Summer	5.133	5.14	2.8309	2.8374	1.9503	1.9462	5.8613	5.8664
Autumn	4.0838	4.0917	3.0805	3.0915	1.4985	1.4955	4.8064	4.8123

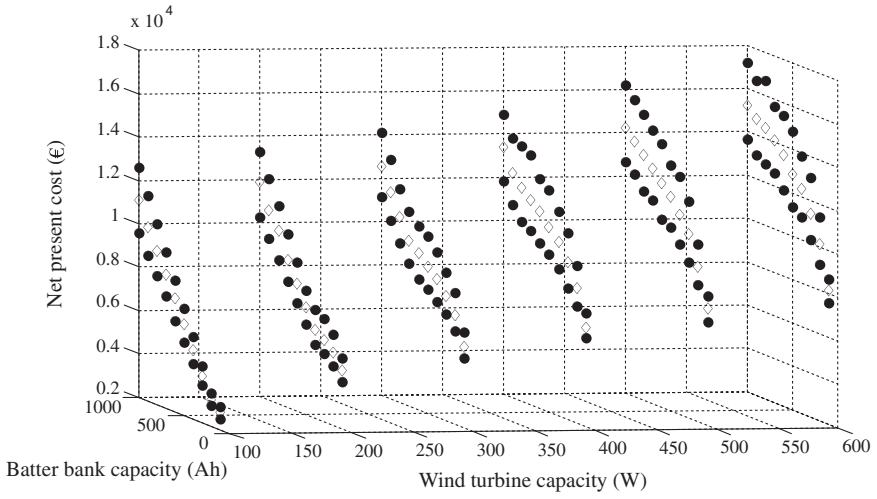

Fig. 11. Expected value of net present cost.

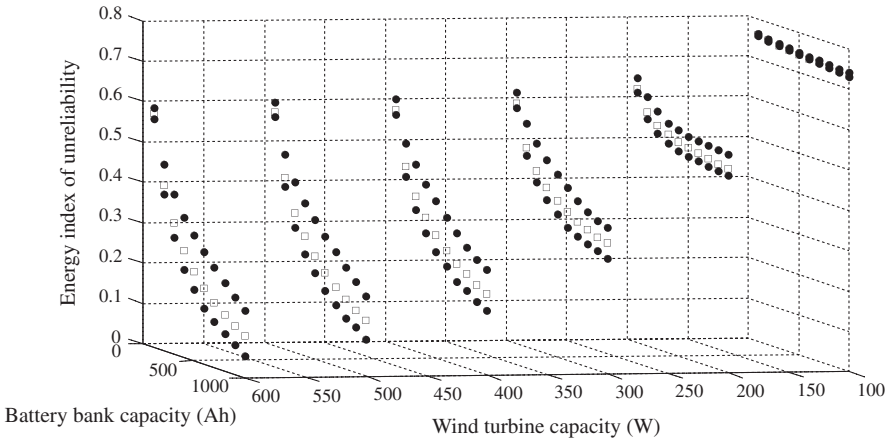

Fig. 12. Expected value of *EIU*.

The ARMA model was fitted to a wind speed time series of 2005 for each season of the year. Table 1 shows the order of the ARMA model, the selected power of transformation, and diagnostic checking of results for each season. A value of $\Delta x = 0.0001$ was used. Table 2 shows the values of the parameters of the ARMA model. Table 3 shows the comparison between observed and simulated values for each season.

The results obtained by stochastic analysis of different system configurations are shown in Figs. 11 and 12, which present the relationship between the expected value of net present cost and energy index of unreliability with a confidence level of 1%. Both figures represent the expected values, the upper limit and the lower limit. These results show that an uncertainty of 17.5% in the battery bank lifetime calculated using the *Ah* throughput model implies about 12% uncertainty in the net present cost. The uncertainty in the system reliability is directly related to the battery bank size and the wind turbine size. For example, in the case of very low battery bank capacity and wind turbine power, there is a high probability that the annual energy demand cannot be satisfied (the system reliability has a very low uncertainty), while if the system storage capacity and wind power generation are increased, under the weather conditions presented in the location of study, the uncertainty presents a higher value.

6. Conclusions

A mathematical model for the stochastic simulation and sizing of small wind energy systems has been presented. The model considers the loss of energy due to voltage stability, coulombic efficiency in charge and discharge process, temperature effects on the battery bank capacity, wind speed variability, and load uncertainty. No other previous work has considered all the aspects included in this paper.

As a study case, a small wind energy system installed in Zaragoza, Spain, was analyzed. The wind/battery system model presented in this paper was compared with the simulation and optimization tool HOMER, which does not consider the charge controller operation nor the influence of temperature on battery bank capacity, and it considers the square root of the battery roundtrip efficiency instead of the coulombic efficiency. The results have shown that if the analysis is carried out without considering the charge controller operation nor the influence of temperature on the battery bank nor the coulombic efficiency, the reliability level obtained in the operation of the physical system could be lower than that obtained in the analysis. In the case of study, an increment of 25% in the capacity of the battery bank would be required to reach a reliability level of 90%.

Different system configurations with wind turbine capacities between 100 W and 600 W and battery bank capacities between 100 A h and 1000 A h were analyzed using Monte Carlo Simulation approach. The wind speed variability was considered using an ARMA model; the uncertainties in the load profile and battery bank lifetime have been considered using random numbers. The results show that an uncertainty of 17.5% in the battery bank lifetime calculated using the *Ah* throughput model implies about 12% uncertainty in the net present cost. According to the monthly temperature behavior of Zaragoza, it does not represent an important factor in the reduction of the battery bank lifetime.

Acknowledgment

This work was supported by the "Ministerio de Ciencia e Innovación" of the Spanish Government under Project ENE2009-14582-C02-01.

References

[1] Independent Evaluation Group. The welfare impact of rural electrification: a reassessment of the costs and benefits. The World Bank; 2008.
[2] Urban F, Benders RMJ, Moll HC. Energy for rural India. Appl Energy 2009;86(1):S47–57.
[3] Fleck B, Huot M. Comparative life-cycle assessment of a small wind turbine for residential off-grid use. Renew Energy 2009;34(12):2688–96.
[4] Bagul AD, Salameh M, Borowy B. Sizing of a stand-alone hybrid wind photovoltaic system using a three-event probability density approximation. Sol Energy 1996;56(4):323–35.
[5] Karaki SH, Chedid RB, Ramadan R. Probabilistic performance assessment of wind energy conversion systems. IEEE Trans Energy Convers 1999;14(2):217–22.
[6] Celik AN. A simplified model for estimating the monthly performance of autonomous wind energy systems with battery storage. Renew Energy 2003;28(4):561–72.
[7] Manwell JF, Rogers A, Hayman G, Avelar CT, McGowan JG, Abddulwahid U, et al. Hybrid2 – a hybrid system simulation model. Theory manual. University of Massachusetts and US National Renewable Energy Laboratory; 2006.
[8] Lambert T, Gilman P, Lilienthal P. Micropower system modeling with HOMER. In: Farret FA, Simões MG, editors. Integration of alternative sources of energy. John Wiley & Sons, Inc.; 2006. p. 379–418.
[9] Dufo-López R, Bernal-Agustín JL, Yusta-Loyo JM, Domínguez-Navarro JA, Ramírez-Rosado IJ, Lujano J, et al. Multi-objective optimization minimizing cost and life cycle emissions of stand-alone PV–wind–diesel systems with batteries storage. Appl Energy 2011;88(11):4033–41.
[10] Morgan TR, Marshall RH, Brinkworth BJ. ARES – a refined simulation program for the sizing and optimisation of autonomous hybrid energy systems. Sol Energy 1997;59(4–6):205–15.
[11] Roy A, Kedare SB, Bandyopadhyay S. Application of design space methodology for optimum sizing of wind–battery systems. Appl Energy 2009;86(12):2690–703.
[12] Roy A, Kedare SB, Bandyopadhyay S. Optimum sizing of wind–battery systems incorporating resource uncertainty. Appl Energy 2010;87(8):2712–27.
[13] Távora CCV, Oliveira FD, Alves CDAS, Martins JH, Toledo OM, Machado NLV. A stochastic method for stand-alone photovoltaic system sizing. Sol Energy 2010;84(9):1628–36.

[14] Zhou W, Lou C, Li Z, Lu L, Yang H. Current status of research on optimum sizing of stand-alone hybrid solar-wind power generation systems. Appl Energy 2010;87(2):380–9.
[15] Jimenez AC, Olson K. Energía renovable para centros de salud rurales. US National Renewable Energy Laboratory; 1998. <http://www.nrel.gov/docs/fy99osti/26224.pdf>.
[16] Manwell JF, McGowan JG. Lead acid battery storage model for hybrid energy systems. Sol Energy 1993;50(5):399–405.
[17] Shepherd CM. Design of primary and secondary cells II. An equation describing battery discharge. J Electrochem Soc 1965;112(7):657–64.
[18] Protogeropoulos C, Marshall RH, Brinkworth BJ. Battery state of voltage modelling and an algorithm describing dynamic conditions for long-term storage simulation in a renewable system. Sol Energy 1994;53(6):517–27.
[19] Ross JN, Markvart T, He W. Modelling battery charge regulation for a stand-alone photovoltaic system. Sol Energy 2000;69(3):181–90.
[20] Schiffer J, Sauer DU, Bindner H, Cronin T, Lundsager P, Kaiser R. Model prediction for ranking lead–acid batteries according to expected lifetime in renewable energy systems and autonomous power-supply systems. J Power Sources 2007;168(1):66–78.
[21] Copetti JB, Chenlo F. Lead/acid batteries for photovoltaic applications. Test results and modeling. J Power Sources 1994;47(1–2):109–18.
[22] Copetti JB, Lorenzo E, Chenlo F. A general battery model for PV system simulation. Prog Photovoltaic 1993;1(4):283–92.
[23] Corbus D, Newcomb C, Baring-Gould EI, Friedly S. Battery voltage stability effects on small wind turbine energy capture. US National Renewable Energy Laboratory; 2002.
[24] IEEE Standards Coordinating Committee 21. IEEE guide for selection, charging, test, and evaluation of lead–acid batteries used in stand-alone photovoltaic (PV) systems. IEEE Std 1361 2003.
[25] Sauer DU, Wenzl H. Batteries|lifetime prediction. In: Encyclopedia of electrochemical power sources; 2009. p. 522–38.
[26] Sauer DU, Wenzl H. Comparison of different approaches for lifetime prediction of electrochemical systems-using lead–acid batteries as example. J Power Sources 2008;176(2):534–46.
[27] Bindner H, Cronin T, Lundsager P, Manwell JF, Abdulwahid U, Baring-Gould I. Lifetime modelling of lead acid batteries. Denmark National Laboratory Risø; 2005.
[28] IEEE Standards Coordinating Committee 29. IEEE recommended practice for installation design and installation of valve-regulated lead–acid storage batteries for stationary applications. IEEE Std 1187-2002.
[29] Brown BG, Katz RW, Murphy AH. Time series models to simulate and forecast wind speed and wind power. J Climate Appl Meteorol 1984;23(8):1184–95.
[30] Dubey SD. Normal and Weibull distributions. Naval Res Logistics Q 1967;14(1):69–79.
[31] Kim TH, White H. On more robust estimation of skewness and kurtosis. Finance Res Lett 2004;1(1):56–73.
[32] Box GEP, Jenkins GM, Reinsel GC. Time series analysis: forecasting and control. 4th ed. Prentice-Hall, Inc.; 2008.
[33] Schwarz G. Estimating the dimension of a model. Ann Stat 1978;6(2):461–4.
[34] Akaike H. A new look at the statistical model identification. IEEE Trans Autom Control 1974;19(6):716–23.
[35] Ljung L. System identification. Theory for the user. PTR Prentice Hall Information and System Sciences Series; 1999.
[36] Ljung GM, Box GEP. On a measure of lack of fit in time series models. Biometrika 1978;65(2):297–303.
[37] Rosenblatt M. Remarks on a multivariate transformation. Ann Math Stat 1952;23(3):470–2.
[38] Yang H, Wei Z, Chengzhi L. Optimal design and techno-economic analysis of a hybrid solar-wind power generation system. Appl Energy 2009;86(2):163–9.
[39] Stevens JW, Corey GP. A study of lead–acid battery efficiency near top-of-charge and the impact on PV system design. IEEE Photovoltaic Spec Conf 1996.
[40] Sexton ED, Olson JB. Coulombic efficiency of a sealed, thin plate, spiral lead–acid battery. In: IEEE battery conference on applications and advances; 1998.

Optimal Design of PV/Wind/Battery Systems by Genetic Algorithms Considering the Effect of Charge Regulation

Juan M. Lujano Rojas, Rodolfo Dufo-López, José L. Bernal-Agustín

Department of Electrical Engineering, University of Zaragoza,
Calle María de Luna 3, 50018, Spain
lujano.juan@gmail.com
{rdufo, jlbernal}@unizar.es

Abstract. Hybrid power systems (HPS) play an important role in the social development of areas located far from the electric grid. The optimal sizing of these systems is difficult to determine due to the variable nature of renewable energy resources and the complex behavior of their components. An important device of HPS is the charge controller as it protects the battery bank against extreme operational conditions, directly affecting the acceptance of charge from the battery bank and consequently the ability of the system to store energy. This paper presents a study about optimization of stand-alone PV/wind/battery hybrid power systems based in a genetic algorithm that considers the effect of charge regulation in the energy capture of the battery bank.

Keywords: Genetic Algorithms, Hybrid power systems.

1 Introduction

Autonomous renewable energy systems are an important option for rural electrification in many places around the world. Designing these types of systems is difficult due to the variability of renewable resource and the complex behavior of some components. Many algorithms have been proposed to find the optimal combination of power sources to meet energy demands. The following possible combinations were tested: [1] direct algorithm [2], design space methodology [3], particle swarm optimization [4], linear programming [5], simulated annealing [6], genetic algorithm [7], and hybrid genetic-simulated annealing [8]. The charge controller protects the battery bank against excessive charge or discharge conditions using voltage set points. For example, when the battery bank voltage reaches a high voltage set point, the charge controller disconnects the renewable generator, and when low voltage set point is reached, the charge controller disconnects the load. In systems with high power from a renewable source, high charge currents produce a premature disconnection of renewable generators; consequently, the state of charge of the battery bank results in low values [9]. In this paper, a study about optimization of hybrid power systems with photovoltaic panels, wind turbines, an inverter, and a lead acid battery bank using a genetic algorithm, which considers the influence of charge controller in the performance of the system, is carried out. The paper is organized as

follows: Section 2 describes the mathematical model of a PV/wind/battery system, and the implementation of the genetic algorithm is explained in Section 3. A case of study is analyzed in Section 4, and conclusions are presented in Section 5.

2 PV/Wind/Battery System Model

The next sections describe mathematical models for each components of a typical hybrid system with several photovoltaic panels, wind turbines, a lead acid battery bank, an inverter, and a load coupled in AC.

2.1 Wind Turbine

Wind turbines are commonly modeled based on their power curve. Fig. 1 shows several wind turbines with small capacities.

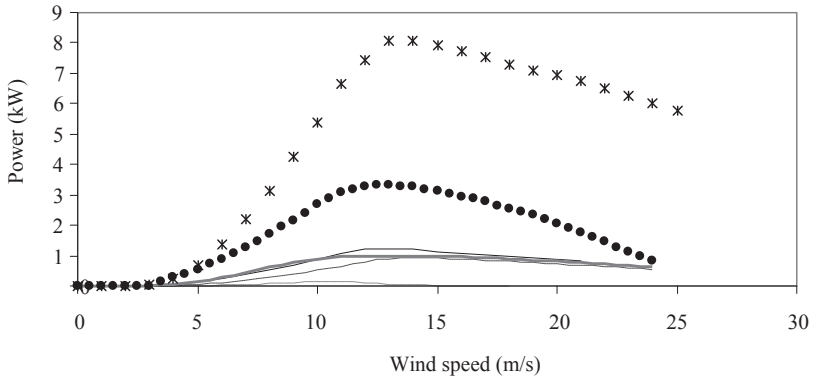

Fig. 1. Typical wind turbines power curves.

2.2 Photovoltaic Panel

The power of the photovoltaic generator is calculated using equations (1) and (2) [10].

$$P_{PV} = P_{STC}\left\{\frac{G}{G_{STC}}\left[1+\alpha(T_c-25)\right]\right\} \quad \textbf{(1)}$$

$$T_c = T_a + \left(\frac{NOCT - 20}{800}\right)G \quad (2)$$

where G is the incident solar radiation in W/m^2, G_{STC} is the solar radiation at standard test conditions, T_c is cell temperature ºC, T_a is ambient temperature in ºC, α is the temperature coefficient in %/ºC, and $NOCT$ is the nominal operation cell temperature in ºC.

2.3 Lead Acid Battery Bank

In this paper, a simplification of the general lead acid battery model proposed in [11] and [12] is used. The capacity of the battery is calculated using equations (3) and (4).

$$C_T = 1.67C_{10}(1 + 0.005\Delta T_a) \quad (3)$$

$$C = \frac{C_T}{1 + 0.67\left(\frac{I}{I_{10}}\right)^{0.9}} \quad (4)$$

where C is the capacity at constant current I, C_T is the maximum capacity, C_{10}, and I_{10} are the capacity and discharge current after 10 hours, respectively.

The efficiency (η_b) during charge ($I>0$) and discharge ($I<0$) is calculated using Equation (5) [12].

$$\eta_b = \begin{cases} 1 - \exp\left[\left(\frac{20.73}{I/I_{10} + 0.55}\right)(SOC - 1)\right] & I > 0 \\ 1 & I < 0 \end{cases} \quad (5)$$

where SOC is the state of charge calculated according to Equation (6) [12].

$$SOC = \begin{cases} \frac{Q}{C}\eta_b & I > 0 \\ 1 - \frac{Q}{C}\eta_b & I < 0 \end{cases} \quad (6)$$

where $Q=|I|t$ is the charge supplied or subtracted during the charge or discharge processes, respectively. The charge regulator disconnects the renewable generators when the battery bank voltage reaches a specific value. Equation (7) [11] allows us to estimate the SOC in this moment and then represents the effect of charge regulation in the acceptance of the battery bank charge.

$$V = (2 + 0.16\frac{Q}{C}) + \frac{I}{C_{10}}(\frac{6}{1 + I^{0.6}} + \frac{0.48}{(1 - Q/C_T)^{1.2}} + 0.036)(1 - 0.025\Delta T_a) \quad (7)$$

where V is battery voltage per cell during the charge process and $\Delta T_a=T_a-25$.

2.4 Inverter

The efficiency (η_p) of the inverter could be described using Equation (8).

$$\eta_p = \frac{P_l}{\varepsilon P_{inv} + (1+\zeta)P_l} \tag{8}$$

where P_l is the alternant current load, P_{inv} is the rated power of the inverter, ε and ζ are parameters determined using experimental data.

3 Mono-Objective Optimization

The problem of finding a combination of photovoltaic panels, wind turbines, and lead acid batteries that minimize the costs of the system, thus guaranteeing a determined level of reliability, is solved using the genetic algorithm described below.

3.1 Optimization Criteria

The variables considered are net present cost (*NPC*) and energy index of unreliability (*EIU*). *NPC* have been defined according to equations (9) and (10) [1].

$$NPC = \frac{(ACC + ARC + AMC)}{CRF(i,j)} \tag{9}$$

$$CRF(i,j) = \frac{i(1+i)^j}{(1+i)^j - 1} \tag{10}$$

where *ACC* is the annualized capital cost, *ARC* is the annualized replacement cost, *AMC* is the annualized maintenance cost, *CRF(i,j)* is the capital recovery factor, *i* is the real interest rate, and *j* is the project lifetime. *EIU* have been defined according to Equation (11).

$$EIU = \frac{ENS}{E_0} \tag{11}$$

where *ENS* is the energy not supplied and E_0 is the total energy demanded.

3.2 Genetic Algorithm Implementation

To find the combination of renewable energy sources and lead acid batteries that minimize the *NPC* during the *j* years, the genetic algorithm could be implemented in the following ways [13]:

1. Adjust the number of individuals in the population (Ψ), number of generations (χ), crossing rate ($\varnothing$), mutation rate (ω), and *EIU* required (EIU_0).

2. An individual is represented as an integer vector $|\varphi|\beta|\lambda|\mu|\delta|\gamma|$ that contains a representation of solar generator manufacturer (φ), number of PV panels in parallel (β), battery manufacturer (λ), number of batteries in parallel (μ), wind generator manufacturer (δ), and number of wind turbines in parallel (γ). The initial population with Ψ individuals is randomly obtained.
3. For each individual in the population, the *NPC* and *EIU* are evaluated, and then an arbitrarily high value of *NPC* is assigned for those individuals with an *EIU* higher than EIU_0.
4. With $k=1,2,..,\Psi$, the aptitude (Φ_k) of individual k is obtained according to its rank in the population, rank 1 for the best individual and rank Ψ for the worst individual. Fitness function is shown in (12).

$$\Phi_k = \frac{(\Psi + 1 - k)}{\sum_{k=1}^{\Psi} (\Psi + 1 - k)} \quad (12)$$

5. Reproduction, crossing, and mutation are carried out to obtain the next generation. Reproduction is done using the roulette-wheel methods, crossing is done using the one crossing point method, and mutation is done by randomly changing the components of some individuals.
6. The steps described from 3 to 5 are repeated until χ generation is reached. The best solution obtained is that which has a lower *NPC* and an *EIU* at least lower than the required EIU_0.

4 Case Study

A PV/wind/battery system installed in the Netherlands in 2009 was analyzed. The installation site is the K13 meteorological station. Wind speed time series are provided by the Royal Netherlands Meteorological Institute [14]. The hourly solar radiation time series was generated synthetically according to Graham and Hollands' methodology [15] using information provided by NASA [16] for this location. The load is assumed to require 900W over 24 hours.

The genetic algorithm explained in Section 3 was implemented in MATLAB to find the combination of PV panels, wind turbines, and battery bank capacity that guarantee at least *EIU*=0.1. The wind turbines considered are showed in Figure 1. For the PV generator, capacities between 0.175kW and 4.375kW were considered, and for the lead acid battery bank, capacities between 200Ah and 3,000Ah and strings between 1 and 10 were considered. The rated capacity of the inverter is 900W with ε=0.0064 and ζ=0.0942. The economic analysis was carried out considering 35 years of project lifetime, a 5% interest rate, and a 3% inflation rate. For wind turbines, we considered 15 years of lifetime and capital cost between 1700€ and 30000€, and operation and maintenance cost between 50€ and 140€, respectively. The lifetime of the inverter is estimated at 20 years and its acquisition cost is estimated at 700€; the operation and maintenance cost is considered negligible. The lifetime of considered batteries is between 8 years and 20 years, and its capital cost is considered 250€/kWh. For a PV panel, its lifetime is considered 20 years, a capital cost of 4€/W is used, and operation and maintenance costs are considered negligible. Fig. 2 shows the evolution of net

present cost in the optimization for 100 individuals in the population, 10 generations, crossing rate of 0.9, and a mutation rate of 0.01. After 10 generations, a hybrid system with 11 PV panels of 175W each, a wind turbine of 1kW, a battery bank of 1,000Ah, and a floating lifetime of 20 years is suggested. The *EIU* value obtained is 0.0675.

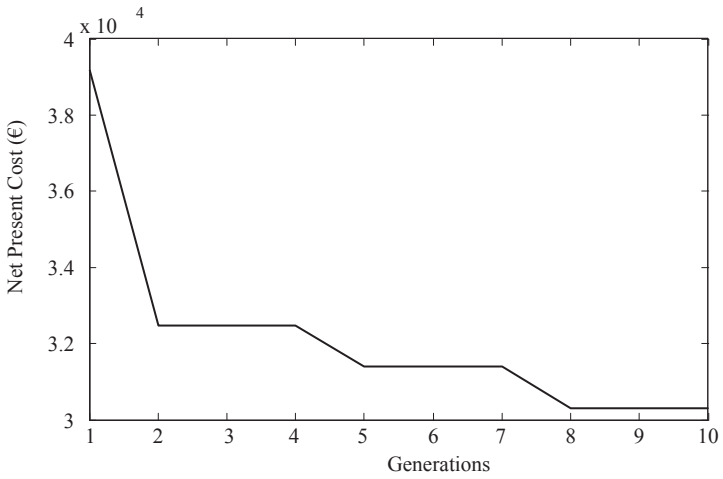

Fig. 2. Evolution of Net Present Cost in the optimization.

5 Conclusions

In this paper, a genetic algorithm was used to find the optimal combinations of photovoltaic panels, wind turbine, and battery bank capacity in a typical hybrid power system to guarantee a determined level of reliability. The model presented in this paper is able to consider the coulombic efficiency, the charge controller operation, and many different types of photovoltaic panels, wind turbines, and battery bank capacities in the mono-objective optimization problem. These characteristics allow us to obtain fast and realistic results from the sizing process.

Acknowledgments

This work was supported by the “Ministerio de Ciencia e Innovación” of the Spanish government under Project ENE2009-14582-C02-01. Furthermore, the authors would like to thank the Royal Netherlands Meteorological Institute and NASA for providing the wind speed and solar radiation data for the case of study presented in this paper.

References

1. Lambert, T., Gilman, P., Lilienthal, P.: Micropower System Modeling with HOMER. In: Farret, F.A., Simões, M.G. (eds.) Integration of Alternative Sources of Energy, pp. 379-418. John Wiley & Sons, Inc (2006)
2. Belfkira, R., Zhang, L., Barakat, G.: Optimal sizing study of hybrid wind/PV/diesel power generation unit. Solar Energy 85, 100-110 (2011)
3. Roy, A., Kedare, S.B., Bandyopadhyay S.: Application of design space methodology for optimum sizing of wind-battery systems. Applied Energy 86, 2690-2703 (2009)
4. Boonbumroong, U., Pratinthong, N., Thepa, S., Jivacate, C., Pridasawas, W.: Particle swarm optimization for AC-coupling stand alone hybrid power systems. Solar Energy 85, 560-569 (2011)
5. Kanase-Patil, A.B., Saini, R.P., Sharma, M.P.: Integrated renewable energy systems for off grid rural electrification of remote area. Renewable Energy 35, 1342-1349 (2010)
6. Ekren, O., Ekren, B.Y.: Size optimization of a PV/wind hybrid energy conversion system with battery storage using simulated annealing. Applied Energy 87, 592-598 (2010)
7. Dufo-López R., Bernal-Agustín J.L., Yusta-Loyo J.M., Domínguez-Navarro J.A., Ramírez-Rosado I.J., Lujano, J., Aso, I.: Multi-objective optimization minimizing cost and life cycle emissions of stand-alone PV-wind-diesel systems with batteries storage. Applied Energy 88, 4033-4041 (2011)
8. Carapellucci, R., Giordano, L.: Modeling and optimization of an energy generation island based on renewable technologies and hydrogen storage systems. International Journal of Hydrogen Energy 37, 2081-2093 (2012)
9. Corbus, D., Newcomb, C., Baring-Gould, E.I., Friedly, S.: Battery voltage stability effects on small wind turbine energy capture. Technical report, U.S. National Renewable Energy Laboratory (2002)
10. Lorenzo, E.: El Generador Fotovoltaico. In: Electricidad solar: Ingeniería de los sistemas fotovoltaicos, pp. 93-120. PROGENSA (1994)
11. Copetti, J.B., Chenlo, F.: Lead/acid batteries for photovoltaic applications. Test results and modeling. Journal of Power Sources 47, 109-118 (1994)
12. Copetti, J.B., Lorenzo, E., Chenlo, F.: A general battery model for PV system simulation. Progress in Photovoltaic 1, 283-292 (1993)
13. Dufo-López, R., Bernal-Agustín, J.L.: Design and control strategies of PV-Diesel systems using genetic algorithms. Solar Energy 79, 33-46 (2005)
14. Royal Netherlands Meteorological Institute, http://www.knmi.nl/
15. Graham, V.A., Hollands, K.G.T.: A method to generate synthetic hourly solar radiation globally. Solar Energy 44, 333-341 (1990)
16. NASA, http://eosweb.larc.nasa.gov/sse/RETScreen/

A Qualitative Evaluation of Operational Conditions in PV/Wind/Battery Systems

Juan M. Lujano-Rojas, Rodolfo Dufo-López, José L. Bernal-Agustín
Department of Electrical Engineering
University of Zaragoza
Zaragoza, Spain
lujano.juan@gmail.com, rdufo@unizar.es, jlbernal@unizar.es

***Abstract*—Hybrid power systems (HPS) play an important role in places located far from electric grids. The sizing of these systems is difficult to determine due to the variable nature of renewable energy resources and the complex behaviour of their components. The battery bank has a significant impact on the performance of hybrid systems due to their complex behaviour and high investment costs. This situation has motivated the development of different approaches to improve the mathematical model of the lead acid battery. However, the accuracy of some of these approaches is still unclear. In this paper, using qualitative information about determined operating conditions, a small capacity hybrid power system installed in Zaragoza is analyzed, concluding that this information could be useful to HPS designers.**

Keywords- hybrid power systems; battery lifetime

I. INTRODUCTION

Autonomous renewable energy systems are an important option for rural electrification. The design of these types of systems is a difficult task due the variability of renewable resource and the complex behaviour of some components. Many studies have been conducted to predict the lifetime of lead acid batteries under determined operating conditions, resulting in the development of three main general types of lifetime models: physic-chemical ageing models, weighted Ah ageing models, and event-oriented ageing models [1]. Physico-chemical ageing models incorporate physical and chemical factors related to mass transport properties, thermodynamic, mechanical, and electrical properties of materials in the ageing process [1,2]. Weighted Ah ageing models, assuming that the lifetimes of batteries depend proportionally of the total Ah throughput [1,2,3], and event-oriented ageing models are based on a pattern recognition approach to identify extreme operating conditions, after which an incremental loss of lifetime is added [1,2]. In an effort to describe the operating conditions of renewable energy systems, in [4] a qualitative analysis has been carried out to develop categories of operating conditions to support system designers. In this paper, these categories proposed in [4] are used to analyze a hybrid system with photovoltaic (PV) panels, wind turbines, and lead acid batteries installed in Zaragoza, Spain. The paper is organized as follows: Section II explains the stress factors in lead acid battery lifetimes. The analysis of PV/Wind/Battery system is described in Section III and conclusions are presented in Section IV.

II. STRESS FACTORS

This section briefly describes some of stress factors proposed in [4] for the categorization process which can be determined using the state of charge (*SOC*) time series.

A. Charge Factor

The charge factor (*CF*) can be used to indicate the operation of battery banks. For example, if *CF* is close to 1, the battery bank operates at a partial cycle with limited recharge, and if *CF* tends to infinity, the operation of battery banks involves a float charge. This factor is calculated using (1).

$$CF = -\frac{\int I \times H(I)dt}{\int I \times H(-I)dt} \tag{1}$$

where $H(.)$ is the Heaviside function and I the battery current ($I>0$ during charge and $I<0$ during discharge).

B. Ah Throughput

Ah throughput (Q_{thrp}) can be used to determine whether or not a battery bank operates at full cycling conditions. This factor is calculated according to (2).

$$Q_{thrp} = -\frac{\int I \times H(-I)dt}{C_n} \tag{2}$$

where C_n is the battery's nominal capacity.

C. Highest Discharge Rate

This factor ($I_{max1\%\_aver}$) is useful in terms of determining the capacity required of the battery bank. To determine it, first using the distribution function of the discharge current (n groups of discharge currents are fixed, and then the cumulative operating time for each group is calculated), the number of current groups (x) required to fulfil the 1% Ah throughput is calculated by means of (3).

$$\sum_{i=n-x}^{n} I_i \times t_i = 0.01 Q_{thrp} C_n \tag{3}$$

Then the average is calculated using (4), where I_{10} is the current of discharge in 10 hours.

$$I_{\max 1\%\_aver} = \frac{0.01 Q_{thrp} C_n}{I_{10} \sum_{i=n-x}^{n} t_i} \tag{4}$$

D. Time Between Full Charges

The time between full charges (*tbfc*) is defined as the average time (measured in days) between the consecutive recharging of the battery bank to *SOC* higher than 90%. This factor is defined according to (5).

$$tbfc = \frac{\int H(90 - SOC)dt}{\eta_{90\%}} \tag{5}$$

where $\eta_{90\%}$ are the times that this event occurs: $SOC_{(t)}>90\%$ and $SOC_{(t-\Delta t)}\leq 90\%$.

E. Partial Cycling

The partial cycling factor (*PC*) is a measurement of the amount of Ah throughput in a specific *SOC* range. This factor is calculated for different *SOC* ranges (A:100-85%, B:85-70%, C:70-55%, D:55-40%, E:40-0%) according to (6).

$$A = -\frac{\int I \times H(SOC - 85) \times H(100 - SOC) \times H(-I)dt}{\int I \times H(-I)dt} \times 100 \tag{6}$$

Then a linear relationship is used to determine the *PC* value according to (7).

$$PC = (A \times 1 + B \times 2 + C \times 3 + D \times 4 + E \times 5)/5 \tag{7}$$

F. Time at Low State of Charge

The time at low *SOC* (*TLS*) is the amount of time with respect to the total duration of the year that the *SOC* is below 35%. This is calculated by using (8).

$$TLS = 100 \times \left(\frac{\int H(35 - SOC)dt}{\int dt} \right) \tag{8}$$

Using this stress factors, in [4], six categories are suggested to analyze the performance of the battery bank. Category 1 represents the typical operation of HPS, in which the renewable generation is undersized and the battery bank operates cyclically with deep discharging and relatively full cycles. Category 2 represents a typical operation of HPS, in which the renewable generation is undersized, but the cycle operation is shallow and, consequently, the Ah throughput is low, *SOC* is high, and full charges are frequent. Category 3 represents HPS, in which the Ah throughput is between low and medium. The charge factor is between high and very high and, very often, the battery bank is fully recharged. Category 4 represents the operation of HPS, in which the Ah throughput is between medium and high with a high partial state of charge, i.e., the HPS operates with deep cycling and infrequent, strong charges. Category 5 represents the operation of an optimally-sized HPS, in which the battery is charged with a medium charge factor, the time between full charges and partial cycling is between low to high, and, consequently, the battery operates between high and medium states of charge. Category 6 represents HPS with a limited charge, which is characterized by an Ah throughput between low and medium and a partial state of charge between low and high. The charge factor is between very low and low, the occurrence of full charge is medium, and, during some periods of time, the battery bank operates at a very low state of charge.

III. Study Case

A typical HPS provided with several PV panels, wind turbines, and a lead acid battery bank is shown in Fig. 1.

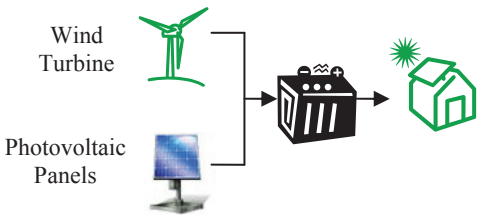

Figure 1. Typical PV/Wind/Battery system.

The PV/Wind/Battery system shown in Fig. 1 that is in place in Zaragoza was used as a study case. The wind speed time series are provided by AEMET [5]; the solar radiation data provided by NASA [6] for this location (Latitude: 41º39'N and Longitude: 0º53'W) were used. Information about renewable resources is shown in Tables I and II and the load profile is shown in Fig. 2. The system analyzed has 24V, 1 PV panel of 175W, 60º of tilt and azimuth 0º, 1 wind turbine with a power curve shown in Fig. 3, and a lead acid battery bank of C_{10}=800Ah. The simulation was carried out using the software HOMER [7] without consideration to the effects of temperature.

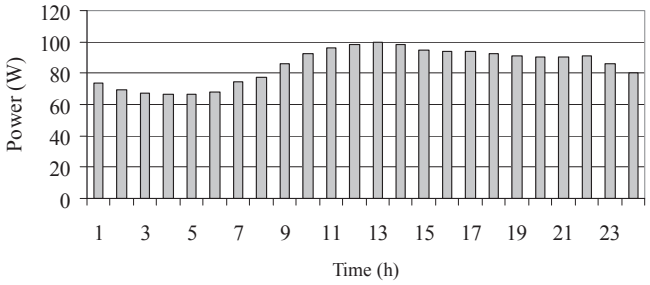

Figure 2. Typical load profile.

Figs. 4 and 5 show the *SOC* time series and its probability distribution. Figs. 6 and 7 show the power production of photovoltaic and wind turbines. Fig. 8 shows the current going into the battery bank.

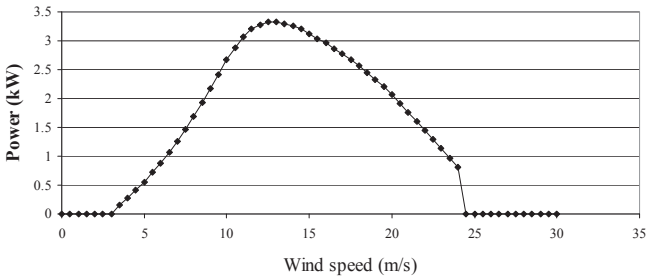

Figure 3. Typical wind turbine power curve.

TABLE I. WIND SPEED CHARACTERISTICS

Zaragoza	
Average wind speed (m/s)	***Standard deviation (m/s)***
4.6644	3.3019

TABLE II. SOLAR RADIATION CHARACTERISTICS

Daily Solar Radiation		
Month	***Clearness Index***	***Daily Radiation (kWh/m^2/d)***
January	0.478	1.890
February	0.564	3.030
March	0.583	4.320
April	0.548	5.200
May	0.544	5.970
June	0.578	6.700
July	0.601	6.770
August	0.578	5.800
September	0.559	4.530
October	0.508	3.030
November	0.485	2.070
December	0.450	1.590

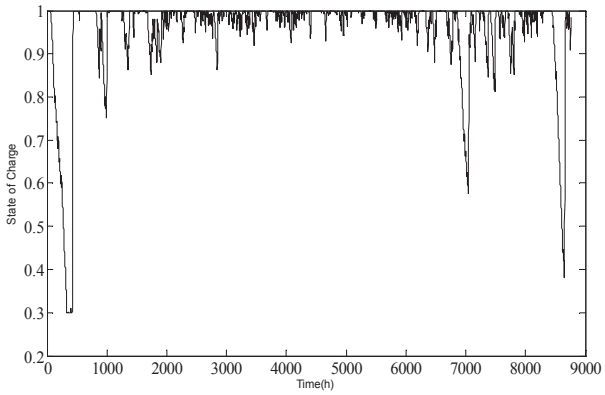

Figure 4. Simulated states of charge.

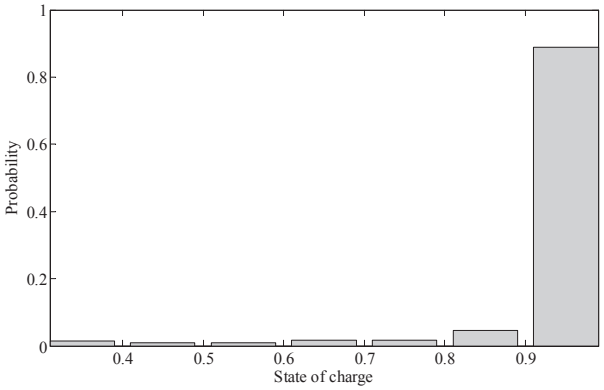

Figure 5. Probability distribution of states of charge.

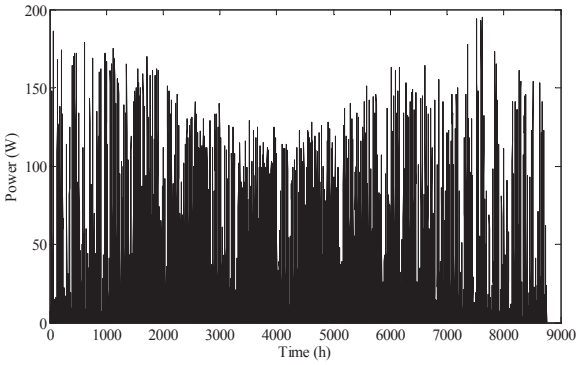

Figure 6. Photovoltaic production.

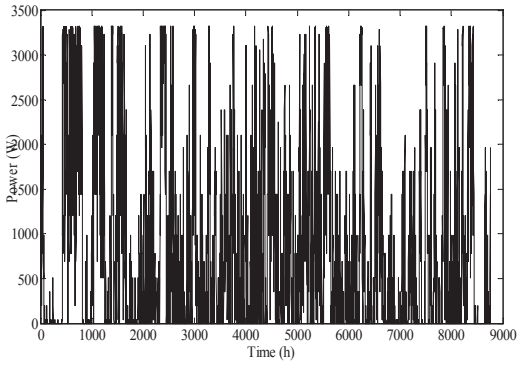

Figure 7. Wind power production.

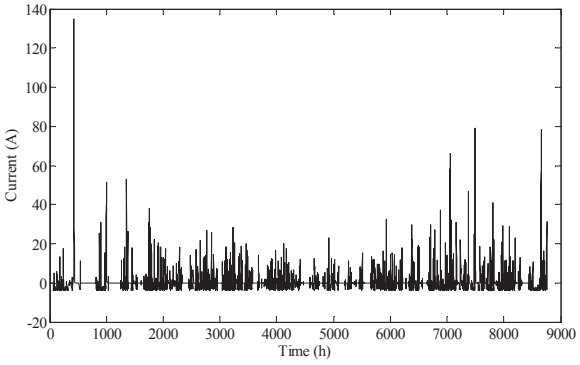

Figure 8. Current of battery bank.

The stress factors obtained are shown in Table III. According to these results and using the relationship between stress factors and intensity levels developed in [4], we can determine that this system presents medium time between full charge, charge factor of high intensity and low discharge rate, Ah throughput, time at low *SOC*, and partial cycling. The category for this system is 3. Fig. 9 shows the radar plot diagram for the system under analysis.

TABLE III. STRESS FACTORS CALCULATED

Stress Factors of Study Case					
***CF* (%)**	**Q_{thrp} ($\times C_{10}$)**	**$I_{max1\%\_aver}$ ($\times I_{10}$)**	***tbfc* (day)**	***TLS* (%)**	***PC* (%)**
116.06	10.85	0.3841	2.13	1.16	26.63

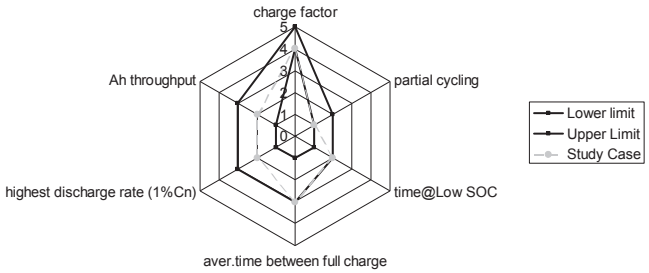

Figure 9. Radar plot diagram of Category 3.

IV. CONCLUSIONS

This paper analyzes a small capacity PV/Wind/Battery system using qualitative information about operating conditions. Estimations of different stress factors such as charge factor, Ah throughput, highest discharge rate, time between full charged, partial cycling, and time at low state of charge have been conducted. According to the results presented in Table III and Fig. 9 the category of operating condition is 3. This category is characterized by a very high risk of corrosion of the positive grid and water loss. This information could be useful in the estimation of the net present cost and a general performance analysis of HPS.

ACKNOWLEDGMENT

This work was supported by the Ministerio de Ciencia e Innovación of the Spanish Government under Project ENE2009-14582-C02-01.

REFERENCES

[1] D.U. Sauer and H. Wenzl, "Comparison of different approaches for lifetime prediction of electrochemical systems-Using lead-acid batteries as example," *Journal of Power Sources*, vol. 176, pp. 534–546, February 2008.

[2] D.U. Sauer and H. Wenzl, "Batteries | Lifetime prediction," in *Encyclopedia of Electrochemical Power Sources*, 2009, pp. 522-538.

[3] J. Schiffer, D.U. Sauer, H. Bindner, T. Cronin, P. Lundsager and R. Kaiser, "Model prediction for ranking lead-acid batteries according to expected lifetime in renewable energy systems and autonomous power supply systems," *Journal of Power Sources*, vol. 168, pp. 66-78, May 2007.

[4] V. Svoboda, H. Wenzl, R. Kaiser, A. Jossen, I. Baring-Gould, J. Manwell, P. Lundsager, H. Bindner, T. Cronin, P. Nøgard, A. Ruddell, A. Perujo, K. Douglas, C. Rodrigues, A. Joyce, S. Tselepis, N. van der Borg, F. Nieuwenhout, N. Wilmot, F. Mattera and D.U. Sauer, "Operating conditions of batteries in off-grid renewable energy systems," *Solar Energy*, vol. 81, pp. 1409-1425, November 2007.

[5] http://www.aemet.es/es/

[6] http://eosweb.larc.nasa.gov/

[7] http://homerenergy.com/

Probabilistic Modeling and Analysis of PV/Wind/Diesel/Battery Systems

Juan M. Lujano-Rojas, Rodolfo Dufo-López, José L. Bernal-Agustín[1]

Department of Electrical Engineering - University of Zaragoza

Calle María de Luna, 3. 50018 Zaragoza (Spain)

lujano.juan@gmail.com; rdufo@unizar.es, jlbernal@unizar.es

Abstract

This paper presents a probabilistic model for hybrid power systems considering photovoltaic panels, wind turbine, conventional diesel or gasoline generator, and a battery bank (PV/Wind/Diesel/Battery system). The model can consider the main sources of uncertainty related to renewable resources, fuel cost, the battery bank's lifetime, energy demand, charge controller operation and coulombic efficiency. As a case study, a hybrid system installed in Zaragoza (Spain) is analyzed. First, the impact of charge controller operation and coulombic efficiency are studied through comparative analysis of the presented model and HOMER model, which is a less accurate model because it does not consider the charge controller operation or the dependence between the coulombic efficiency and state of charge. The results show a difference between both models of approximately 33% in the number of hours of operation of a conventional generator, 31% in fuel consumption, and 31% in net present cost for hybrid power system configurations with low storage capacity. However, these differences are lower when the capacity of the battery bank is incremented because the charge currents are reduced, the acceptance of charge by the battery bank is improved, and the effect of the charge controller is minimized. Furthermore, a probabilistic analysis has been carried out for different sizes of battery banks, obtaining the uncertainty in the net present cost, which depends on fuel cost and the battery bank's lifetime.

Keywords: hybrid power systems, coulombic efficiency, charge controller, probabilistic modeling.

1. Introduction

Stand-alone hybrid power systems are useful for satisfying energy demands in remote areas where there is not access to electricity. In this context, several models and optimization techniques have been carried out to sizing hybrid power systems.

HOMER [1] is a very frequently used computational tool for hybrid power system design. This software evaluates all possible combinations of components, of the hybrid system, to determine the system configuration that minimizes the net present cost. Furthermore, this tool can consider hybrid power systems, including photovoltaic (PV) panels, wind turbines, small hydro, biomass power, lead-acid batteries, a diesel generator, fuel cells, and hydrogen storage. Another tool, HOGA [2], is a computer program for optimal sizing of hybrid power systems, which includes wind turbines, PV panels, small hydro, lead-acid batteries, a diesel generator, fuel cells, and hydrogen storage. This computational tool uses genetic algorithms to obtain the optimal system, taking much less computational time than evaluating all possible combinations. HOGA can consider the net present cost, energy not supplied, and CO_2 emissions as objectives in the mono- or multi-objective optimization.

[1] Corresponding author. Tel.: +34 976761921; fax: +34 976762226.
E-mail address: jlbernal@unizar.es (J.L. Bernal-Agustín).

In addition to the two mentioned tools, several researchers have applied other techniques for the design of hybrid systems. This way, Boonbumroong et al. [3] presented an application of the Particle Swarm Optimization (PSO) and the constriction coefficient algorithm to design a typical hybrid power system. This methodology was applied to size a hybrid system that includes PV arrays, wind turbines, a battery bank, and an inverter. Reached results were compared with the one obtained using the rule-of-thumb method and HOMER software, concluding that the PSO algorithm substantially reduces the required time to find the optimal configuration. Belfkira et al. [4], using the DIviding RECTangles (DIRECT) algorithm, developed an optimization model for hybrid wind/PV/diesel systems to minimize the total cost while the energy required is covered. This methodology was implemented to design a hybrid system installed in Senegal, and the results showed the influence of the load profile and renewable resources in the optimal configuration of the hybrid system. Furthermore, the authors conclude that the size of the battery bank is a relevant parameter, because it can significantly reduce the number of operating hours of the diesel generator and the total cost.

Recently, Kaldellis et al. [5] presented a study about electrification for remote consumers, in a Greek island region of medium-high solar potential, using PV-diesel hybrid systems and storage. The applied methodology evaluated the possible combinations of PV panels, battery bank size, and diesel generator capacity, calculating the long-term electricity generation cost for 10 and 20 years of operation, respectively. Results showed different optimal configurations when these operation time periods were considered. These results reveal the importance of using long-term data about the renewable resources and probabilistic assessment in the design process. In this sense, Kaplani and Kaplanis [6] developed a simulation model for stand-alone PV systems that could also be adapted to system with diesel generators. The proposed methodology was applied to design some PV systems installed in various European cities. The stochastic PV sizing methodology suggests a 37% reduction in pick power of PV generator and battery storage capacity compared to the results reached using a conventional methodology. Similar results can be found were founded by Távora et al. [7], who presented a comparative study of deterministic and probabilistic approaches to design PV systems. The results showed that the deterministic method could oversize the system. Karaki et al. [8] applied a probabilistic methodology to estimate the production costs of a wind-diesel system. A wind farm model was built using the joint probability distribution function of the total available wind power, while the diesel generator model was obtained using convolution methods. The production costs associated with the diesel system were estimated using the expected energy that is not supplied and a de-convolution process in reverse economic order. Giannakoudis et al. [9] presented a model for optimization and power management of hybrid systems with hydrogen storage adapting the simulated annealing algorithm to consider uncertainty (stochastic annealing). The variables under uncertainty included the solar radiation, the wind speed, and the efficiencies of the electrolyzer and fuel cell. The objective function considered was the net present value of investment over the lifetime of the system. Tan et al. [10] developed a methodology for stochastic sizing of a battery bank in an uninterruptible power system with a PV generator using a Monte Carlo simulation approach. In this methodology, first a random event of load profile, weather conditions, and failure was generated, and the required energy capacity was calculated. This process was repeated a number of times. Then the results were statistically analyzed using the cumulative distribution function and, finally, the battery capacity was economically evaluated considering a determined confidence level. Another technique, applying Monte Carlo

simulation and a reliability analysis methodology, including battery storage for PV systems with diesel generators, was developed by Moharil and Kulkarni [11].

Other authors have published studies that have shown the importance of battery storage in the reduction of operating hours of diesel generators and total net present cost [4,12,13]. This is a relevant topic because the charge controller operation and the coulombic efficiency have an important influence on the acceptance of the battery bank's charge, and consequently on the ability of the system to meet the energy demand. However, these factors are not considered in many studies and simulation models [1,2]. Otherwise, the use of long-term data and the consideration of uncertainty of the potential of renewable resources in the simulation and optimization process are determinant factors in the optimal sizing of hybrid systems [6,7].

In this paper, a probabilistic model based in a Monte Carlo simulation approach of a PV/Wind/Diesel/Battery system is developed and the influence of charge controller and coulombic efficiency in its performance is analyzed. This research work is a continuation of our previous one presented in [14].

This work is presented as follows:

- The PV/Wind/Diesel/Battery system model
- Stochastic modeling of the renewable resources
- The case study
- Conclusions.

2. PV/Wind/Diesel/Battery system model

The hybrid power system being analyzed is shown in Fig. 1. The lead acid battery bank, the wind turbine, and the photovoltaic generator are connected to the AC bus through the inverter. The model of this system will be carefully described in the following sections.

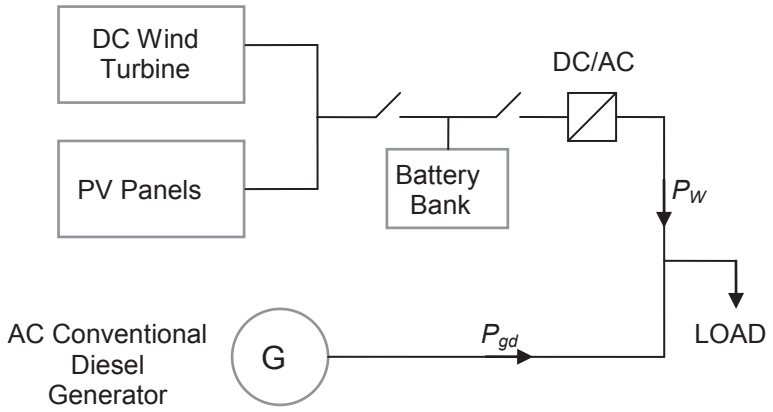

Fig. 1. Hybrid power system

2.1 Photovoltaic panel model

The output power of the photovoltaic panel (P_{PV}) could be estimated using Eq. (1) and its efficiency can be estimated by means of Eq. (2) [15].

$$P_{PV} = AG\eta_{PV} \tag{1}$$

$$\eta_{PV} = \eta_{STC}\left[1 + \alpha(T_c - 25)\right] \tag{2}$$

where A is the area of the photovoltaic panel in m^2, G is the incident solar radiation in W/m^2, η_{PV} is the efficiency in a determined operating condition, η_{STC} is the efficiency at standard test conditions, T_c is the cell temperature in degrees C, and α is the temperature coefficient in %/degrees C. Combining Eqs. (1) and (2), the production of photovoltaic panel could be expressed in terms of power obtained under standard test conditions (P_{STC}).

$$P_{PV} = P_{STC}\left\{\frac{G}{1000}\left[1 + \alpha(T_c - 25)\right]\right\} \tag{3}$$

$$T_c = T_a + \left(\frac{NOCT - 20}{800}\right)G \tag{4}$$

where T_a is the ambient temperature in degrees C and $NOCT$ is the nominal operation cell temperature in degrees C.

2.2 Wind turbine model

Frequently, the wind generator is represented using the power curve provided by the manufacturer; Fig. 2 shows a normalized power curve of a typical wind turbine of low rated power and horizontal axes. The start-up wind speed is between 3 to 4 m/s, and the rated wind speed is between 14 to 15 m/s. Generally, if the wind speed is higher than 14 or 18 m/s, the output power is between 30% and 70% of the rated power [13].

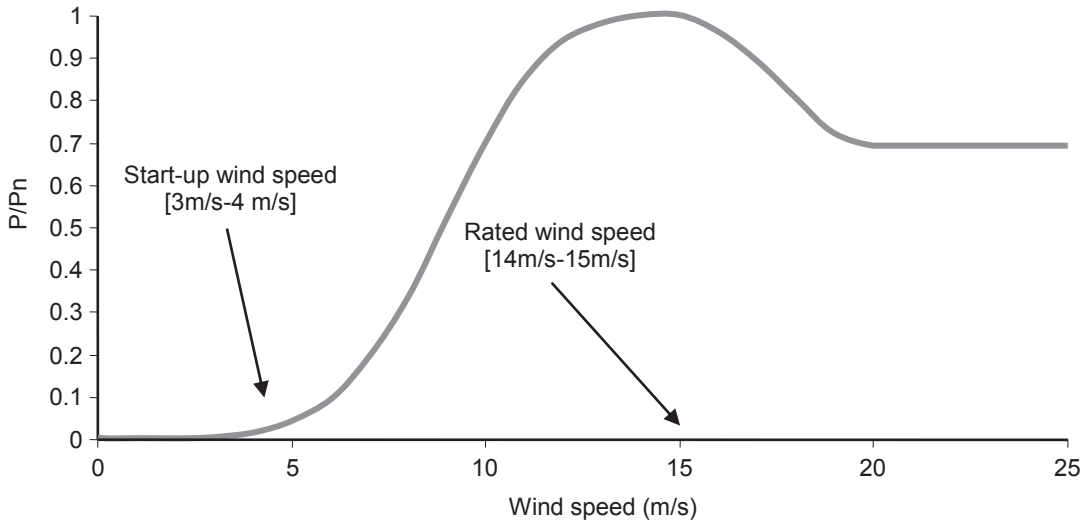

Fig. 2. Typical power curve of wind turbine

2.3 Diesel or gasoline generator model

The fuel consumption of a conventional generator is an important variable in the hybrid system performance analysis. The fuel consumption (F_l) is calculated using Eq. (5).

$$F_l = m_1 P_{gdn} + m_2 P_{gd} \tag{5}$$

where P_{gdn} is the rated power, P_{gd} is the output power, and the constants m_1 and m_2 could be determined using data provided by the manufacturer. For a diesel generator, typical values for these constants are m_1=0.085 *l/kWh* and m_2=0.246 *l/kWh* [16], while for a gasoline generator, typical values are m_1=0.2 *l/kWh* and m_2=0.5 *l/kWh* [17].

2.4 The inverter model

The inverter is modeled calculating its efficiency (η_i) for the power transmission from the DC bus to AC bus. The efficiency is variable with the AC load and can be represented by means of Eq. (6).

$$\eta_i = \frac{P_l}{m_3 P_{inv} + (1 + m_4) P_l} \tag{6}$$

where P_l is the load in the AC bus, P_{inv} is the rated power of the inverter, m_3 and m_4 are parameters fitted using data provided by the manufacturer. Fig. 3 shows a typical efficiency curve for m_3=0.0119 and m_4=0.0155.

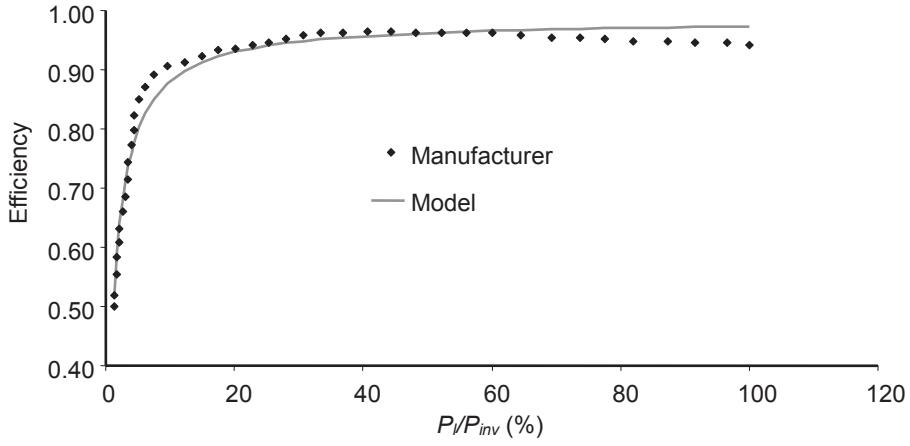

Fig. 3. Typical efficiency curve for an inverter

2.5 Lead acid battery and charge controller model

The lead acid battery model used in this paper is a simplified version of Copetti's model [18,19]. An extended discussion of other lead acid battery models and lifetime estimation methods can be found in reference [14], in which this simplified version was used for probabilistic modeling of small capacity wind energy systems using a Monte Carlo simulation approach.

The battery capacity (C) is calculated using Eqs. (7) and (8) [18,19].

$$C_T = 1.67 C_{10}(1 + 0.005\Delta T_a) \tag{7}$$

$$C = \frac{C_T}{1 + 0.67\left(\frac{I}{I_{10}}\right)^{0.9}} \tag{8}$$

where C_T is the maximum capacity of the battery, I is the charge or discharge current, $\Delta T_a = T_a - 25$ is the change in the temperature from the reference of 25º C, and C_{10} and I_{10} are the capacity and current in 10 hours at 25º C, respectively.

The state of charge (SOC) is estimated by means of Eq. (9) [19].

$$SOC = \begin{cases} \frac{Q}{C}\eta_b & I > 0 \\ 1 - \frac{Q}{C}\eta_b & I < 0 \end{cases} \tag{9}$$

where $Q = |I|t$ represents the charge supplied to the battery (charge process) or supplied by the battery (discharge process) during the time of interest t, while η_b is the coulombic efficiency calculated according to Eq. (10) [19] for the charge ($I>0$) and discharge ($I<0$) processes.

$$\eta_b = \begin{cases} 1 - \exp\left[\left(\frac{20.73}{I/I_{10} + 0.55}\right)(SOC - 1)\right] & I > 0 \\ 1 & I < 0 \end{cases} \tag{10}$$

The charge controller protects the battery bank against overcharging or overdischarging by disconnecting the renewable generators or the load, respectively. During the charge process, the charge controller operation can affect the energy capture of the battery as it prematurely disconnects the renewable generators when the voltage increases suddenly, producing a low state of charge in the battery bank [20]. The charge controller is an important component of the hybrid system that is not considered by several simulation and optimization tools available nowadays. The battery voltage during the charge process can be estimated using Eq. (11) [18]. For a determined charge controller set-point (the set-point at which the charge controller protects the battery from overcharging by disconnecting the renewable generators), the Q value and the state of charge in the moment at which the charge controller disconnects the renewable generators can be calculated using Eq. (11). For example, if the charge controller set-point is 2.50 V per cell, by using Eq. (11), the upper limit of the state of charge due to operation of the charge controller could be determined calculating the Q value with V=2.50 V.

$$V = (2 + 0.16\frac{Q}{C}) + \frac{I}{C_{10}}(\frac{6}{1 + I^{0.6}} + \frac{0.48}{(1 - Q/C_T)^{1.2}} + 0.036)(1 - 0.025\Delta T_a) \tag{11}$$

This simplification in the lead acid battery model presented in [18,19] allows us to estimate the effects of the voltage stability on the DC bus and the coulombic efficiency in the state of charge without calculating the battery voltage in detail, thus reducing the computational effort, which is desirable in a probabilistic model based on Monte Carlo simulations. The lower limit of the state of charge is the minimum value recommended by the manufacturer; the charge controller disconnects the load when this value is reached.

Similar to the model presented in [14], in this paper, the *Ah* throughput model is implemented considering 17.5% error [21]. In this battery, a lifetime model assumes that the amount of energy that can be cycled through the battery is fixed. Using the depth of discharge versus the cycles to failure curve frequently provided by the manufacturer, the estimated throughput energy (Q_t) can be calculated using Eq. (12) [21].

$$Q_t = \frac{1}{N_p}\sum_{i=1}^{N_p} C_{10}(DOD_i)(CF_i) \tag{12}$$

where DOD_i and CF_i are points of the depth of discharge versus the cycles to failure curve and N_p is the total number of points considered. Calculating the total ampere-hours cycled by the battery bank from the simulation of the hybrid system and comparing this value with the expected throughput determines the battery lifetime.

3. Model of the renewable resources

The stochastic analysis of a PV/Wind/Diesel/Battery system based in a Monte Carlo simulation approach requires that a model be able to consider the main sources of uncertainty in the power obtained from the photovoltaic panels and wind turbine.

3.1 Stochastic modeling of photovoltaic generator.

The output power of the photovoltaic generator can be estimated by means of the model described in section 2.1. The hourly solar radiation could be synthetically generated using the stochastic procedure proposed by Graham and Hollands [22]. However, if hourly global radiation data are available, the methodology to fit an autoregressive moving average (ARMA) model described by Kamal and Jafri [23] is suggested. The uncertainty related to the production of the photovoltaic generator could be modeled using a Gaussian distribution with mean and standard deviation of -15% and 9.45%, respectively. This probability distribution models the uncertainty related to climate variability, solar radiation, transposition model, power rating of modules, dirt and soiling, snow, and other errors [24].

3.2 Stochastic modeling of wind power generation.

If the wind speed time series is known, the wind turbine output power is calculated using the model described in section 2.2. Some studies [25,26] have shown the ability of the ARMA model to represent the mean characteristics of the hourly average wind speed time series such as the diurnal non-stationarity, non-Gaussian shape of its probability distribution function (PDF), and the autocorrelation between successive wind speeds. The mathematical formulation of ARMA model is presented in Eq. (13).

$$\hat{W}_{(t)} = \varphi_1 \hat{W}_{(t-1)} + \ldots + \varphi_p \hat{W}_{(t-p)} + \varepsilon_{(t)} - \theta_1 \varepsilon_{(t-1)} - \ldots - \theta_q \varepsilon_{(t-q)} \tag{13}$$

where $\hat{W}_{(t)}$ is the transformed and standardized wind speed of hour t, $\varphi_1,\ldots,\ \varphi_p$ are the autoregressive (AR) parameters, $\theta_1,\ldots,\ \theta_q$ are the moving average (MA) parameters, and $\varepsilon_{(t)},\ \varepsilon_{(t-1)},\ldots,\ \varepsilon_{(t-q)}$ are random variables with mean zero and standard deviation of σ. The estimation of autoregressive and moving average parameters require carrying out the processes of transformation and standardization, estimation, and diagnostic checking.

The transformation and standardization processes are necessary because the PDF of the wind speed time series is frequently a Weibull distribution, which make it necessary to transform the measured wind speed time series to another with Gaussian PDF. This transformation is carried out using a power *m* in Eq. (14) [27].

$$U_{T(t)} = U_{(t)}^{\ m} \text{ with } t = 1,...,n \tag{14}$$

where $U_{(t)}$ is the measured wind speed time series with *n* observations, and $U_{T(t)}$ is the transformed time series. The transformed time series become a stationary one ($W_{(t)}$) by means of the standardization process of Eq. (15) [27].

$$W_{(t)} = \frac{U_{T(t)} - \mu_{h(t)}}{\sigma_{h(t)}} \text{ with } t = 1,...,n \tag{15}$$

where $\mu_h(h)$ and $\sigma_h(h)$ with $h=1,2,....24$ are the hourly mean and standard deviation of the transformed wind speed time series ($U_{T(t)}$). It is assumed that these variables have a periodical behavior, that is to say, $\mu_h(h=25) = \mu_h(h=1)$ and $\sigma_h(h=25) = \sigma_h(h=1)$ [27].

During the estimation process, the autoregressive and moving average parameters are calculated, and these are finally validated during the diagnostic checking process. Details about all these processes can be found in [14].

To simulate a wind speed time series, first Eq. (13) is evaluated. Then, the transformed values of the simulated wind speed time series ($\hat{U}_{T(t)}$) are calculated using Eq. (16).

$$\hat{U}_{T(t)} = \mu_{h(t)} + \sigma_{h(t)} \hat{W}_{(t)} \tag{16}$$

Finally, the simulated wind speed time series ($\hat{U}_{(t)}$) is obtained applying the probability transformation described in Fig. 4 [29], where the curve of the left-hand side is the cumulative distribution function (CDF) of the time series $\hat{U}_{T(t)}$ and the curve of the right-hand side is the CDF of the measured wind speed time series under uncertainty $\beta U_{(t)}$. The factor β represents the uncertainty due to long-term variations in the average wind speed. This idea is expressed in Eq. (17).

$$\beta = \frac{\psi}{\omega} \tag{17}$$

where ψ is a random variable normally distributed with mean and standard deviation equal to that obtained from the historical data, and ω is the average of the wind speed time series measured $U_{(t)}$. The algorithm used to calculate the inverse of the CDF in discrete form presented in our previous work [14] could be used, but taking into consideration the time series $\beta U_{(t)}$ instead the measured time series $U_{(t)}$.

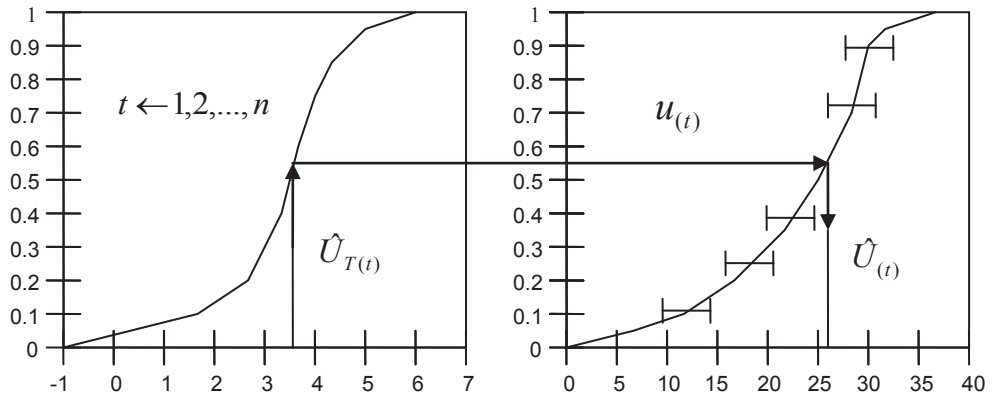

Fig. 4. Probability transformation

4. The case study

The probabilistic model presented in the previous section was used to analyze a PV/Wind/Diesel/Battery system installed in Zaragoza, Spain. The hourly wind speed and ambient temperature time series of 2005 and monthly averages between 1953 and 2010 provided by AEMET [29] were considered. Fig. 5 shows the histogram of seasonal average wind speed, while its total average and standard deviation are shown in Table 1. Fig. 6 shows the global horizontal radiation and clearness index provided by NASA [30], and Fig. 7 shows the monthly average ambient temperature.

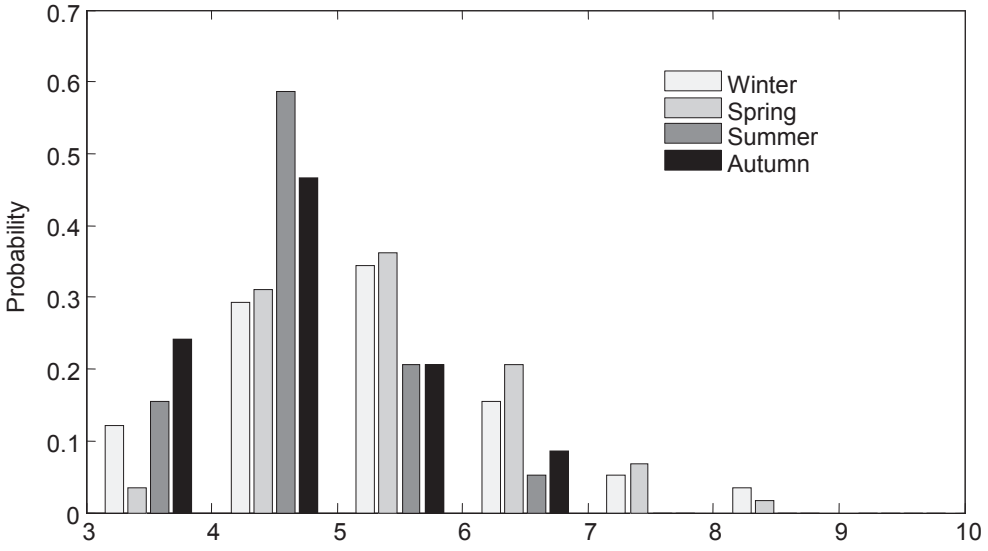

Fig. 5. Histogram of seasonal average wind speed between 1953 and 2010

Table 1
Seasonal characteristics from 1953 to 2010 in Zaragoza

Season	Average wind speed	Standard deviation
Winter	5.3322	1.5329
Spring	5.4598	1.2853
Summer	4.6920	1.0417
Autumn	4.6546	1.3004

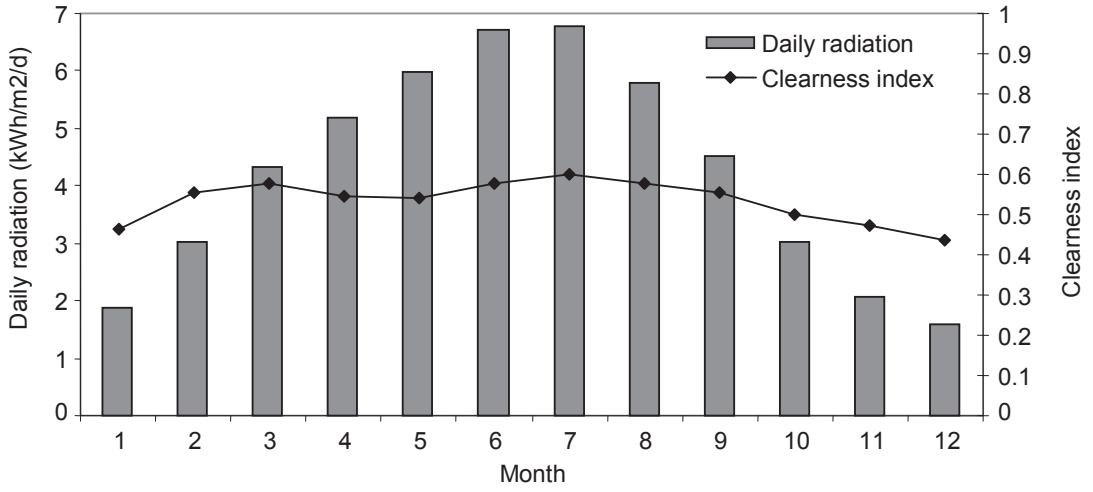

Fig. 6. Monthly average global horizontal radiation and clearness index in Zaragoza

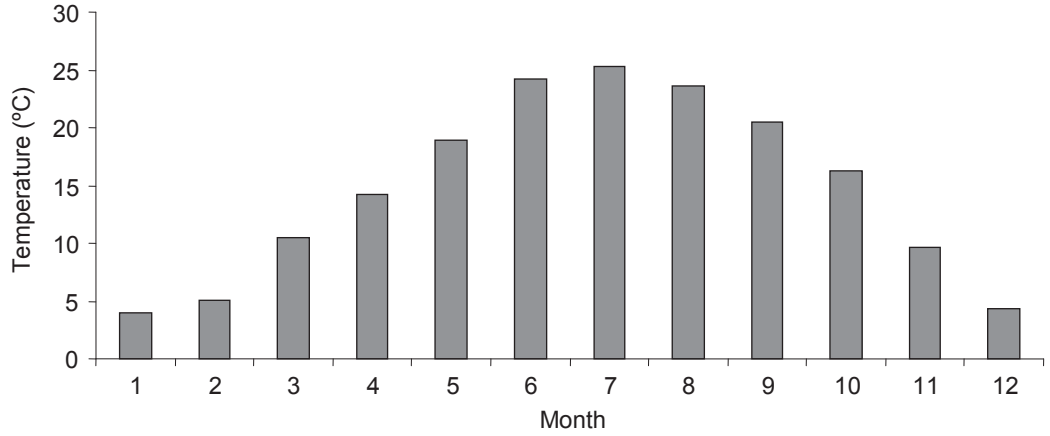

Fig. 7. Monthly average temperature in Zaragoza

The typical load profile considered is shown in Fig. 8, which is composed of three household appliances of 150W, 100W, and 100W, respectively. However, there is uncertainty in the possible hour at which each appliance could be used. For example, the first appliance typically operates between 17h and 22h, but it could be used between 1h and 24h. In a similar way, the second appliance typically operates between 19h and 21h, but it could be used between 17h and 24h. The third appliance typically operates during all hours of the day.

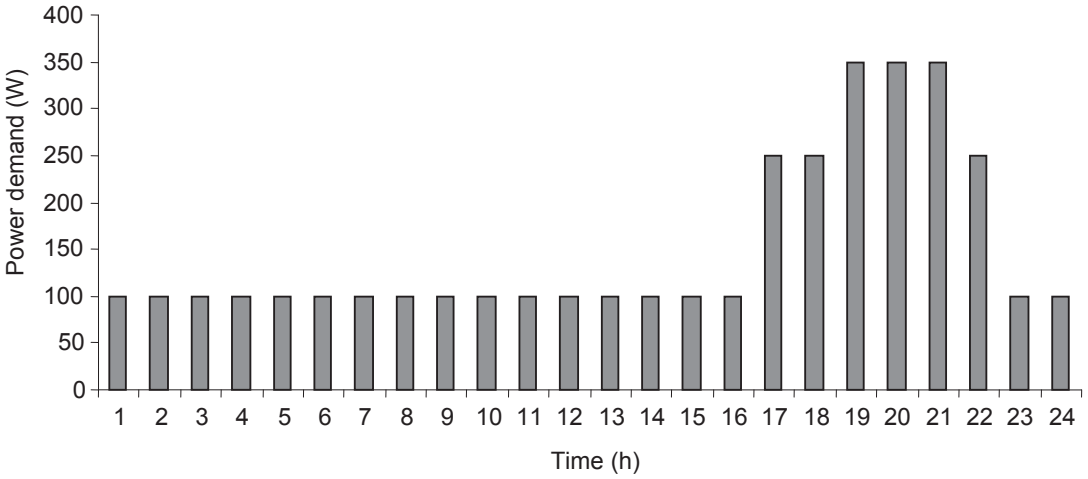

Fig. 8. Typical load profile

The photovoltaic generator is conformed by a panel with output power under standard test conditions (P_{STC}) of 175W, temperature coefficient (α) of -0.485%/ºC, nominal operation cell temperature (*NOCT*) of 47.5ºC, 60º tilt angle, and open circuit voltage of 44.4V. The rated power of the wind turbine is 1,000W; it is installed at 20 m height. The renewable generators and battery bank of 24V are coupled to the AC bus through

an inverter of 500W. The conventional generator considered is based in gasoline, and its rated power is 500W. Different batteries with capacities between 100Ah and 1,000Ah have been considered, and the capacity curves are shown in Fig. 9.

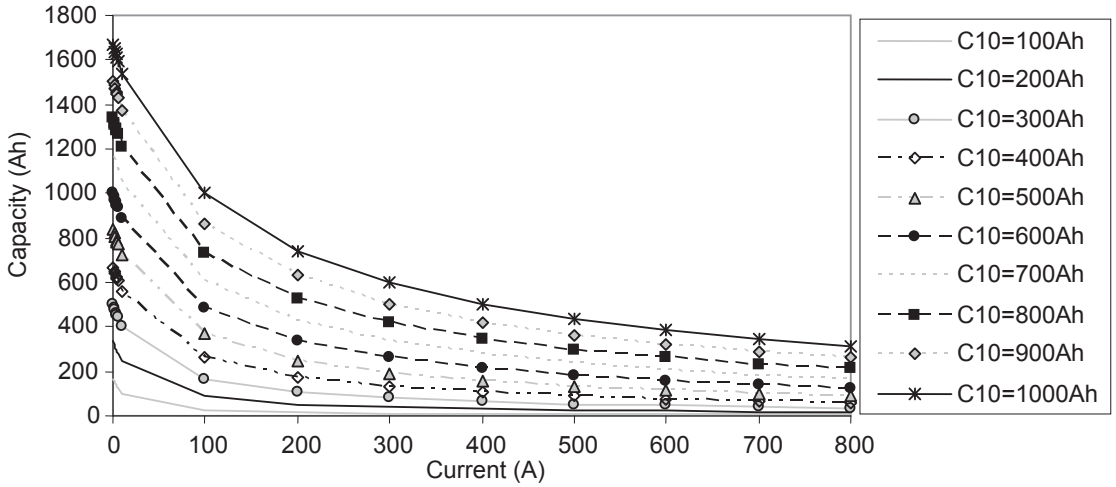

Fig. 9. Capacity curves for different batteries considered

The hours of operation of the gasoline generator, the fuel consumption, and the net present cost were the variables considered to analyze the performance of the PV/Wind/Diesel/Battery system under study. A simulation process determined the hours of operation and fuel consumption, while the net present cost (*NPC*) was calculated using Eqs. (18) and (19).

$$NPC = \frac{(ACC + ARC + AMC)}{CRF(i,j)} \tag{18}$$

$$CRF(i,j) = \frac{i(1+i)^j}{(1+i)^j - 1} \tag{19}$$

where *ACC* is the annualized capital cost, *ARC* is the annualized replacement cost, *AMC* is the annualized maintenance cost, *j* is the project lifetime, *i* is the annual real interest rate, and *CRF(i,j)* is the capital recovery factor [31].

The capital and replacement costs of the wind turbine, the photovoltaic panel, the inverter, and the gasoline generator are assumed to be 3,200€, 500€, 400€, and 250€, respectively. The lifetimes of the wind turbine, the photovoltaic panel, and the inverter are assumed to be 15 years, 20 years, and 15 years, respectively. The lifespan of the gasoline generator is estimated to be 1,000h. The capital and replacement costs of the battery bank are estimated at 250€/kWh, and its floating lifetime is 9 years with 300 cycles at 70% depth of discharge. The operation and maintenance costs for the wind turbine, the photovoltaic panel, the inverter, and the lead acid batteries were negligible. The operation and maintenance costs of the gasoline generator are estimated 0.2€/h. An inflation rate of 3% and a nominal interest rate of 4.5% have been assumed for a project lifetime of 30 years.

4.1. Effect of the coulombic efficiency and charge controller operation.

The general performance and the impacts of coulombic efficiency and charge controller operation were analyzed in a PV/Wind/Diesel/Battery system with a photovoltaic panel of 175W, a wind turbine of 1,000W, an inverter of 500W, a gasoline generator of 500W with fuel cost of 1.2 €/l, and a battery bank with capacities between 100Ah and 5,000Ah under the weather conditions described previously and taking into account the load profile presented in Fig. 8. For each configuration evaluated, the model of the hybrid system presented in section 2, which considered the operation of the charge regulator and coulombic efficiency, was compared with the HOMER model, which does not consider the charge controller operation and uses the coulombic efficiency as a fixed value equal to the square root of the battery roundtrip efficiency. The comparative results obtained for the hours of operation of a gasoline generator, fuel consumption, and net present cost are shown in Figs. 10, 11, and 12, respectively. According to this comparative analysis, there are important differences between the simulations obtained using both models when the system configurations have low storage capacities. In systems with small storage capacity, the charge currents are high, the high voltage set-point of the charge controller is reached prematurely, and consequently the renewable generators are disconnected, producing a low state of charge of the battery bank and an important increment in the number of hours of operation and fuel consumption of a gasoline generator, which incrementally affect the net present cost compared to the results obtained using a HOMER model. The maximum difference between both models is observed when the battery bank's capacity is 100Ah; for this configuration, the difference between the hours of operation of the gasoline generator, fuel consumption, and net present cost are about 33%, 31%, and 31%, respectively. Otherwise, when the battery bank's capacity is incremented, similar results could be obtained using both models, because in this case the charge currents are reduced, the battery bank can accept more energy (see Eq. (8) with $I \rightarrow 0$), the DC voltage does not reach high values prematurely, and, consequently, the effect of the charge controller is minimized.

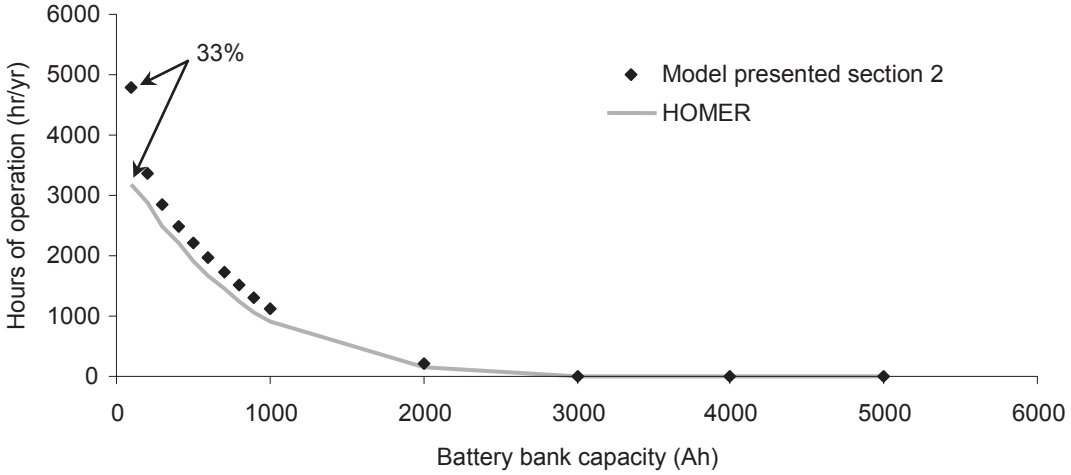

Fig. 10. Hours of operation

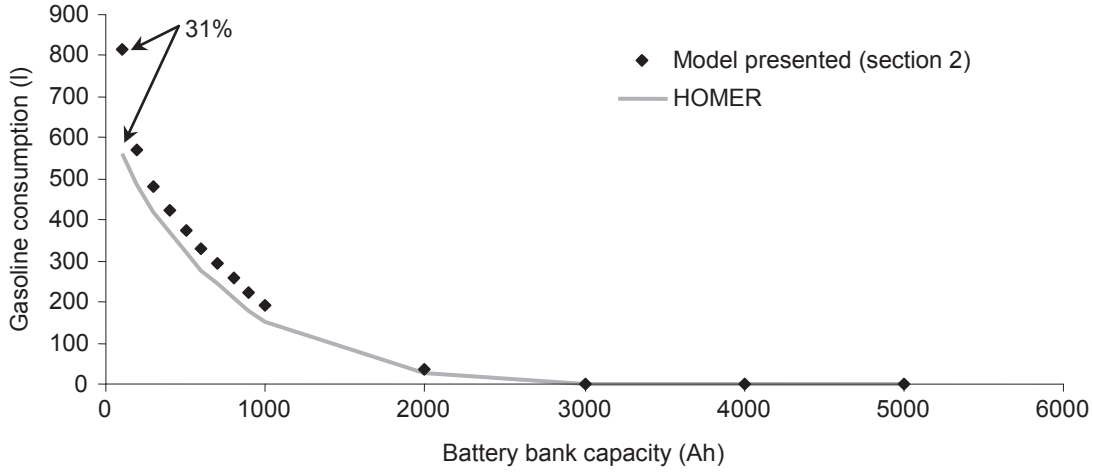

Fig. 11. Gasoline consumption

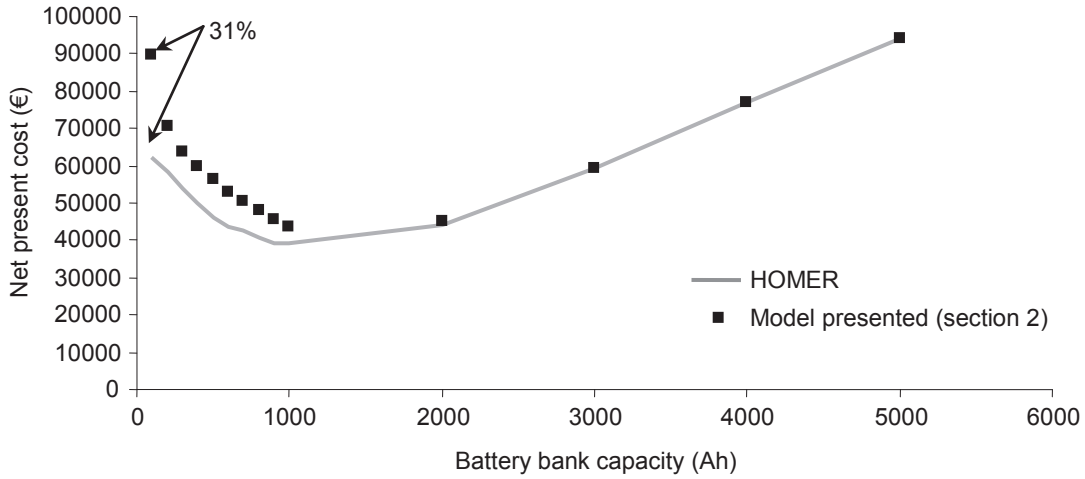

Fig. 12. Net present cost

4.2. Probabilistic analysis.

The probabilistic analysis was carried out according to the methodology described in section 3. The uncertainty related to the production of the photovoltaic generator was modeled using a Gaussian distribution with mean and standard deviation of -15% and 9.45%, respectively. The parameters of the ARMA model were fitted using the methodology presented in [14] and are shown in Table 2. The parameter ψ in Eq. (17) was represented as a random number with Gaussian PDF (according to the histogram of Fig. 5), with mean and standard deviation shown in Table 1. The uncertainty of the load profile was considered by randomly modeling the hour at which a particular household

appliance is used. For example, if the household appliance of 150W can operate for 6h between 1h and 24h, its operation was modeled as an energy block (150W×6h); the hour that use of the appliance started was selected randomly for each day. The battery bank's lifetime was estimated using the *Ah* throughput model with 17.5% error. After analyzing historical data of gasoline prices in Spain between 2007 and 2011 provided by [32], the uncertainty in gasoline prices was modeled as a random number with Gaussian PDF with mean 1€/l and uncertainty 9.50%.

Table 2
ARMA model parameters

Season	φ_1	φ_2	φ_3	φ_4	φ_5	φ_6	φ_7	φ_8	φ_9	σ
Winter	0.6563	0.0786	0.1581	-0.0501	0.0105	0.031	0.0275	-0.0215	0.0655	0.4184
Spring	0.6422	0.1336	0.0818	0.011	-0.0109	0.0187	0.0168	-0.0326	0.0562	0.5312
Summer	0.7049	0.1039	0.0907	-0.0055	-0.0405	0.0893	-0.0305	---------	---------	0.509
Autumn	0.6429	0.1435	0.0567	-0.0249	0.0368	0.0156	0.0133	0.0428	---------	0.5171

The hourly solar radiation model proposed by Graham and Hollands [22] and the uncertainty related to the production of the photovoltaic generator modeled by means of Gaussian PDF with mean of -15% and standard deviation of 9.45% were used to synthetically generate 100 scenarios of photovoltaic power generation. The stochastic simulation model of wind speed time series presented in section 3.2 was used to synthetically generate 100 scenarios (100 Monte Carlo simulations) of wind power generation. The rated power of each household appliance and the uncertainty related to its possible hour of operation were used to randomly generate 100 scenarios, considering an additional 25% error.

Fig. 13 shows the expected value of net present cost with its uncertainty interval calculated at a 10% confidence level. For hybrid system configurations with battery banks of low capacity (about 100Ah), the uncertainty in the net present cost is meanly influenced by the uncertainty in the prices of fuel (9.50%), being approximately 7%. When the capacity of the battery bank is incremented, the uncertainty in the net present cost is influenced jointly by the uncertainty in the prices of fuel (9.50%) and the uncertainty in the determination of the battery bank's lifetime (17.5%), reaching about 28% for a system configuration with 1,000Ah. The uncertainty of the net present cost in systems with high storage capacity is mainly influenced by the uncertainty in the determination of the battery bank's lifetime (17.5%), reaching approximately 20% for a system configuration with 5,000Ah.

5. Conclusions

This paper describes a mathematical model for probabilistic analysis and simulation of hybrid power system with photovoltaic panels, wind turbine, conventional diesel or gasoline generator, and a battery bank (PV/Wind/Diesel/Battery system) based on a Monte Carlo simulation approach. This model can consider the main uncertain sources related to the output power of renewable generators, determination of the battery bank's lifetime, energy demand, and fuel cost as well as charge controller operation and coulombic efficiency of the battery bank.

As a case study, a hybrid power system installed in Zaragoza was analyzed. The effects of charge controller operation and coulombic efficiency in the number of hours of

operation of a conventional (diesel or gasoline) generator, fuel consumption, and net present cost were analyzed and the results obtained were compared with those obtained from a HOMER model, which does not consider charge controller operation and used a fixed value of coulombic efficiency during the charge and discharge processes instead of the coulombic efficiency definition that depends directly of the state of charge and charge current of the battery bank. The comparative results have shown important differences between both models for system configurations with high renewable rated power and low storage capacity. However, if the capacity of the battery bank is increased, these differences are reduced because the charge currents are reduced, the acceptance of the charge of the battery bank is improved, and the effect of the charge controller is minimized.

A probabilistic analysis was carried out considering a 17.5% error in the determination of the battery bank's lifetime and a 9.5% error in fuel cost as well as the uncertainty related to the wind power potential and photovoltaic generator power production. For a hybrid system configuration with storage capacity of 100Ah, the uncertainty in the net present cost was estimated at about 7%, influenced mainly by the uncertainty in fuel costs. If the battery bank's capacity is increased to 1,000Ah, the uncertainty in the net present cost was estimated at about 28%, influenced jointly by the uncertainties in fuel costs and the battery bank's lifetime. Finally, for a battery bank of 5,000Ah, the uncertainty in the net present cost was estimated at about 20%, influenced mainly by the uncertainty in determining the battery bank's lifetime.

Acknowledgements

This work was supported by the Ministerio de Ciencia e Innovación of the Spanish government under Project ENE2009-14582-C02-01.

References

[1] Lambert T, Gilman P, Lilienthal P. Micropower system modeling with HOMER. In: Farret FA, Simões MG. Integration of alternative sources of energy, John Wiley & Sons, Inc; 2006, p. 379-418.

[2] Bernal-Agustín JL, Dufo-López, R. Efficient design of hybrid renewable energy systems using evolutionary algorithms. Energy Convers and Management 2009;50(3):479-89.

[3] Boonbumroong U, Pratinthong N, Thepa S, Jivacate C, Pridasawas W. Particle swarm optimization for AC-coupling stand alone hybrid power systems. Sol Energy 2011;85(3):560-69.

[4] Belfkira R, Zhang L, Barakat G. Optimal sizing study of hybrid wind/PV/diesel power generation unit. Sol Energy 2011;85(1):100-10.

[5] Kaldellis J, Zafirakis D, Kavadias K, Kondili E. Optimum PV-diesel hybrid systems for remote consumers of the Greek territory. Appl Energy 2012;doi:10.1016/j.apenergy.2011.12.010

[6] Kaplani E, Kaplanis S. A stochastic simulation model for reliable PV system sizing providing for solar radiation fluctuations. Appl Energy 2012;doi:10.1016/j.apenergy.2011.12.016

[7] Távora CCV, Oliveira FD, Alves CDAS, Martins JH, Toledo OM, et al. A stochastic method for stand-alone photovoltaic system sizing. Sol Energy 2010;84(9):1628-36.

[8] Karaki SH, Chedid RB, Ramadan R. Probabilistic production costing of diesel-wind energy conversion systems. IEEE Trans. Energy Convers. 2000;15(3):284-89.

[9] Giannakoudis G, Papadopoulos AI, Seferlis P, Voutetakis S. Optimum design and operation under uncertainty of power systems using renewable energy sources and hydrogen storage. Int J Hydrog Energy 2010;35(3):872-91.

[10] Tan CW, Green TC, Hernandez-Aramburo CA. A stochastic method for battery sizing with uninterruptible-power and demand shift capabilities in PV (photovoltaic) systems. Energy 2010;35(12):5082-92.

[11] Moharil RM, Kulkarni PS. Reliability analysis of solar photovoltaic system using hourly mean radiation data. Sol Energy 2010;84(4):691-702.

[12] Saheb-Koussa D, Haddadi M, Belhamel M. Economic and technical study of hybrid system (wind-photovoltaic-diesel) for rural electrification in Algeria. Appl Energy 2009;86(7-8):1024-30.

[13] Jimenez AC, Olson K. Renewable energy for rural health clinics. U.S. National Renewable Energy Laboratory; 1998.

[14] Lujano-Rojas JM, Dufo-López R, Bernal-Agustín. Optimal sizing of small wind/battery systems considering the DC voltage stability effect on energy capture, wind speed variability, and load uncertainty. Appl Energy 2012;doi:10.1016/j.apenergy.2011.12.035

[15] Lorenzo E, Araujo G., Cuevas A., Egido M. Miñano J., Zilles R. Solar Electricity. Engineering of Photovoltaic Systems. PROGENSA; 1994. p. 316.

[16] Skarstein O, Ulhen K. Design considerations with respect to long-term diesel saving in wind/diesel plants. Wind Engin 1989;13(2):72-87.

[17] Dufo-López R, Bernal-Agustín JL, Yusta-Loyo JM, Domínguez-Navarro JA, Ramírez-Rosado IJ, Lujano J, et al. Multi-objective optimization minimizing cost and life cycle emissions of stand-alone PV-wind-diesel systems with batteries storage. Appl Energy 2011;88(11):4033-41.

[18] Copetti JB, Chenlo F. Lead/acid batteries for photovoltaic applications. Test results and modeling. J Power Sources 1994;47(1-2):109-18.

[19] Copetti JB, Lorenzo E, Chenlo F. A general battery model for PV system simulation. Prog Photovolt 1993;1(4):283-92.

[20] Corbus D, Newcomb C, Baring-Gould EI, Friedly S. Battery voltage stability effects on small wind turbine energy capture. U.S. National Renewable Energy Laboratory; 2002.

[21] Bindner H, Cronin T, Lundsager P, Manwell JF, Abdulwahid U, Baring-Gould I. Lifetime modelling of lead acid batteries. Denmark National Laboratory Risø, 2005.

[22] Graham VA, Hollands KGT. A method to generate synthetic hourly solar radiation globally. Sol Energy 1990;44(6):333-41.

[23] Kamal L, Jafri YZ. Stochastic modeling and generation of synthetic sequences of hourly global solar irradiation at Quetta, Pakistan. Renew Energy 1999;18(4):565-72.

[24] Thevenard D, Pelland S. Estimating the uncertainty in long-term photovoltaic yield predictions. Sol Energy 2011; doi:10.1016/j.solener.2011.05.006

[25] Kamal L, Jafri YZ. Time series models to simulate and forecast hourly averaged wind speed in Quetta, Pakistan. Sol Energy 1997;61(1):23-32.

[26] Nfaoui H, Buret J, Sayigh AAM. Stochastic simulation of hourly average wind speed sequences in Tangiers (Morocco). Sol Energy 1996;56(3):301-14.

[27] Brown BG, Katz RW, Murphy AH. Time series models to simulate and forecast wind speed and wind power. J Clim and Appl Meteorol 1984;23(8):1184-95.

[28] Rosenblatt M. Remarks on a multivariate transformation. Ann Mathematical Stat 1952;23(3):470-2.

[29] Agencia Estatal de Meteorología (Meteorological Agency). http://www.aemet.es

[30] Atmospheric Science Data Center. http://eosweb.larc.nasa.gov/sse/RETScreen/

[31] Yang H, Wei Z, Chengzhi. Optimal design and techno-economic analysis of a hybrid solar-wind power generation system. Appl Energy 2009;86(2):163-69.

[32] Corporation of Strategic Reserves of Oil-based products. http://www.cores.es/

Forecast of Hourly Average Wind Speed Using ARMA Model with Discrete Probability Transformation

Juan M. Lujano-Rojas, José L. Bernal-Agustín, Rodolfo Dufo-López, and José A. Domínguez-Navarro

Department of Electrical Engineering, University of Zaragoza,
Calle María de Luna 3, 50018, Spain
lujano.juan@gmail.com,
{jlbernal,rdufo,jadona}@unizar.es

Abstract. In this paper the methodology for wind speed forecasting with ARMA model is revised. The transformation, standardization, estimation and diagnostic checking processes are analyzed and a discrete probability transformation is introduced. Using time series historical data of three weather stations of the Royal Netherlands Meteorological Institute, the forecasting accuracy is evaluated for prediction intervals between 1 and 10 hours ahead and compared with artificial neural network training by back-propagation algorithm (BP-ANN). The results show that for the wind speed time series under study, in certain cases the ARMA model with discrete probability transformation can improve the BP-ANN at least 17.71%.

Keywords: Wind Speed Forecasting, Autoregressive Moving Average Model (ARMA), Artificial Neural Network.

1 Introduction

Wind speed and power predictions are important aspects for the wholesale energy market, wind farm owners and power system operators [1]. The autoregressive moving average model (ARMA) is a conventional statistical method for wind speed prediction that is based on analyzing historical data. This model frequently achieves accurate results in short-term prediction [2]. Brown [3] proposed a general model that considers the non-Gaussian shape of the probability distribution function (PDF), the diurnal non-stationarity and the autocorrelation of wind speed. This model is used by Daniel and Chen [4] for evaluating the forecasting accuracy of wind speed in Jamaica. Torres et al. [5] compared the forecasting accuracy between the ARMA and persistence models using time series data of five weather stations in Spain for prediction intervals between 1 and 10 hours ahead. The results show that for an interval prediction of 1 hour in advance the ARMA model improved the persistence model from 2–5% and, for an interval of 10 hours, 12–20%. In [6-8], comparative studies between ARMA and artificial neural network (ANN) models are shown. However, the ARMA models used in these studies do not consider the non-Gaussian shape of the PDF. This must be considered because the PDF of wind speed time series follows

M. Zhu (Ed.): Electrical Engineering and Control, LNEE 98, pp. 1003–1010.
springerlink.com

a Weibull distribution, making the direct application of stochastic models difficult for its analysis [9]. Reference [10] presents a comparative analysis of three types of ANN for forecasts 1 hour ahead, concluding that the most suitable ANN depends on the time series under study and the index error used to evaluate the forecasting accuracy.

In this paper, the methodology for wind speed forecasting with the ARMA model is revised. The transformation, standardization, estimation and diagnostic checking processes are analyzed and a Discrete Probability Transformation (DPT) is introduced. The forecasting error is evaluated for prediction intervals between 1 and 10 hours ahead using hourly average wind speed data of three weather stations in Netherlands. The ARMA model with discrete probability transformation (ARMA+DPT) is compared with an ANN training with back-propagation algorithm (BP-ANN).

2 Materials and Methods

The hourly average wind speed time series of weather stations Volkel (January 2007, 2008 and 2009), K13 (February 2007, 2008 and 2009) and Valkenburg (March 2007, 2008 and 2009) are used to fit the ARMA model (2007 and 2008 for each station) and evaluate the forecasting error (2009 for each station). These time series are provided by the Royal Netherlands Meteorological Institute [11].

2.1 ARMA Model

The mathematical formulation of the autoregressive moving average (ARMA) model is:

$$\hat{W}_{(t)} = \varphi_1 \hat{W}_{(t-1)} + \ldots + \varphi_p \hat{W}_{(t-p)} + a_{(t)} - \theta_1 \varepsilon_{(t-1)} - \ldots - \theta_q \varepsilon_{(t-q)} \quad (1)$$

Where $\hat{W}_{(t)}$ is the transformed and standardized wind speed of hour t, $\varphi_1,\ldots,\varphi_p$ are the autoregressive parameters, $\theta_1,\ldots,\theta_q$ are the moving average parameters, $\varepsilon_{(t)}$, $\varepsilon_{(t-1)},\ldots,$ $\varepsilon_{(-qt)}$ are random variables with an average value of zero and a standard deviation of σ. The fit of the ARMA model to the wind speed time series of interest requires the transformation, standardization, estimation and diagnostic checking processes.

2.1.1 Transformation and Standardization

The Weibull PDF is frequently used in the time series analysis. In order to analyze a determined wind speed time series it is necessary to transform the series to another one that has a Gaussian PDF. This transformation is [3]:

$$U_{T(t)} = U_{(t)}^{\ m} \text{ with } t = 1,\ldots,n \quad (2)$$

Where $U_{(t)}$ is the wind speed time series of interest, $U_{T(t)}$ is the transformed wind speed time series with Gaussian PDF, m is the power transformation and n is the number of hourly wind speed observations. The power transformation m is calculated from Weibull shape k. Dubey (1967) [12] showed that for shape factors between 3.26 and 3.60, the Weibull PDF is similar to the Gaussian PDF, thus the power

transformation of equation (2) with m between k/3.60 and k/3.26 adequately describes the Gaussian PDF. The selected value of this range is m value, for which the coefficient of skewness (SK) is closest to zero. The coefficient of skewness is calculated by equation (3) [13].

$$SK = \frac{Q_3 + Q_1 - 2Q_2}{Q_3 - Q_1} \tag{3}$$

Where $Q_1=C^{-1}(0.25)$, $Q_2=C^{-1}(0.5)$ and $Q_3=C^{-1}(0.75)$ are the first, second and third quartiles, respectively. $C^{-1}(.)$ is the inverse of the Cumulative Distribution Function (CDF) calculated by the algorithm of the Fig. 3 (Section 2.1.4).

The transformed wind speed time series is not stationary. In order to be stationary it is necessary to subtract the hourly average and divide per the hourly standard deviations. If $\mu_h(h)$ and $\sigma_h(h)$ with h=1,2,…, 24 are the hourly average and standard deviation of transformed wind speed series, respectively, it is assumed that these functions are periodic: $\mu_h(t=25)=\mu_h(h=1)$ and $\sigma_h(t=25)=\sigma_h(h=1)$ [3]. The transformed and standardized series ($W_{(t)}$) is:

$$W_{(t)} = \frac{U_{T(t)} - \mu_{h(t)}}{\sigma_{h(t)}} \tag{4}$$

2.1.2 Estimation

The plots of autocorrelation function (ACF) and partial autocorrelation function (PACF) of the series of Equation (4) have useful information to determine the value of order p and q of the ARMA model [14].

Others approach for selecting the p and q values are Bayesian Information Criterion (BIC) [15] and Akaike Information Criterion (AIC) [16]. The optimal value of p and q are selected minimizing the respective criterion BIC or AIC of the equations (5) and (6), respectively.

$$BIC(p,q) = n\log(\sigma_{(p,q)}{}^2) + (p+q)\log(n) \tag{5}$$

$$AIC(p,q) = n\log(\sigma_{(p,q)}{}^2) + 2(p+q) \tag{6}$$

$$\sigma_{(p,q)}{}^2 = \frac{\sum_{t=1}^{n}(W_{(t)} - \hat{W}_{(t)})^2}{n-(p+q)} \tag{7}$$

Where $\sigma_{(p,q)}{}^2$ is the variance of the residual, $\hat{W}_{(t)}$ is the value calculated by the ARMA model. The autoregressive and moving average parameters are calculated by minimization of the quadratic prediction error criterion [17].

2.1.3 Diagnostic Checking

The statistical checking is made by the Ljung-Box test [18]. In this test the statistical S is compared with the chi-square distribution χ_α^2 with L-p-q degrees of freedom. If $\chi_\alpha^2 > S$ then the model is adequate for the significance level α. The statistical S is calculated by Equation (8).

$$S = n(n+2)\sum_{\Omega=1}^{L}\frac{r_\Omega^{\,2}}{(n-\Omega)} \tag{8}$$

Where L is a number of lags considered and r_Ω is the correlation coefficient of the residuals corresponding to lag Ω.

2.1.4 Forecasting with ARMA Model

The forecasting process starts by evaluating expressions (9) and (10).

$$\hat{W}_{(t+l)} = \varphi_1 W_{(t-1+l)} + \ldots + \varphi_p W_{(t-p+l)} + \varepsilon_{(t+l)} - \theta_1 \varepsilon_{(t-1+l)} - \ldots - \theta_q \varepsilon_{(t-q+l)} \tag{9}$$

$$\hat{U}_{T(t+l)} = \mu_{h(t+l)} + \sigma_{h(t+l)} \hat{W}_{(t+l)} \tag{10}$$

Where l=1,…,hrp, hrp are the hours ahead of forecasting. An important fact is that the values of equation (10) can be negative, so depending of the m value, undoing the transformation process using the power $1/m$ is difficult. For this reason, in this paper the undoing of the transformation process is made with the probability transformation in the discrete form. Using this transformation process, the PDF of the equation (10) will be the PDF of the original wind speed time series. This probability trans-formation is based in Equation (11) [19] and the forecasting values $\hat{U}_{(t+l)}$ are calcula-ted by Equation (12).

$$C(\hat{U}_{(t+l)}) = u_{(t+l)} = \hat{C}_T(\hat{U}_{T(t+l)}) \tag{11}$$

$$\hat{U}_{(t+l)} = C^{-1}(\hat{C}_T(\hat{U}_{T(t+l)})) \tag{12}$$

Where C is the CDF in discrete form of the original wind speed time series $U_{(t)}$, $\hat{C}_T$ is the CDF of Equation (10), assuming a Gaussian CDF with average and standard deviation equal to the transformed time series and $u_{(t+l)}$ is a variable with uniform density function in [0,1]. Once $u_{(t+l)}$ is calculated with Equation (11), it is necessary to calculate the value of $\hat{U}_{(t+l)}=C^{-1}(u_{(t+l)})$. The first step is to build the vector $\boldsymbol{x}$, whose elements are zero until $ceil(\max(U_{(t)}))$ with t=1,2,…,n in step Δx. The next step is to build the vector $\boldsymbol{C}$, whose elements are the cumulative probabilities of each element of vector $\boldsymbol{x}$. Finally, the forecasted value of wind speed $\hat{U}_{(t+l)}$ is calculated by the algorithm of Figure 1. The function $size(\boldsymbol{C})$ calculates the number of rows of vector $\boldsymbol{C}$.

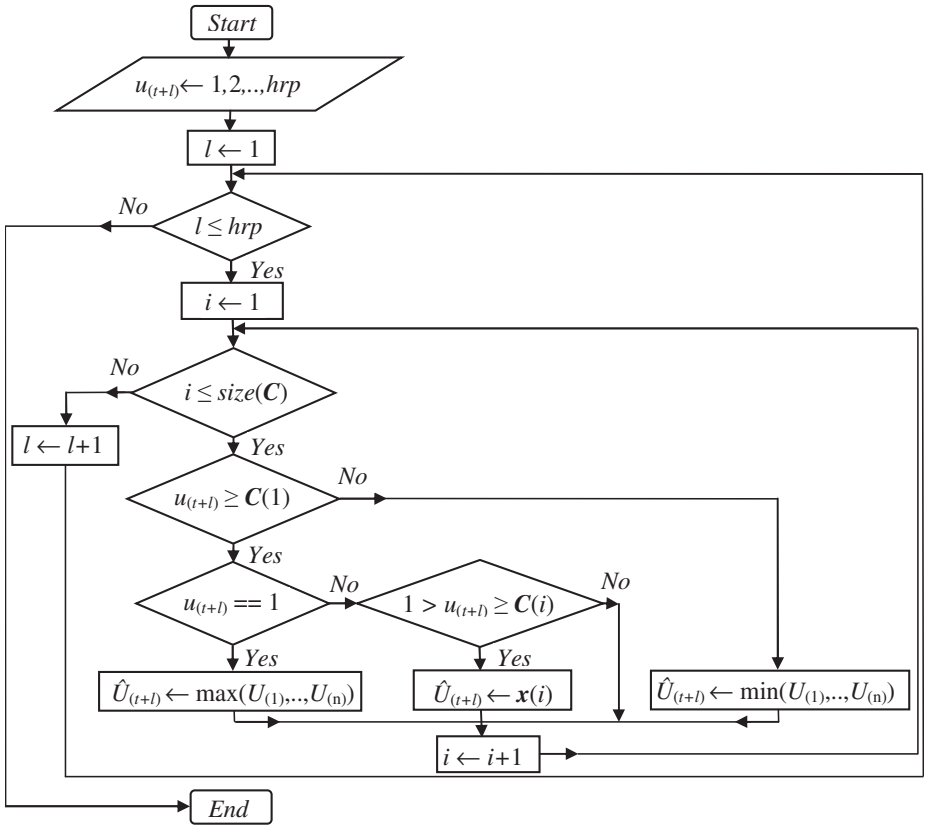

Fig. 1. Algorithm to calculate the inverse of the CDF in discrete form.

2.1.5 BP-ANN Model

The artificial neural network training by back-propagation algorithm (BP-ANN) used for hourly average wind speed forecasting is shown in Fig. 2.

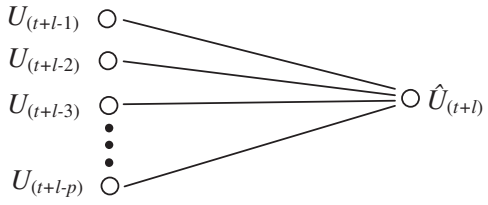

Fig. 2. Artificial neural network for wind speed forecasting.

The data used for training the artificial neural network is scaled between 0.1 and 0.9 to avoid the saturation regions of the sigmoid function.

3 Results

A program in MATLAB has been developed to fit the ARMA model with discrete probability transformation (ARMA+DPT) and BP-ANN to the wind speed time series of January, February and March of 2007 and 2008 for the Volkel, K13 and Valkenburg stations, respectively. The 2009 data for each station and month combination were used to evaluate the forecasting error. The results of transformation, standardization, estimation and diagnostic checking processes are summarized in Table 1. In tables 2, 3 and 4, the comparison among forecasting errors indices is shown: mean bias error (MBE), root mean square error (RMSE), mean absolute bias error (MABE) and correlation coefficient (R).

4 Conclusion

In this paper, the methodology for wind speed prediction with the ARMA model is carefully reviewed. The transformation, standardization, estimation and diagnostic checking processes are analyzed and a discrete probability transformation is introduced for undoing the transformation process necessary to calculate the autoregressive and moving average parameters of the ARMA model. This model was used as a prediction tool and has been compared with the artificial neural network training by the back-propagation algorithm. According to the results shown in the Tables 2, 3 and 4, the ARMA+DPT model present in average RMSE errors between 0.90 and 1.89 m/s and MABE errors between 0.63 and 1.39 m/s, while the BP-ANN model present higher average RMSE errors, between 0.95 and 2.05 m/s and higher average MABE errors, between 0.72 and 1.56 m/s for intervals prediction between 1 and 10 hours ahead, respectively. Figures 17, 18 and 19 show that the ARMA+DPT in certain cases can improve the BP-ANN by as much as 17.71%; however, in other cases the BP-ANN error can be 0.9% smaller than the ARMA+DPT model.

Table 1. Parameters of ARMA+DPT model for each station.

Parameter/Station	Volkel	K13	Valkenburg
(p,q)	(2,0)	(5,0)	(7,0)
L-p-q	147	132	142
$\chi_{0.05}^2$	176.2938	159.8135	170.8092
S	143.1374	137.8389	154.9721
m	0.7162	0.6899	0.6269
φ_1	0.9014	1.0225	0.9210
φ_2	0.0487	0.0150	0.0173
φ_3	-----	0.0024	0.0359
φ_4	-----	-0.0480	-0.0210
φ_5	-----	-0.0211	-0.0295
φ_6	-----	-----	0.0438
φ_7	-----	-----	-0.0174
k	2.3353	2.25	2.0436
Criterion	AIC	AIC	AIC
Δx		0.0001	

Table 2. Forecasting errors (Volkel).

$l(h)$	Volkel					
	BP-ANN			ARMA+DPT		
	RMSE	MABE	R	RMSE	MABE	R
1	0.9750	0.7123	0.9142	0.8691	0.5714	0.9241
2	1.1982	0.8692	0.8656	1.0547	0.7097	0.8879
3	1.3531	0.9805	0.8243	1.1596	0.7828	0.8632
4	1.4959	1.0858	0.7825	1.2793	0.8751	0.8326
5	1.6316	1.1950	0.7364	1.3899	0.9382	0.8024
6	1.7451	1.2642	0.6930	1.4960	1.0168	0.7698
7	1.8598	1.3561	0.6431	1.5865	1.0750	0.7419
8	1.9457	1.4107	0.6137	1.6018	1.1096	0.7431
9	2.0668	1.5201	0.5407	1.7507	1.2042	0.6842
10	2.1068	1.5652	0.4943	1.8121	1.2774	0.6492

Table 3. Forecasting errors (K13).

$l(h)$	K13					
	BP-ANN			ARMA+DPT		
	RMSE	MABE	R	RMSE	MABE	R
1	0.8802	0.6747	0.9671	0.8789	0.5989	0.9674
2	1.0489	0.7972	0.9528	1.0705	0.7533	0.9515
3	1.2238	0.9270	0.9353	1.2795	0.9069	0.9313
4	1.3589	1.0109	0.9195	1.4179	1.0146	0.9146
5	1.4839	1.1252	0.9044	1.5478	1.1445	0.8999
6	1.6193	1.2432	0.8838	1.6471	1.2304	0.8823
7	1.8601	1.3519	0.8483	1.9063	1.3775	0.8457
8	1.8986	1.4056	0.8421	1.9441	1.4217	0.8420
9	2.0141	1.5466	0.8232	1.9005	1.4359	0.8458
10	1.9873	1.4650	0.8234	2.0244	1.5064	0.8214

Table 4. Forecasting errors (Valkenburg).

$l(h)$	Valkenburg					
	BP-ANN			ARMA+DPT		
	RMSE	MABE	R	RMSE	MABE	R
1	1.0081	0.7779	0.9380	0.9521	0.7048	0.9449
2	1.1910	0.9330	0.9128	1.0935	0.8157	0.9256
3	1.3945	1.0750	0.8765	1.2158	0.9056	0.9086
4	1.5402	1.2119	0.8467	1.3302	1.0016	0.8877
5	1.6996	1.3384	0.8080	1.4590	1.1203	0.8639
6	1.8082	1.4060	0.7793	1.5904	1.1965	0.8389
7	1.9382	1.5316	0.7404	1.6971	1.2914	0.8112
8	2.0466	1.6378	0.7042	1.7202	1.3218	0.8067
9	2.0129	1.6190	0.7154	1.7490	1.3378	0.7979
10	2.0649	1.6530	0.6967	1.8301	1.3936	0.7748

Acknowledgments

This work was supported by the "Ministerio de Ciencia e Innovación" of the Spanish Government under Project ENE2009-14582-C02-01.

References

1. Barthelmie, R.J., Murray, F., Pryor, S.C.: The economic benefit of short-term forecasting for wind energy in the UK electricity market. Energy Policy 36, 1687–1696 (2008)
2. Lei, M., Shiyan, L., Chuanwen, J., Hongling, L., Yan, Z.: A review on the forecasting of wind speed and generated power. Renewable and Sustainable Energy Reviews 13, 915–920 (2009)
3. Brown, B.G.: Time series models to simulate and forecast wind speed and wind power. Journal of Climate and Applied Meteorology 23, 1184–1195 (1984)
4. Daniel, A.R., Chen, A.A.: Stochastic simulation and forecasting of hourly average wind speed sequences in Jamaica. Solar Energy 33, 571–579 (1991)
5. Torres, J.L., García, A., De Blas, M., De Francisco, A.: Forecast of hourly average wind speed with ARMA models in Navarre (Spain). Solar Energy 79, 65–77 (2005)
6. Sfetsos, A.A.: A comparison of various forecasting techniques applied to mean hourly wind speed time series. Renewable Energy 21, 23–35 (2000)
7. Cadenas, E., Rivera, W.: Wind speed forecasting in the south coast of Oaxaca, México. Renewable Energy 32, 2116–2128 (2007)
8. Palomares-Salas, J.C., De la Rosa, J.J.G., Ramiro, J.G., Melgar, J., Agüera, A., Moreno, A.: ARIMA vs. Neural Networks for wind speed forecasting. In: IEEE International Conference on Computational Intelligence for Measurement Systems and Applications, pp. 129–133. IEEE Computer Society Press, Los Alamitos (2009)
9. Nfaoui, H., Buret, J., Sayigh, A.A.M.: Stochastic simulation of hourly average wind speed sequences in Tangiers (Morocco). Solar Energy 56, 301–314 (1996)
10. Gong, L., Jing, S.: On comparing three artificial neural networks for wind forecasting. Applied Energy 87, 2313–2320 (2010)
11. Royal Netherlands Meteorological Institute, `http://www.knmi.nl/`
12. Dubey, S.D.: Normal and Weibull distributions. Naval Research Logistics Quarterly 14, 69–79 (1967)
13. Kim, T.H., White, H.: On more robust estimation of skewness and kurtosis. Finance Research Letters 1, 56–73 (2004)
14. Box, J.E.P., Jenkins, G.M.: Time series analysis: forecasting and control. Prentice-Hall, Inc., Englewood Cliffs (1976)
15. Schwarz, G.: Estimating the dimension of a model. The Annals of Statistics 6, 461–464 (1978)
16. Akaike, H.: A new look at the statistical model identification. IEEE Transactions on Automatic Control 19, 716–723 (1974)
17. Ljung, L.: System Identification. Theory for the user. PTRInformation and System Sciences Series. Prentice-Hall, Englewood Cliffs (1999)
18. Ljung, G.M., Box, G.E.P.: On a measure of lack of fit in time series models. Biometrika 65, 297–303 (1978)
19. Rosenblatt, M.: Remarks on a multivariate transformation. Annals of Mathematical Statistics 23, 470–472 (1952)
20. Rojas, R.: Neural Networks. Springer, Berlin (1996)

Renewable Energy 44 (2012) 288–295

Contents lists available at SciVerse ScienceDirect

Renewable Energy

journal homepage: www.elsevier.com/locate/renene

Optimum load management strategy for wind/diesel/battery hybrid power systems

Juan M. Lujano-Rojas [a], Cláudio Monteiro [b,c], Rodolfo Dufo-López [a], José L. Bernal-Agustín [a,*]

[a] Department of Electrical Engineering, University of Zaragoza, 50018 Zaragoza, Spain
[b] FEUP, Fac. Engenharia Univ. Porto, Portugal
[c] INESC – Instituto de Engenharia de Sistemas e Computadores do Porto, Porto, Portugal

ARTICLE INFO

Article history:
Received 4 August 2011
Accepted 25 January 2012
Available online 8 February 2012

Keywords:
Load management strategy
Hybrid system
Controllable loads

ABSTRACT

This paper discusses a novel load management strategy for the optimal use of renewable energy in systems with wind turbines, a battery bank, and a diesel generator. Using predictions concerning wind speed and power, controllable loads are used to minimize the energy supplied by the diesel generator and battery bank, subject to constraints imposed by the user's behavior and duty cycle of the appliances. We analyzed a small hybrid power system in Zaragoza, Spain, and the results showed load management strategy allowed improvement in the wind power use by shifting controllable loads to wind power peaks, increasing the state of the charge in the battery bank, and reducing the diesel generator operating time, when compared to a case without load management.

1. Introduction

Management of hybrid power systems has two important components: a strategy for controlling energy sources and load management. In an important study, Barley and Winn [1] proposed the following general control strategies for systems with renewable energy sources, a diesel generator and a battery bank: the frugal dispatch strategy, the load following strategy, the state of charge (SOC) setpoint strategy, and the full power/minimum run time (FPMRT) strategy. In the frugal dispatch strategy, the intersection of the diesel energy cost curve with the battery wear cost line determines a critical load. If the net load (the difference between load and power from renewable sources) is higher than the critical load, the diesel generator is used; otherwise, the batteries are discharged. In the load following strategy, the diesel generator runs to match the instantaneous net load and never charges the batteries. In the state of charge (SOC) setpoint strategy, the diesel generator operates at full power until the SOC reaches the setpoint previously arranged. In the FPMRT strategy, the diesel generator operates for a predetermined length of time, charging the batteries with the excess energy, and then is disconnected. The authors used the predictive dispatch strategy as a benchmark for evaluating these strategies and found the actual use of the diesel generator and the battery bank depended on the critical load value in the future.

Ashari and Nayar [2] developed a control strategy for systems with renewable energy sources, diesel generators, and battery banks that uses power demand, battery bank voltage, and minimum power of a diesel generator to decide when to charge or discharge the battery bank and start or stop the diesel generator, i.e., the optimal strategy operation is searched, determining the load setpoint to start and stop the diesel generator and the SOC setpoint to charge the battery bank.

More recently, Dufo-López and Bernal-Agustín [3] analyzed combining the load following strategy and the state of charge set-point strategy proposed, by Barley and Winn [1], in photovoltaic systems combined with other sources of energy. They found that if the net load is lower than the critical load, the state of charge setpoint strategy should be applied; otherwise, the load following strategy should be applied.

Yamamoto et al. [4] proposed a predictive control method for systems with photovoltaic panels, diesel generators, and battery bank. Their strategy used the forecast of photovoltaic production and an hourly load profile to decide on the diesel generator output power. If the SOC of the battery bank was between 0.5 and 0.7, the diesel generator started and, when the SOC was higher than 0.7, the diesel generator stopped.

Concerning load management, Groumpos et al. [5] did the first work in stand-alone photovoltaic systems with a system located in the village of Schuchuli, Arizona (USA). In this system, four load

* Corresponding author. Tel.: +34 976761921; fax: +34 762226.
E-mail address: jlbernal@unizar.es (J.L. Bernal-Agustín).

0960-1481/$ – see front matter © 2012 Elsevier Ltd. All rights reserved.
doi:10.1016/j.renene.2012.01.097

priorities and four SOC setpoints (0.5, 0.4, 0.3 and 0.2) were established. For example, if the battery bank was discharging and the SOC setpoints values were sequentially reached, the loads were disconnected beginning with the lowest priority. Otherwise, if the battery bank was charging and the SOC setpoints values were sequentially reached, the loads were reconnected. The same authors, Groumps and Papegeorgiou, proposed in [6] an optimal load management technique for a stand-alone photovoltaic system based on three major categories of load classifications: an operational classification (DC and AC loads), a system classification (uncontrollable, controllable, and semi-controllable loads), and a priority classification (useful, essential, critical, and emergency loads). In this method, using the controllable load, the general load curve is manipulated to minimize the integral of the square of the net load over a 24-h period in order to reduce the required battery bank capacity and total life cycle costs.

Khouzam and Khouzam [7] developed a methodology for load management in stand-alone photovoltaic systems wherein the loads were classified into four general categories according to their priorities: convenient, essential, critical, and emergency; the priority of the battery bank was variable and dependent on the SOC. The optimal management was based on the maximization of an objective function that depended on the load priorities and was subject to the availability of an energy supply.

In another study, Moreno et al. [8] implemented a fuzzy controller to be applied to load management in stand-alone photovoltaic systems. The variable considered was supply expectancy predicted 1 h ahead in order to decide in real time whether to connect or disconnect the load according to its priority. Salah et al. [9] proposed a load management method for a domestic grid-connected photovoltaic system without batteries. In this approach, the photovoltaic generator was considered a complementary source of energy. This technique uses the fuzzy logic controller to decide in real time which appliance must be connected, the photovoltaic panel or the electric grid. The decision is made after considering photovoltaic and operating power, the priority of the appliances, and the maximum time the appliances are connected to the photovoltaic generator. This approach allows continuous energy savings. Ammar et al. [10] proposed a methodology for daily optimum management of a household photovoltaic system connected to the electrical grid without a battery bank. This approach uses predictions concerning photovoltaic generator production the next day to plan the connection times of appliances to the photovoltaic generator. The decision is made considering the duty cycle for each appliance. Similar criteria were used by Salah et al. in [9]. Finally, Thiaux et al. [11] analyzed the influence of the load profile shape on the energy cost of the life cycle of stand-alone photovoltaic systems. Their results showed the gross energy requirements are minimized when the load and photovoltaic production profiles are similar.

According to these papers, renewable power sources forecasting, control strategies for power sources, and load management are important in reducing the life cycle cost of a determined stand-alone hybrid power system. In this paper, we describe a novel load management strategy developed for the optimal use of renewable energy in systems with wind turbines, a battery bank, and a diesel generator.

This paper is organized as follows. In section 2, we provide a description of the wind/diesel/battery hybrid power system model. In section 3, we explain the prediction of the hourly average wind speed with the ARMA model. In section 4, we carefully detail the proposed load management strategy. We illustrate the load management strategy with a case study described in section 5, and we draw conclusions in the final section of the paper.

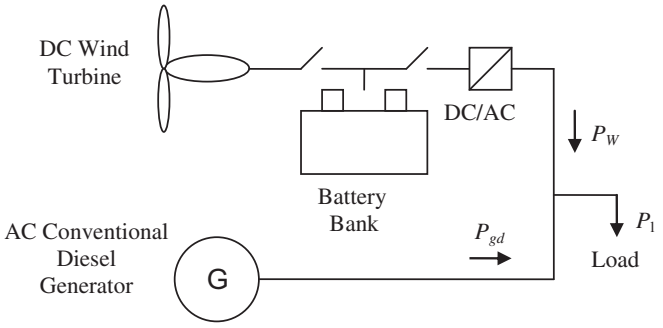

Fig. 1. AC coupled hybrid power system.

2. Wind/diesel/battery hybrid power system model

The system under study is the AC coupled hybrid power system [12] shown in Fig. 1. In this system, the small capacity wind turbine and the battery bank are coupled through a power inverter to an AC bus. The next sections describe the mathematical models for each component of the system.

2.1. Small capacity wind turbine model

The typical power curve of a small capacity wind turbine with horizontal axes is shown in Fig. 2; this curve can be obtained using data in discrete form frequently provided by the manufacturer. In this type of wind turbine, the start-up wind speed is between 3 and 4 m/s, and the rated power is reached for wind speeds between 14 and 15 m/s. When the wind speed is higher than 14 or 18 m/s, the power production falls to between 30 and 70% of the rated power [13].

2.2. Lead acid battery bank and charge controller model

Coppeti and Chenlo [14] proposed that a lead acid battery model is able to adequately represent the complex behavior of the charge and discharge processes in the battery [15]; however, their mathematical formulation was very complex because it needed to solve a nonlinear equations system for each hour of simulation. Therefore, for the purposes of this paper, we simplified this model, which is normalized with respect to the total ampere-hours that may be charged or discharged in 10 h at 25 °C (C_{10} capacity), and it considers the low current operation and temperature effects of the battery capacity. Equations (1) and (2) show the capacity equation [14].

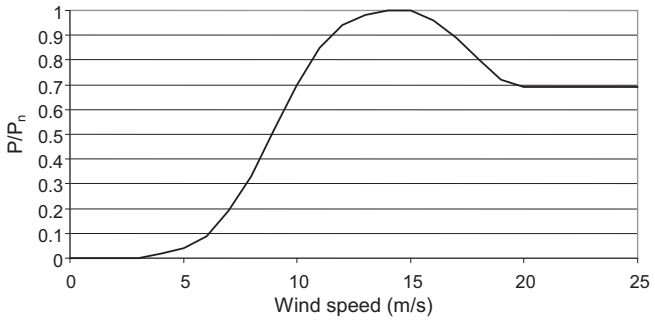

Fig. 2. Typical power curve of small wind turbine.

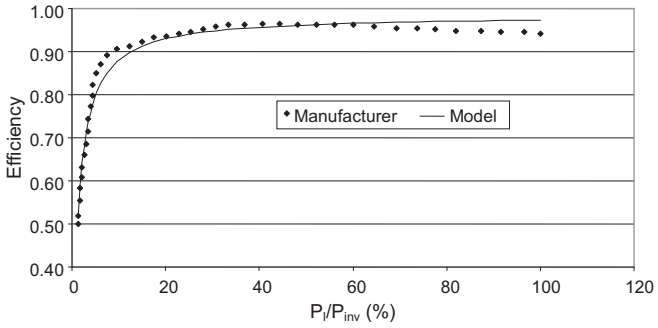

Fig. 3. Typical inverter efficiency curve.

$$C_T = 1.67C_{10}(1 + 0.005\Delta T_a) \tag{1}$$

$$C = \frac{C_T}{1 + 0.67\left(\frac{I}{I_{10}}\right)^{0.9}} \tag{2}$$

where $\Delta T_a = T_a - 25$ is the temperature variation from the reference of 25 °C, and T_a is the ambient temperature in °C, C_T is the maximum capacity of the battery (Ah), and C is the ampere-hours capacity at the charge or discharge constant current I (A).

During the charge process ($I > 0$), the coulombic efficiency is defined as the ratio of the number of coulombs that effectively have been stored in the battery to the number of coulombs supplied to the battery; in contrast, during the discharge process ($I < 0$), the coulombic efficiency is defined as the ratio of the number of coulombs that can be discharged from the battery to the number of coulombs initially stored in it. The coulombic efficiency (η_b) during the discharge and charge process is calculated using equation (3) [16].

$$\eta_b = \begin{cases} 1 - \exp\left[\left(\frac{20.73}{I/I_{10} + 0.55}\right)(SOC - 1)\right] & I>0 \\ 1 & I < 0 \end{cases} \tag{3}$$

where I_{10} (A) is the charge or discharge current in 10 h at 25 °C. The state of charge (SOC) of the battery (value between 0 and 1) is calculated using equation (4).

$$SOC = \begin{cases} \frac{Q}{C}\eta_b & I>0 \\ 1 - \frac{Q}{C}\eta_b & I < 0 \end{cases} \tag{4}$$

where $Q = |I|t_b$ (Ah) is the charge supplied by the battery (discharge) or to the battery (charge) during a particular time t_b (h). An important factor in the operation of the hybrid power system using lead acid batteries is the effect of voltage stability on energy capture. This is important because high charge currents produce a DC bus with high voltage, and the charge controller disconnects the wind turbine before the battery bank is completely charged [17], so it is necessary to consider the charge controller in the hybrid system model, although it is not considered in most of the models used to simulate and optimize this kind of system. Considering the joint effect of ambient temperature, coulombic efficiency, and charge controller operation allows a high degree of accuracy in the simulation of the system.

The battery voltage at which the charge controller disconnects the wind turbine is between 2.40 and 2.55 V per cell [18] and, during this process, the battery voltage per cell (V) may be approximated by equation (5) [14].

$$V = \left(2 + 0.16\frac{Q}{C}\right) + \frac{I}{C_{10}}\left(\frac{6}{1 + I^{0.6}} + \frac{0.48}{(1 - Q/C_T)^{1.2}} + 0.036\right) \times (1 - 0.025\Delta T_a) \tag{5}$$

For example, if the charge controller setpoint is 2.50 V per cell, the equation (5) allows one to estimate the Q value at which the

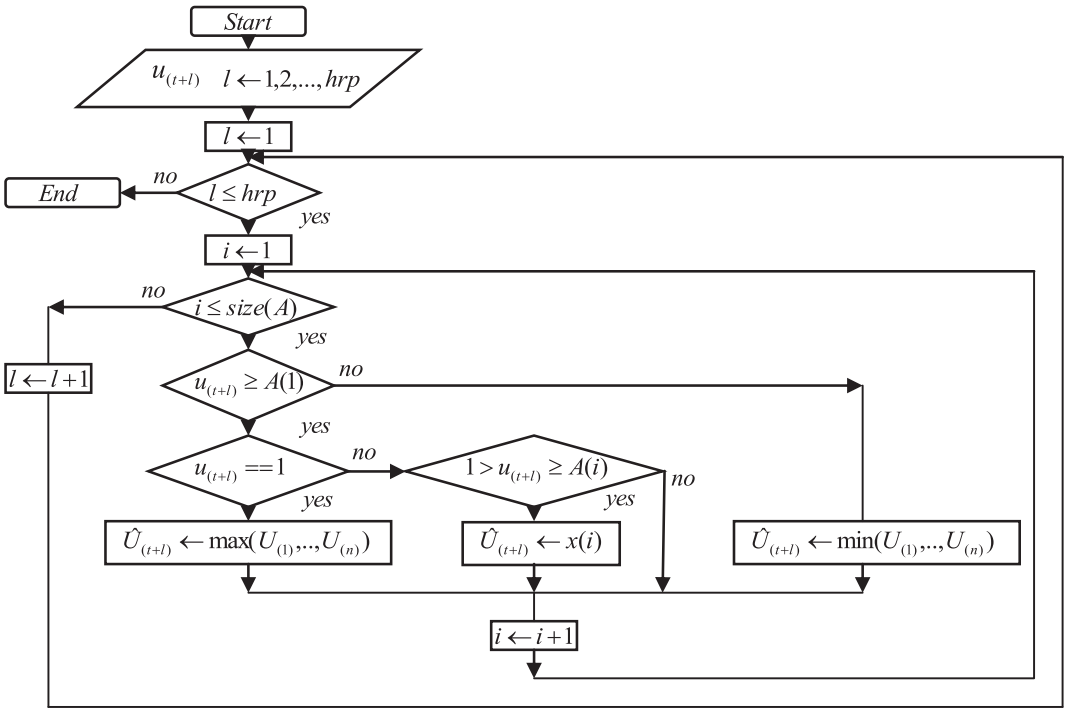

Fig. 4. Algorithm to calculate the inverse of the CDF in discrete form.

battery voltage is 2.50 V per cell and, therefore, the moment at which the charge controller disconnects the wind generator, (the state of charge of the battery bank limited at this value). During the discharge process, when the state of charge is equal to the minimum value specified by the battery manufacturer, the charge controller disconnects the load of the battery bank to prevent over-discharge.

2.3. Inverter model

The inverter is modeled by its efficiency (η_i) calculated by equation (6).

$$\eta_i = \frac{P_l}{k_0 P_{inv} + (1 + k_1) P_l} \tag{6}$$

where P_l is the load in the AC bus, P_{inv} is the rated power of the inverter, and k_0 and k_1 are parameters determined from the data supplied by the manufacturer. Fig. 3 shows the efficiency curve of a typical power inverter with $k_0 = 0.0119$ and $k_1 = 0.0155$. An important consideration is that the efficiency drops when the load is lower than 10% of the rated power.

2.4. Diesel generator model

The fuel consumption of the diesel generator, F_l (1), is calculated using equation (7).

$$F_l = k_2 P_{gdn} + k_3 P_{gd} \tag{7}$$

where P_{gdn} (kW) is the rated power of the diesel generator, P_{gd} (kW) is the power generated at the time of interest, and k_2 and k_3 are parameters determined from the data supplied by the manufacturer (the typical values for these parameters are $k_2 = 0.085$ l/kWh and $k_3 = 0.246$ l/kWh [19]).

3. Hourly wind speed prediction method

Hourly average wind speed forecasting using only the time series is typically made with an autoregressive moving average (ARMA) model. The methodology to fit the ARMA model was presented in [20] and will be briefly explained in the next sections.

3.1. ARMA model

The autoregressive moving average (ARMA) model is:

$$\hat{W}_{(t)} = \phi_1 \hat{W}_{(t-1)} + \ldots + \phi_p \hat{W}_{(t-p)} + \varepsilon_{(t)} - \theta_1 \varepsilon_{(t-1)} - \ldots - \theta_q \varepsilon_{(t-q)} \tag{8}$$

where $\hat{W}_{(t)}$ is the transformed and standardized wind speed time series, $\phi_1,\ldots, \phi_p$ are the autoregressive parameters, $\theta_1,\ldots, \theta_q$ are the moving average parameters, and $\varepsilon_{(t)}$, $\varepsilon_{(t-1)},\ldots$, $\varepsilon_{(t-q)}$ are random variables with a mean of zero and a standard deviation of σ. Calculation of autoregressive and moving average parameters requires transformation, standardization, estimation, and diagnostic checking processes.

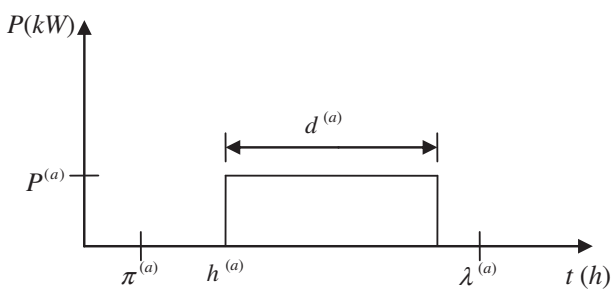

Fig. 5. Idealized load profile of appliance *a*.

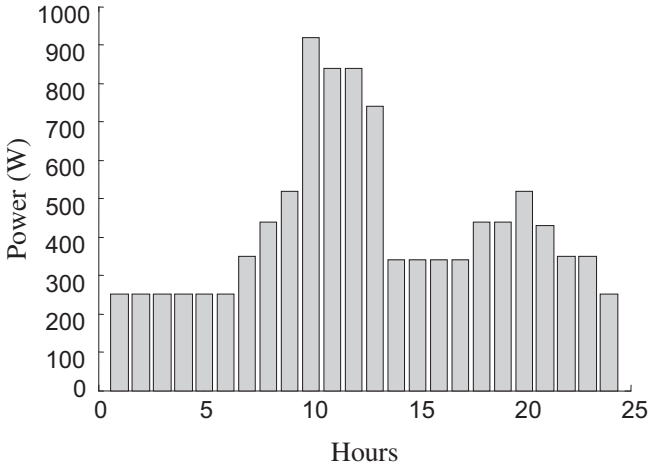

Fig. 6. Typical load profile for case study.

3.1.1. Transformation and standardization

The probability density function (PDF) of a wind speed time series frequently is a Weibull distribution with a determined shape factor *k*, so the first step in the wind speed time series analysis consists of transforming the time series to another one that has a Gaussian PDF. This transformation is shown in equation (9) [21]:

$$U_{T(t)} = U_{(t)}^{m} \text{ with } t = 1, \ldots, n \tag{9}$$

where $U_{(t)}$ is the wind speed time series under study, $U_{T(t)}$ is the time series with a Gaussian PDF, n is the total number of observations, and m is the power transformation between k/3.60 and k/3.26, according to Dubey (1967) [22]. The selected value of m is that for which the coefficient of skewness (SK) is closest to zero. The coefficient of skewness is calculated by equation (10) [23].

$$SK = \frac{Q_3 + Q_1 - 2Q_2}{Q_3 - Q_1} \tag{10}$$

where $Q_1 = A^{-1}(0.25)$, $Q_2 = A^{-1}(0.5)$, and $Q_3 = A^{-1}(0.75)$ are the first, second, and third quartiles, respectively. $A^{-1}(.)$ is the inverse of

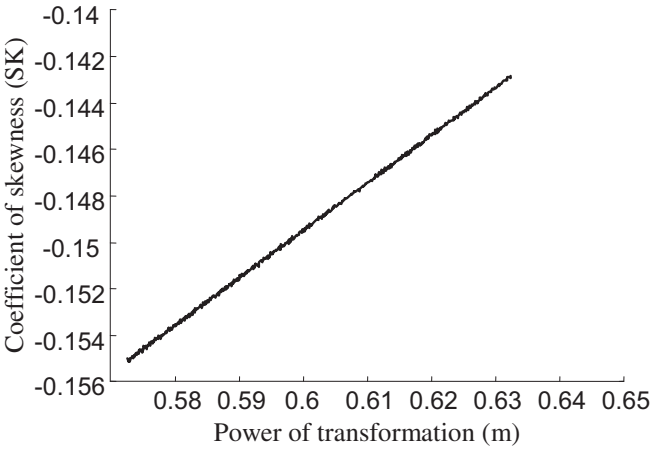

Fig. 7. Coefficient of skewness vs. power of transformation.

Table 1
Characteristics of ARMA model.

(p,q)	L-p-q	$\chi^2(\alpha = 0.05)$	S	m	ϕ_1	ϕ_2	k	Criterio	Δx
(2,0)	73	93.9453	86.2816	0.6323	0.7225	0.2178	2.0615	BIC	0.0001

the Cumulative Distribution Function (CDF) calculated using the algorithm shown in Fig. 4 (Section 3.1.4). In order for the time series $U_{T(t)}$ to be stationary, it is necessary to subtract the hourly average and divide by the hourly standard deviations. If $\mu_h(h)$ and $\sigma_h(h)$ with $h = 1,2,\ldots,24$ are the hourly average and standard deviation of transformed wind speed series, respectively, it is assumed that these functions are periodic: $\mu_h(h = 25) = \mu_h(h = 1)$ and $\sigma_h(h = 25) = \sigma_h(h = 1)$ [21]. The transformed and standardized series ($W_{(t)}$) is:

$$W_{(t)} = \frac{U_{T(t)} - \mu_{h(t)}}{\sigma_{h(t)}} \tag{11}$$

3.1.2. Estimation

The order of the ARMA (*p*,*q*) model can be estimated using the plots of autocorrelation function (ACF) and partial autocorrelation function (PACF). For example, in a pure autoregressive process of order *p*, the ACF tails off, while PACF has a cut-off value after lag *p* [24]. Others' approaches use the Bayesian Information Criterion (BIC) [25] and Akaike Information Criterion (AIC) [26]. The *p* and *q* values are selected, minimizing the respective criterion BIC or AIC of equations (12) and (13).

$$BIC(p,q) = n\log\left(\sigma^2_{(p,q)}\right) + (p+q)\log(n) \tag{12}$$

$$AIC(p,q) = n\log\left(\sigma^2_{(p,q)}\right) + 2(p+q) \tag{13}$$

$$\sigma^2_{(p,q)} = \frac{\sum_{t=1}^{n}\left(W_{(t)} - \hat{W}_{(t)}\right)^2}{n-(p+q)} \tag{14}$$

where $\sigma^2_{(p,q)}$ is the variance of the residual and $\hat{W}_{(t)}$ is the value calculated by the ARMA model. The autoregressive and moving average parameters are calculated by minimizing the quadratic prediction error criterion [27].

3.1.3. Diagnostic checking

The verification and statistical checking of the ARMA model fitted in the previous steps is carried out using the test of randomness proposed by Ljung and Box [28], which is determined according to the statistics of equation (15).

$$S = n(n+2)\sum_{\beta=1}^{L}\frac{r_\beta^2}{(n-\beta)} \tag{15}$$

where *L* is a number of lags considered and r_β is the correlation coefficient of the residuals corresponding to lag β. Under the null hypothesis of randomness, the asymptotic distribution of *S* is chi-square with *L-p-q* degrees of freedom $\chi^2(L\text{-}p\text{-}q)$. The null hypothesis of randomness, considering a determined level of significance α, is rejected if the statistics *S* is higher than $\chi^2_\alpha(L\text{-}p\text{-}q)$.

3.1.4. Forecasting of hourly average wind speed with the ARMA model

The first step in wind speed forecasting is to evaluate equations (16) and (17).

$$\hat{W}_{(t+l)} = \phi_1 W_{(t-1+l)} + \ldots + \phi_p W_{(t-p+l)} + \varepsilon_{(t+l)} - \theta_1\varepsilon_{(t-1+l)} - \ldots - \theta_q\varepsilon_{(t-q+l)} \tag{16}$$

$$\hat{U}_{T(t+l)} = \mu_{h(t+l)} + \sigma_{h(t+l)}\hat{W}_{(t+l)} \tag{17}$$

where $l = 1,\ldots,hrp$ and *hrp* are the hours ahead of prediction. In order to undo the transformation process, it is necessary to apply the probability transformation in the discrete form. Using this transformation, the PDF of hourly wind speed predicted will be the PDF of the original wind speed time series. This probability transformation is based on equation (18) below [29], and the forecasting values $\hat{U}_{(t+l)}$ are calculated using the next following equation (19).

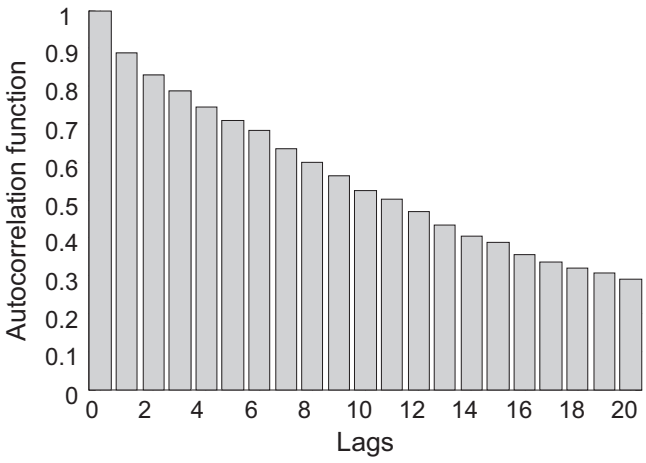

Fig. 8. Autocorrelation function.

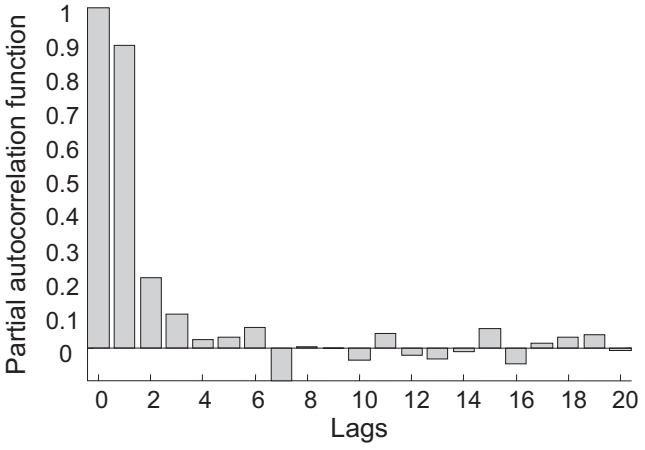

Fig. 9. Partial autocorrelation function.

Table 2
Forecasting errors 24 h ahead.

Index of error	Error
MBE (m/s)	−0.2600
RMSE (m/s)	2.5638
MABE (m/s)	1.9954
R	0.4635

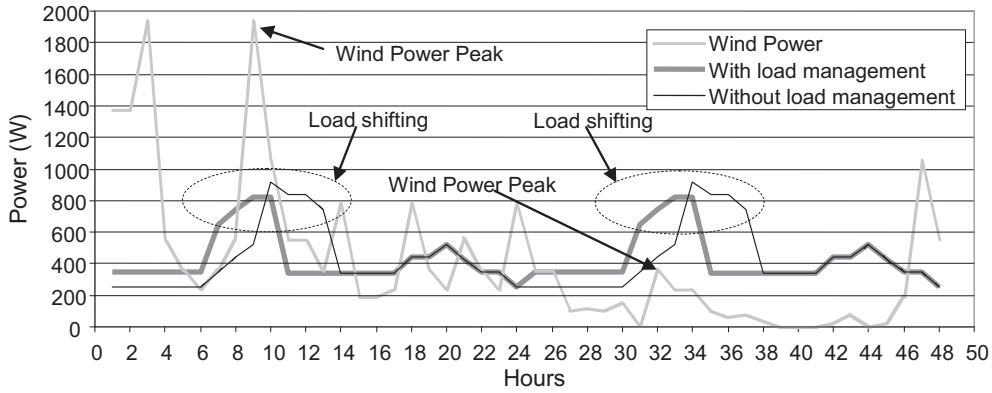

Fig. 10. Wind power and load profiles for 5th and 6th of August 2005.

$$A\left(\hat{U}_{(t+l)}\right) = u_{(t+l)} = \hat{A}_T\left(\hat{U}_{T(t+l)}\right) \tag{18}$$

$$\hat{U}_{(t+l)} = A^{-1}\left(\hat{A}_T\left(\hat{U}_{T(t+l)}\right)\right) \tag{19}$$

where A is the CDF in a discrete form of the original wind speed time series $U_{(t)}$, $\hat{A}_T$ is the CDF of the Gaussian distribution with a mean and standard deviation equal to the transformed time series $U_{T(t)}$, and $u_{(t+l)}$ is a random variable uniformly distributed and calculated using equation (18). To calculate the $\hat{U}_{(t+l)} = A^{-1}(u_{(t+l)})$ value, it is necessary to build the vector x, whose elements are zero *ceil* (max($U_{(t)}$)) with $t = 1,2,\ldots,n$ in step Δx. The next step is to build the vector A, whose elements are the cumulative probabilities of each element of vector x. The predicted value of the hourly wind speed $\hat{U}_{(t+l)}$ is calculated using the algorithm in Fig. 4. In this figure, the function *size* (A) calculates the number of rows of vector A.

4. Predictive load management

The load demand of the hybrid power system of Fig. 1 may be managed to reduce the daily fuel consumption; this is done using controllable loads when wind speed will be high.

If a is the number of controllable loads, Fig. 5 shows its idealized load profile.

Where $\pi^{(a)}$ is the earliest hour at which appliance a must start its operation, $\lambda^{(a)}$ is the latest hour at which appliance a must end its operation, $d^{(a)}$ is the duration of the operation of appliance a, $h^{(a)}$ is the possible hour at which appliance a will start its operation, $P^{(a)}$ is the power required by appliance a, and T (h) is the period of management. The load management consists of making forecasts of the hourly average wind speed and wind power in $T = 24$ h ahead. Using these predictions, it is possible to set the hour at which the appliance a will start its operation for minimizing the energy supplied by the controllable power sources (diesel generator and battery bank), using the load following strategy. In this paper, the optimization is made by testing all possible combinations. The mathematical formula of this problem is:

$$\min f = \sum_{l=1}^{l=T} k_4 \Psi(LHV)\left(k_2 P_{gdn} + k_3 P_{gd}(l)\right) + k_5 V_{DC}(\Delta \mathrm{SOC})C \tag{20}$$

It is subject to the following constraints:

$$P_l(l) = P_W(l) + P_{gd}(l) \text{ with } l = 1,2,\ldots,T \tag{21}$$

$$h^{(a)} \geq \pi^{(a)} \text{ with } a = 1,2,.. \tag{22}$$

$$h^{(a)} + d^{(a)} \leq \lambda^{(a)} \tag{23}$$

where f (kWh) is the entire amount of energy supplied by the diesel generator and the battery bank during the period of management T, Ψ is the density of fuel (0.82 kg/l), *LHV* is the lower heating value of fuel (43.2 MJ/kg), V_{DC} is the nominal voltage of the DC bus, ΔSOC is

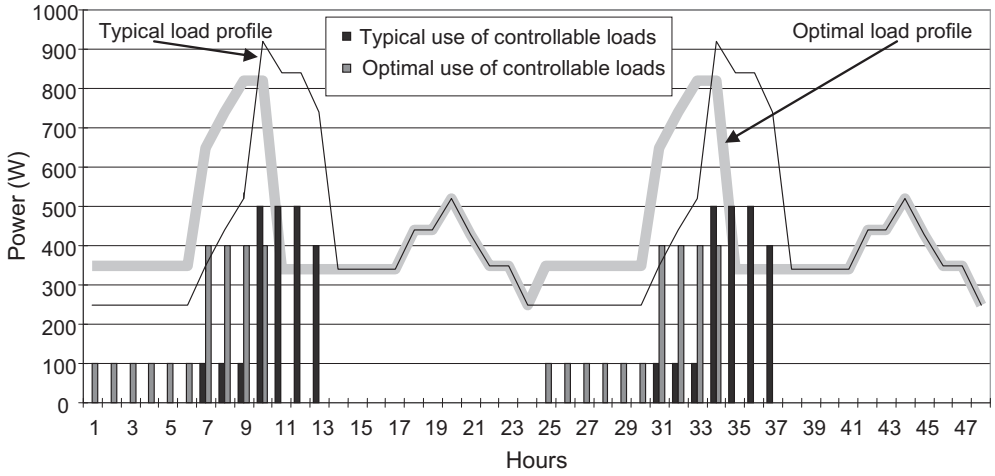

Fig. 11. Controllable loads management for 5th and 6th of August 2005.

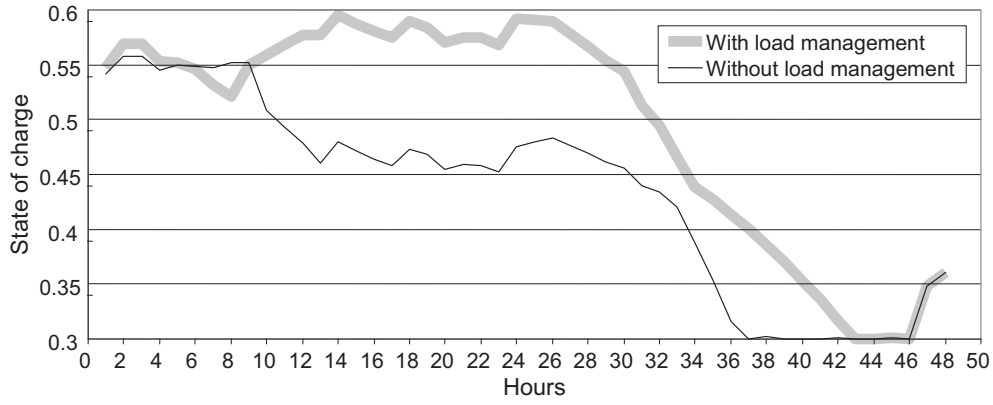

Fig. 12. State of charge for 5th and 6th of August 2005.

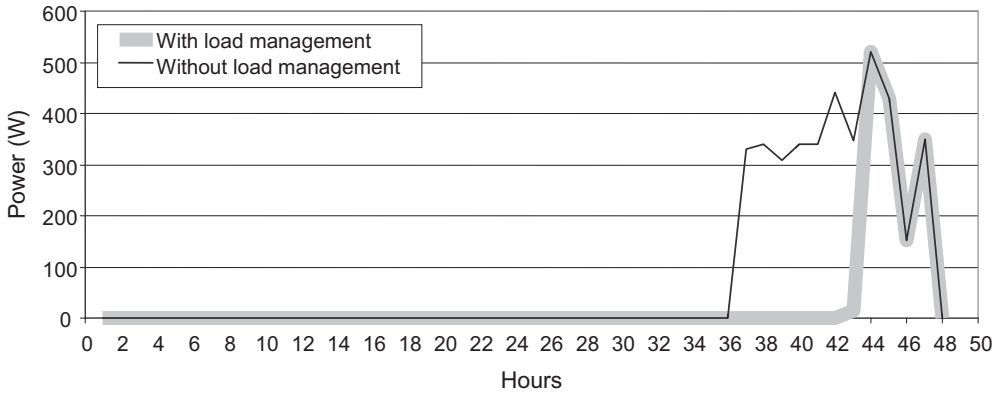

Fig. 13. Diesel generator output power for 5th and 6th of August 2005.

the decrement of the state of the charge when the battery bank is discharged, and k_4 and k_5 are conversion factors ($k_4 = 2.7 \times 10^{-4}$ and $k_5 = 10^{-3}$). $P_l(l)$, $P_W(l)$, and $P_{gd}(l)$ are the power levels demanded by the load, the total power produced by the wind turbine and battery bank, and the power produced by the diesel generator, respectively, during hour l, expressed in kW. The variables $\pi^{(a)}$ and $\lambda^{(a)}$ are imposed by the user of the hybrid power system and $d^{(a)}$ is imposed by the duty cycle of appliance a.

5. Case study

The load management strategy is illustrated using the system shown in Fig. 1 with a typical power demand (P_l) shown in Fig. 6. The system has two controllable loads ($a = 1,2$) that frequently operate for between 7 and 18 h ($\pi^{(1)} = 7$ and $\lambda^{(1)} = 18$) and between 1 and 24 h ($\pi^{(2)} = 1$ and $\lambda^{(2)} = 24$), consuming 400 W during 4 h and 100 W during 6 h, respectively. The system has a small wind turbine of 3500 W, a diesel generator of 1 kW, an inverter of 1 kW, and a battery bank of 6 cells in serial, 2 V, and $C_{10} = 1000$ Ah. The data collected in July 2005 in Zaragoza was used to fit the ARMA model. The forecasting error was calculated using data collected in August 2005. Fig. 7 shows the coefficient of skewness for different values of the power transformation shown in section 3.1.1 and the selected value shown in Table 1. Figs. 8 and 9 show the autocorrelation functions and partial autocorrelation function of transformed and standardized wind speed time series in July. The forecasting errors index containing the mean bias error (MBE), root mean square error (RMSE), mean absolute bias error (MABE), and correlation coefficient (R) are shown in Table 2. The load management strategy proposed in this paper and load following strategy, using the typical load profile of the Fig. 6, were applied to control the system of the study case simulated in August 2005 in Zaragoza without considering the temperature effects. The simulation of August 5th and 6th is shown in Figs. 10–13 Figs. 10 and 11 show the load is shifting to the wind power peak, i.e., the load profile with load management minimizing the energy supplied by the diesel generator and the battery bank (equation (20), with constraints (21), (22) and (23)). Fig. 12 shows the effect of the load shifting in the state of charge, which allows improving wind power use, increasing the state of the battery bank charge, and reducing the number of hours the diesel generator is operated, according to Fig. 13. For this case study, compared with the case without load management, the energy supplied by the diesel generator is reduced 4.6%.

6. Conclusions

In this paper we propose an optimum load management technique for hybrid systems with wind power, a battery bank, and a diesel generator. A controllable loads strategy is used to minimize the energy supplied by the diesel generator and battery bank, subject to constraints imposed by the user's behavior and duty cycle of the appliances. The results show that the load management strategy allows improvement of wind power usage by shifting controllable loads to wind power peaks (Figs. 10 and 11), increasing the state of charge in the battery bank (Fig. 12), and reducing the diesel generator operation time (Fig. 13), compared to the case without load management. However, due to a forecasting error in the hourly wind speed, in some cases the load shifting of the controllable loads may not be optimal.

Acknowledgments

This work was supported by the "Ministerio de Ciencia e Innovación" of the Spanish Government under Project ENE2009-14582-C02-01.

References

[1] Barley CD, Winn B. Optimal dispatch strategy in remote hybrid power systems. Solar Energy 1996;58(4–6):165–79.
[2] Ashari M, Nayar CV. An optimum dispatch strategy using set points for a photovoltaic (PV)–diesel–battery hybrid power system. Solar Energy 1999; 66(1):1–9.
[3] Dufo-López R, Bernal-Agustín JL. Design and control strategies of PV–diesel systems using genetic algorithms. Solar Energy 2005;79(1):33–46.
[4] Yamamoto S, Park JS, Takata M, Sasaki K, Hashimoto T. Basic study on the prediction of solar irradiation and its application to photovoltaic-diesel hybrid generation system. Solar Energy Materials and Solar Cells 2003;75(3–4): 577–84.
[5] Groumpos PP, Cull RC, Ratajczak AF. An overview of control aspects of a village stand-alone photovoltaic power system. IEEE Transaction on Power Apparatus and Systems 1984;103(10):2845–53. PAS.
[6] Groumps PP, Papegeorgiou G. An optimum load management strategy for stand-alone photovoltaic power systems. Solar Energy 1991;46(2):121–8.
[7] Khouzam K, Khouzam L. Load prioritization and shedding in photovoltaic power systems. Solar Cells 1991;31(6):505–11.
[8] Moreno A, Julve J, Silvestre S, Castañer L. A fuzzy logic controller for stand alone PV systems. IEEE Photovoltaic; 2000:1618–21. Specialists Conference.
[9] Salah CB, Chaabene M, Ammar MB. Multi-criteria fuzzy algorithm for energy management of a domestic photovoltaic panel. Renewable Energy 2008; 33(5):993–1001.
[10] Ammar MB, Chaabene M, Elhajjaji A. Daily energy planning of a household photovoltaic panel. Applied Energy 2010;87(7):2340–51.
[11] Thiaux Y, Seigneurbieux J, Multon B, Ahmed HB. Load profile impact on the gross energy requirement of stand-alone photovoltaic systems. Renewable Energy 2010;35(3):602–13.
[12] Moutawakkil K, Elster S. Re hybrid systems: coupling of renewable energy sources on the AC and DC side of the inverter. Refocus 2006;7(5):46–8.
[13] Jimenez AC, Olson K. Energía renovable para centros de salud rurales. USA: National Renewable Energy Laboratory, http://www.nrel.gov/docs/fy99osti/26224.pdf; 1998. Available from:.
[14] Copetti JB, Chenlo F. Lead/acid batteries for photovoltaic applications. Test results and modeling. Journal of Power Sources 1994;47(1–2):109–18.
[15] Achaibou N, Haddadi M, Malek A. Lead acid batteries simulation including experimental validation. Journal of Power Sources 2008;185(2):1484–91.
[16] Copetti JB, Lorenzo E, Chenlo F. A general battery model for PV system simulation. Progress in Photovoltaics 1993;1(4):283–92.
[17] Corbus D, Newcomb C, Baring-Gould EI, Friedly S. Battery voltage effects on small wind turbine energy capture. USA: National Renewable Energy Laboratory. Available at: http://www.nrel.gov/docs/fy02osti/32511.pdf; 2002.
[18] IEEE Standards Coordinating Committee 21. IEEE guide for selection, charging, test, and evaluation of lead-acid batteries used in stand-alone photovoltaic systems. IEEE Std; 2003. 1361.
[19] Skarstein O, Ulhen K. Design considerations with respect to long-term diesel saving in wind/diesel plants. Wind Engineering 1989;13(2):72–87.
[20] Lujano-Rojas JM, Bernal-Agustín JL, Dufo-López R, Domínguez-Navarro JA. Forecast of hourly average wind speed using ARMA model with discrete probability transformation. Lecture Notes in Electrical Engineering 98. Springer-Verlag; 2011. p. 1003–10.
[21] Brown BG, Katz RW, Murphy AH. Time series models to simulate and forecast wind speed and wind power. Journal of Climate and Applied Meteorology 1984;23(8):1184–95.
[22] Dubey SD. Normal and Weibull distributions. Naval Research Logistics Quarterly 1967;14(1):69–79.
[23] Kim TH, White H. On more robust estimation of skewness and kurtosis. Finance Research Letters 2004;1(1):56–73.
[24] Box JEP, Jenkins GM. Time series analysis: forecasting and control. Upper Saddle River, NJ: Prentice-Hall, Inc; 1976.
[25] Schwarz G. Estimating the dimension of a model. The Annals of Statistics 1978;6(2):461–4.
[26] Akaike H. A new look at the statistical model identification. IEEE Transactions on Automatic Control 1974;19(6):716–23.
[27] Ljung L. System identification. Theory for the user. PTR Prentice Hall; 1999. Information and System Sciences Series.
[28] Ljung GM, Box GEP. On a measure of lack of fit in time series models. Biometrika 1978;65(2):297–303.
[29] Rosenblatt M. Remarks on a multivariate transformation. Annals of Mathematical Statistics 1952;23(3):470–2.

Energy Policy 45 (2012) 671–679

Contents lists available at SciVerse ScienceDirect

Energy Policy

journal homepage: www.elsevier.com/locate/enpol

Optimum residential load management strategy for real time pricing (RTP) demand response programs

Juan M. Lujano-Rojas [a], Cláudio Monteiro [b,c], Rodolfo Dufo-López [a], José L. Bernal-Agustín [a,*]

[a] Department of Electrical Engineering, University of Zaragoza, Spain
[b] FEUP, Faculty of Engenharia University of Porto, Portugal
[c] INESC-Instituto de Engenharia de Sistemas e Computadores do Porto, Porto, Portugal

ARTICLE INFO

Article history:
Received 3 November 2011
Accepted 8 March 2012
Available online 28 March 2012

Keywords:
Smart grid
Demand response
Electric vehicle

ABSTRACT

This paper presents an optimal load management strategy for residential consumers that utilizes the communication infrastructure of the future smart grid. The strategy considers predictions of electricity prices, energy demand, renewable power production, and power-purchase of energy of the consumer in determining the optimal relationship between hourly electricity prices and the use of different household appliances and electric vehicles in a typical smart house. The proposed strategy is illustrated using two study cases corresponding to a house located in Zaragoza (Spain) for a typical day in summer. Results show that the proposed model allows users to control their diary energy consumption and adapt their electricity bills to their actual economical situation.

1. Introduction

Energy demand is increasing in many countries as a result of economic and industrial developments; consequently, many governments are working to provide reliable electrical energy. However, problems related with restrictions in electricity prices by means of a price ceiling and flat rates have produced a difference between marginal electricity generation costs and energy consumption cost of electricity. This increases the growth of demand faster than the growth of generation capacity. In addition, the volatility of wholesale electricity prices affects the retailer's ability to generate profit and increase the investment uncertainty (Kim and Shcherbakova, 2011). The demand response (DR) is defined as changes in the electricity consumption patterns of end consumers to reduce the instantaneous demand in times of high electricity prices. A change in consumption patterns could be made by means of a change in the price of electricity (Price-Based Programs) or incentive payments (Incentive-Based Programs Albadi and El-Saadany, 2008). Time-of-Use (TOU) is a particular type of Price-Based Program whereby peak periods have higher prices than prices during off-peak periods; consequently, the users change their use of electricity. This type of DR program is particularly convenient for residential users (Eissa, 2011).

Recently, many studies have been carried out to determine how end-users can adjust their load level according to a determined DR program. Molderink et al. (2010) developed an algorithm for the control of energy streams on a single house and a large group of houses. It is assumed that every house has microgenerators, heat and electricity buffers, appliances, and a local controller. In this approach, global and local controllers are used in three steps. First, a prediction is made for production and consumption for one day ahead, and then the local controller determines the aggregated profile and sends it to the global controller. Second, the plan for each house is made for the next day. Third, the algorithm decides how the demand is matched. Two examples were analyzed, and the results showed that it is possible to plan for a fleet of houses based on a one-day prediction; however, any forecasting error affects the outcomes of this approach. Houwing et al. (2011) analyzed the importance of the micro-Combined Heat and Power systems (micro-CHP) as a special type of distributed generation (DG) technology. The model-predictive control (MPC) proposed to make a demand response, minimizing the cost of the domestic energy use, subject to operational constraints and assuming the perfect prediction of energy demand and electricity prices. The results showed that the costs are between 1% and 14% lower than the standard control strategies.

Mohsenian-Rad and Leon-Garcia (2010) developed a residential load control for real-time pricing (RTP) environments where the electricity payment and the waiting time for the operation of each appliance are minimized in response to the variable real-time prices. First, a price prediction is made for a determined scheduling horizon. Next, an objective function that considers the total electricity payment and the total cost of waiting (cost of using appliances at later hours) into the scheduling horizon is minimized. Mohsenian-Rad et al. (2010) presented a demand side

* Corresponding author. Tel.: +34 976761921; fax: +34 976762226.
E-mail address: jlbernal@unizar.es (J.L. Bernal-Agustín).

0301-4215/$ - see front matter © 2012 Elsevier Ltd. All rights reserved.
http://dx.doi.org/10.1016/j.enpol.2012.03.019

management model where, for a fleet of residential consumers, the optimal energy consumption schedule for each consumer is determined by minimizing the energy cost in the system based on game theory. Conejo et al. (2010) presented a demand response model that minimizes the cost of energy consumption considering the load-variation limits, hourly load, and price prediction uncertainty. This model assumes that prices and decisions in the prior $t-1$ h are known; in the actual moment (hour t), the price and power demand are known, and the prices in the next $24-t$ h are estimated using an autoregressive integrated moving average (ARIMA)-based model with a confidence interval. Using this information, the optimization model establishes a floor for daily consumption, and ramping down/up limits are solved, obtaining the energy consumption in the current hour t and the demand at the beginning of hour $t+1$. Finally, this procedure is repeated each hour on a scheduling horizon of 1 day.

Sianaki et al. (2010) proposed a methodology for demand response that considers the customers' preferences for the use of certain appliances during peak hours by means of the Analytic Hierarchy Process. This quantification of customer preferences is used to decide what appliances must be used during the peak hours, solving the Knapsack Problem, wherein the numerical priority obtained by the Analytic Hierarchy Process for a certain appliance is considered as a measure of the profit obtained by its use. The authors conclude that this method allows improvement both in customers' budgets and the global energy consumption on the electrical grid. Tanaka et al. (2011) presented a methodology to minimize the power flow fluctuation in the smart grid with a fleet of houses using optimally a battery bank and a heat pump, concluding that this methodology allows for the reduction of the electric power consumption and the cost of electricity.

An important aspect is that the success of a determined DR program depends widely on awareness, attitude, and behavioral adaptation of consumers (Bartusch et al., 2011). However, according to results obtained by Gyamfi and Krumdieck (2011), customers are very sensitive to the energy prices. In scientific articles previously mentioned, the motivation and intention of consumers to participate in the DR program is represented in different ways. For example, Mohsenian-Rad and Leon-Garcia (2010) use a factor that is equal to 1 when a strict cost reduction is required, slightly higher than 1 when a medium cost reduction is required, and much higher than 1 when a cost reduction is not required. However, this type of representation might be a simplistic way to effectively reflect the relationship between the reduction in the electricity bill and the economic situation of the consumers. Based on this reasoning, this paper proposes a load management strategy that considers the power-purchase of energy of the consumers in a real-time pricing DR program optimizing the negotiation between the consumer and retailer.

The paper is organized as follows. Section 2 explains the smart grid infrastructure required for the real-time pricing demand response program implementation, and the mathematical modeling of household appliances and electric vehicles. Section 3 describes in detail the load management strategy proposed. Section 4 analyzes two study cases of a residential consumer in a real-time pricing demand response in the Iberian Peninsula. Finally, Section 5 gives conclusions.

2. Mathematical model of system

The load management based on the real-time prices requires an electricity grid that allows for active participation of consumers in demand response programs to supply electricity economically and efficiently. This electricity grid is known as the "smart grid." Future smart grids will be provided with a communication infrastructure that can be categorized into three classes: wide area network (WAN), field area network (FAN), and home area network (HAN). A WAN is used to exchange real-time measurements between the control center and electric devices located in power plants, substations, and distributed storage. A FAN allows communication between distribution substations, distribution feeders, transformers, and customers' homes. A HAN allows communication between loads, sensors, and appliances in homes. An Energy Services Interface (ESI) is a secure two-way communication interface between the utility and the customers. An ESI can receive hourly prices from the utility and inform the customers; using a web-based Energy Management System (EMS) or In-Home Display (IHD) connected to the ESI, customers can respond to the pricing signal (Wang et al., 2011). For a typical house provided with a smart meter, wind turbine, photovoltaic (PV) panels, several household appliances, and an electric vehicle (EV), the technique proposed in this paper consists of using information about wholesale energy prices, the power of renewable sources and temperature, energy demand, and user behavior to determine optimal demand response for the following day, considering the power-purchase of energy of the consumers. Fig. 1 describes the load management strategy proposed, where, using ESI, the user is informed about the actual and forecasted values of energy prices, energy consumption, and renewable power. Then, using a diary planner for the next day—expressed by means of the user's power-purchase of energy and predictions of wholesale energy prices, renewable power productions, and energy demand—the EMS can determine the optimal use of household appliances for the next day and the best time to use the electric vehicle, subject to the conditions imposed by a specific trip.

The next section describes a mathematical model of household appliances and electric vehicles of a typical residential consumer.

2.1. Energy demand modeling

2.1.1. Household appliances

Let $n=1,2,3,\ldots,N$ be the household appliances. In this paper, it is assumed that a typical household appliance n can be modeled by means of an idealized load profile, as shown in Fig. 2. Here, h_n is the possible hour at which the appliance will start its operation, P_n is its power required, and d_n is the duration of its operation. The matrix of all possible load profiles for this appliance $PDCA_n$ (Possible Demand Curve of the Appliance n) can be obtained using the algorithm shown in Fig. 3. The matrix $PDCA_n$ will have 24 columns, and its number of rows will be a variable value called R_n, while the variables r and l are counters used by the algorithm.

Additionally, a row with zeros must be added to the matrix $PDCA_n$ to consider the option of shutting down the appliance n.

2.1.2. Electric vehicle

Environmental factors related to greenhouse gas emissions, petroleum-based transportation, and air pollution are promoting

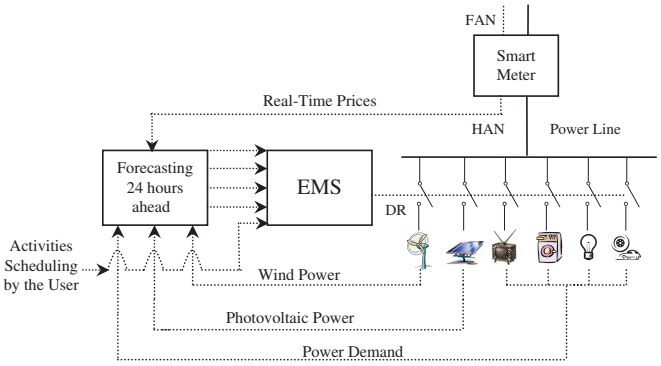

Fig. 1. Smart house and load management strategy.

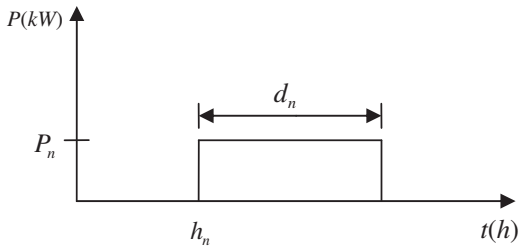

Fig. 2. Idealized load profile of household appliances.

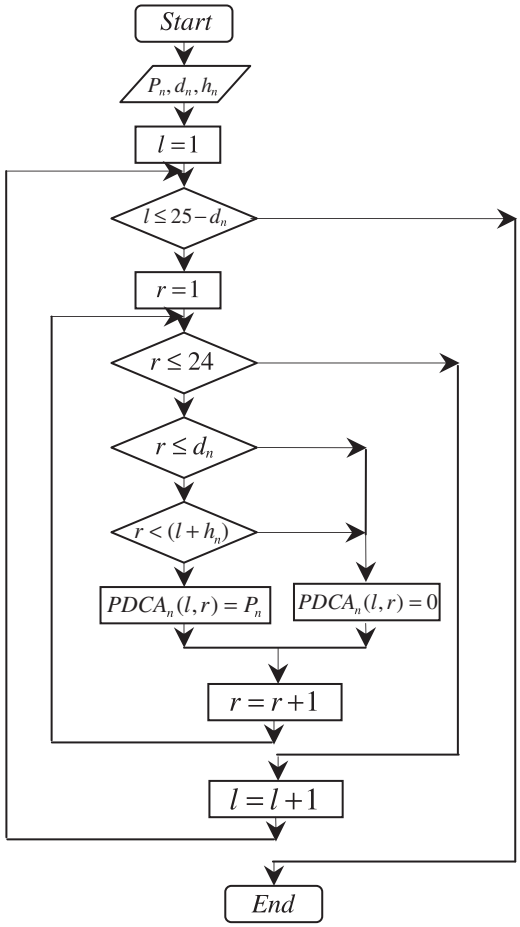

Fig. 3. Algorithm to find $PDCA_n$.

the development of EVs. For these reasons, it is expected that EVs will be an important electric load in the urban environments; therefore, this is considered in our analysis. Recently, there are plug-in hybrid electric vehicles that use nickel-metal hydride and lithium ion batteries (Bradley and Frank, 2009); however, for simplicity and illustrative purposes, in our optimal load management strategy, a lead acid battery model will be considered.

Copetti and Chenlo (1994) developed a general lead acid battery model to represent the complex battery behavior; however, its mathematical formulation is complex because we need to solve a nonlinear equations system for each hour of simulation; for this reason, a simplification is used. The following Equations represent the capacity model normalized with respect to the total ampere-hours that might be charged or discharged in 10 h at 25 °C (C_{10} capacity):

$$C_T = 1.67C_{10}(1+0.005\Delta T_a) \tag{1}$$

$$C = \frac{C_T}{1+0.67(|I|/I_{10})^{0.9}} \tag{2}$$

where $\Delta T_a = T_a - 25$ is the temperature variation from the reference of 25 °C, T_a is the ambient temperature in °C, C_T is the maximum capacity of the battery and C is the ampere-hours capacity at the charge or discharge constant current I.

The Coulombic efficiency (η_b) during the discharge ($I<0$) and charge ($I>0$) processes is calculated using the following equation (Copetti et al., 1993):

$$\eta_b = \begin{cases} 1-\exp\left[\left(\frac{20.73}{I/I_{10}+0.55}\right)(SOC-1)\right], & I>0 \\ 1, & I<0 \end{cases} \tag{3}$$

where I_{10} is the charge or discharge current in 10 h at 25 °C. The state of charge (SOC) of the battery is calculated by

$$SOC = \begin{cases} \frac{Q}{C}\eta_b, & I>0 \\ 1-\frac{Q}{C}\eta_b, & I<0 \end{cases} \tag{4}$$

where $Q=|I|t$ is the charge supplied by the battery (discharge) or to the battery (charge) during time t. During the charge process, the battery voltage at which the charge controller disconnects the power source is assumed to be 2.5 V/cell; during this process, the battery voltage per cell might be approximated by (Copetti and Chenlo, 1994)

$$V = \left(2+0.16\frac{Q}{C}\right)+\frac{I}{C_{10}}\left(\frac{6}{1+I^{0.6}}+\frac{0.48}{(1-Q/C_T)^{1.2}}+0.036\right)(1-0.025\Delta T_a) \tag{5}$$

Eq. (5) allows us to estimate the Q value at which the battery voltage is 2.5 V per cell and, therefore, the state of charge in the moment at which the charge controller disconnects the power sources. During the discharge process, when the state of charge is equal to the minimum value specified by the battery manufacturer, the charge controller disconnects the traction system to prevent over-discharge.

Let $k=1,2,3,\ldots,K$ be the number of electric vehicles in the house. A matrix $PDCEV_k$ (Possible Demand Curve of the Electric Vehicle k) can be made similar to the one used to represent all possible load profiles of household appliances ($PDCA_n$) but using the lead acid battery model presented above to estimate power required from the electric grid to charge the battery bank of EV considering a determined level of autonomy. The matrix $PDCEV_k$ will have 24 columns, and its number of rows will be a variable value called F_k.

3. Optimum load management strategy

As explained in Section 2, the optimum load management strategy requires forecasting of renewable power production, load, and electricity prices for the next day. Then, using the activity scheduling by the user—expressed as the power-purchase of energy—the negotiation between utility and user is optimized. The next sections present a survey about predictions of interest, show users how to express the activities scheduling, and describe the optimization problem and its solution methodology to determine the optimal demand response of the user for the next day.

3.1. Ensemble forecasting

Several models have been developed to forecast wind speed and power using different types of information. Lei et al. (2009) divided the forecasting methods into four categories: physical model, conventional statistical model, spatial correlation model, and artificial intelligence model. The *physical model* uses information about terrain, obstacles, pressure, and temperature to predict wind speed. The result obtained with this model can be used as the

auxiliary input of a *statistical model*, which is based on analyzing historical data. *Spatial correlation* models consider the spatial relationship between the wind speeds at different places. The models based on *artificial intelligence* use an artificial neural network (ANN), fuzzy logic, or a support vector machine to make predictions of wind speed and wind power. The photovoltaic power prediction can be made using models based on artificial intelligence and statistical analysis such as ANNs, autoregressive moving average (ARMA) process, Bayesian inference, and Markov chains (Paoli et al., 2010).

However, other approaches based on analyses of satellite data and numerical weather predictions present greater accuracy for horizons of more than 5 h (Kleissl, 2010). Aggarwal et al. (2009) divided the electricity price forecasting methodologies in three main categories: game theory-based models, simulation-based models, and time series analysis-based models. *Game theory* models consider the strategies of the market participants to maximize their benefits. *Simulation* models consider system operational conditions by means of optimal power flow. *Time series* classification includes statistical techniques such as ARMA models, ANNs, and data mining. Artificial intelligence models have been applied to analyze the relationship between energy consumption patterns and temperature behavior. Some examples of this type of approach have been proposed by Abdel-Aal (2004a, 2004b) and Fan et al. (2009). Electric vehicles will be an important load whose patterns of use must be known. In the load management strategy proposed in this paper, the home-arrival time of the EV must be predicted. Wang et al. (2011) have developed a probability distribution of this variable to analyze the impact of plug-in hybrid electric vehicles on power systems; however, statistical analysis could also be considered.

3.2. Activity scheduling by user

An example of the power-purchase of energy of the user is shown in Table 1. For the household appliance n, the column VUA_n (Value to User of the household Appliance n) contains the hourly values assigned by the consumer to use this appliance during a determined hour of the following day. According to Table 1, the consumer could pay €0.05 per kWh to use the household appliance n from 16:00 to 18:00 h. Similarly, the column $VUEV_k$ (Value to User of the Electric Vehicle k) contains the hourly values assigned by the consumer to use the electric vehicle k during a determined hour of the next day. According to Table 1, the consumer would pay 7 cents of euro per kWh to travel with the EV k from 11:00 to 15:00 h. It is assumed that the energy required for an EV k to travel from 11:00 to 15:00 h is bought previously between the 1:00 and 10:00 h; when the consumer comes back home (16:00 h), the EV is reconnected, and consequently, the consumer must negotiate with the utility again. Other possibilities of use of EVs can be included in the model simply by changing the value to use the EV in determined hours of the following day. Additionally the user must express the required level of autonomy for future travel with the EV. This methodology allows us to express the diary planning consumption for one day ahead in terms of the interest shown in using a determined household appliance or EV at a determined time—this interest is conveniently expressed in €/kWh. Table 1 shows the input information to EMS, which optimizes the negotiation between retailer and consumer.

Table 1
Activities scheduling by the user for the next day.

t (h)	VUA_1 (€/kWh)	VUA_n (€/kWh)	$VUEV_1$ (€/kWh)	$VUEV_k$ (€/kWh)
1	0	0	0.15	0.07
2	0	0	0.15	0.07
3	0	0	0.15	0.07
4	0	0	0.15	0.07
5	0	0	0.15	0.07
6	0	0	0.15	0.07
7	0	0	0.15	0.07
8	0	0	0	0.07
9	0	0	0	0.07
10	0	0	0	0.07
11	0	0	0.15	0
12	0.1	0	0.15	0
13	0.1	0	0.15	0
14	0.1	0	0.15	0
15	0.1	0	0.15	0
16	0.1	0.05	0.15	0.07
17	0.1	0.05	0.15	0.07
18	0	0.05	0.15	0.07
19	0	0	0.15	0.07
20	0	0	0.15	0.07
21	0	0	0.15	0.07
22	0	0	0.15	0.07
23	0	0	0.15	0.07
24	0	0	0.15	0.07

3.3. Optimization problem

The optimal demand response for the next day, considering the power-purchase of energy of the user, could be determined by maximizing the difference between the amount of money the user can pay and the cost of obtaining the required energy from the grid, which is related to the energy market prices.

Let $n=1,2,3,\ldots,N$ be the number of household appliances and $k=1,2,3,\ldots,K$ the number of electric vehicles in the house. The matrix $PDCA_n$ with R_n rows and 24 columns, and the matrix $PDCEV_k$ with F_k rows and 24 columns, are determined according to the Sections 2.1.1 and 2.1.2, respectively. Let α_n be an integer number contained in the interval $[1,R_n]$ and β_k an integer number contained in the interval $[1,F_k]$. For a specific combination of load profiles for different household appliances indicated by the row α_n in the matrix $PDCA_n$, and the different charge profiles for the electric vehicles indicated by the row β_k in the matrix $PDCEV_k$, the objective function described above could be represented mathematically using

$$f=\sum_{i=1}^{i=24}\left[\begin{array}{l}\left(\sum_{n=1}^{n=N}VUA_n(i)PDCA_n(\alpha_n,i)+\sum_{k=1}^{k=K}VUEV_k(i)PDCEV_k(\beta_k,i)\right)\\ -EP(i)\left(\sum_{n=1}^{n=N}PDCA_n(\alpha_n,i)+\sum_{k=1}^{k=K}PDCEV_k(\beta_k,i)\right)\\ +EP(i)(WP(i)+PVP(i))\end{array}\right] \quad (6)$$

where f is the difference between the amount of money that the user can pay and the cost of obtaining the required energy from the grid, $VUA_n(i)$ is the user value of household appliance n in the hour i, $PDCA_n(\alpha_n,i)$ is the power demanded by household appliance n in the hour i, $VUEV_k(i)$ is the user value to travel in electric vehicle k in the hour i, $PDCEV_k(\beta_k,i)$ is the power demanded by electric vehicle k during charge process in the hour i, $EP(i)$ is the forecasted electricity prices in the hour i and $WP(i)$ and $PVP(i)$ are the forecasted wind power and photovoltaic power in the hour i, respectively. In Eq. (6), the first term represents the power-purchase of energy of the consumer, while the second term represents the cost of the required energy, and the third term represents the benefits obtained due to selling wind and photovoltaic energy back to the grid. The number of possible combinations (N_c) in the optimization problem to maximize the objective function of Eq. (6) depends on the operation time of the different appliances (d_n) and on the number of appliances according to

$$N_c=(26-d_1)(26-d_2)\cdots(26-d_n)\cdots(26-d_N) \quad (7)$$

Fig. 4 shows in a semi-logarithmic graph the behavior of the number of possible combinations when the number of appliances is between 1 and 20, and their operation time ($d_1,d_2,\ldots,d_n,\ldots,d_N$) is

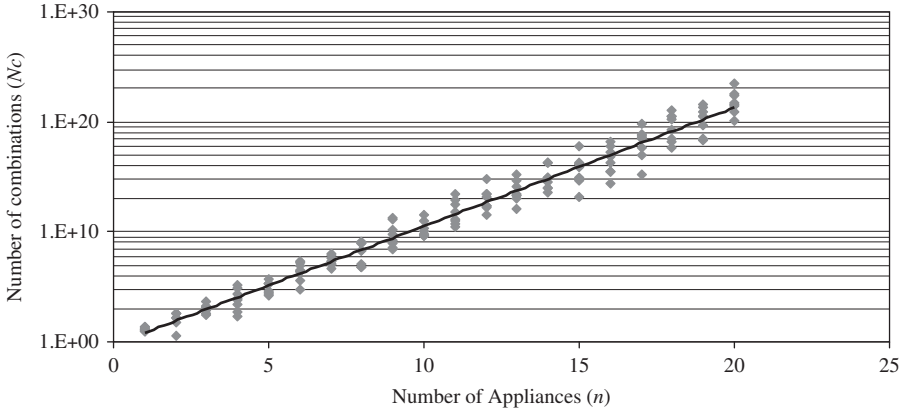

Fig. 4. Relationship between number of combinations (N_c) and number of appliances (N).

represented as a integer random variable between 1 and 24. According to these results, the number of possible combinations grows exponentially ($N_c=0.5566e^{2.4809n}$, $R^2=0.9765$) with the number of appliances considered.

Considering the nonlinear nature of the optimization problem and the number of possible combinations, we concluded that heuristic optimization techniques should be applied. Heuristic optimization techniques do not ensure finding a global optimal solution, but they can find very good solutions while consuming a low computational time. The proposed methodology requires solving the optimization problem at the end of the present day in order to reduce uncertainty in the ensemble of forecasting. Thus, the problem of finding the combination of household appliances' load profiles and EV trips that maximize the objective function of Eq. (6) can be solved using a heuristic optimization technique. In this case, we used a genetic algorithm (Goldberg, 1989) that, for a determined number of individuals in the population (P_o), number of generations (G_o), crossing rate (C_o) and mutation rate (M_o), can be implemented in the following way:

1. The initial population is obtained randomly, where an individual is an integer vector such as this: $|\alpha_1|\alpha_2|\ldots|\alpha_n|\ldots|\alpha_N|\beta_1|\beta_2|\ldots|\beta_k|\ldots|\beta_K|$ with $n=1,2,3,\ldots,N$; $k=1,2,3,\ldots,K$ and $\alpha_1, \alpha_2,\ldots,\alpha_n,\ldots,\alpha_N \in [1,R_n]$; $\beta_1,\beta_2,\ldots,\beta_k,\ldots,\beta_K \in [1,F_k]$.
2. For each individual in the population, the objective function (f) of Eq. (6) is evaluated.
3. The fitness function (F_{it}) of individual p is determined according to its rank in the population (rank 1 is assigned to the best individual, which maximizes f defined by Eq. (6), and rank P_o to the worst individual, which minimizes f). The fitness function is shown as

$$F_{it}=\frac{(P_o+1)-p}{\sum_{p=1}^{P_o}(P_o+1-p)} \quad \text{with} \quad p=1,2,\ldots,P \tag{8}$$

4. Reproduction, crossing, and mutation are carried out on the obtained solutions, defining the next generation. Reproduction is made using the roulette-wheel method, where the selection probability of a determined individual is proportional to its fitness. The crossing between two individuals is made by the "one crossing point" method with a crossing rate C_o ($0<C_o<1$), which defines how many descendants will be produced in each generation. The mutation is made by randomly changing the components of some individuals, whose quantity is defined by the mutation rate M_o ($0<M_o<1$), which determines the number of individuals which will be mutated in each generation.
5. The process in steps 2–4 is repeated until G_o generations are reached. The best solution obtained is the one that has the highest value of f, and then the optimal load profile of each household appliance and travel with the EV fitted to the power-purchase of energy of the consumer is determined.

4. Study cases

To illustrate the load management strategy proposed in this paper, a residential house located in Zaragoza (Spain) is analyzed. The house has a television of 0.12 kW ($n=1$), air conditioner of 1 kW ($n=2$), computer of 0.1 kW ($n=3$), 15 bulbs of 10 W ($n=4$), other household appliances with total consumption of 0.15 kW ($n=5$), a wind turbine of 3 kW, and an EV with a battery bank of $C_1=53$ Ah and 312 V ($k=1$). Two cases have been considered, as presented in the next sections.

4.1. Case study determining the best time to use EV

During the previous day of our analysis, the user specified his plan to EMS using Table 1 linked to ESI. Specifically for this day, the user, according to his power-purchase, could pay 1 c€/kWh to watch television between 14 h and 23 h, 10 c€/kWh to use the air conditioner for 5 h between 13 h and 22 h, 10 c€/kWh to use the computer between 9 h and 20 h, 10 c€/kWh to use the lights between 21 h and 23 h, 10 c€/kWh to use the other household appliances during the 24 h period, and 5 c€/kWh to use the EV for 5 h at any time of the day. According to Section 3, predictions 24 h ahead of electricity prices, ambient temperature, and wind power are simulated. Analyzing information published by Foley et al. (2012), Aggarwal et al. (2009), Hahn et al. (2009), and Abdel-Aal (2004a), wind power forecasting error of 20%, energy prices forecasting error of 10%, ambient temperature forecasting error of 10% and load forecasting error of 2% have been considered.

The household appliances and EV were modeled according to Section 2. For example, for the air conditioner ($n=2$, $P_2=1$ kW, and $d_2=5$ h), the matrix of all possible load profiles derived from all possible uses ($PDCA_2$) is built using the algorithm presented in Fig. 3. The transpose matrix of $PDCA_2$ is shown in Table 2. Note that a row with zeros in $PDCA_2$ has been included to consider the option of shutting down the air conditioner ($R_2=21$).

Initially, the battery bank of the EV has an *SOC* of 35%, and then the user connects the EV to the grid to increment the *SOC* to 60% or higher. It is estimated that 11.7% of energy stored in the battery bank is spent during travel, and when the user returns with the EV, he will reconnect it to the grid to recharge its battery bank. The transpose matrix of the load for each possible travel with the EV ($PDCEV_1$) under these autonomy requirements is shown in Table 3, assuming that the EV is charged optimally, maintaining

the voltage at a constant value. Note that a row with zeros in $PDCEV_1$ has been included to consider the option of no travel with the EV ($F_1=13$).

Tables similar to Table 2 were built for other household appliances, and then the optimum load management strategy, explained in Section 3, was implemented in MATLAB considering $P_o=1000$, $G_o=30$, $C_o=95\%$, and $M_o=1\%$. The evolution of the genetic algorithm is shown in Fig. 5. The total number of possible combinations is 2,812,992, and the implemented program evaluates about 28 combinations per second.

Table 2
Transpose matrix $PDCA_2$.

Possible load curves																				
1	2	3	4	5	6	7	8	9	10	11	12	13	14	15	16	17	18	19	20	21
1	0	0	0	0	0	0	0	0	0	0	0	0	0	0	0	0	0	0	0	0
1	**1**	0	0	0	0	0	0	0	0	0	0	0	0	0	0	0	0	0	0	0
1	**1**	**1**	0	0	0	0	0	0	0	0	0	0	0	0	0	0	0	0	0	0
1	**1**	**1**	**1**	0	0	0	0	0	0	0	0	0	0	0	0	0	0	0	0	0
1	**1**	**1**	**1**	**1**	0	0	0	0	0	0	0	0	0	0	0	0	0	0	0	0
0	**1**	**1**	**1**	**1**	**1**	0	0	0	0	0	0	0	0	0	0	0	0	0	0	0
0	0	**1**	**1**	**1**	**1**	**1**	0	0	0	0	0	0	0	0	0	0	0	0	0	0
0	0	0	**1**	**1**	**1**	**1**	**1**	0	0	0	0	0	0	0	0	0	0	0	0	0
0	0	0	0	**1**	**1**	**1**	**1**	**1**	0	0	0	0	0	0	0	0	0	0	0	0
0	0	0	0	0	**1**	**1**	**1**	**1**	**1**	0	0	0	0	0	0	0	0	0	0	0
0	0	0	0	0	0	**1**	**1**	**1**	**1**	**1**	0	0	0	0	0	0	0	0	0	0
0	0	0	0	0	0	0	**1**	**1**	**1**	**1**	**1**	0	0	0	0	0	0	0	0	0
0	0	0	0	0	0	0	0	**1**	**1**	**1**	**1**	**1**	0	0	0	0	0	0	0	0
0	0	0	0	0	0	0	0	0	**1**	**1**	**1**	**1**	**1**	0	0	0	0	0	0	0
0	0	0	0	0	0	0	0	0	0	**1**	**1**	**1**	**1**	**1**	0	0	0	0	0	0
0	0	0	0	0	0	0	0	0	0	0	**1**	**1**	**1**	**1**	**1**	0	0	0	0	0
0	0	0	0	0	0	0	0	0	0	0	0	**1**	**1**	**1**	**1**	**1**	0	0	0	0
0	0	0	0	0	0	0	0	0	0	0	0	0	**1**	**1**	**1**	**1**	**1**	0	0	0
0	0	0	0	0	0	0	0	0	0	0	0	0	0	**1**	**1**	**1**	**1**	**1**	0	0
0	0	0	0	0	0	0	0	0	0	0	0	0	0	0	**1**	**1**	**1**	**1**	**1**	0
0	0	0	0	0	0	0	0	0	0	0	0	0	0	0	0	**1**	**1**	**1**	**1**	0
0	0	0	0	0	0	0	0	0	0	0	0	0	0	0	0	0	**1**	**1**	**1**	0
0	0	0	0	0	0	0	0	0	0	0	0	0	0	0	0	0	0	**1**	**1**	0
0	0	0	0	0	0	0	0	0	0	0	0	0	0	0	0	0	0	0	**1**	0

Fig. 6 shows forecasted and actual values of electricity prices and ambient temperature 24 h ahead of a typical summer day based on information provided by the Spanish electrical market operator OMEL (http://www.omel.es) and the Spanish meteorological agency AEMET (http://www.aemet.es). Typically, the residents of this house use their air conditioner between 18 h and 22 h—assuming that this house has a good thermal insulation—so the air conditioner could be used in the daytime hours, during which electricity prices are low. In this sense, Fig. 7 shows the load shifting recommended by load management strategy regarding the use of the air conditioner for this day.

The user of the EV typically travels between 8:00 h and 13:00 h. However, in the plan, the user has expressed flexibility to use the EV on this day. Under the travel conditions explained above, Fig. 8 shows the results obtained by the load management strategy about the use of the EV; note that if the user travels with the EV at 8:00 h ($SOC=61.7\%$) and returns at 13:00 h ($SOC=50\%$), electricity to recharge the battery bank will be bought when electricity prices will be high. However, if the user travels with the EV at 19:00 h ($SOC=77.7\%$) and returns at 23:00 h, the autonomy of EV is incremented and its battery bank is charged when energy prices are low.

The user has specified a value of 1 c€/kWh to watch television between 14 h and 23 h, which, according to the hourly prices shown previously in Fig. 6, is a very low value, and the load management strategy recommends shutting down the television. Fig. 9 shows a comparison between typical and optimal load profiles, which allows the reduction of the electricity bill of 21.7%. These results could be shown by EMS through ESI to give the users an incentive to change their energy consumption pattern. Note that according to Fig. 9, the load management strategy allows users to reach an important reduction of energy consumption in hours of high electricity prices.

4.2. Case study selecting time to use EV

In a typical situation, we can consider that the consumer needs to use EV from 8:00 to 13:00 h and can pay 5 c€/kWh for the

Table 3
Transpose matrix $PDCEV_1$.

Possible travel												
1	2	3	4	5	6	7	8	9	10	11	12	13
3.42	3.42	3.42	3.42	3.42	3.42	3.42	3.42	3.42	3.42	3.42	3.42	0.00
3.36	3.36	3.36	3.36	3.36	3.36	3.36	3.36	3.36	3.36	3.36	3.36	0.00
3.02	3.02	3.02	3.02	3.02	3.02	3.02	3.02	3.02	3.02	3.02	3.02	0.00
2.24	2.24	2.24	2.24	2.24	2.24	2.24	2.24	2.24	2.24	2.24	2.24	0.00
1.99	1.99	1.99	1.99	1.99	1.99	1.99	1.99	1.99	1.99	1.99	1.99	0.00
1.68	1.68	1.68	1.68	1.68	1.68	1.68	1.68	1.68	1.68	1.68	1.68	0.00
1.65	1.65	1.65	1.65	1.65	1.65	1.65	1.65	1.65	1.65	1.65	1.65	0.00
0.00	1.51	1.51	1.51	1.51	1.51	1.51	1.51	1.51	1.51	1.51	1.51	0.00
0.00	**0.00**	1.31	1.31	1.31	1.31	1.31	1.31	1.31	1.31	1.31	1.31	0.00
0.00	**0.00**	**0.00**	1.10	1.10	1.10	1.10	1.10	1.10	1.10	1.10	1.10	0.00
0.00	**0.00**	**0.00**	**0.00**	1.12	1.12	1.12	1.12	1.12	1.12	1.12	1.12	0.00
0.00	**0.00**	**0.00**	**0.00**	**0.00**	1.07	1.07	1.07	1.07	1.07	1.07	1.07	0.00
2.45	**0.00**	**0.00**	**0.00**	**0.00**	**0.00**	0.81	0.81	0.81	0.81	0.81	0.81	0.00
2.07	2.45	**0.00**	**0.00**	**0.00**	**0.00**	**0.00**	0.82	0.82	0.82	0.82	0.82	0.00
1.76	2.07	2.45	**0.00**	**0.00**	**0.00**	**0.00**	**0.00**	0.84	0.84	0.84	0.84	0.00
1.35	1.76	2.07	2.45	**0.00**	**0.00**	**0.00**	**0.00**	**0.00**	0.78	0.78	0.78	0.00
1.29	1.35	1.76	2.07	2.45	**0.00**	**0.00**	**0.00**	**0.00**	**0.00**	0.56	0.56	0.00
1.10	1.29	1.35	1.76	2.07	2.45	**0.00**	**0.00**	**0.00**	**0.00**	**0.00**	0.48	0.00
1.13	1.10	1.29	1.35	1.76	2.07	2.45	**0.00**	**0.00**	**0.00**	**0.00**	**0.00**	0.00
1.10	1.13	1.10	1.29	1.35	1.76	2.07	2.45	**0.00**	**0.00**	**0.00**	**0.00**	0.00
0.95	1.10	1.13	1.10	1.29	1.35	1.76	2.07	2.45	**0.00**	**0.00**	**0.00**	0.00
0.82	0.95	1.10	1.13	1.10	1.29	1.35	1.76	2.07	2.45	**0.00**	**0.00**	0.00
0.85	0.82	0.95	1.10	1.13	1.10	1.29	1.35	1.76	2.07	2.45	**0.00**	0.00
0.83	0.85	0.82	0.95	1.10	1.13	1.10	1.29	1.35	1.76	2.07	2.45	0.00

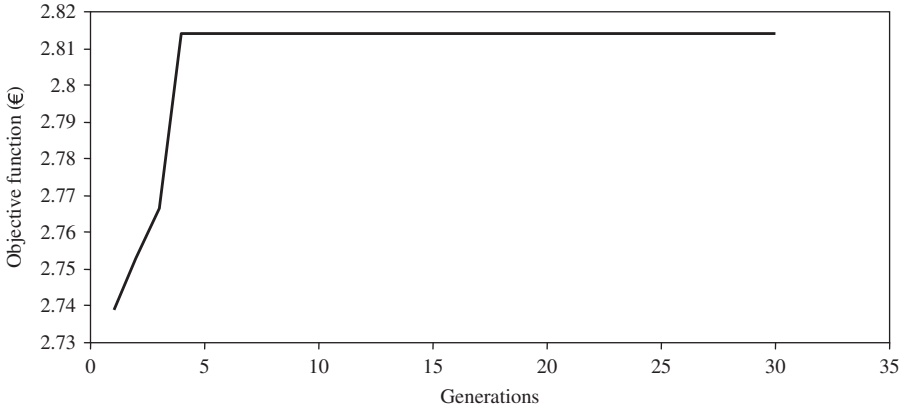

Fig. 5. Evolution of genetic algorithm optimization.

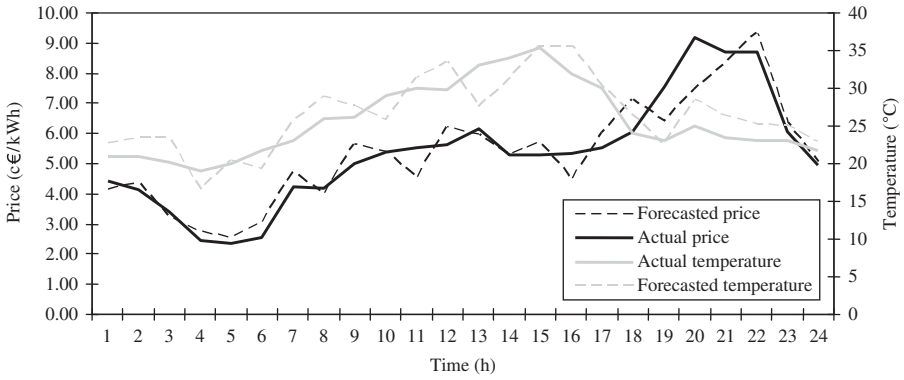

Fig. 6. Energy prices and temperature for a typical day of summer.

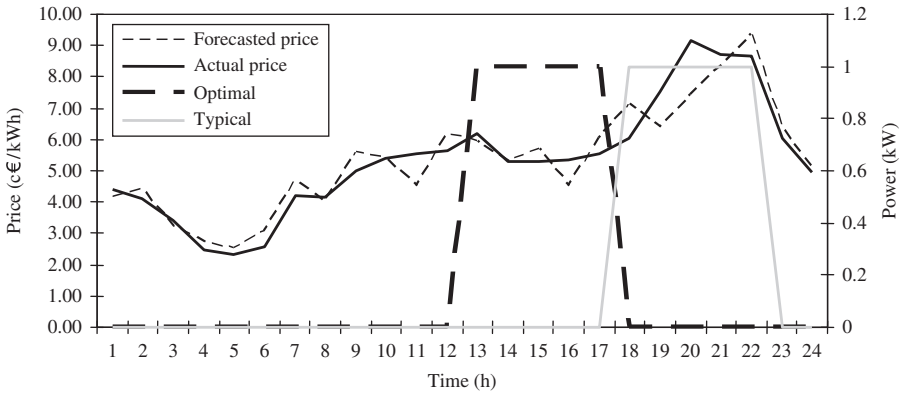

Fig. 7. Comparison of typical and optimal use of air conditioner.

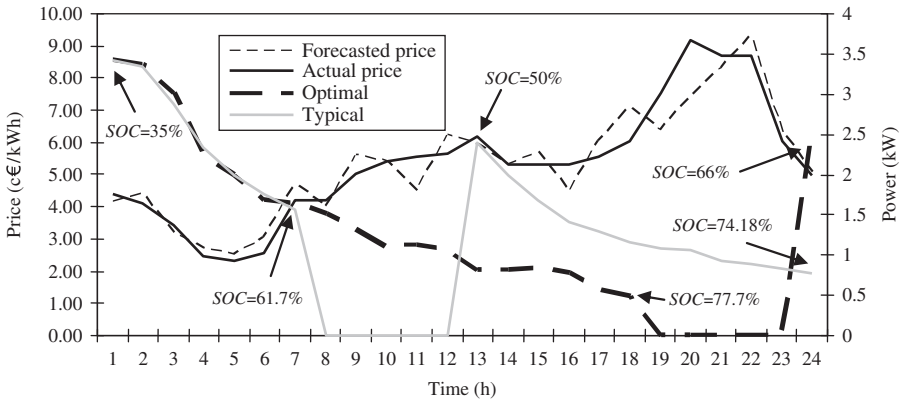

Fig. 8. Illustration of optimal use of EV for 5 h.

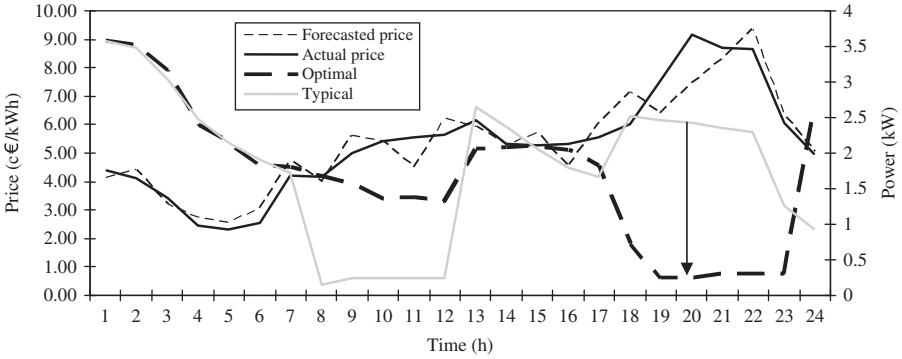

Fig. 9. Comparison between typical and optimal load profiles.

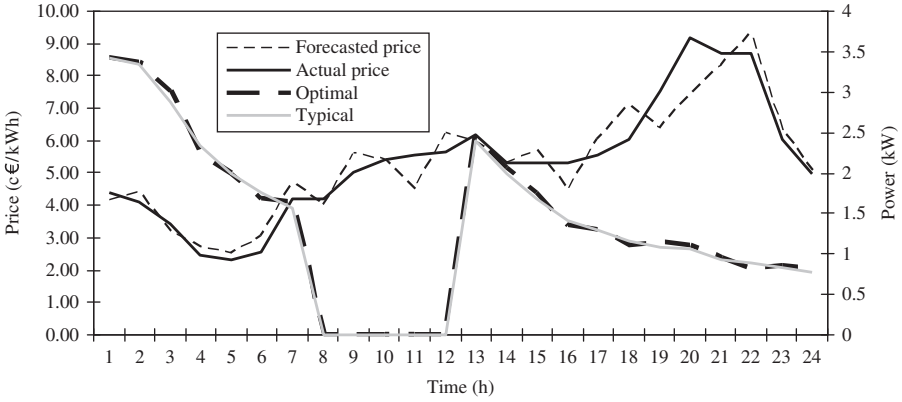

Fig. 10. Illustration of the required use of EV during 5 h.

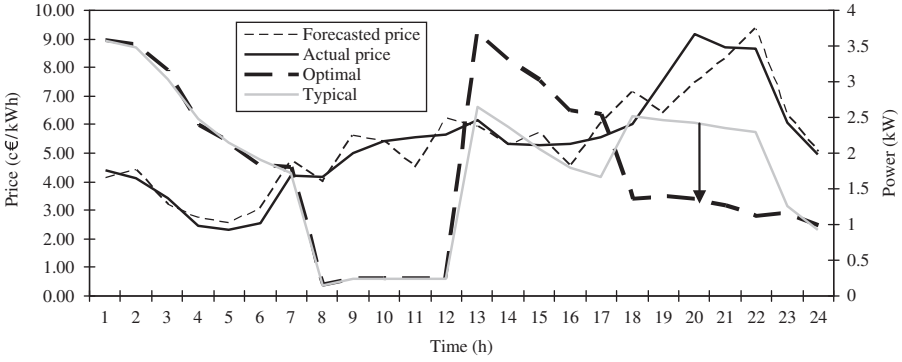

Fig. 11. Comparison between typical and optimal load profiles under typical use of EV.

energy required from the grid to charge its battery bank. It is expected that the user comes home and reconnects the EV at 13:00 h. The conditions for the other appliances are the same as previously analyzed in Section 4.1. Fig. 10 shows the results obtained from the optimization process, where the use of EV is required by the consumer. Fig. 11 shows a comparison between the typical and optimal load profiles. Under these conditions, the reduction of the electricity bill is 8%, mainly due to air conditioner use.

An important aspect to consider is that a forecasting error of electricity prices could affect the ability of the load management strategy to determine optimal scheduling for different appliance usages and traveling with EVs, while a forecasting error of renewable power could affect the estimation of benefits obtained from selling renewable energy to grid.

5. Conclusions

In this paper, an optimal load management strategy for residential consumers is shown that utilizes the communication infrastructure of the future smart grid, predictions of electricity prices, energy demand, renewable power production, and power-purchase of energy of the consumer to determine—through the negotiation between retailer and consumer—the optimal utilization of different appliances and EVs. Two study cases, of a residential

consumer in Zaragoza (Spain), have been analyzed. Results show that the proposed model allowed users to reduce their electricity bill between 8% and 22% for the typical summer day analyzed and adapt the electricity bill to their actual economical situation.

Acknowledgments

This work was supported by the Ministerio de Ciencia e Innovación of the Spanish Government, under Project ENE2009-14582-C02-01.

References

Abdel-Aal, R.E., 2004a. Hourly temperature forecasting using abductive networks. Engineering Applications of Artificial Intelligence 17, 543–556.
Abdel-Aal, R.E., 2004b. Short-term hourly load forecasting using abductive networks. IEEE Transactions on Power Systems 19, 164–173.
Aggarwal, S.K., Saini, L.M., Kumar, A., 2009. Electricity price forecasting in deregulated markets: a review and evaluation. Electrical Power and Energy Systems 31, 13–22.
Albadi, M.H., El-Saadany, E.F., 2008. A summary of demand response in electricity markets. Electric Power Systems Research 78, 1989–1996.
Bartusch, C., Wallin, F., Odlare, M., Vassileva, I., Wester, L., 2011. Introducing a demand-based electricity distribution tariff in the residential sector: demand response and customer perception. Energy Policy 39, 5008–5025.
Bradley, T.H., Frank, A.A., 2009. Design, demonstrations and sustainability impact assessments for plug-in hybrid electric vehicles. Renewable and Sustainable Energy Reviews 13, 115–128.
Conejo, A.J., Morales, J.M., Baringo, L., 2010. Real-time demand response model. IEEE Transactions on Smart Grid 1, 236–242.
Copetti, J.B., Chenlo, F., 1994. Lead/acid batteries for photovoltaic applications. Test results and modeling. Journal of Power Sources 47, 109–118.
Copetti, J.B., Lorenzo, E., Chenlo, F., 1993. A general battery model for PV system simulation. Progress in Photovoltaic 1, 283–292.
Eissa, M.M., 2011. Demand side management program evaluation based on industrial and commercial field data. Energy Policy 39, 5961–5969.
Fan, S., Chen, L., Lee, W.J., 2009. Short-term load forecasting using comprehensive combination based on multimeteorological information. IEEE Transactions on Industry Applications 45, 1460–1466.
Foley, A.M., Leahy, P.G., Marvuglia, A., McKeogh, E.J., 2012. Current methods and advances in forecasting of wind power generation. Renewable Energy 37, 1–8.
Goldberg, D.E., 1989. Genetic Algorithms in Search, Optimization and Machine Learning. Addison-Wesley Professional.
Gyamfi, S., Krumdieck, S., 2011. Price, environment and security: exploring multi-modal motivation in voluntary residential peak demand response. Energy Policy 39, 2993–3004.
Hahn, H., Meyer-Nieberg, S., Pickl, S., 2009. Electric load forecasting methods: tools for decision making. European Journal of Operational Research 199, 902–907.
Houwing, M., Negenborn, R.R., De Schutter, B., 2011. Demand response with micro-CHP systems. Proceedings of the IEEE 99, 200–213.
Kim, J., Shcherbakova, A., 2011. Common failures of demand response. Energy 36, 873–880.
Kleissl, J., 2010. Current state of art in solar forecasting. California Institute for Energy and Environment. Available at: 〈http://uc-ciee.org/all-documents/a/457/113/nested〉.
Lei, M., Shiyan, L., Chuanwen, J., Hongling, L., Yan, Z., 2009. A review on the forecasting of wind speed and generated power. Renewable and Sustainable Energy Reviews 13, 915–920.
Mohsenian-Rad, A.H., Leon-Garcia, A., 2010. Optimal residential load control with price prediction in real-time electricity pricing environments. IEEE Transactions on Smart Grid 1, 120–133.
Mohsenian-Rad, A.H., Wong, V.W.S., Jatkevich, J., Schober, R., Leon-Garcia, A., 2010. Autonomous demand-side management based on game-theoretic energy consumption scheduling for the future smart grid. IEEE Transactions on Smart Grid 1, 320–331.
Molderink, A., Bakker, V., Bosman, M.G.C., Hurink, J.L., Smit, G.J.M., 2010. Management and control of domestic smart grid technology. IEEE Transactions on Smart Grid 1, 109–119.
Paoli, C., Voyant, C., Muselli, M., Nivet, M.L., 2010. Forecasting of preprocessed daily solar radiation time series using neural networks. Solar Energy 84, 2146–2160.
Sianaki, O.A., Hussain, O., Tabesh, A.R., 2010. A knapsack problem approach for achieving efficient energy consumption in smart grid for end-users' life style. In: Proceedings of the IEEE conference CITRES, pp. 159–164.
Tanaka, K., Yoza, A., Ogimi, K., Yona, A., Senjyu, T., Funabashi, T., Kim, C.H., 2011. Optimal operation of DC smart house system by controllable loads based on smart grid topology. Renewable Energy 39, 132–139.
Wang, W., Xu, Y., Khanna, M., 2011. A survey on the communication architectures in smart grid. Computer Networks 55, 3604–3629.
Wang, J., Liu, C., Ton, D., Zhou, Y., Kim, J., Vyas, A., 2011. Impact of plug-in hybrid electric vehicle on power systems with demand response and wind power. Energy Policy 39, 4016–4021.

2. Resumen

En esta tesis doctoral se analiza la simulación y dimensionado óptimo de sistemas basados en fuentes renovables, tanto aislados como conectados a la red eléctrica, así como el desarrollo de estrategias de gestión de la demanda que sirvan de soporte a los usuarios de este tipo de sistemas con el fin de optimizar su consumo de energía eléctrica.

2.1 Objetivos

Los objetivos de este trabajo de investigación son los siguientes:

1. Analizar el modelado de los diferentes componentes de un sistema híbrido típico aislado alimentado mediante energía eólica, energía solar, generación convencional y almacenamiento con baterías de plomo ácido.

2. Analizar las diferentes técnicas de optimización determinística y probabilística para el dimensionado y simulación de un sistema híbrido típico aislado alimentado mediante energía eólica, energía solar, generación convencional y almacenamiento mediante baterías de plomo ácido.

3. Desarrollar estrategias de gestión de la demanda haciendo uso de la predicción de variables meteorológicas, tales como la velocidad del viento, la radiación solar y la temperatura ambiente, que permitan un mejor funcionamiento de los sistemas híbridos aislados de la red eléctrica. Los sistemas considerados están compuestos, principalmente, por aerogeneradores, paneles solares, generadores convencionales y almacenamiento de energía eléctrica.

4. Analizar las principales características de la futura Red Eléctrica Inteligente, y en particular la infraestructura tecnológica que permite la comunicación entre el distribuidor de la energía eléctrica y los consumidores.

5. Analizar el modelado de los diferentes componentes del sistema eléctrico doméstico alimentado por la red eléctrica, aerogenerador y paneles fotovoltaicos, asumiendo que las tarifas pueden cambiar dinámicamente de acuerdo con la hora del día (*RTP, Real Time Pricing*).

6. Desarrollar estrategias óptimas de gestión de la demanda para un consumidor residencial.

2.2 Metodología

La metodología que se ha seguido para alcanzar los objetivos propuestos en esta tesis doctoral, ha sido:

1. Revisión bibliográfica de los diferentes modelos matemáticos de aerogeneradores, paneles solares, banco de baterías de plomo ácido, inversor y generación convencional.

2. Revisión bibliográfica de las técnicas de modelado y optimización determinística de sistemas híbridos aislados de la red eléctrica.

3. Revisión bibliográfica de las técnicas de modelado y optimización probabilística de sistemas híbridos aislados de la red eléctrica.

4. Revisión bibliográfica de las técnicas de predicción de velocidad del viento, radiación solar y temperatura ambiente.

5. Desarrollo e implementación de una estrategia de gestión de la demanda que permita optimizar el uso del banco de baterías y de la fuente de generación convencional en un sistema híbrido aislado de la red eléctrica.

6. Revisión bibliográfica sobre la estructura de la futura red eléctrica inteligente.

7. Revisión bibliográfica de las principales técnicas de predicción de precios de la energía eléctrica.

8. Desarrollo de una estrategia de Adaptación de la Demanda de un consumidor típico residencial con varios electrodomésticos y vehículo eléctrico.

2.3 Revisión bibliográfica y principales aportaciones.

En general, la gestión de sistemas para la generación de electricidad puede realizarse mediante la gestión de la generación, mediante la gestión de la demanda, o mediante ambas técnicas. Estas estrategias pueden aplicarse a sistemas que están conectados a la red eléctrica así como a sistemas que están aislados de la misma. En el presente trabajo de investigación se realiza un análisis amplio (tanto desde el punto de vista

determinístico como probabilístico) de la simulación y el dimensionado óptimo de sistemas aislados basados en fuentes renovables y conectados a la red eléctrica, así como del desarrollo de estrategias de gestión de la demanda que sugieran al usuario la forma óptima en la que los electrodomésticos podrían ser usados.

Un elevado número de estudios previos han demostrado la importancia de los sistemas híbridos basados en fuentes renovables (fotovoltaica y/o eólica con baterías y/o generador de combustión interna) para la electrificación rural [13,14,15] y en la reducción de gases de efecto invernadero [16]. El dimensionado y control de este tipo de sistemas es un aspecto que ha sido estudiado por muchos investigadores. HOMER [17] es una herramienta computacional desarrollada por el Laboratorio Nacional de Energías Renovables de Estados Unidos (*U.S. National Renewable Energy Laboratory*), y se utiliza frecuentemente para la simulación y diseño óptimo de sistemas híbridos. HOMER utiliza, cuando se aplica en diseño, un método enumerativo que evalúa todas las posibles soluciones. Belfkira *et al.* [18] aplicaron el algoritmo DIRECT (*Dividing Rectangles*) para el dimensionado óptimo de sistemas con paneles fotovoltaicos, aerogeneradores y generadores diesel, minimizando el coste total. Boonbumroong *et al.* [19] utilizaron la técnica del Enjambre de Partículas con Constricción de Coeficientes (*Particle Swarm Optimization with Constriction Coefficienct*) para el dimensionado de un sistema con paneles fotovoltaicos, aerogeneradores, baterías y un inversor bidireccional. Los resultados obtenidos fueron comparados con HOMER, obteniendo como conclusión que la metodología propuesta permite reducir considerablemente el tiempo necesario para encontrar la configuración óptima. Hakimi y Moghaddas-Tafreshi [20] optimizaron, mediante la técnica del Enjambre de Partículas (*Particle Swarm Optimization*), el dimensionado de sistemas con aerogeneradores, pilas de combustibles, electrolizador, tanque de hidrogeno, reformador e inversor, obteniendo una alta fiabilidad por la existencia de pilas de combustible, ya que servían de apoyo a los aerogeneradores. HOGA [21] es una herramienta computacional desarrollada en la Universidad de Zaragoza para la optimización de sistemas híbridos mediante Algoritmos Evolutivos. Ekren y Ekren [22] utilizaron recocido simulado (*Simulated Annealing*) para optimizar el dimensionado de un sistema, instalado en Turquía, con paneles fotovoltaicos, aerogeneradores y baterías.

Considerar la variabilidad de los recursos renovables en el dimensionado óptimo de sistemas híbridos es un aspecto importante que ha sido objeto de investigación por parte

de muchos autores. Bagul *et al.* [23] propusieron una metodología que consiste en estimar la función de densidad de probabilidad de la energía, que fluye a través del banco de baterías usando información sobre los recursos renovables, y las especificaciones de los fabricantes, obteniendo el dimensionado óptimo de los componentes al considerar un determinado nivel de fiabilidad. Karaki *et al.* [24,25] desarrollaron una técnica basada en determinar el valor esperado de la energía para recargar el banco de baterías usando la distribución de probabilidad conjunta de los recursos renovables y la curva de duración de la demanda, determinando la configuración óptima teniendo en cuenta los costes de capital y la fiabilidad. Roy *et al.* [26] implementaron una metodología que consistía en identificar el conjunto de posibles soluciones para la configuración del sistema híbrido, de forma que la configuración óptima se determinaba utilizando la distribución de probabilidad de los recursos renovables. Távora *et al.* [27] compararon las metodologías determinística y probabilística, concluyendo que la metodología determinística puede dar como resultado la instalación de sistemas cuya capacidad de generación esté por encima de la requerida para obtener un determinado nivel de fiabilidad. Giannakoudis *et al.* [28] presentaron una metodología de optimización utilizando el algoritmo de recocido simulado adaptado (*Stochastic Annealing*), considerando la incertidumbre. Tan *et al.* [29] desarrollaron una metodología para el dimensionado óptimo de un sistema de energía ininterrumpida que consideraba la aleatoriedad de los recursos mediante simulaciones de Monte Carlo. En esta metodología, en primer lugar se generaban aleatoriamente unas condiciones de demanda, radiación solar y fallo de los equipos involucrados, y a continuación se calculaba la capacidad energética requerida, repitiéndose este procedimiento un determinado número de veces. Los resultados obtenidos se analizaban estadísticamente y, finalmente, el banco de baterías se seleccionaba considerando un determinado nivel de significación.

El control de los sistemas híbridos tiene dos importantes componentes: la estrategia para controlar las fuentes de energía y la gestión de la demanda. En un relevante estudio, Barley y Winn [30] propusieron las siguientes estrategias generales de control para sistemas con fuentes de energía renovables, un generador diesel y un banco de baterías:

- La Estrategia de Despacho Frugal (*Frugal dispatch strategy*)
- La Estrategia de Seguimiento de la Demanda (*Load following strategy*)
- La Estrategia de Ajuste del Estado de Carga (*State of charge setpoint strategy*)

- La Estrategia de Funcionamiento a Plena Potencia al Mínimo Tiempo (*Full power/minimum run time*).

En la Estrategia de Despacho Frugal, la intersección de la curva de costes del generador diesel con la curva de costes correspondiente al uso de la batería determina la carga crítica. Con dicha estrategia, si la demanda neta (diferencia entre la demanda y la potencia proveniente de las fuentes renovables) es mayor que la carga crítica, se utiliza el generador diesel, en otro caso se carga el banco de baterías. En la Estrategia de Seguimiento de la Demanda, el generador diesel se utiliza para satisfacer únicamente la demanda neta. En la Estrategia de Ajuste del Estado de Carga, el generador diesel opera a plena potencia para cargar las baterías hasta un determinado valor de estado de carga previamente ajustado. En la Estrategia de Funcionamiento a Plena Potencia al Mínimo Tiempo, el generador diesel opera durante un intervalo de tiempo predeterminado, cargando las baterías con la energía excedente, y después se desconecta. Ashari y Nayar [31] desarrollaron una estrategia de control que utiliza la demanda de energía, el voltaje del banco de baterías y la potencia mínima a la que es recomendable que funcione el generador diesel para decidir cuándo cargar o descargar el banco de baterías, y cuándo arrancar o detener el generador diesel. La estrategia de operación óptima se obtiene determinando el valor de la demanda crítica para arrancar y detener el generador diesel, y el ajuste del estado de carga al cual debe ser cargado el banco de baterías. Dufo-López y Bernal-Agustín [32] propusieron una estrategia de control que combinaba la Estrategia de Seguimiento de la Demanda y la Estrategia de Ajuste del Estado de Carga propuestas por Barley y Winn [30]. En esta estrategia combinada, si la demanda neta era menor que la demanda crítica, se aplicaba la Estrategia de Ajuste del Estado de Carga, en otro caso se utilizaba la Estrategia de Seguimiento de la Demanda. Yamamoto *et al.* [33] propusieron una estrategia de control en la que se utilizaba la predicción de la potencia proveniente de las fuentes de energías renovables y el perfil de carga horario para determinar la potencia del generador diesel. Si el estado de carga del banco de baterías se encontraba entre 0.5 y 0.7, el generador diesel se arrancaba para cargar el banco de baterías, y cuando el estado de carga era superior a 0.7, el generador diesel se apagaba.

En lo concerniente a la gestión de la demanda en sistemas híbridos aislados de la red eléctrica, Groumps *et al.* [34] realizaron el primer trabajo sobre sistemas fotovoltaicos aislados analizando un sistema instalado en la Villa de Schuchuli, Arizona (USA). En

este sistema se establecieron cuatro categorías de prioridad y cuatro ajustes del estado de carga (0.5, 0.4, 0.3 y 0.2). Al aplicar la estrategia de gestión, si el banco de baterías se descargaba y el ajuste del estado de carga se alcanzaba secuencialmente, las cargas se desconectaban comenzando por la de menor prioridad, y si el banco de baterías se cargaba y el ajuste del estado de carga se alcanzaba secuencialmente, las cargas se reconectaban. Más tarde, Groumps y Papegeorgiou [35] propusieron una técnica de gestión óptima de la demanda, para sistemas fotovoltaicos aislados, basada en tres categorías principales de clasificación de la carga: una clasificación de acuerdo con la operación (cargas en DC o AC), una clasificación de acuerdo al sistema (Incontrolable, Controlable y Semi-controlable) y una clasificación de acuerdo con la prioridad (Útil, Esencial, Crítica y de Emergencia). En esta técnica de gestión, usando las cargas controlables, la curva de carga general se modificaba con el fin de minimizar la integral del cuadrado de la carga neta en un período de 24 horas con el fin de reducir la capacidad necesaria del banco de baterías y los costes relacionados con el ciclo de vida del sistema. Khouzam y Khouzam [36] desarrollaron una metodología para la gestión de la demanda en sistemas fotovoltaicos autónomos en la que las cargas se clasificaban en cuatro categorías generales de acuerdo a su nivel de prioridad (Conveniente, Esencial, Crítica y de Emergencia), siendo la prioridad del banco de baterías variable y dependiente del estado de carga. La gestión óptima se basaba en la maximización de una función objetivo, que dependía de la prioridad de la carga sujeta a restricciones de disponibilidad para suplir la energía. En otro estudio, Moreno *et al.* [37] implementaron un controlador basado en lógica difusa para la gestión de la demanda en sistemas fotovoltaicos autónomos. En esta técnica la variable considerada fue la esperanza de suplir la demanda durante la siguiente hora, siendo esta variable utilizada para decidir, en tiempo real, si se desconectaba o conectaba una determinada carga teniendo en cuenta su nivel de prioridad.

En cuanto a la gestión de la demanda en sistemas conectados a la red eléctrica, Salah *et al.* [38] desarrollaron una metodología para la gestión de la demanda doméstica. En este trabajo el generador fotovoltaico se consideraba una fuente complementaria de energía y se utilizaba un controlador basado en lógica difusa para decidir en tiempo real qué electrodoméstico debía ser conectado al generador fotovoltaico o a la red eléctrica. La decisión se tomaba considerando la potencia del generador fotovoltaico, la potencia doméstica demandada, la prioridad de cada uno de los electrodomésticos y el tiempo de

operación requerido por cada uno de ellos. Se obtuvo la conclusión de que esta técnica permitía obtener un ahorro de energía continuo. Ammar *et al.* [39] propusieron una metodología para la gestión óptima de la demanda en consumidores residenciales conectados a la red eléctrica sin baterías, utilizando predicciones diarias de la potencia proveniente del generador fotovoltaico para decidir el tiempo que un determinado electrodoméstico estará conectado al generador fotovoltaico. Esta decisión se tomaba considerando la energía que cada electrodoméstico requiere para su funcionamiento. Un criterio similar fue utilizado por Salah *et al.* [38]. Thiaux *et al.* [40] analizaron la influencia de la forma del perfil de consumo en el coste de la energía durante el ciclo de vida de un sistema fotovoltaico autónomo. Los resultados de este estudio mostraron que las necesidades de energía se reducen cuando el perfil de carga y la producción fotovoltaica son similares.

La Adaptación de la Demanda (*DR, Demand Response*), se define como el cambio en el modelo de consumo de la electricidad, por parte de los consumidores, para reducir la demanda en horas en las que los precios de la electricidad son altos, o cuando la fiabilidad del sistema está en peligro. Los cambios en el modelo de consumo se pueden conseguir a través de cambios en el precio de la electricidad o a través de incentivos [41]. Así, la Adaptación de la Demanda modificando el modelo de consumo puede reducir la incertidumbre y los problemas relacionados con las diferencias entre los costes de generación y el precio de venta de la energía eléctrica [7], y también puede mejorar la eficiencia y la fiabilidad de la infraestructura disponible, además de reducir la volatilidad en los precios de la energía [41].

La implementación de estrategias para la Adaptación de la Demanda requiere de una red eléctrica equipada con una tecnología que facilite la fluida comunicación entre el distribuidor de la energía y todos los usuarios beneficiarios de la misma. Hoy en día este concepto de red eléctrica se denomina Red Eléctrica Inteligente (*Smart Grid*). Los programas de Adaptación de la Demanda pueden clasificarse en dos categorías: Programas Basados en Incentivos (*IBP, Incentive-Based Programs*) y Programas Basados en Precios (*PBP, Price-Based Programs*). Los *IBP* están basados en pagos o descuentos por participar en el programa, mientras que los *PBP* están basados en precios que cambian dinámicamente en cada hora. Los programas *IBP* están clasificados en Programas Clásicos (*Classical Programs*) y Programas Basados en el Mercado (*Market-Based Programs*). Los programas clásicos son los Programas de

Control Directo de Carga (*Direct Load Control Programs*) y los Programas de Carga Interrumpible (*Interruptible/Curtaible Load Programs*); mientras que los Programas Basados en el Mercado son los Programas de Adaptación de la Demanda durante Emergencia (*Emergency DR Programs*), Licitación de Demanda (*Demand Bidding*), Capacidad del Mercado (*Capacity Market*) y Mercado de Servicios Auxiliares (*Ancillary Services Market*). En los Programas Clásicos *IBP* los consumidores reciben un pago semejante a un vale de descuento. En los Programas de Control Directo de Carga la empresa de distribución puede desconectar cargas del consumidor participante después de una breve notificación, mientras que en los Programas de Carga Interrumpible los participantes son convocados para reducir su consumo a un valor predefinido. En los *PBP* el cambio en los precios se define de diferentes formas: de acuerdo a la hora a la cual se utiliza la energía eléctrica (*TOU, Time of Use*), si la energía eléctrica se utiliza durante situaciones de emergencia o de alto precio (*CPP, Critical Peak Pricing*), estableciendo altos precios durante los días de demanda extrema (*ED-CPP, Extreme Day CPP*), y programas que reflejan directamente al usuario los costes de generación de la electricidad en cada hora (*RTP, Real Time Pricing*) [41]. Los programas *TOU* son los que habitualmente utilizan los consumidores residenciales [42].

Los programas de Adaptación de la Demanda se han implementados en varios países. En los Estados Unidos existen varios programas de Adaptación de la Demanda, administrados por el Operador Independiente del Sistema (*ISO, Independent System Operator*) o por el Operador Regional del Sistema de Transmisión (*RTO, Regional Transmission Operator*). Ejemplos de estos tipos de operadores son el Operador Independiente del Sistema de Nueva York y el Operador de la Interconexión PJM. Existen diferentes programas de Adaptación de la Demanda, en los que el consumidor puede participar usando estrategias de control de la demanda para reducir su consumo de acuerdo a un determinado precio o señal de emergencia [43]. En el Reino Unido los sectores industrial y comercial pueden acordar programas *TOU* y/o Programas de Carga Interrumpible con la empresa de distribución eléctrica. Muchos usuarios participan en programas con la opción de obtener descuentos en el precio de la energía durante la noche. En Italia los Programas de Carga Interrumpible son aplicados a las grandes industrias, reduciendo su consumo a un valor de carga predefinido. En España se han desarrollado dos programas de Adaptación de la Demanda para los grandes consumidores, uno está dirigido por el sistema y otro está dirigido por el precio. En el

programa dirigido por el sistema los consumidores pueden participar voluntariamente en el programa, de forma que el operador del sistema de transmisión (*TSO, Transmission System Operator*) puede solicitar a estas industrias que limiten su demanda durante periodos que van desde 45 minutos hasta 12 horas. En el programa dirigido por el precio el *TSO* puede aplicar el *TOU* en siete periodos del año [44]. En China los programas de Adaptación de la Demanda han sido implementados para mejorar la fiabilidad y el factor de carga. En Pekín se ha incrementado la diferencia de precios entre las horas que se encuentran dentro y fuera del pico de demanda. Así, los consumidores industriales han acordado Programas de Carga Interrumpible, utilizando equipos de almacenamiento de energía y cargas controladas. En Jiangsu se han aplicado Programas de Carga Interrumpible a consumidores industriales, se ha promovido el uso de equipos de almacenamiento de energía, se han aplicado tarifas *TOU* y se ha implementado el control de máquinas industriales [45].

Se han desarrollado diversos estudios sobre cómo el usuario final puede ajustar su demanda de acuerdo a un determinado programa de Adaptación de la Demanda. Molderink *et al.* [46] desarrollaron un algoritmo para el control de los flujos de energía en una casa o en un gran conjunto de casas. En el algoritmo propuesto se asumía que cada casa poseía micro-generadores, cogeneración, electrodomésticos y un controlador local. En este enfoque existen tres etapas. En la primera se realizaba la predicción de las producciones de generación renovable y de los consumos en un día, y con esta información el controlador local determinaba el perfil agregado y lo enviaba al controlador global. En la segunda etapa se realizaba la planificación para cada una de las casas y, finalmente, en la tercera etapa el algoritmo decidía cómo satisfacer la demanda. Mohsenian-Rad y Leon-Garcia [47] desarrollaron un control de carga residencial para consumidores acogidos a programas *RTP* en el que el pago por la electricidad y el tiempo de espera para utilizar un determinado electrodoméstico se minimizaba teniendo en cuenta los precios que cambian dinámicamente. En primer lugar, para un determinado horizonte de tiempo, se realizaba la predicción de los precios de la electricidad, y a continuación se minimizaba una función objetivo que consideraba el pago total por la electricidad y el coste total por utilizar un determinado electrodoméstico después de la hora requerida. Mohsenian-Rad *et al.* [48] presentaron un modelo para la gestión de la demanda en programas *IBP* en el que, para un conjunto de consumidores residenciales, la planificación óptima del consumo de cada

consumidor se obtenía minimizando el coste de la energía mediante teoría de juegos. Conejo *et al.* [49] presentaron un modelo de respuesta de la demanda que minimizaba el coste de la energía consumida considerando los límites de variación de la carga, demanda horaria e incertidumbre en la predicción de los precios. Sianaki *et al.* [50] propusieron una metodología que analizaba la preferencia de los consumidores por utilizar un cierto electrodoméstico durante la hora de máximo consumo mediante un proceso Analítico Jerárquico (*Analytic Hierarchy Process*), utilizándose esta información para decidir qué electrodoméstico debe ser usado durante la hora de máximo consumo.

2.3.1 Influencia de la temperatura, el regulador de carga y la eficiencia culómbica del banco de baterías en el funcionamiento de los pequeños sistemas eólicos.

La Figura 7 muestra un sistema híbrido típico compuesto por una turbina eólica y un banco de baterías de plomo ácido, que satisface una determinada demanda de energía.

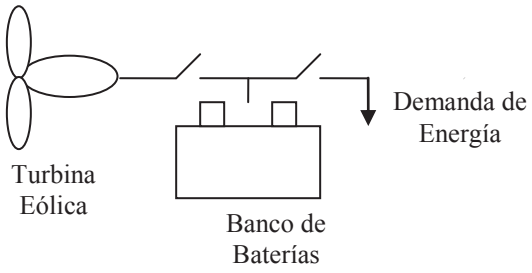

Figura 7. Sistema eólico con almacenamiento

Un componente de gran importancia en este tipo de sistemas es el controlador de carga, que tiene como principal objetivo proteger al banco de baterías contra condiciones de operación extremas como la sobrecarga y la sobredescarga, utilizando como indicador la tensión entre sus terminales. Cuando la tensión del banco de baterías alcanza el ajuste de nivel alto del regulador de carga, este asume que el banco de baterías está completamente cargado y desconecta el generador de energía (turbina eólica y/o paneles fotovoltaicos), mientras que cuando la tensión del banco de baterías alcanza el ajuste de nivel bajo del regulador, este asume que el banco de baterías está descargado y desconecta la carga. Basándose en resultados experimentales, Baring-Gould *et al.* [58] y Corbus *et al.* [59] demostraron que el regulador de carga puede tener un efecto importante sobre la habilidad del banco de baterías para almacenar energía. Corbus *et al* [59] analizando diferentes sistemas compuestos por una turbina eólica y un banco de baterías, y concluyeron que en sistemas con gran capacidad de generación eólica y poca capacidad de almacenamiento, la tensión del banco de baterías alcanza prematuramente

el ajuste de nivel alto del regulador de carga, y como consecuencia el aerogenerador se desconecta y el estado de carga del banco de baterías no alcanza el nivel adecuado. Este hecho se ilustra en la Figura 8, donde se observa que para un ajuste de nivel alto del regulador de carga de 2,25 V/celda, si el banco de baterías se carga con la corriente de carga en 5 horas (C/5), cuando la tensión alcanza 2,25 V el estado de carga del banco de baterías es del 45%. Se aprecia que a medida que se reduce la corriente de carga, se tarda más tiempo en alcanzar el ajuste del nivel alto del regulador, y por lo tanto el banco de baterías es capaz de aceptar más energía. Si el banco de baterías se carga con la corriente de carga en 8 horas (C/8), entonces el estado de carga será del 61%. Si la corriente de carga se reduce a la necesaria para cargar el banco en 10 horas (C/10), el estado de carga conseguido será del 65%; y finalmente, si el banco de baterías se carga con la corriente de carga en 20 horas (C/20), el estado de carga será del 78%.

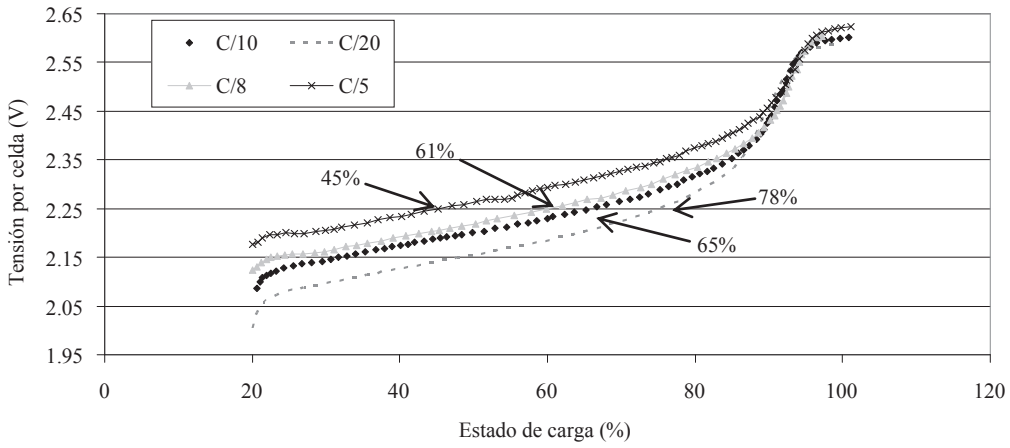

Figura 8. Tensión vs. Estado de carga en una batería de plomo ácido [59]

Por otro lado, la eficiencia culómbica del banco de baterías es otro factor que afecta significativamente a su capacidad para aceptar carga. La eficiencia culómbica varía considerablemente de acuerdo con el estado de carga, mostrando valores muy bajos para estados de carga altos. Esta pérdida de eficiencia está relacionada con las reacciones de gaseo que se producen en el banco de baterías durante la carga [60]. Stevens y Corey [61] analizaron varios sistemas fotovoltaicos, y concluyeron que la baja eficiencia culómbica en altos estados de carga podría dar lugar a una reducción substancial en la energía almacenada. Esta situación se produce porque un porcentaje elevado de la energía disponible se utiliza para satisfacer pérdidas en lugar de utilizarse para cargar el banco de baterías.

En [51] se muestra uno de los trabajos de investigación desarrollados durante la realización de esta tesis doctoral, en el que se utilizó una simplificación del modelo

general de la batería de plomo ácido propuesto por Copetti *et al.* [62,63], se presentó un modelo de un sistema híbrido compuesto por una turbina eólica y un banco de baterías capaz de considerar el efecto, en el funcionamiento general del sistema, del ajuste del nivel alto de tensión del regulador de carga, la eficiencia culómbica del banco de baterías y la temperatura ambiente. El efecto de estas variables se analizó mediante la simulación de un sistema instalado en Zaragoza, y los resultados de esta simulación se compararon con los obtenidos utilizando HOMER, que no considera el efecto del regulador de carga, la eficiencia culómbica ni la temperatura ambiente sobre la operación del sistema híbrido. En la Figura 9 se muestra la comparación entre las distribuciones de probabilidad del estado de carga en un sistema con 100Ah de capacidad en 10 horas, obtenidas utilizando HOMER y con el modelo presentado en [51]. Estos resultados muestran cómo el efecto conjunto de la pérdida de eficiencia culómbica y la operación del regulador de carga puede dificultar que el estado de carga del banco de baterías alcance valores altos. Sin embargo, los resultados obtenidos mediante HOMER sugieren una mayor probabilidad de obtener estados de carga elevados debido a que no considera la relación existente entre la eficiencia culómbica y el estado de carga, y tampoco tiene en cuenta la operación del regulador de carga ni el efecto de la temperatura.

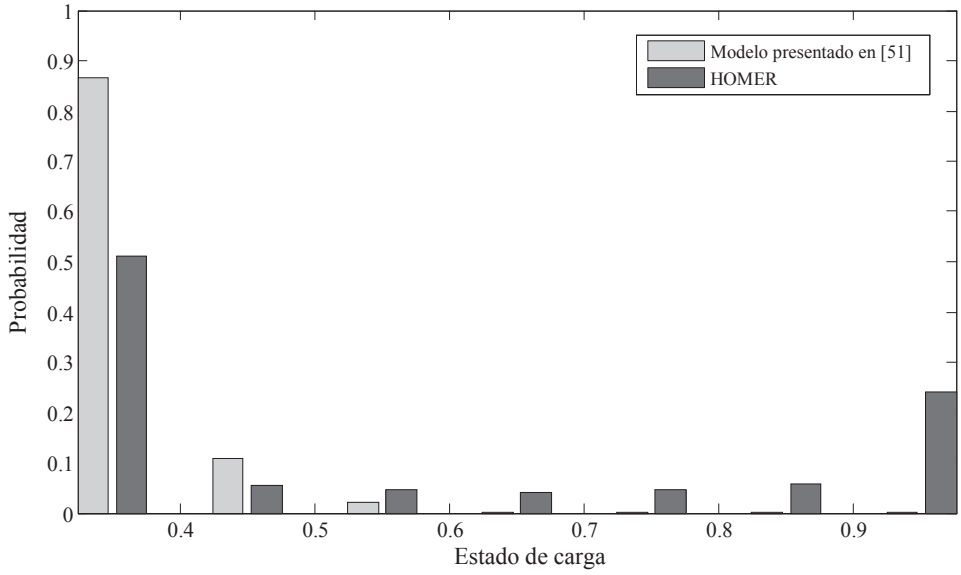

Figura 9. Comparación entre distribuciones de probabilidad del estado de carga (C_{10}=100Ah)

En la Figura 10 se muestra el comportamiento de la falta de fiabilidad (*Unreliability*) del sistema cuando se consideran capacidades del banco de baterías comprendidas entre 100Ah y 1000Ah. Considerando estos resultados, si se requiere un nivel de fiabilidad

del 90%, y no se consideran en la simulación factores como la operación del controlador de carga, ni la eficiencia culómbica y la temperatura ambiente, un banco de baterías con capacidad de 800Ah sería el adecuado. Sin embargo, si se consideran estos factores, el banco de baterías debería ser de 1000Ah. Esto podría dar lugar a que el nivel de fiabilidad del sistema, tras ser instalado, fuese menor que el calculado al utilizar HOMER. Es decir, si se instala un sistema analizado con HOMER, el nivel de fiabilidad real será menor que el esperado, por lo que será necesario incrementar la capacidad del banco de baterías. En el ejemplo que se ha mostrado el aumento debería ser del 25%.

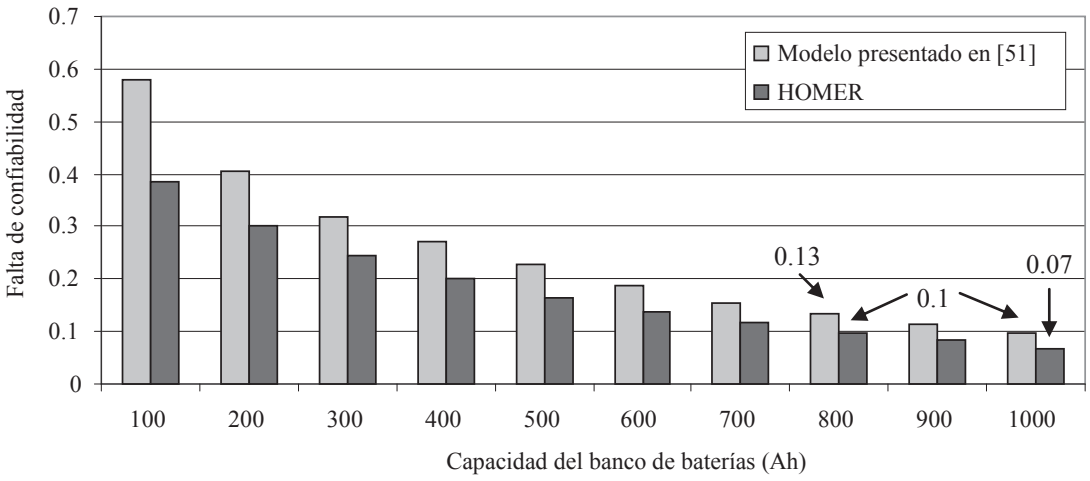

Figura 10. Falta de confiabilidad para diferentes capacidades del banco de baterías

El modelo matemático de un sistema típico, presentado en [51], compuesto por una turbina eólica y un banco de baterías, se amplió incorporando el modelo de un generador fotovoltaico compuesto por uno o más paneles fotovoltaicos, y el modelo de un inversor en el que se considera la eficiencia variable en función de la potencia de salida. En [52] este modelo se utilizó para desarrollar una metodología, basada en un algoritmo genético, para el dimensionado óptimo de este tipo de sistemas. Con esta metodología es posible encontrar la combinación óptima de componentes que garantice un determinado nivel de fiabilidad, considerando factores de gran importancia, como son la eficiencia culómbica, la operación del regulador de carga y la temperatura ambiente. La metodología presentada en este trabajo se ilustró mediante el diseño de un sistema localizado en los Países Bajos. Se consideraron, como posibles elementos para el diseño, las turbinas eólicas cuya curva de potencia se muestra en la Figura 11, un generador fotovoltaico con capacidad comprendida entre 175W y 4.375kW, un banco de baterías cuyas celdas podían tener una capacidad comprendida entre 200Ah y

3000Ah (con un máximo de 10 celdas conectadas en paralelo), y un inversor de 900W. Teniendo en cuenta otras variables relacionadas con aspectos económicos, como los costes de capital y las tasas de interés e inflación, se obtuvo la configuración de componentes que minimizaba el coste neto considerando 35 años de vida útil del sistema, y garantizando un nivel de fiabilidad del 90%. Una vez transcurridas 10 generaciones del algoritmo genético, la configuración óptima encontrada constaba de 11 paneles fotovoltaicos de 175W de potencia cada uno, una turbina eólica de 1kW y un banco de baterías de 1000Ah. En la Figura 12 se muestra la evolución del coste neto actualizado durante cada generación del proceso de optimización.

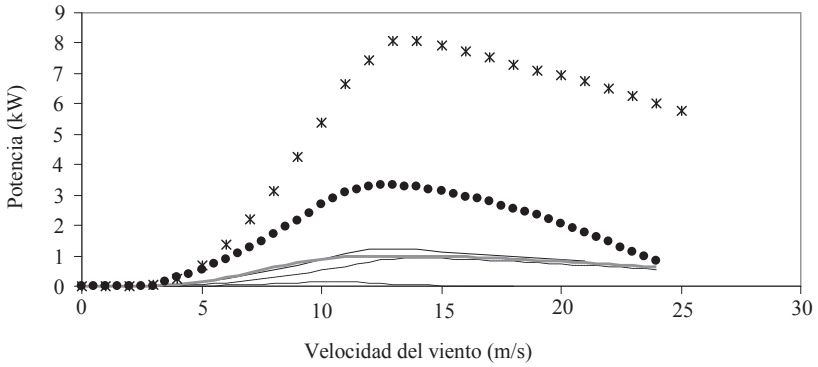

Figura 11. Curvas de potencia de diferentes turbinas eólicas

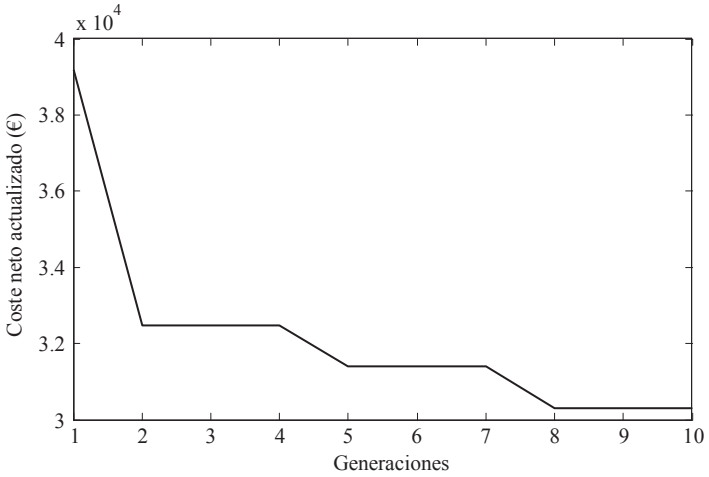

Figura 12. Evolución del coste neto actualizado durante la optimización

Como se ha podido observar, el banco de baterías es uno de los componentes más importantes de un sistema híbrido. El banco de baterías no solo afecta de forma importante al balance energético del sistema sino que también afecta de forma determinante a la rentabilidad del mismo. Esto se debe a que el banco de baterías es uno

de los componentes más costosos del sistema y a que su tiempo de vida operativa es una variable difícil de determinar, ya que depende en gran medida de las condiciones meteorológicas a las que el sistema híbrido está sometido. Por lo tanto, si no se tiene certeza del número de veces que será necesario reemplazar el banco de baterías, podrían obtenerse costes no previstos muy elevados al final de la vida útil del sistema, viéndose afectada su rentabilidad.

2.3.2 Análisis y efecto de la incertidumbre en la vida útil del banco de baterías, la variabilidad del viento y la demanda en pequeños sistemas eólicos.

Existen varios trabajos en los que se han desarrollado modelos con el fin de determinar el tiempo de vida del banco de baterías. Los tres tipos de modelos que se han desarrollado son:

- Los modelos físico-químicos (*Physico-chemical ageing models*). Los modelos físico-químicos se basan en un conocimiento detallado de los factores físicos y químicos relacionados con el proceso de envejecimiento.

- Los modelos *Ah* (Ampere-hora) ponderados (*Weighted Ah ageing models*). Los modelos *Ah* ponderados asumen que la vida de la batería depende proporcionalmente de los *Ah* descargados del banco de baterías. Los *Ah* que han sido descargados del banco de baterías se multiplican por un factor de ponderación que se ajusta de acuerdo con las condiciones operativas. Se dice que el banco de baterías ha alcanzado su vida útil cuando los *Ah* ponderados totales han excedido un determinado valor que se ha obtenido a partir de las condiciones de operación nominales.

- Los modelos orientados por eventos (*Event-oriented ageing models*). Los modelos orientados por eventos estiman el tiempo de vida de la batería identificando condiciones de operación extremas [64].

Utilizando la experiencia e información proveniente de expertos, Svoboda *et al.* [65] desarrollaron diferentes categorías de operación típicas, para el banco de baterías, basadas en la determinación de factores de estrés relacionados con la magnitud de la corriente de descarga, el tiempo transcurrido entre recargas sucesivas, la cantidad de *Ah* descargados en condiciones de bajo estado de carga, y el tiempo durante el cual el banco de baterías permanece en esta condición. En [53] se han utilizado estas

categorías de operación para evaluar cualitativamente el desempeño del banco de baterías de un sistema híbrido situado en Zaragoza, siendo este trabajo parte de esta tesis doctoral. En la Figura 13 se muestra la serie temporal del estado de carga que se utilizó para determinar la magnitud de los diferentes factores de estrés necesarios con el fin de determinar la categoría de operación del banco de baterías, que en este caso se caracterizaba por mantener un alto estado de carga durante la mayor parte del tiempo. Con esa serie temporal del estado de carga en ocasiones se producían descargas a altas corrientes y recargas frecuentes, lo que daba lugar a un elevado riesgo de corrosión de la rejilla positiva, un elevado riesgo de pérdida de agua y un alto riesgo de pérdida de masa activa, sin embargo existía un muy bajo riesgo de sulfatación irreversible o degradación de la masa activa, así como de la polarización inversa de la célula, y de la estratificación o congelación del electrolito [65].

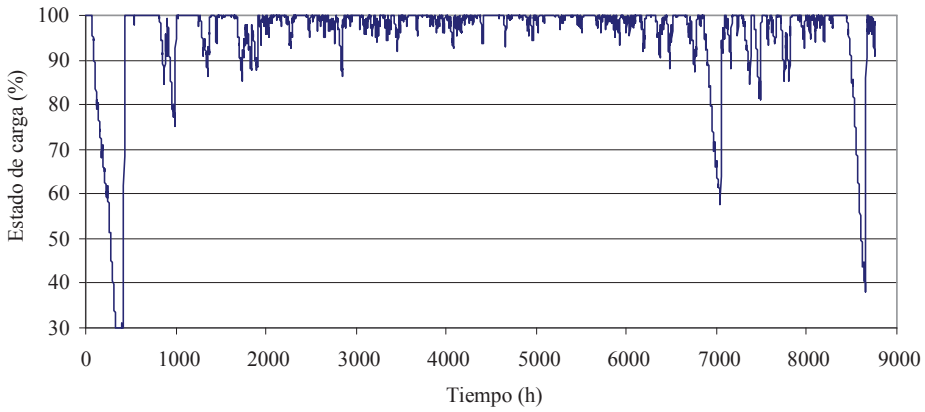

Figura 13. Serie temporal del estado de carga

El modelo *Ah*, sin considerar los factores de ponderación, ha sido implementado en muchas herramientas de simulación y optimización de sistemas híbridos. En [66] se validó experimentalmente este modelo de envejecimiento considerando baterías de plomo ácido con placas planas OGi y con placas tubulares OPzS bajo perfiles de generación eólica y fotovoltaica. Bajo condiciones de generación eólica, los resultados mostraron un 16,7% de error en la estimación de la vida de la batería de placas planas OGi y un 17,5% de error en la estimación de la vida de la batería de placas tubulares OPzS. Utilizando estos resultados, en [51] el modelo de envejecimiento *Ah*, sin considerar los factores de ponderación, se incorporó al modelo probabilístico, basado en la técnica de simulación por Monte Carlo, de un sistema híbrido similar al que se muestra en la Figura 7. Este modelo incorpora la variabilidad del recurso eólico

mediante un modelo Auto Regresivo de Media Móvil que considera las principales características de las series temporales de viento, como son la forma no Gaussiana de su distribución de probabilidad, su característica no estacionaria y su autocorrelación de alto orden. Además, este modelo considera la incertidumbre relacionada con el perfil de la demanda. Utilizando este modelo probabilístico, en [51] se estudió el efecto, en el coste neto actualizado del sistema, de la incertidumbre en la determinación de la vida útil de la batería. Como resultado se obtuvo que un 17,5% de incertidumbre en la vida del banco de baterías da lugar a, aproximadamente, un 12% de incertidumbre en el coste neto actualizado. En la Figura 14 se muestra el valor esperado del coste neto actualizado con su correspondiente grado de incertidumbre para distintas capacidades del banco de baterías y potencia nominal de la turbina eólica, considerando un nivel de significación del 1%.

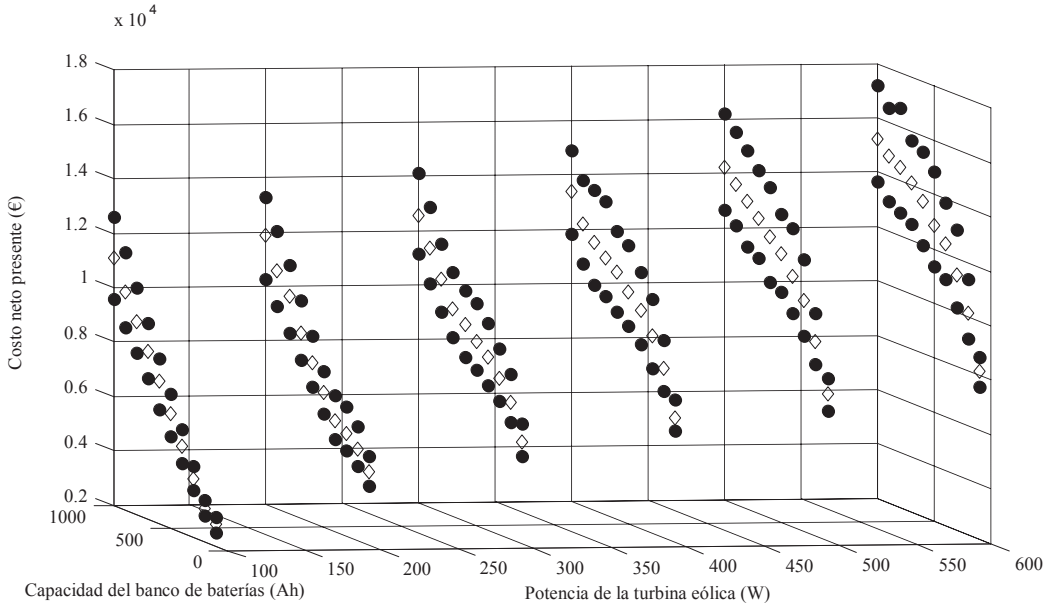

Figura 14. Valor esperado del costo neto presente

La incertidumbre en el grado de fiabilidad en un sistema similar al mostrado en la Figura 7 está directamente relacionada con la capacidad del banco de baterías, con la potencia nominal de la turbina eólica, y con las condiciones meteorológicas de la localidad donde se pretende instalar el sistema. La Figura 15 muestra los resultados obtenidos del análisis de la fiabilidad para distintas capacidades del banco de baterías y potencia nominal de la turbina eólica, considerando un nivel de significación del 1%.

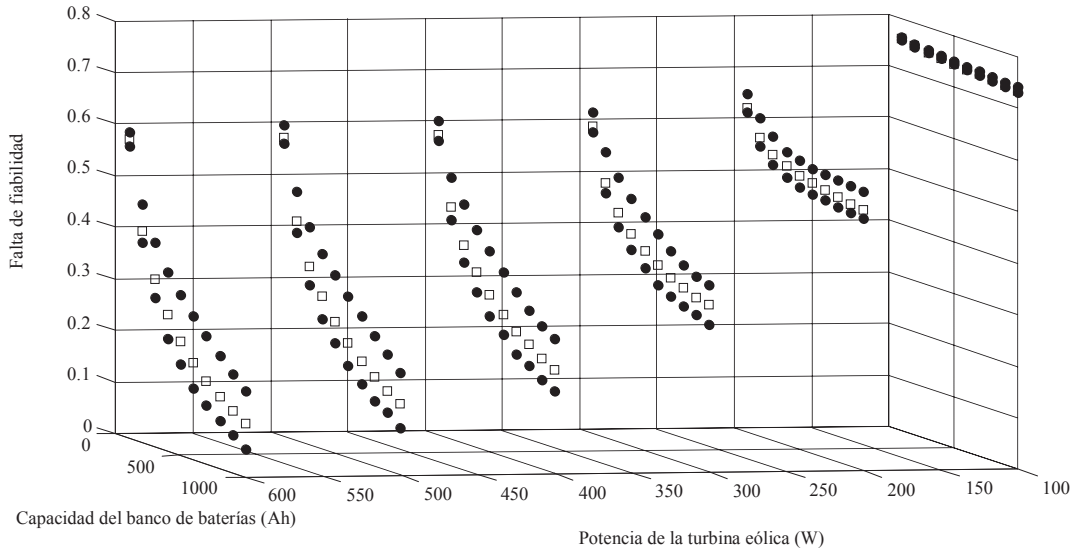

Figura 15: Valor esperado del análisis de fiabilidad.

Generalmente aquellos sistemas que demandan mucha energía o que requieren de un gran nivel de fiabilidad incluyen entre sus componentes un generador convencional, que puede proveer potencia de forma segura y controlable, pero que debido a los altos precios del combustible producen a lo largo de la vida útil del sistema costes muy elevados. Por otro lado, en este tipo de sistemas el banco de baterías juega un papel importante, ya que permite reducir el número de horas de operación del generador convencional almacenando la energía excedente que proviene de las fuentes de energías renovables. El modelo probabilístico de un sistema híbrido compuesto por una turbina eólica y un banco de baterías que se había presentado en [51], se mejoró en [54] mediante la incorporación de paneles fotovoltaicos, un generador convencional y un inversor que permite considerar demandas de energía en corriente alterna. Además, el modelo probabilístico se amplió incluyendo la incertidumbre del recurso eólico relacionada con las variaciones a largo plazo, la incertidumbre en la producción del generador fotovoltaico y la incertidumbre en los costes del combustible.

2.3.3 Influencia de la temperatura, el regulador de carga y la eficiencia culómbica del banco de baterías en sistemas híbridos con generación convencional.

El efecto de la eficiencia culómbica y de la operación del regulador de carga en el funcionamiento de un sistema provisto de un generador fotovoltaico, un aerogenerador, un banco de baterías y un generador convencional, se analizaron en un sistema localizado en Zaragoza. Los resultados se compararon con los obtenidos utilizando HOMER, que, como se ha explicado anteriormente, no considera ninguno de estos

factores. Los resultados comparativos entre las horas de operación del generador convencional, el consumo de combustible y el coste neto actualizado, se muestran en las Figuras 16, 17 y 18, respectivamente. Considerando este análisis comparativo, existen importantes diferencias entre la simulación obtenida mediante ambos modelos cuando la configuración del sistema tiene baja capacidad de almacenamiento. En sistemas con pequeña capacidad de almacenamiento las corrientes de carga son altas, la tensión correspondiente al nivel alto del regulador de carga se alcanza prematuramente y, por lo tanto, los generadores renovables se desconectan, produciéndose un bajo estado de carga del banco de baterías, y un incremento significativo en el número de horas de operación y en el consumo de combustible del generador convencional, incrementándose el coste neto actualizado real en comparación con los resultados obtenidos utilizando HOMER. La máxima diferencia en los resultados obtenidos con ambos modelos se produce cuando el banco de baterías tiene una capacidad de 100Ah. Para esta configuración la diferencia entre las horas de operación del generador convencional, su consumo de combustible y el coste neto actualizado, son de, aproximadamente, 33%, 31% y 31%, respectivamente. Cuando la capacidad del banco de baterías se incrementa, se obtienen resultados bastante similares para los dos modelos, ya que en este caso las corrientes de carga son reducidas y, en consecuencia, el banco de baterías puede aceptar más carga y la tensión correspondiente al nivel alto del regulador no se alcanza prematuramente.

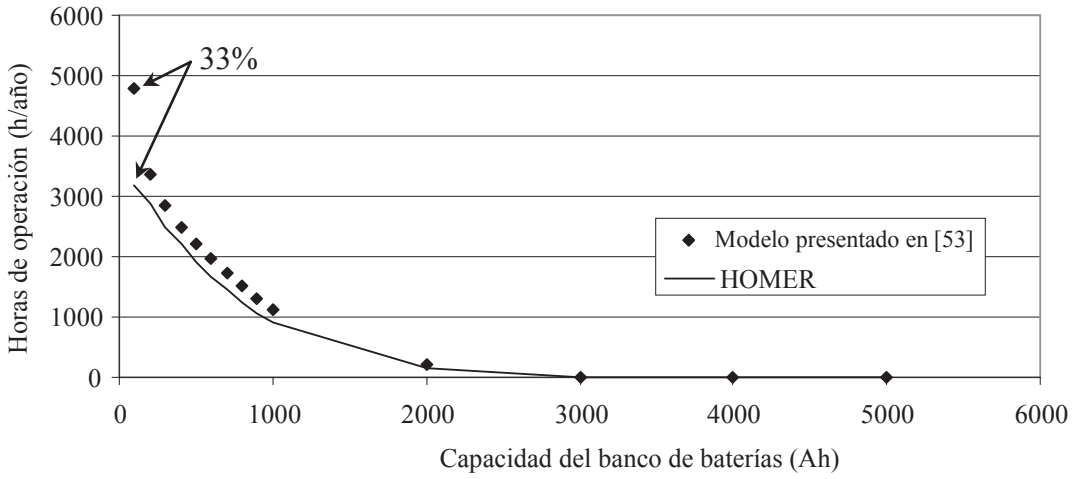

Figura 16. Comparación entre las horas de operación del generador convencional

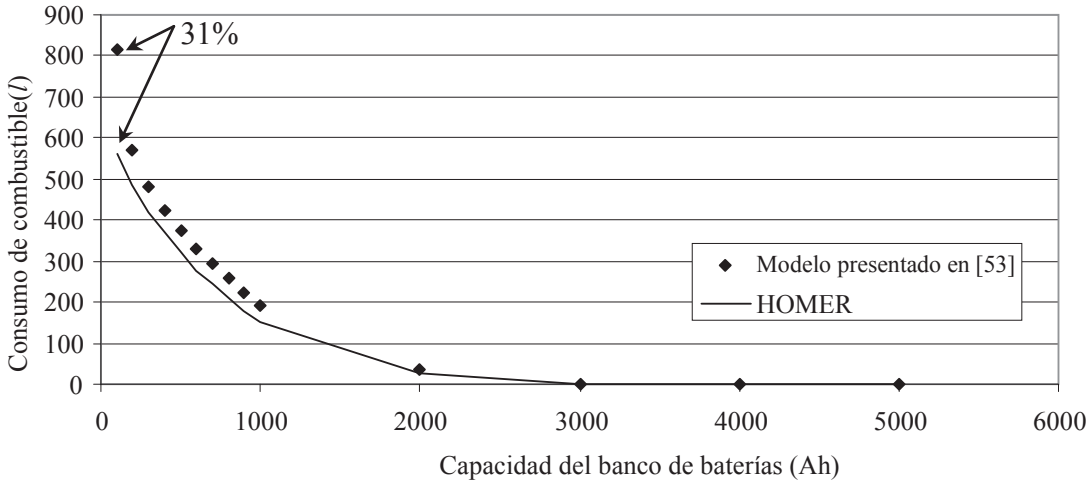

Figura 17. Comparación entre el consumo de combustible

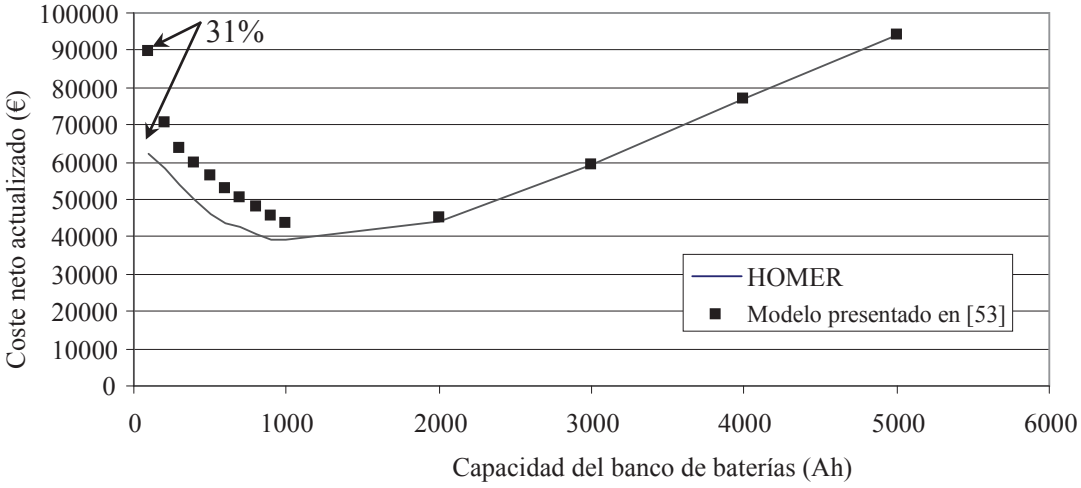

Figura 18. Comparación entre el coste neto actualizado

2.3.4 Efecto de la incertidumbre en la vida útil del banco de baterías y los precios del combustible en sistemas híbridos con generación convencional.

En otro caso de estudio, utilizando el modelo probabilístico desarrollado, se analizó el efecto de la incertidumbre del recurso eólico relacionada con las variaciones a largo plazo, la incertidumbre en la producción del generador fotovoltaico, la incertidumbre en los costes del combustible y la incertidumbre en el perfil de demanda de energía en un sistema localizado en Zaragoza que previamente se había dimensionado. En la Figura 19 se muestra el valor esperado del coste neto actualizado con su correspondiente intervalo de incertidumbre, calculado considerando un nivel de significación del 10%. Cuando la configuración del sistema híbrido tiene baja capacidad de almacenamiento

(alrededor de 100Ah), la incertidumbre en el coste neto actualizado es del 7%, estando principalmente influenciada por la incertidumbre en los precios del combustible. A medida que la capacidad del banco de baterías aumenta, la incertidumbre en el coste neto actualizado está influenciada conjuntamente tanto por la incertidumbre en el precio del combustible como por la incertidumbre en la determinación de la vida útil del banco de baterías, alcanzando una incertidumbre del 28% para una configuración con capacidad de almacenamiento de 1000Ah. Finalmente, la incertidumbre en el coste neto actualizado de sistemas con muy alta capacidad de almacenamiento está básicamente influenciada por la incertidumbre en la determinación de la vida útil del banco de baterías, alcanzando alrededor del 20% para una configuración con capacidad de almacenamiento de 5000Ah.

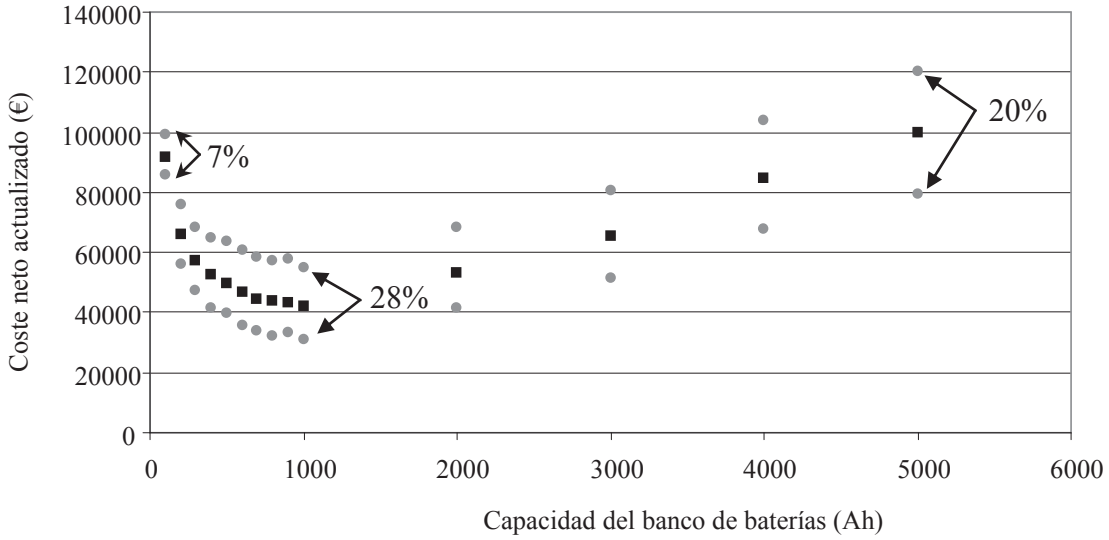

Figura 19. Valor esperado del coste neto actualizado.

2.3.5 Predicción de velocidades horarias de viento y su aplicación en estrategias de gestión de la demanda en sistemas aislados.

La predicción ha sido durante mucho tiempo una herramienta muy útil en la gestión de sistemas de energía eléctrica con una elevada penetración de energías renovables. Esta herramienta es también útil en la gestión de la demanda de consumidores residenciales, los cuales, haciendo uso de la información proveniente de la predicción, están preparados para hacer un uso adecuado de sus electrodomésticos en función de su propio beneficio o ahorro económico. La aplicación de esta idea a un sistema aislado de la red eléctrica provisto de generación eólica requiere del conocimiento de una técnica de predicción de potencia eólica o, en su defecto, de velocidad de viento. El modelo

Auto Regresivo de Media Móvil es un método estadístico que ha sido frecuentemente referenciado en la literatura como una técnica de predicción de velocidades horarias de viento a corto plazo. En [55] se describen en detalle los procesos de Transformación y Estandarización de la serie temporal de viento, así como la estimación de parámetros del modelo Auto Regresivo de Media Móvil y su correspondiente verificación estadística. También se describe el procedimiento necesario para la predicción de velocidades horarias de viento, incorporado una transformación de probabilidad en pasos discretos con el fin de considerar la forma de la distribución de probabilidad de la serie temporal de viento bajo análisis. Utilizando datos históricos de tres estaciones meteorológicas ubicadas en los Países Bajos, se realizó un análisis comparativo entre el error de predicción obtenido utilizando el modelo Auto Regresivo de Media Móvil y una red neuronal entrenada mediante el algoritmo de Retro-Propagación para horizontes de predicción entre 1 y 10 horas. De acuerdo con los resultados obtenidos, en algunos casos el modelo Auto Regresivo de Media Móvil mejoró los resultados alcanzados mediante la red neuronal en, al menos, un 17,71%.

La metodología descrita en [55] para la predicción de velocidades horarias de viento puede ser utilizada en el desarrollo de una estrategia que permita a los usuarios utilizar adecuadamente los recursos energéticos disponibles. Supóngase que se desea sugerir al usuario del sistema híbrido de la Figura 20 cómo podría usar sus electrodomésticos para aprovechar al máximo el recurso eólico disponible en su localidad.

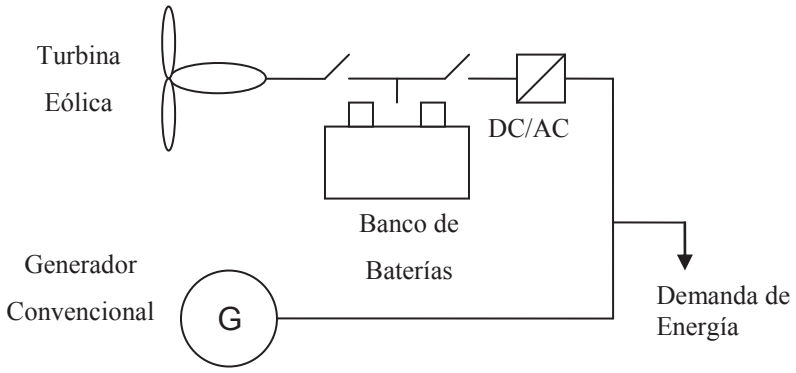

Figura 20. Sistema híbrido típico.

La demanda de energía del sistema híbrido bajo estudio podría ser gestionada para reducir el consumo diario de energía proveniente del generador convencional. Esto es posible si se utilizan las cargas controlables del sistema cuando se prevé que la velocidad del viento será alta. Como aplicación de esta idea, se desarrolló una estrategia

de gestión de la demanda que utiliza la predicción de velocidades promedio horarias de viento en un horizonte de 24 horas [56]. Usando esta predicción es posible determinar la hora a la que cada electrodoméstico debe ser utilizado con el objetivo de minimizar la energía suplida por las fuentes controlables de energía, que en este caso son el generador convencional y el banco de baterías. Esta idea se analizó utilizando como ejemplo un sistema localizado en Zaragoza con el perfil de carga que se muestra en la Figura 21.

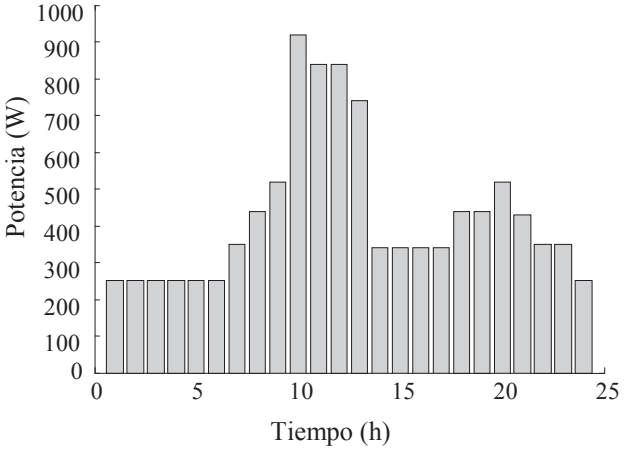

Figura 21. Perfil de carga típico para el caso de estudio

En el caso que se estudió se consideró que el usuario disponía de dos cargas controlables que frecuentemente se utilizan entre las 7:00 y las 18:00 horas, y entre la 1:00 y las 24:00 horas, consumiendo 400W durante 4 horas y 100W durante 6 horas, respectivamente. El sistema disponía de una turbina eólica de 3500W, un generador diesel de 1kW, un inversor de 1kW y un banco de baterías de 1000Ah. A modo de ejemplo del funcionamiento del sistema al aplicar la estrategia de gestión de la demanda propuesta, las Figuras 22 y 23 muestran, para los días 5 y 6 de agosto de 2005, que la curva de carga se desplaza hacia las horas en las que la potencia eólica alcanza valores elevados, y en consecuencia la energía suplida por el generador convencional y el banco de baterías se minimiza. Las Figuras 24 y 25 muestran el efecto del desplazamiento de la carga en el estado de carga del banco de baterías y en el número de horas de operación del generador diesel. En general la estrategia de gestión de la demanda propuesta permite mejorar, en comparación con el caso en el que el perfil de carga se mantuviese rígido, el uso de la potencia disponible del viento, aumentando el estado de carga del banco de baterías y reduciendo el número de horas de operación del generador diesel.

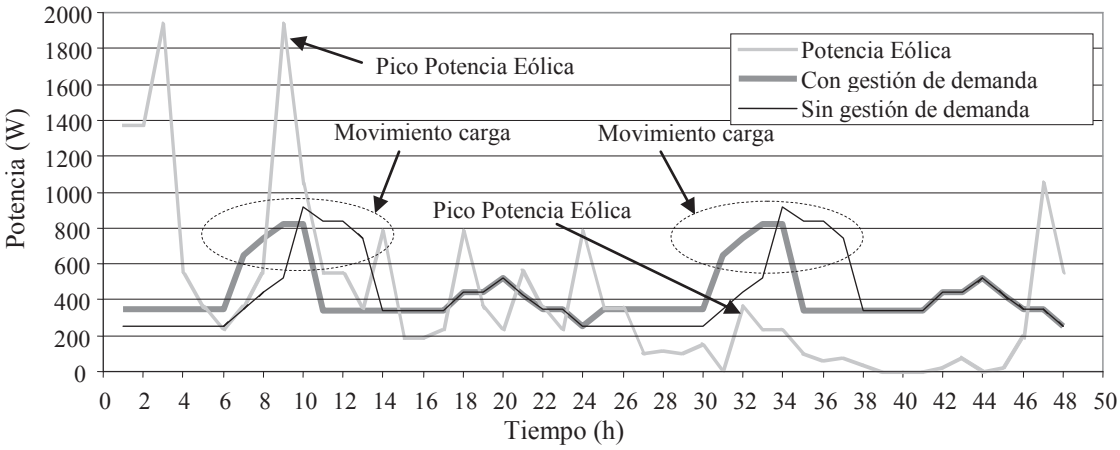

Figura 22. Potencia eólica y perfiles de carga para los días 5 y 6 de agosto de 2005

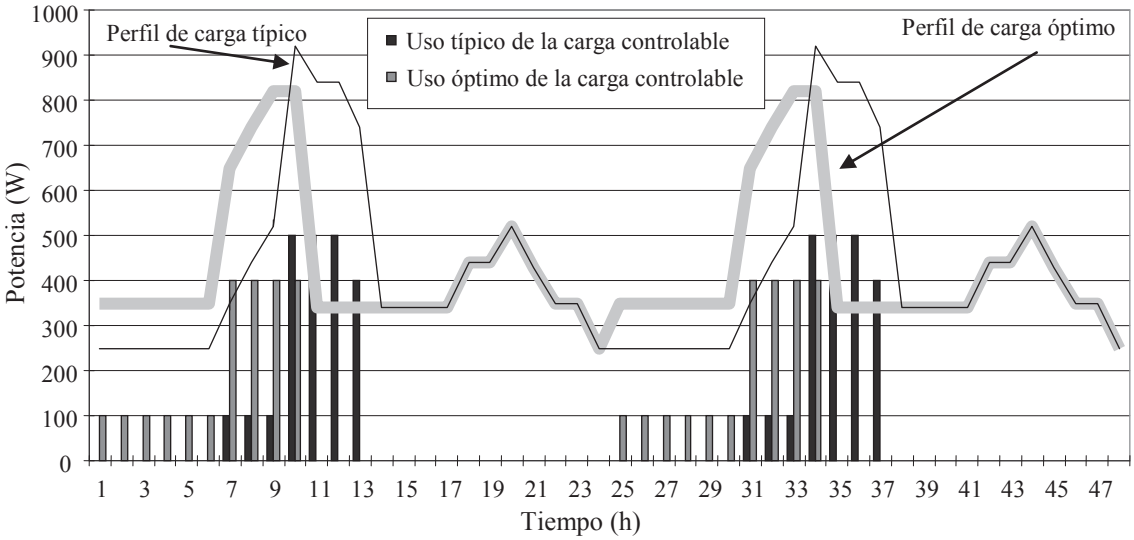

Figura 23. Gestión de la carga controlable para los días 5 y 6 de agosto de 2005

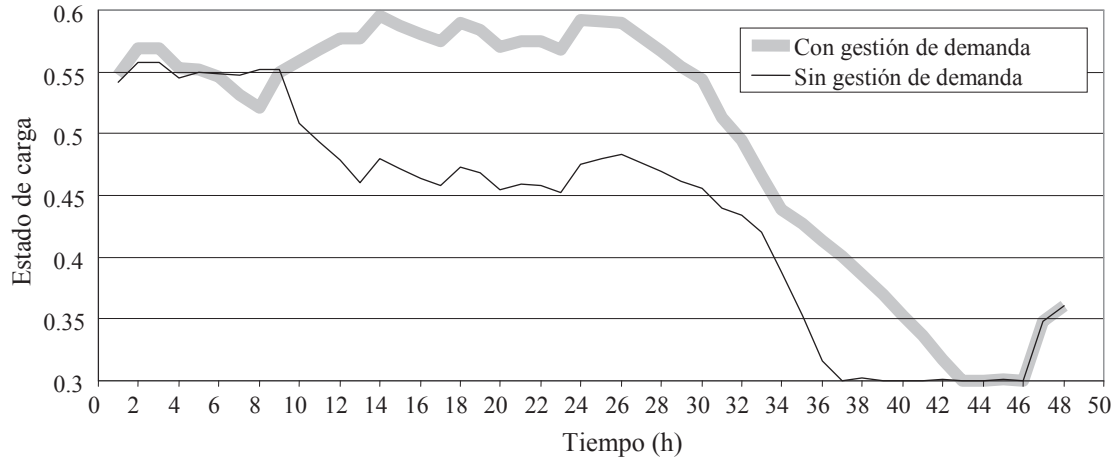

Figura 24. Estado de carga del banco de baterías para los días 5 y 6 de Agosto de 2005

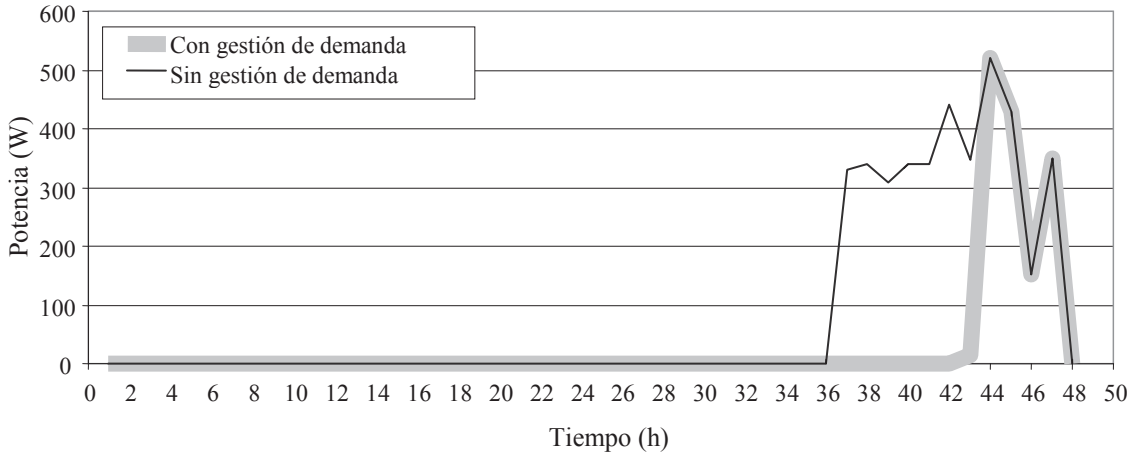

Figura 25. Potencia suministrada por el generador diesel los días 5 y 6 de Agosto de 2005.

2.3.6. Optimización de la gestión de la demanda en sistemas residenciales conectados a la red eléctrica.

Teniendo en cuenta el auge que tiene hoy en día el concepto de la nueva Red Eléctrica Inteligente (*Smart Grid*), es posible que en un futuro los usuarios residenciales compren la energía eléctrica a precios que varíen dinámicamente a lo largo del día, en función de los costes de generación. La implementación de la Red Eléctrica Inteligente puede permitir que los costes de generación se vean reflejados directamente en el precio al que los usuarios residenciales adquieren la energía eléctrica. Para el logro de este objetivo es necesario que la futura Red Eléctrica Inteligente permita la comunicación directa entre las empresas de distribución de energía eléctrica y los consumidores. Este tipo de comunicación puede llevarse a cabo mediante el uso de redes de ordenadores y mediante la Interfaz de Servicios de Energía (ISE), que es la interfaz que establece la comunicación entre el distribuidor de energía eléctrica y los consumidores. Esta interfaz puede recibir los precios horarios de la energía provenientes de la empresa distribuidora e informar al consumidor. Utilizando un Sistema de Gestión de la Energía (SGE) conectado a la Interfaz de Servicios de Energía, los consumidores pueden decidir cómo utilizar sus electrodomésticos en respuesta a las señales de precios que reciban.

A partir del planteamiento descrito, en [57] se desarrolló una técnica de Adaptación de la Demanda que, usando predicciones de los precios de la energía, la producción de potencia de las fuentes renovables y la demanda, además del poder adquisitivo de los consumidores, determinaba la manera óptima en la que estos deben utilizar sus electrodomésticos. Para ello se consideró una casa equipada con un Medidor de Energía

Inteligente (*Smart Meter*), una turbina eólica, un generador fotovoltaico, varios electrodomésticos y un vehículo eléctrico.

En la Figura 26 se muestra la estrategia de gestión de la demanda propuesta, donde a través de la Interfaz de Servicios de Energía (conectada a una pantalla), se le informa al usuario del valor actual y de la predicción para las próximas 24 horas de los precios de la electricidad, del consumo de energía y de la potencia de los generadores renovables. Posteriormente, utilizando la planificación del usuario para el día siguiente, expresada mediante su poder adquisitivo y por el conjunto de predicciones indicadas anteriormente, el Sistema de Gestión de la Energía (SGE) puede determinar, estableciendo la óptima negociación entre la empresa distribuidora y el usuario, el uso que este debe hacer de sus electrodomésticos durante el día siguiente. Una vez realizado este proceso de optimización, mediante la Interfaz de Servicios de Energía, el Sistema de Gestión de la Energía informa al usuario acerca de cuánto podría reducir su factura de electricidad si se lleva a cabo el uso sugerido de los electrodomésticos. De esta manera se incentiva al usuario a hacer uso de sus electrodomésticos de forma racional teniendo en cuenta su poder adquisitivo.

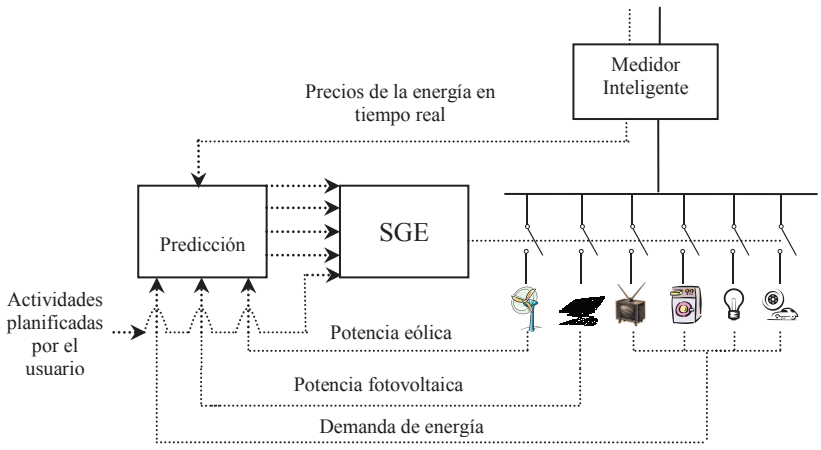

Figure 26. Casa inteligente y su estrategia para la gestión de la demanda.

El análisis de esta estrategia de gestión de la demanda se realizó considerando un consumidor residencial durante un día típico de verano en la ciudad de Zaragoza, en una casa inteligente equipada con un televisor, un sistema de aire acondicionado, un ordenador, varias lámparas, otros electrodomésticos de uso cotidiano y un vehículo eléctrico. En nuestro análisis se han considerado dos posibles situaciones. En la primera situación el usuario, de acuerdo a su poder adquisitivo, indica en el día previo a nuestro análisis que podría pagar 1 c€/kWh por ver la televisión entre las 14:00 y las 23:00

horas, 10 c€/kWh por usar el aire acondicionado entre las 13:00 y las 22:00 horas durante 5 horas, 10 c€/kWh por usar el ordenador entre las 9:00 y las 20:00 horas, 10 c€/kWh por usar las lámparas entre las 21:00 y las 23:00 horas, 10 c€/kWh por usar los otros electrodomésticos durante las próximas 24 horas, y 5 c€/kWh por usar el vehículo eléctrico durante 5 horas en cualquier momento del día siguiente.

En la Figura 27 se muestran los valores predichos y actuales de los precios de la energía y la temperatura ambiente para el día típico de verano bajo estudio.

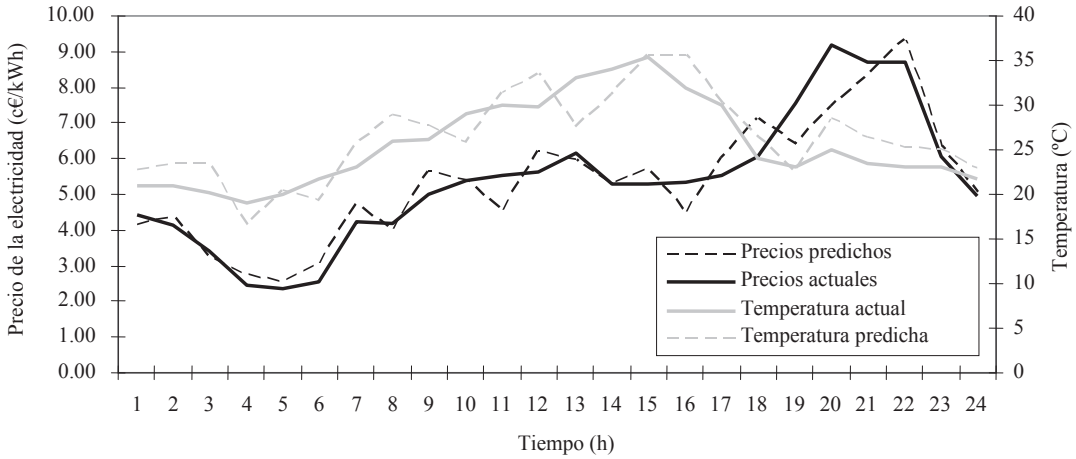

Figura 27. Precios de la energía eléctrica y temperatura ambiente.

Habitualmente los residentes de esta casa utilizan el aire acondicionado entre las 18:00 y las 22:00 horas, ya que, asumiendo que esta casa tiene un buen aislamiento térmico, el aire acondicionado podría utilizarse durante las horas del día en las que los precios de la electricidad son bajos. En este sentido, en la Figura 28 se muestra el uso recomendado para este electrodoméstico.

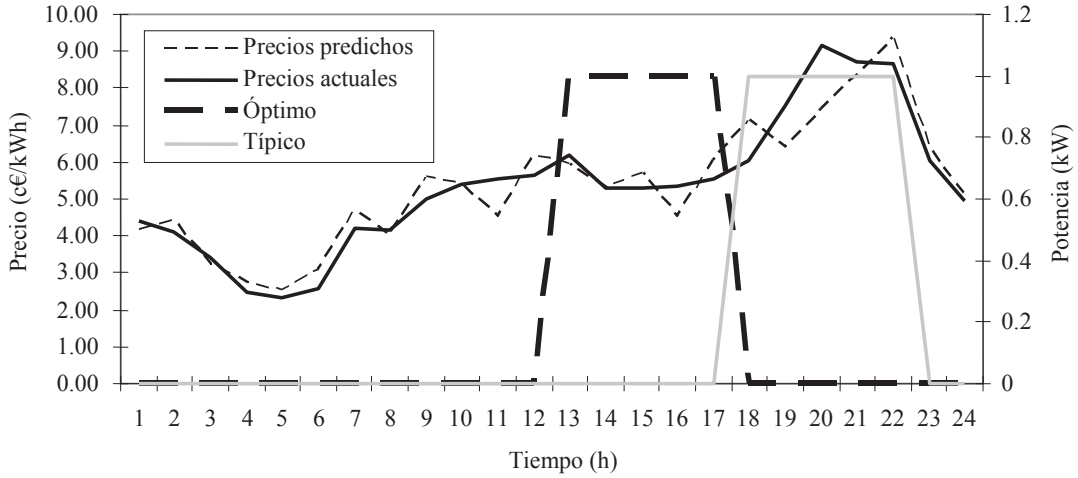

Figura 28. Comparación entre el uso típico y óptimo del aire acondicionado.

El usuario del vehículo habitualmente viaja entre las 8:00 y las 13:00 horas. Sin embargo, en su planificación para este día específico el usuario ha expresado flexibilidad en su uso, siendo necesario un grado de autonomía correspondiente a un estado de carga (*EC*) del banco de baterías del vehículo de, al menos, el 60%. La Figura 29 muestra los resultados al aplicar la estrategia de gestión de la demanda al uso del vehículo eléctrico. Nótese que si el usuario comienza su viaje a las 8:00 (*EC*=61,7%) y regresa a las 13:00 horas (*EC*=50%), la electricidad necesaria para recargar el banco de baterías se adquirirá cuando su precio es elevado, mientras que si el usuario comienza su viaje a las 19:00 (*EC*=77.7%) y regresa a las 23:00 horas, la autonomía del vehículo es mayor y el banco de baterías se recarga cuando los precios de la energía son más bajos.

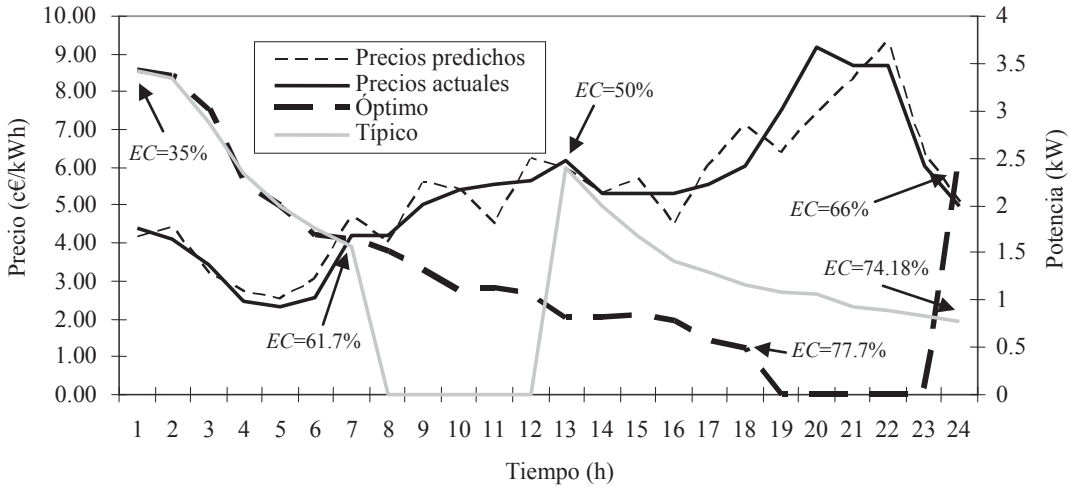

Figura 29. Ilustración del uso óptimo del vehículo eléctrico en la primera situación.

Considerando los precios horarios mostrados previamente en la Figura 27, el usuario ha especificado que puede pagar 1 c€/kWh por utilizar el televisor entre las 14:00 y las 23:00 horas, siendo este un valor muy bajo para el coste de la electricidad, por lo que la estrategia de gestión de la demanda recomienda no utilizar el televisor. La Figura 30 muestra la comparación entre las curvas de demanda típica y óptima para esta situación, observándose que es posible obtener una reducción en la factura de electricidad de, aproximadamente, un 22%.

En otra situación que se estudió, el usuario comunica en su planificación la necesidad de utilizar el vehículo entre las 8:00 y las 13:00 horas pagando 5 c€/kWh por la energía eléctrica requerida. En esta situación no se expresa flexibilidad alguna en el uso del

vehículo eléctrico. Las especificaciones de uso para los otros electrodomésticos permanecen iguales a las de la situación anterior. La Figura 31 muestra el uso sugerido por la estrategia de gestión de la demanda bajo estas condiciones, que coincide con los requerimientos del usuario debido a que este puede pagar la suficiente cantidad de dinero por la energía necesaria para realizar el viaje en el momento solicitado y recargar el banco de baterías del mismo posteriormente.

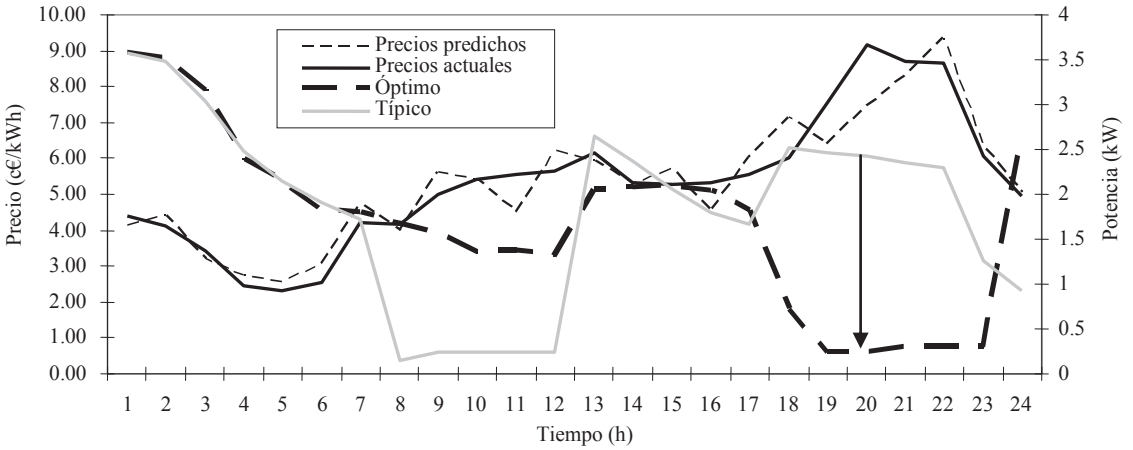

Figura 30. Comparación entre las curvas de demanda típica y óptima en la primera situación.

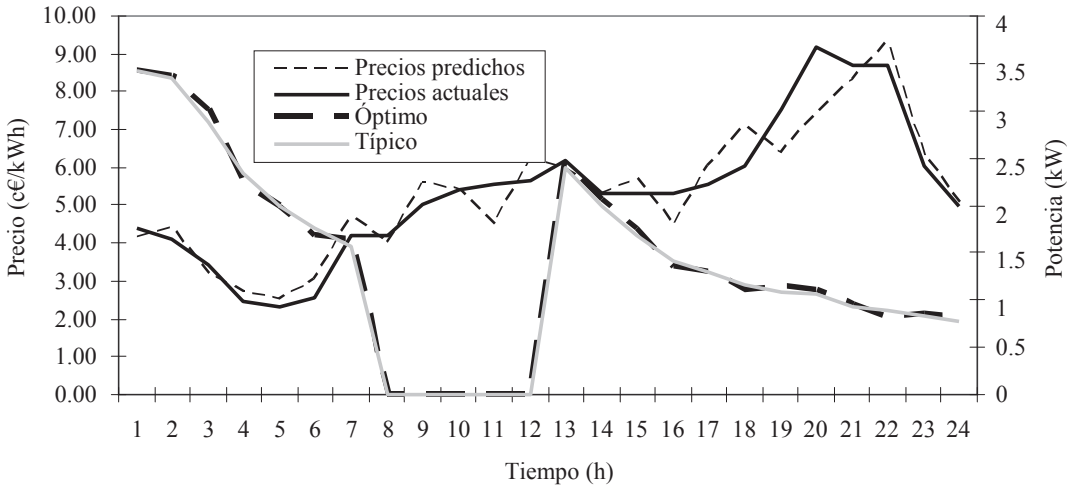

Figura 31. Ilustración del uso óptimo del vehículo eléctrico en la segunda situación.

La Figura 32 muestra la comparación entre las curvas de demanda típica y óptima para esta situación, observándose que es posible obtener una reducción en la factura de la electricidad de, aproximadamente, un 8%.

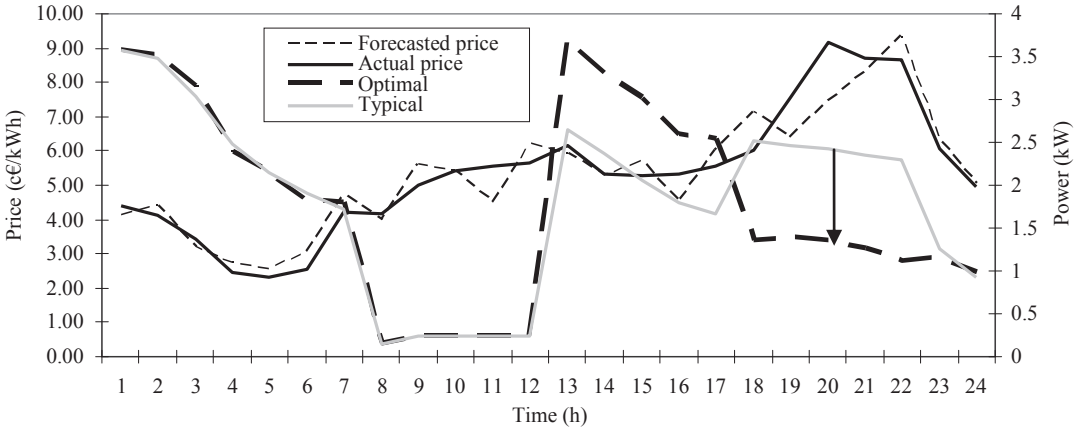

Figura 32. Comparación entre las curvas de demanda típica y óptima en la segunda situación.

2.4 Conclusiones

En esta tesis doctoral se han analizado, de forma detallada, los principales aspectos relacionados con el funcionamiento de los sistemas eléctricos aislados y conectados a la red eléctrica basados en fuentes de energía renovable. En lo referente al análisis de los sistemas aislados de la red eléctrica, se ha analizado el efecto de la eficiencia culómbica y del regulador de carga en la fiabilidad de los sistemas eólicos con baterías. También se ha tratado la estimación de las horas de operación, consumo de combustible y coste neto actualizado de los sistemas que utilizan como respaldo un generador convencional. Por otra lado, se ha desarrollado un modelo probabilístico que permite considerar la incertidumbre existente en la estimación de la vida del banco de baterías, la incertidumbre asociada a los precios del combustible, la producción del generador fotovoltaico, el perfil típico de carga, así como la variabilidad de los recursos eólico y solar. Además, teniendo en cuenta la importancia que tiene el uso racional de la energía eléctrica, en esta tesis se ha desarrollado una novedosa técnica para la gestión de la demanda de sistemas aislados de la red eléctrica que sugiere al usuario del mismo el mejor momento para hacer uso de sus electrodomésticos, reduciendo el consumo de combustible y mejorando el uso de la energía almacenada en el banco de baterías. Finalmente, considerando sistemas conectados a la red eléctrica, se ha desarrollado una estrategia de Adaptación de la Demanda para consumidores residenciales que, haciendo uso de las capacidades de comunicación de la futura Red Eléctrica Inteligente, determina mediante la optimización de la negociación entre el usuario y la empresa de distribución de energía eléctrica, la forma en que el consumidor debe utilizar sus electrodomésticos considerando sus preferencias y su poder adquisitivo.

Los resultados obtenidos sugieren importantes mejoras en los modelos que se utilizan habitualmente en la simulación y optimización de sistemas híbridos, específicamente en la consideración del regulador de carga como un importante elemento del sistema, y en la estimación de la vida útil del banco de baterías. Además, las estrategias para la gestión de la demanda, presentadas en este trabajo de investigación, pueden ayudar a que los usuarios de sistemas aislados o conectados a la red eléctrica realicen un uso eficiente de las fuentes de energía locales, y adapten sus patrones de consumo de electricidad a su condición económica actual.

3. Versión en inglés

A continuación se incluye la versión en inglés de esta tesis doctoral.

Analysis and optimal load management in grid-connected and stand-alone electrical systems based on renewable energy sources

By

Juan M. Lujano-Rojas

Department of Electrical Engineering

University of Zaragoza

Introduction

Energy is a fundamental instrument in social and productive development in every region in the world. For a long time, global energy consumption has been growing, according to the Energy Information Administration [1], and it is expected that global energy consumption will to reach 770 quadrillion BTU in 2035, a 53% increase compared to the energy consumption of 2008. This expected increase is due to the robust economic growth and expanding population in some developing countries, while countries with advanced economies, such as those belonging to the Organization for Economic Co-operation and Development (OECD), have been affected in an important way by the worldwide economic recession, from which they are still recovering slowly. As shown in Figure 1, the growth of energy demand in countries that belong to the OECD is estimated to be an average annual rate of 0.6%, while the growth of energy demand in countries that do not belong to OECD is estimated to be an average annual rate of 2.3% [1].

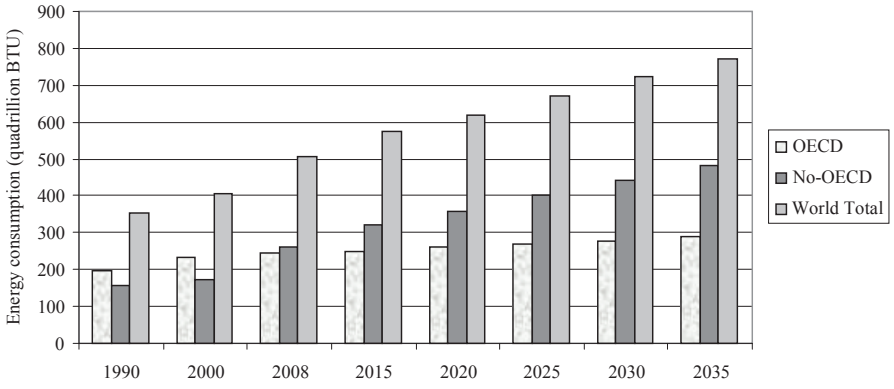

Figure 1. World energy consumption [1]

During the global economic recession, China and India have maintained a significant level of economic growth and, consequently, a significant increase in their energy consumption. In 2008, the energy consumption of both countries represented 21% of the world's energy consumption, while for 2035, it is estimated that both countries will consume 31%. Moreover, in 2009, the United States had just recovered from the downturn, while China and India reached economic growth of 12.4% and 6.9%, respectively. According to Figure 2, as a consequence of this situation, for the first time, the energy consumption of China was higher than the energy consumption of the United States. It is estimated that, in 2035, the energy demand of China will be higher than the energy demand of the United States by about 68% [1].

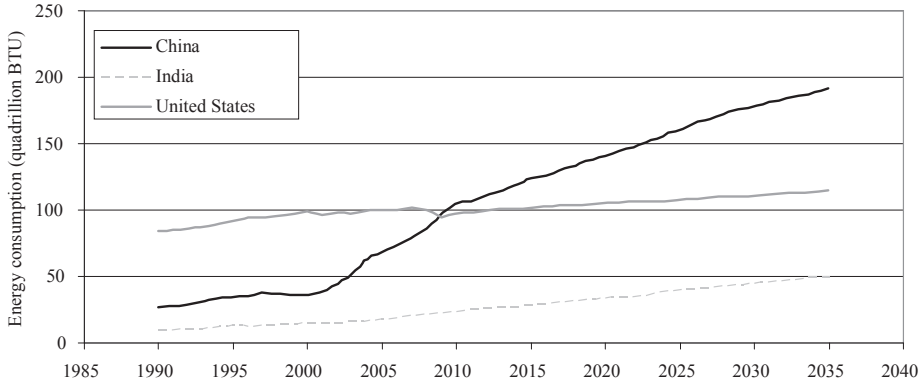

Figure 2. Energy consumption of the United States, China, and India [1]

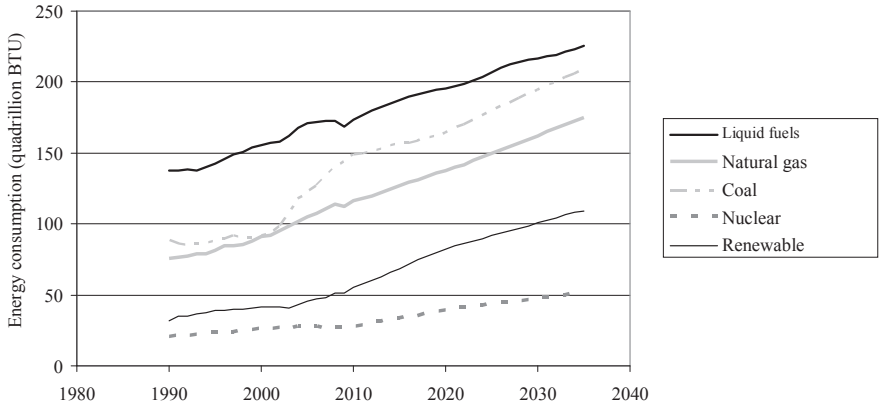

Figure 3. World energy consumption by type of fuel [1]

On the other hand, according to the future tendencies presented in Figure 3, it is estimated that the consumption of liquid fuels will increase at an average annual rate of 1% because it is likely that the prices of oil and other liquid fuels will stay relatively

high. The global consumption of natural gas will increase at an average annual rate of 1.6%, motivated by its use in industrial process and electric power generation. The consumption of coal will increase at an average annual rate of 1.5%, due mainly to the fast economic growth of the countries that do not belong to the OECD in Asia. There is an important uncertainty about the growth of nuclear energy related to the plants' safety and radioactive waste disposal that could make the installation of new plants difficult. Renewable energies are the fastest-growing energy sources; their consumption will increase at an average annual rate of 2.8%, motivated by the high prices of fuel, the environmental impact of fossil fuel use, and government incentives offered in many countries [1].

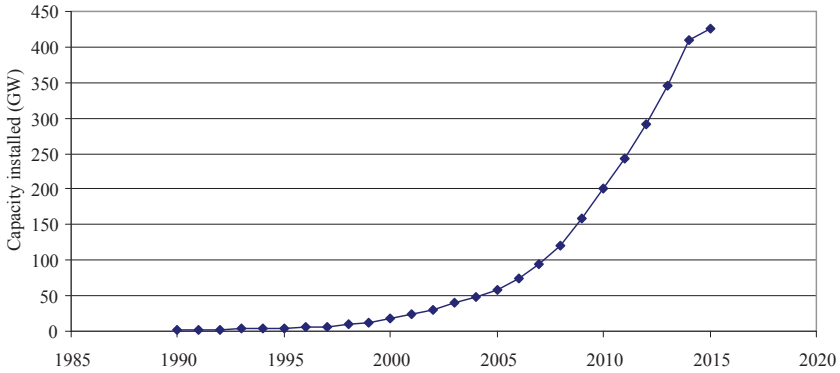

Figure 4. World wind energy capacity installed [3]

Wind energy has recently experienced an important development. Figure 4 shows the evolution of the rated capacity installed around the world, which is expected to reach 425 GW in 2015 [2]. The five countries with the highest installed capacity are China, the United States, Germany, Spain, and India. China is the electricity market with highest wind energy capacity; it reached 42.3 GW of installed capacity in 2010. Due to their good wind energy resource, it is expected the capacity installed will reach 90 GW in 2015 and 200 GW in 2020. In 2011, the United States reached 40.2 GW of capacity installed. With this capacity, they have were able to supply about 2% of their total energy requirements, and it is expected that the capacity installed will increase to the point that it will satisfy 20% of their electric energy demand in 2030. Germany and Spain are the main producers of wind energy in Europe. In 2010, Germany reached 27.2 GW of capacity installed, providing 6.2% of their energy demand, and it is expected that, in 2020, the capacity installed onshore will reach 45 GW, while the capacity installed offshore will reach 10 GW. In 2010, Spain reached 20.7 GW of capacity

installed, representing 16.6% of their electric energy demand. It is expected that, in 2020, the wind energy capacity installed onshore will reach 40 GW, while the capacity installed offshore will reach 5 GW. In 2010, India reached 13.1 GW of capacity installed [2].

As shown in Figure 5, solar photovoltaic energy has grown considerably in recent years, mainly motivated by the reduction in the manufacturing cost of solar photovoltaic, technological advances, and the government incentives offered in many countries, reaching 40 GW of capacity installed in 2010, of which 85% corresponded to grid-connected systems [4].

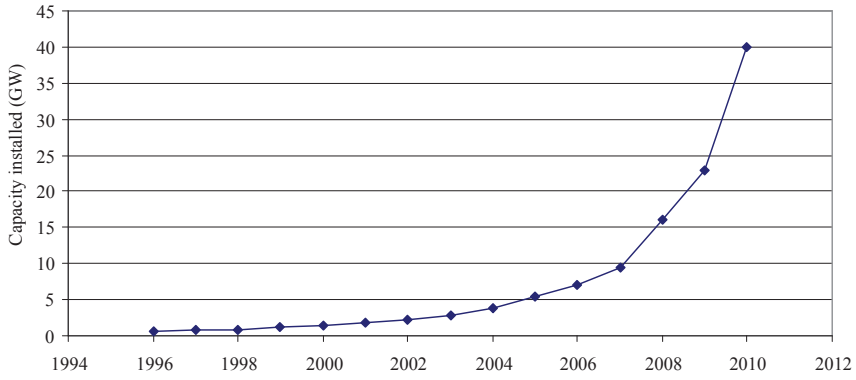

Figure 5. World capacity installed of solar photovoltaic energy [4].

Figure 6 presents the main producers of solar photovoltaic energy.

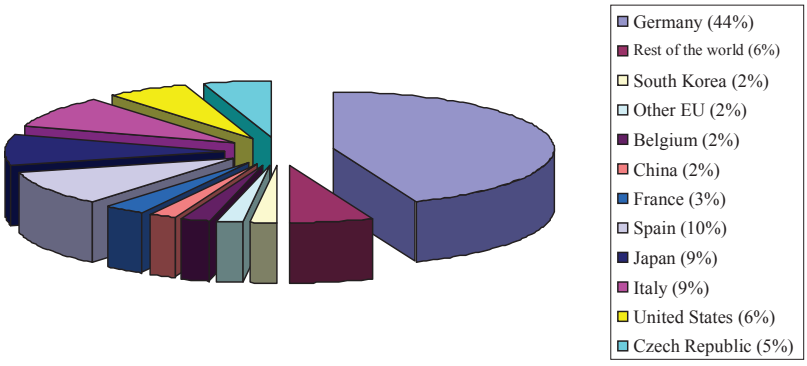

Figure 6. Capacity installed of solar photovoltaic energy by country [5].

The Czech Republic has increased their capacity installed from almost zero in 2008 to 2 GW in 2010, while India and China have accumulated 102 MW and 893 MW, respectively. The countries with the highest capacity installed of solar photovoltaic energy are Germany, Italy, Spain, and the United States. Many grid-connected systems

are installed in countries that belong to the OECD, while many isolated systems are installed in developing countries such as China and India, due mainly to their large rural populations [5].

As explained previously, the actual energy situation is characterized by the growth of world energy consumption as a consequence of the robust economic development of countries with emerging economies, in addition to a considerable increase in the electricity generation capacity installed to satisfy the energy demand. In this expansion of the capacity installed of power generation are included different sources such as natural gas, coal, nuclear energy, fossil fuels, and renewable energies. Renewable energies have been quickly growing in recent years, driven by problems related to environmental factors, the depletion of oil and natural gas reserves, and technological advances that have allowed a considerable reduction in manufacturing costs. Wind energy and solar energy have garnered big interest around the world. In the specific case of wind energy (which, according to Figures 4 and 5, has greater capacity installed than solar photovoltaic energy), its impact in the power system is mainly related to its penetration level and the flexibility of the system [6]. On the one hand, if the penetration level is increased, the impact of wind energy in the power system will be higher; i.e., the uncertainty related to wind power could considerably increase the production costs when the penetration level is high. The fluctuations of wind power could affect the operation of other dispatchable generation units because the intermittence of wind power could drive other generation units to operate far from the optimal point. On the other hand, if the flexibility level of the system is increased, more wind energy can be integrated into the system; i.e., during periods of low demand and high production of wind power, a reduction in the power production from wind farms is necessary to maintain the energy balance of the system; this decision depends on the penetration level of wind power and the flexibility of the system [6]. Another important aspect is that problems related to restrictions imposed on electricity prices, such as price ceilings, flat rates, and other regulatory restrictions, have produced a significant difference between the marginal cost of power generation and the price at which consumers obtain the energy. As a consequence of this difference, in many countries, the growth of demand for energy is higher than the growth of the capacity installed; i.e., the growth in the capacity of power generation has been affected by the fact that the electricity prices do not reflect the real marginal cost. While the development of the population and economic growth require the consumption of large quantities of energy,

the liberalization of the electric energy sector is perceived as a risky policy that could drive the loss of welfare for consumers in the short term; this situation makes growth and development difficult due to the inhibition of the restructuring process [7].

As a solution to the problems related to the growth of energy demand and the growth in the penetration level of wind energy, several authors have proposed using massive storage of electric energy as an option that could convert random sources of energy in dispatchable power plants. Anagnostopoulos *et al.* [8] and Varkani *et al.* [9] proposed using a reversible hydraulic system to recover excess electric energy from wind farms due to the limitations required for the balanced operation of the electric grid. This idea could help the growth of the wind energy capacity installed and increase the economic benefits derived from it. Recently, Fertig *et al.* [10] proposed using a combination of a compressed air energy storage system and a wind farm to provide dispatchable power. Bernal-Agustín *et al.* [11], analyzing the shape of the demand curve, proposed using the excess energy produced during off-peak hours to generate hydrogen and store it in a hydrogen tank; this energy could then be sold to the electric grid during peak hours. Dufo-López *et al.* [12] proposed a similar idea but using different types of batteries. On the other hand, the flexibility of the power system can be increased using demand side management to incentivize consumers to use electric energy during hours of high wind power production [6].

In this doctoral thesis is carried out a deep analysis of the operation and modeling of electrical systems isolated and connected to an electric grid that uses renewable energies, along with the development of strategies to manage the energy demand to help residential consumers find the optimal use for their household appliances. The main results and novelties found in this research work are presented in the following group of scientific articles:

1. Lujano-Rojas JM, Dufo-López R, Bernal-Agustín JL. Optimal sizing of small wind/battery systems considering the DC bus voltage stability effect on energy capture, wind speed variability, and load uncertainty. **Applied Energy** 2012;93:404-412.

2. Lujano-Rojas JM, Monteiro C, Dufo-López R, Bernal-Agustín JL. Optimum load management strategy for wind/diesel/battery hybrid power systems. **Renewable Energy** 2012;44:288-295.

3. Lujano-Rojas JM, Monteiro C, Dufo-López R, Bernal-Agustín JL. Optimum residential load management strategy for real time pricing (RTP) demand response programs. **Energy Policy** 2012;45:671-679.

4. Lujano-Rojas JM, Dufo-López R, Bernal-Agustín JL. Optimal design of PV/Wind/Battery systems by genetic algorithms considering the effect of charge regulation. International Conference on Mechanical and Electronic Engineering (ICMEE 2012). **This paper will be published in Lecture Notes in Electrical Engineering.**

5. Lujano-Rojas JM, Dufo-López R, Bernal-Agustín JL. A qualitative evaluation of operational conditions in PV/Wind/Battery systems. Asia-Pacific Power and Energy Engineering Conference (APPEEC 2012). **Available at IEEEXplore.**

6. Lujano-Rojas JM, Bernal-Agustín JL, Dufo-López R, Domínguez-Navarro JA. Forecast of hourly average wind speed using ARMA model with discrete probability transformation. **Lecture Notes in Electrical Engineering 98**. Springer-Verlag; 2011. p. 1003-1010.

Summary

This research work presents an extensive analysis and the development of optimal demand response strategies for hybrid power systems and residential grid-connected systems that use uses renewable energies. The development of these tasks requires the carrying out of several objectives by means of a determined methodology.

Objectives

The main objectives of this doctoral thesis are:

1. To analyze the modeling of the different components of a typical hybrid power system that has a wind turbine, several photovoltaic panels, conventional generation, and a lead acid battery bank.

2. To analyze the simulation and optimization techniques of a typical hybrid power system that has a wind turbine, several photovoltaic panels, conventional generation, and a lead acid battery bank.

3. To develop strategies for optimal load management using hourly forecasting of wind speed, solar radiation, and ambient temperature to improve the performance of hybrid power systems that have a wind turbine, several photovoltaic panels, conventional generation, and a lead acid battery bank.

4. To analyze the main characteristics of a future smart grid, specifically a technological infrastructure that allows bidirectional communication between the retailer and the consumers.

5. To analyze the modeling of the different components of a typical residential electric system connected to a smart grid that has a wind turbine, several photovoltaic panels, and household appliances in a real-time pricing environment.

6. To analyze strategies for the optimal load management for a typical residential consumer in a real-time pricing environment.

Methodology

The methodology carried out in this thesis is presented next:

1. Carry out a literature review on the different mathematical models of wind turbines, photovoltaic panels, lead acid batteries, inverters, and conventional generation.

2. Carry out a literature review on the deterministic modeling and optimization of hybrid power systems.

3. Carry out a literature review on the probabilistic modeling and optimization of hybrid power system.

4. Carry out a literature review on forecasting techniques of hourly wind speed, solar radiation, and ambient temperature.

5. Develop and implement a strategy for load management that allows optimization of the performance of the battery bank and conventional generation in a typical hybrid power system.

6. Carry out a literature review on the infrastructure of smart grids.

7. Carry out a literature review on the main techniques to forecast wholesale energy market prices.

8. Develop a demand response strategy for a typical residential consumer connected to a smart grid considering a wind turbine, several photovoltaic panels, several household appliances, and an electric vehicle.

Literature review and the main contributions of this doctoral thesis

The management of power systems can be carried out by means of controlling the sources of power, managing demand, or both. These strategies can be applied to grid-connected systems or isolated systems. In this research work, the isolated and grid-connected systems are analyzed, and strategies to manage the energy demand of residential consumers of these types of systems are developed.

Many studies have shown the importance of hybrid power systems in rural electrification [13,14,15] and reduction of the emission of greenhouse gases [16]. The sizing and control of hybrid systems is an important factor that has been studied by many authors. The Hybrid Optimization Model for Electric Renewables (HOMER) [17] is a computational tool developed by the U.S. National Renewable Energy Laboratory that is used frequently for the simulation and optimization of hybrid systems in testing all possible combinations. Belfkira *et al.* [18] implemented the Dividing Rectangles (DIRECT) algorithm for the optimal sizing of a system that has several photovoltaic panels, a wind turbine, and a diesel generator, minimizing the total cost. Boonbumroong *et al.* [19] used particle swarm with a constriction coefficient for the optimal sizing of a typical hybrid system with several photovoltaic panels, a wind turbine, a battery bank, and a bidirectional inverter. The results obtained were compared with HOMER, and it was concluded that the proposed methodology considerably reduced the time required to find the optimal configuration. Hakimi and Moghaddas-Tafreshi [20] used particle swarm optimization to size a system with a wind turbine, fuel cells, an electrolyzer, a hydrogen tank, a reformer, and an inverter, obtaining high reliability due to the fact that the fuel cells are a backup for the wind turbine. Hybrid Optimization by Genetic Algorithms (HOGA) [21] is a computational tool developed by the University of Zaragoza for the simulation and optimization of a hybrid system using genetic algorithms. Ekren and Ekren [22] used simulated annealing for the optimal sizing of a hybrid system comprising several photovoltaic panels, a wind turbine, and batteries installed in Turkey.

Considering the variability of renewable resources in the optimization of a hybrid system is an important factor that has been studied by several authors. Bagul *et al.* [23] proposed a methodology that consists of estimating the probability density function of the energy that flows by means of the battery bank's using information about the renewable resources and technical data provided by the manufacturers, obtaining the optimal configuration of components considering a determined confidence level. Karaki *et al.* [24,25] developed a sizing technique based on finding the expected value of the energy available to recharge the battery bank using the joint probability distribution function of the renewable resource and the duration curve of the energy demand, determining the optimal configuration considering the capital cost and the reliability of the system. Roy *et al.* [26] implemented a methodology that consists of identifying the

set of all possible configurations of a hybrid system, and then the optimal configuration is determined using the probability distribution function of the renewable resources. Távora *et al.* [27] compared the deterministic and probabilistic approaches and concluded that the deterministic approach could suggest a configuration for a hybrid system with over-estimated generation capacity for a determined level of reliability. Giannakoudis *et al.* [28] presented an optimization methodology using simulated annealing adapted to consider uncertainty (stochastic annealing). Tan *et al.* [29] developed a methodology for the optimal sizing of a battery bank in an uninterruptible power system that has a photovoltaic generator using a Monte Carlo simulation approach. The first step of this methodology consists of generating a random event for a load profile, weather conditions, and failure. Then, under these operating conditions, in the second step, the required storage capacity is calculated. This process is repeated a specified number of times. Finally, the results are statistically analyzed using the cumulative distribution function, and the storage capacity is economically selected considering a determined confidence level.

The control of hybrid power systems has two important components: the strategies to control the energy sources and energy demand management. In an important paper, Barley and Winn [30] proposed the following general strategies to control hybrid systems: the frugal discharge strategy, load following strategy, state of charge setpoint strategy, and full power/minimum run time strategy. In the frugal discharge strategy, the intersection of the cost curve of the diesel generator and the cost curve of the use of the battery bank determines the critical load. In this strategy, if the net load (the difference between the load and the renewable power) is higher than the critical load, the diesel generator is used; in other cases, the battery bank is discharged. In the load following strategy, the diesel generator is used only to meet the net load. In the state of charge setpoint strategy, the diesel generator is used to charge the battery bank up to a predefined value. In the full power/minimum run time strategy, the diesel generator operates during a predefined interval of time, charging the battery bank with the excess energy. Ashari and Nayar [31] developed a strategy that uses the load demand, the voltage of the battery bank, and the minimum operating power of the diesel generator to decide when to charge or discharge the battery bank and when the diesel generator must be started or stopped. The optimal strategy is obtained, determining the critical load at which the diesel generator must be started or stopped and the setpoint of state of charge

at which the battery bank must be discharged. Dufo-López and Bernal-Agustín [32] proposed a control strategy that combines the load following strategy and the state of charge setpoint strategy proposed previously by Barley and Winn [30]. In this combined strategy, if the net load is lower than the critical load, the state of charge setpoint strategy is applied; in other cases, the load following strategy is used. Yamamoto *et al.* [33] proposed a strategy that uses predictions of the hourly power production of the renewable energy sources and the load demand to determine the operating power of the diesel generator. If the state of charge of the battery bank is between 0.5 and 0.7, the diesel generator starts to charge the battery bank, and when the state of charge is higher than 0.7, the diesel generator is shut off.

Several authors have analyzed the load management in hybrid power systems. Groumps *et al.* [34] carried out the first research work about a standalone photovoltaic system, analyzing a system installed in the Village of Schuchuli, Arizona (USA). In the operative strategy of this system, four categories of priority and four settings of state of charge (0.5, 0.4, 0.3, and 0.2) were considered. For example, if the battery bank is discharged and the settings of state of charge are reached sequentially, the loads are sequentially disconnected starting with the load with the lowest priority level. Otherwise, if the battery bank is charged and the settings of state of charge are reached sequentially, the loads are sequentially reconnected. In another paper, Groumps and Papegeorgiou [35] proposed a technique for load management in standalone photovoltaic systems based on three main categories of load classification: a classification according to load operation (DC and AC loads), a classification according to the system operation (uncontrollable, controllable, and semi-controllable loads), and a classification according to the priority (useful, essential, critical, and emergency loads). In this strategy, using controllable loads, the load curve is manipulated to minimize the integral of the square of the net load over a 24-hour period to reduce the required capacity of the battery bank. Khouzam and Khouzam [36] developed a methodology to manage the load in a standalone photovoltaic system classifying the loads into four categories according to their priority level: convenient, essential, critical, and emergency. The priority of the battery bank is a variable that depends on its state of charge. The optimal load management is based on the maximization of an objective function that depends on the priority level of the load subject to constraints of the availability to supply the energy demand. Moreno *et al.* [37] implemented a fuzzy logic

controller for the load management in standalone photovoltaic systems. This controller considers the expected supply forecasted one hour ahead to decide whether to connect or disconnect a determined load according to the priority level.

The load management in residential grid-connected systems has been analyzed by many authors. Salah *et al.* [38] developed a methodology in which the photovoltaic generator is considered a complementary power source and then, using a fuzzy logic controller, it is decided which household appliance must be connected to the photovoltaic generator and the electrical grid. The decision is made considering the power production of the photovoltaic generator, the energy required by each appliance, and its priority level. According to the results obtained, this methodology allows continuous energy savings to be obtained. Ammar *et al.* [39] proposed a strategy for load management for residential consumers using daily predictions of the power production of the photovoltaic generator to decide the time at which a determined appliance will be connected to the photovoltaic generator. This decision is made considering the energy required by each appliance. A similar criterion was proposed by Salah *et al.* [38]. Thiaux *et al.* [40] analyzed the influence of the load profile shape in the cost of energy during the lifetime of a typical standalone photovoltaic system. The results have shown that the energy required is reduced when the load profile and the photovoltaic power production are similar.

Demand response (DR) is defined as the changes in the electricity consumption patterns of the end consumers to reduce their energy demand in times of high electricity prices. The changes in the behavior and the consumption pattern of the consumers could be carried out through changes in electricity prices (price-based programs) or incentive payments (incentive-based programs) [41]. In this way, demand response's changing the electricity consumption pattern of the end consumers can reduce problems related to the difference between the marginal generation costs and the price at which the end consumers obtain the energy [7]; additionally, demand response can improve the efficiency and the reliability of the available infrastructure and reduce the volatility of electricity prices [41].

The implementation of demand response programs requires an electrical grid that has the technology to allow communication between the consumers and the retailer; this concept of the electrical grid is known as a smart grid. DR programs have been divided

mainly into two categories: incentive-based programs (IBPs) and price-based programs (PBPs). IBPs are based on participation payments such as bill credits or discounted rates, while PBPs are based on dynamic pricing rates. IBP are classified in classical programs and market-based programs. Classic IBPs include direct load control programs and interruptible/curtailable load programs, while market-based IBPs include emergency DR programs, demand bidding, capacity markets, and ancillary services markets. In classic IBPs, the customers receive participation payments such as bill credits or discounts. Thus, in direct load control programs, utilities can shut down participant equipment on short notice, while in interruptible/curtailable load programs, participants are asked to reduce their load to predefined values. PBPs have several rates such as time of use (TOU), critical peak pricing (CPP), extreme day pricing (EDP), extreme day CPP (ED-CPP), and real-time pricing (RTP). In TOU during peak periods, the rate is higher than the rate during the off-peak periods. CPP is used during emergencies or when wholesale electricity prices are high for days. ED-CPP has high prices in effect during the 24h of an extreme day. In RTP, the real cost of electricity in the wholesale market is passed on to the consumers [41]. TOU programs have been shown to be particularly convenient for residential consumers [42].

Demand response programs have been implemented in many countries around the world. In the United States, several DR programs in organized wholesale markets are administered by independent system operator/regional transmission operators (ISO/RTOs); some examples are the New York Independent System Operator (NYISO) and PJM Interconnection (PJM), which offer different DR programs in which end customers can participate using energy management control strategies to reduce their load according to price or emergency signals [43]. In the United Kingdom, industrial and commercial sectors are able to engage in TOU and/or interruptible/curtailable load contracts with suppliers. Many customers are enrolled in programs with the option to obtain discounted electricity rates at night. In Italy, interruptible programs are applied to very large industries, which must reduce their loads to predefined values. Spain has developed two DR programs for large industrial consumers: system-led and price-led. In system-led programs, consumers are able to participate in DR programs voluntarily, and then the transmission system operator (TSO) can request that these industries limit their demand during periods from 45 minutes to 12 hours. In price-led programs, the TSO can apply TOU rates in seven periods of the year [44]. In China, demand response

programs have been implemented to improve the system reliability and load factor. In Beijing, the difference between off-peak and on-peak was increased, industrial consumers signed interruptible/curtailable load contracts, the use of energy storage equipment was encouraged, and loads were controlled. In Jiangsu, interruptible/curtailable load programs have been applied to industrial consumers, the use of energy storage devices was promoted, TOU rates were applied, and industrial machines were controlled [45].

Many authors have analyzed how residential consumers could adapt their power demand according to a determined DR program. Molderink *et al.* [46] developed a strategy for DR to control the energy streams in a single house and a large group of houses. In this methodology, the system has a global controller, and every house must be provided with microgenerators, heat and electricity buffers, several appliances, and a local controller. The global and local controllers are used in three steps: in the first step, a prediction of production and consumption is made one day ahead, and then the local controller determines the aggregated profile and sends them to the global controller. In the second step, the planning for each house for the next day is made, and finally, in the third step, the algorithm decides how the demand is matched. Two examples are analyzed, and the results show that it is possible to make a plan for a group of houses based on a prediction made one day ahead; however, forecasting errors affect the effectiveness of this approach. Mohsenian-Rad and Leon-Garcia [47] developed a methodology for the load management of residential consumers enrolled in real-time pricing demand response programs. In this approach, the electricity payment and the waiting time for the operation of each appliance are minimized in response to variable real-time prices. For a determined scheduling horizon, the price forecasting is made, and then an objective function that considers the total electricity payment and the total cost of waiting (the cost of the use of appliances at later hours) in the scheduling horizon is minimized. Mohsenian-Rad *et al.* [48] presented a residential load control model in which, for a group of residential consumers, the optimal energy consumption schedule for each consumer is determined, minimizing the energy cost in the system based on game theory. The approach proposed by Conejo *et al.* [49] consists of minimizing the cost of energy consumption considering the load-variation limits, hourly load, and price prediction uncertainty. This methodology assumes that the prices and decisions in the prior t-1 hours are known, the price and power demand are known in the actual moment

(hour *t*), and the prices in the next 24-*t* hours are estimated using an autoregressive integrated moving average (ARIMA) based model with a confidence interval. Using this information, an optimization model establishing a floor for daily consumption and ramping down/up limits is developed, obtaining the energy consumption in the current hour *t* and the demand at the beginning of hour *t*+1; finally, this procedure is repeated for each hour on a scheduling horizon of one day. The methodology proposed by Sianaki *et al.* [50] can consider the preferences of the customers regarding the use of certain appliances during peak hours by means of the analytic hierarchy process. The customers' preferences are used to decide what appliances must be used during peak hours, solving the knapsack problem, where the numerical priority obtained by the analytic hierarchy process for a certain appliance is considered as a measure of the profit obtained by its use.

Influence of the temperature, charge regulation, and coulombic efficiency of the battery bank in the performance of small wind/battery systems

Figure 7 shows a typical small-capacity wind energy system composed of a wind turbine and a lead acid battery bank, which supply a determined energy demand.

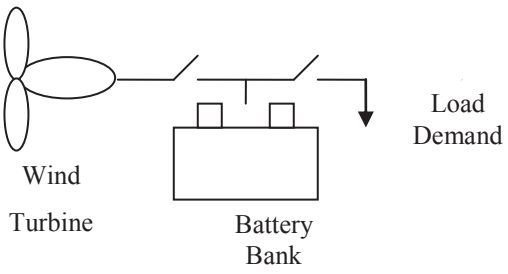

Figure 7. Small-capacity wind battery system

The charge controller is an important component in standalone systems with lead acid batteries. The charge controller protects the battery bank against extreme operating conditions such as over-discharge or over-charge by measuring the voltage on its terminals; i.e., if the battery bank reaches the low voltage setpoint, the charge controller disconnects the load. Otherwise, when the battery bank reaches the high voltage setpoint, the charge controller disconnects the renewable generator. Using experimental data, Baring-Gould *et al.* [58] and Corbus *et al.* [59] showed that the charge regulator could affect the ability of the battery bank to store energy. Corbus *et al* [59], analyzing different small wind energy systems, concluded that, in systems with high wind power generation and small storage capacity, the voltage of the battery bank reaches the high

voltage setpoint prematurely, the charge controller disconnects the renewable generator, and, consequently, the state of charge of the battery bank stays low. This fact is illustrated in Figure 8. For a typical high-voltage setpoint of 2.25 V/cell, if the battery bank is charged with charge current in 5 hours (C/5), when the voltage reaches 2.25 V/cell, the state of charge will be 45%. Note that if the charge current is reduced, more time is required to reach the high voltage setpoint, and, consequently, the battery bank can accept more energy. If the battery bank is charged with the charge current in 8 hours (C/8), the state of charge will be 61%. If the charge current is reduced to the charge current in 10 hours (C/10), the state of charge will be 65%, and, finally, if the charge current is C/20, the state of charge will be 78%.

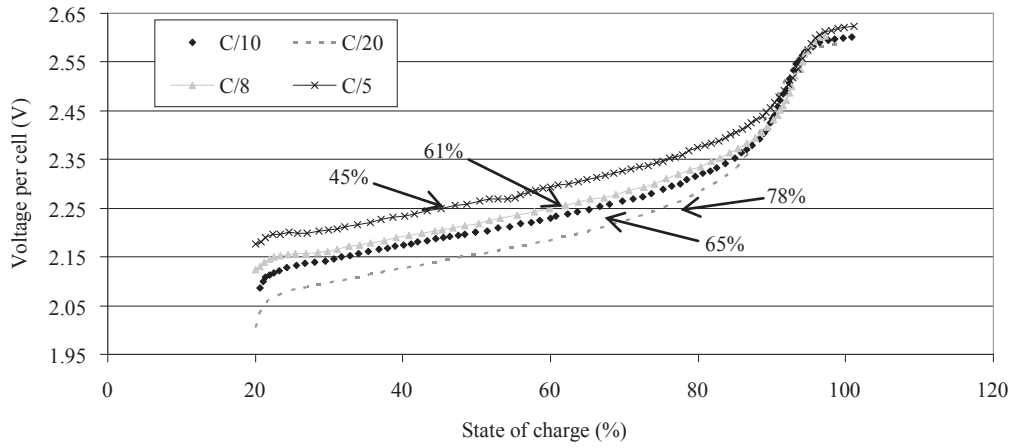

Figure 8. Voltage vs. state of charge in a lead acid battery [59]

Otherwise, the coulombic efficiency of the battery bank is another important factor that could significantly affect its ability to store energy. The coulombic efficiency varies considerably according to the state of charge, presenting a very low value when the state of charge is high. This loss of efficiency is related to the gassing reactions during the charge process [60]. Stevens and Corey [61], analyzing photovoltaic systems, concluded that the low coulombic efficiency during a high state of charge can result in a reduction of the energy stored due to the fact that the energy available from the photovoltaic generator is used to satisfy this loss instead of charging the battery bank.

In [51], using a simplification of the lead acid battery model proposed by Copetti *et al.* [62,63], a small wind energy system was analyzed considering the joint effect of the charge controller operation, the coulombic efficiency of the battery bank, and the ambient temperature in the performance of the system. The effect of these factors was

analyzed through the simulation of a system installed in Zaragoza, and the results obtained were compared with those obtained using HOMER, which does not consider these factors. Figure 9 shows a comparison between the probability distribution function of the state of charge of a system with 100Ah of storage capacity using HOMER and the model presented in [51]. The results show how the joint effect of the loss of coulombic efficiency and the charge controller operation could make hard the acceptance of battery bank charging. However, the results obtained using HOMER suggest a higher probability of obtaining a high state of charge due to the fact that this model does not consider the relation between the coulombic efficiency and the state of charge, the operation of the charge controller, and the ambient temperature.

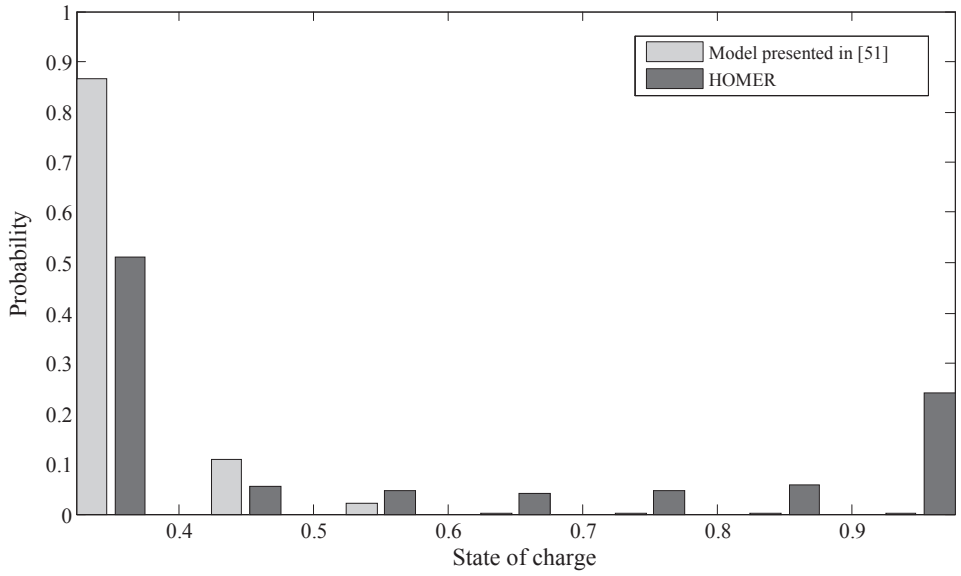

Figure 9. Comparison between the probability distribution functions of states of charge (C_{10}=100Ah)

Figure 10 shows the results obtained from a reliability analysis considering battery bank capacities between 100Ah and 1000Ah. According to these results, if a reliability level of 90% and factors related to the charge controller operation, coulombic efficiency, and ambient temperature are not considered, a battery bank capacity of 800Ah is required. However, if these factors are considered, a battery bank of 1000Ah is recommended. These results suggest that the reliability level obtained during the operation of the physical system could be lower than that obtained using the HOMER model; i.e., if a system analyzed with HOMER is installed, the reliability level could be lower than expected, and, consequently, an increase in the battery bank capacity could be required. In our study case, this increase is 25%.

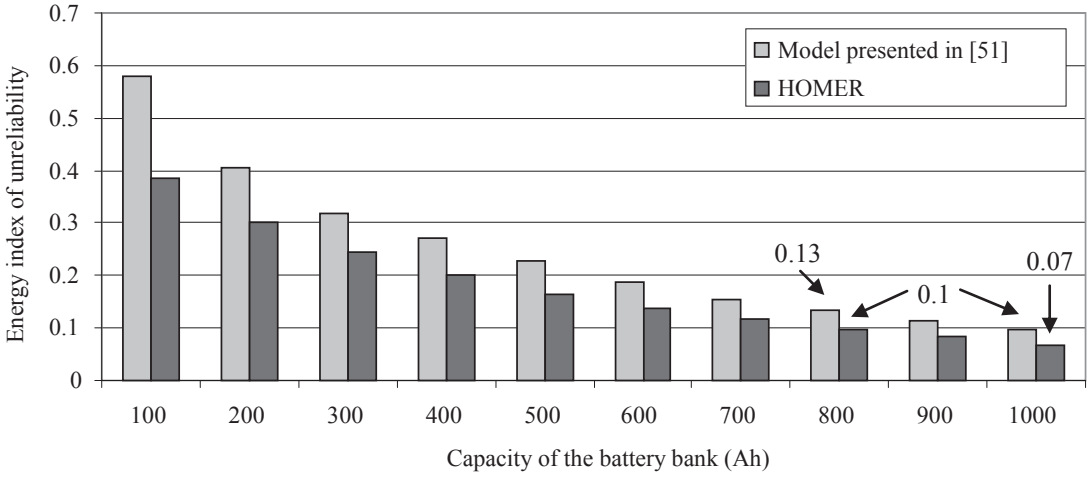

Figure 10. Unreliability for different battery bank capacities

The mathematical model of a typical small wind energy system presented in [51] was improved by incorporating the model of a typical photovoltaic generator and an inverter. In [52], this model was used to develop a methodology for the optimal sizing of hybrid systems based on genetic algorithms, which allows the determination of the optimal configuration of components in the hybrid system to guarantee an established reliability level considering the coulombic efficiency, charge controller operation, and ambient temperature. This methodology was illustrated by means of the optimal sizing of a hybrid system to be installed in the Netherlands, considering wind turbines with the power curves shown in Figure 11, a photovoltaic generator with capacities between 175W and 4.375kW, lead acid batteries with capacities between 200Ah and 3000Ah and strings between 1 and 10, and an inverter of 900W. Considering other economic variables such as capital cost, interest, and inflation rates, the optimal capacity of the photovoltaic generator, wind turbine, and battery bank was found that minimized the net present cost during 35 years of lifetime, guaranteeing a 90% reliability level. After 10 generations of the genetic algorithm, the optimal configuration found had 11 photovoltaic panels of 175W each, a wind turbine of 1kW, and a battery bank of 1000Ah. Figure 12 shows the evolution of the net present cost during the optimization process.

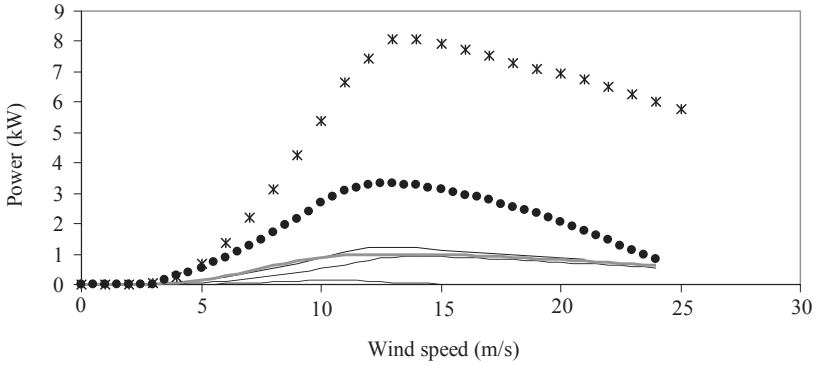

Figure 11. Power curves of different wind turbines

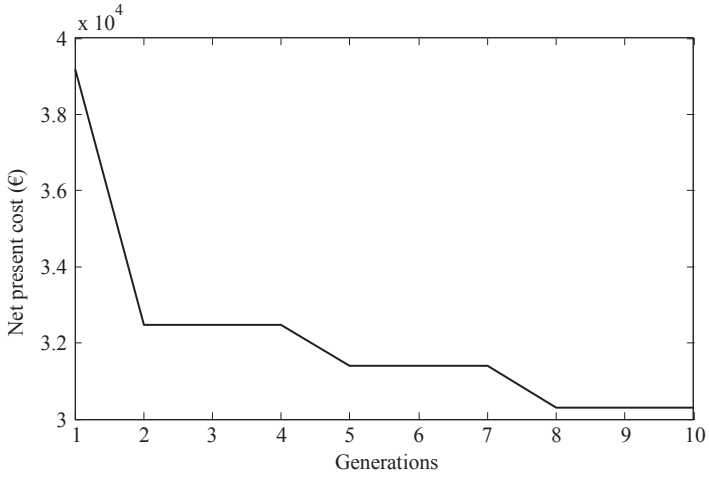

Figure 12. Evolution of the net present cost during the optimization

It has been shown that the battery bank is one of the most important components in a hybrid system. The battery bank affects not only the performance of the system but also its profitability due to the fact that this is one of the most expensive components in the system and that its lifetime is difficult to determine. The problem is that, if the uncertainty regarding the battery bank lifetime is large, the net present cost could be too high at the end of the lifetime of the system, and, consequently, the system could not be profitable.

Effect of uncertainty related to the battery bank lifetime, wind speed variability, and load profile uncertainty in small-capacity wind energy systems.

Many studies have been carried out to determine the battery bank lifetime; as a result of these studies, three types of ageing models have been developed: physico-chemical ageing models, weighted Ah ageing models, and event-oriented ageing models. Physico-chemical ageing models are based on a detailed knowledge of physical and

chemical factors related to the ageing process, while weighted Ah ageing models are based on the assumption that the lifetime of the battery bank is proportionally related to the total Ah throughput. In the implementation of this ageing model, the actual Ah throughput is multiplied by a weight factor fitted according to the actual operating conditions. Finally, the battery bank lifetime is reached when the total Ah throughput exceeds a limit value calculated from nominal conditions. The event-oriented aging model determines the reduction in the battery bank lifetime by identifying extreme operating conditions by means of the pattern recognition approach [64]. Using information provided by experts, Svoboda *et al.* [65] developed different operating categories for the battery bank based on the calculation of stress factors related to the discharge current, time between successive recharge, and Ah throughput during low state of charge conditions. In [53], these operating categories were used for the qualitative evaluation of the operating conditions of the battery bank of a hybrid system installed in Zaragoza. Figure 13 shows the time series of state of charge, which was used to calculate the stress factors required to determine the operating categories of the battery bank. The study case analyzed was characterized by a high state of charge during many hours of the year, in some hours of high discharge currents, and frequent recharges, which produce a high risk of corrosion of the positive grid, a very high risk of water loss, and high risk of active mass shedding. However, there is a low risk of irreversible sulphation or active mass degradation, reverse polarization of cells, and stratification or freezing of the electrolyte [65].

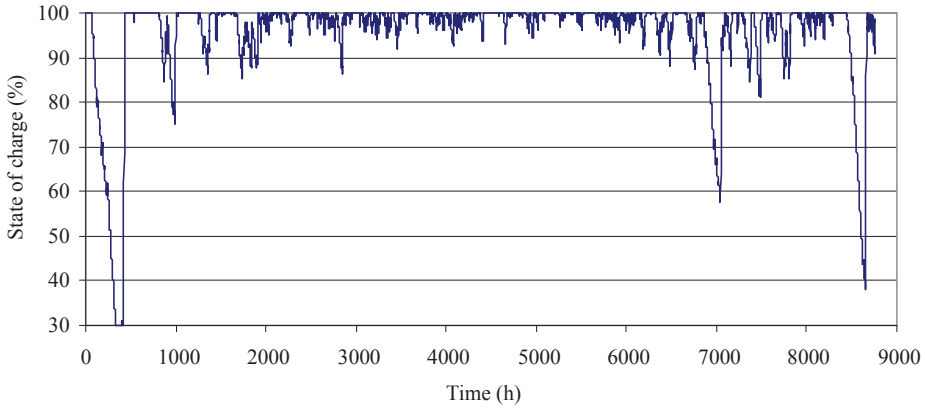

Figure 13. Time series of state of charge

The Ah ageing model (i.e. the weighted Ah ageing models without considering the weight factors) has been implemented in many computational tools for the simulation

and optimization of hybrid systems. In [66], the researchers carried out an experimental validation considering lead acid batteries of flat-plate OGi and tubular OPzS operating under wind and photovoltaic generation profiles. Specifically, in wind generation conditions, the results obtained showed an error of 16.7% in the estimation of the lifetime of the flat-plate OGi battery and an error of 17.5% in the estimation of the lifetime of the tubular OPzS battery. Based on these results, in [51], the Ah ageing model (without considering the weight factors) was incorporated in the probabilistic model of the small wind energy system shown in Figure 7 using the Monte Carlo simulation approach. This model can consider the variability of wind resources by means of the auto regressive moving average (ARMA) model, which considers the main features of wind speed time series: no-Gaussian shape of its probability distribution function, no stationarity, and a high-order autocorrelation. Additionally, this model can consider the uncertainty related to the load profile. Using this stochastic model, [51] analyzed the effect of uncertainty regarding the battery lifetime on the net present cost. The results showed that 17.5% uncertainty in the battery bank lifetime produces about 12% uncertainty in the net present cost. Figure 14 shows the net present cost and its uncertainty interval for different battery bank capacities and the rated power of the wind turbines considering a confidence level of 1%.

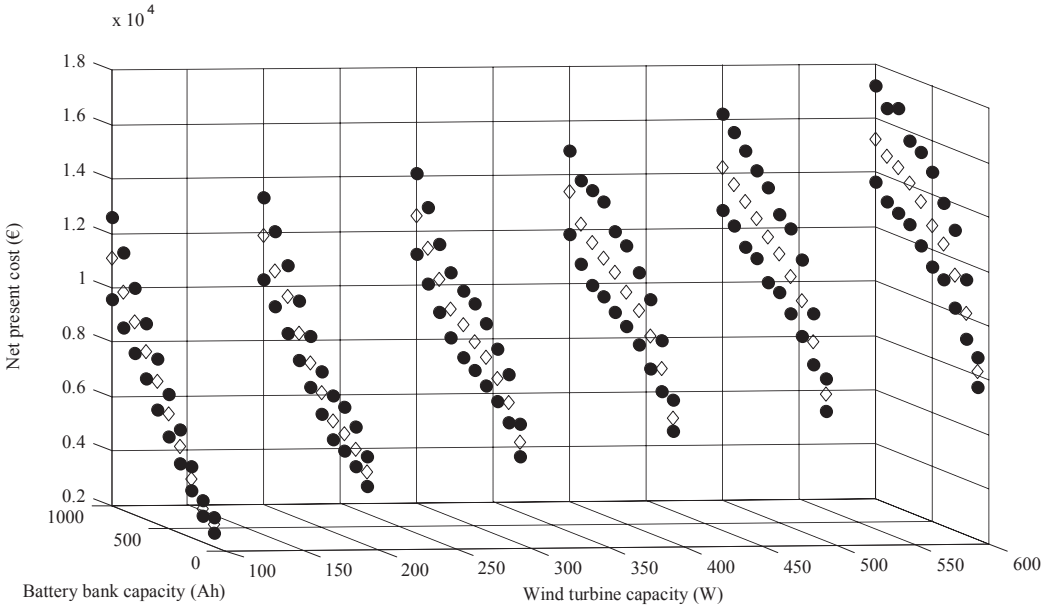

Figure 14. Expected value of the net present cost

The system shown in Figure 7 was used to analyze the effect of uncertainty regarding the reliability of the system. In these systems, reliability is related to the battery bank capacity, the rated power of the wind turbine, and the weather conditions of the place of installation. Figure 15 shows the results obtained from the reliability analysis for different battery bank capacities and rated power of the wind turbines considering a confidence level of 1%.

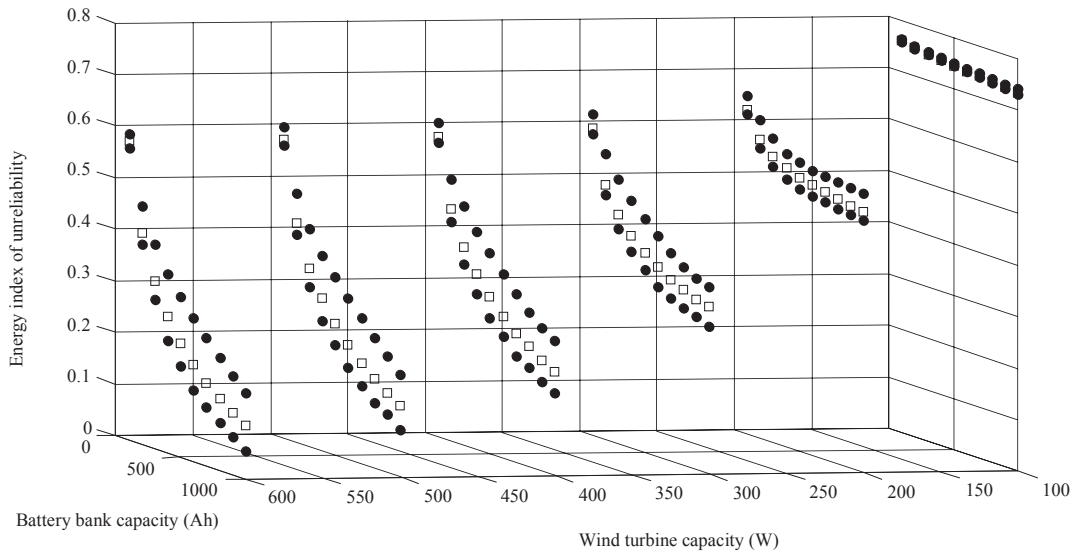

Figure 15. Expected value of the energy index of unreliability

Frequently, hybrid power systems need to meet large energy demands or require high reliability levels; in these situations, the systems commonly incorporate a conventional generator, which provides dispatchable power, but due to the relatively high prices of the fuel, the use of conventional generation increases the net present cost considerably. However, the battery bank has an important role due to the fact that it can reduce the number of operating hours of the conventional generator, storing the excess energy from the renewable generators. The probabilistic model of a typical wind energy system presented in [51] was improved in [54], incorporating a photovoltaic generator, a conventional generator, and an inverter. Additionally, this probabilistic model was improved, incorporating the long-term uncertainty related to the wind resource, the uncertainty related to the photovoltaic generator, and the uncertainty related to the fuel prices.

Influence of the temperature, charge regulation, and coulombic efficiency of the battery bank in the performance of hybrid systems with conventional generation.

The effect of the coulombic efficiency and operation of the charge controller of the battery bank in a typical hybrid system that has a photovoltaic generator, a wind turbine, and a conventional generator was analyzed in a system located in Zaragoza. The results obtained were compared with those obtained using HOMER, which does not consider these factors. The results obtained from the comparative analysis between the hours of operation of the conventional generator, its fuel consumption, and the net present cost of the system are shown in Figures 16, 17, and 18, respectively. According to this analysis, there are important differences between the simulations of the two models when the system has low storage capacity. Systems with low storage capacity have high charge currents, so the high voltage setpoint of the charge controller is reached prematurely and renewable generators are disconnected, producing a low state of charge for the battery bank, an increase in the number of hours of operation of the conventional generator and its fuel consumption, and, consequently, a considerable increase in the net present cost compared with the results obtained using the HOMER model. The highest difference between both models was obtained with a battery bank of 100Ah. For this configuration, the difference between the hours of operation of the conventional generator, its fuel consumption, and the net present cost of the system were about 33%, 31%, and 31%, respectively. When the battery bank capacity is increased, the results obtained from the comparative analysis are very similar due to the fact that, in these cases, the charge currents are reduced, the high voltage setpoint is not reached prematurely, and the battery bank can accept more energy.

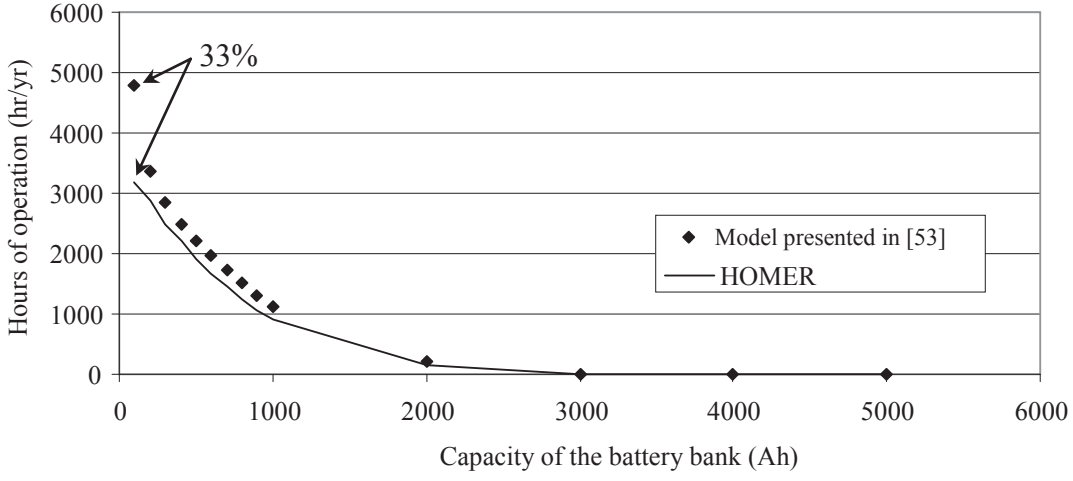

Figure 16. Comparison of the hours of operation

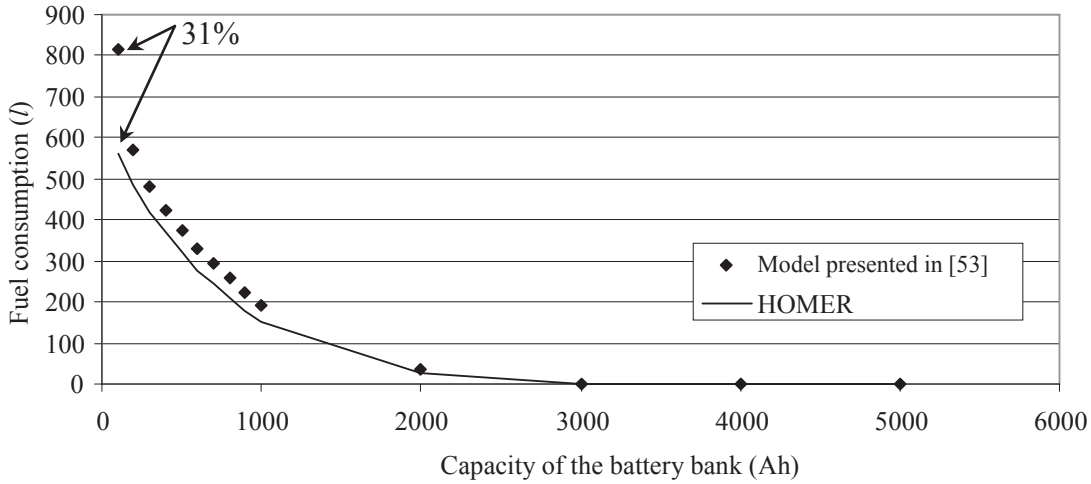

Figure 17. Comparison of fuel consumption

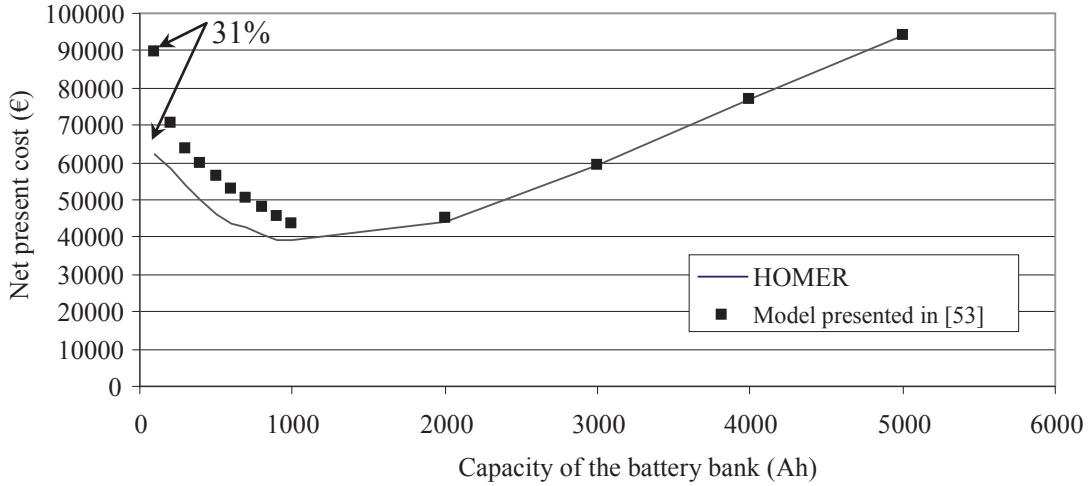

Figure 18. Comparison of the net present costs

Effect of uncertainty related to the battery bank lifetime and fuel prices in the performance of hybrid systems with conventional generation

In another case study, using the stochastic model developed previously, the effect of the long-term uncertainty related to the wind resource, the uncertainty in the power production of the photovoltaic generator, the uncertainty in the fuel prices, and the uncertainty in the load profile was analyzed in a hybrid system installed in Zaragoza and sized previously. Figure 19 shows the expected value of the net present cost and its uncertainty interval calculated considering a 10% confidence level. When the configuration of the hybrid system has low storage capacity (100Ah), the uncertainty in the net present cost is about 7%, influenced by the uncertainty in the fuel prices. If the capacity of the battery bank is increased, the uncertainty in the net present cost is jointly influenced by the uncertainty in the fuel prices and the uncertainty in the lifetime of the

battery bank, reaching about 28% for a hybrid system with a capacity of 1000Ah. Finally, the uncertainty in the net present cost of systems with high storage capacity is influenced mainly by the uncertainty in the battery bank lifetime, reaching about 20% for a hybrid system with a capacity of 5000Ah.

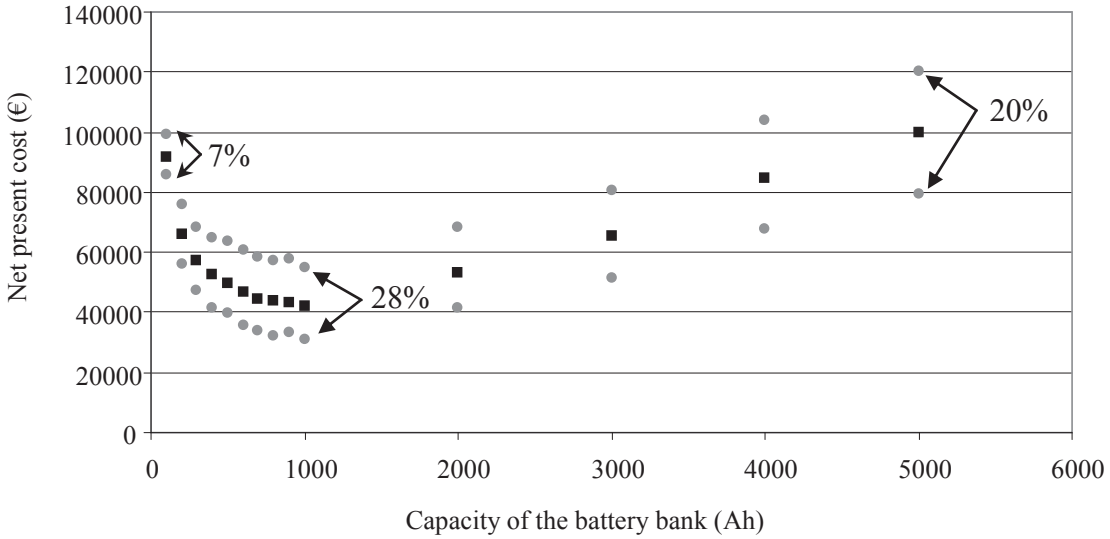

Figure 19. Expected value of the net present cost

Forecasting of hourly wind speed and its application in the development of load management strategies in hybrid systems

The concept of forecasting has long been a useful tool in the management of power systems with high penetration of renewable energy. In addition, this concept is useful in the residential load management. Residential consumers, using information provided by forecasting process, could use their household appliances in a convenient way to save money. The implementation of this idea in a hybrid system that has a wind turbine requires using a forecasting technique to predict the future values of wind power or wind speed. The auto regressive moving average (ARMA) model is a stochastic method frequently used in the literature as a forecasting technique for hourly wind speeds in the short term. In [55], a methodology to predict hourly average wind speeds using the ARMA model is described. The transformation, standardization, estimation, and diagnostic checking processes are carefully analyzed, and a discrete probability transformation has been incorporated to consider the shape of the probability density function of the original wind speed time series under study. Using data from three meteorological stations located in the Netherlands, a comparative analysis of forecasting errors obtained using the ARMA model with discrete probability transformation and an artificial neural network trained by back-propagation was carried out considering

forecasting intervals between 1 and 10 hours. The results obtained showed that, in some cases, the ARMA model with discrete probability transformation could improve the artificial neural network by at least 17.71%.

The methodology described in [55] to forecast hourly average wind speeds could be used in an illustrative form to develop a strategy for the load management in the typical standalone hybrid power system shown in Figure 20.

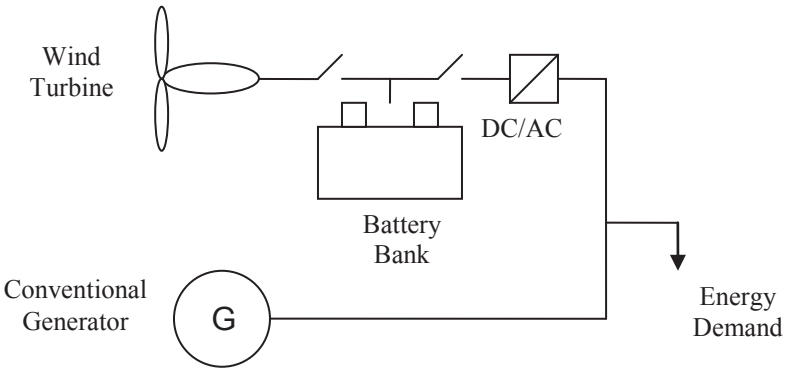

Figure 20. Typical hybrid system

The energy demand of the hybrid system under study could be managed to reduce the daily energy consumption of the conventional generator. This is possible using the controllable loads of the system when the wind speed is high. The load management strategy presented in [56] uses the prediction of the hourly average wind speed 24 hours ahead to determine when each household appliance must be used, minimizing the energy supplied by the controllable loads of the system (conventional generator and battery bank). This idea was analyzed using as an example a hybrid system installed in Zaragoza with the load profile presented in Figure 21.

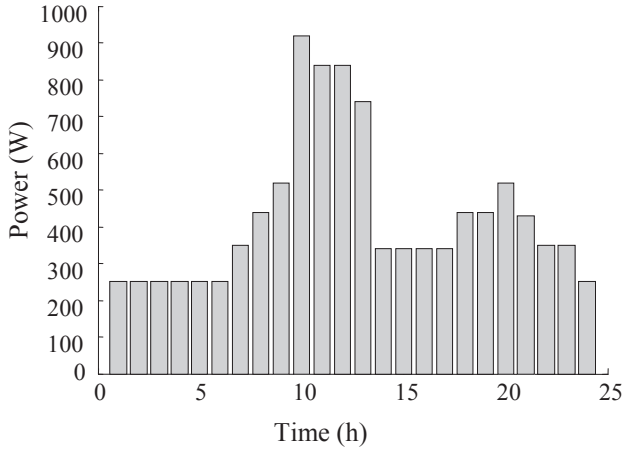

Figure 21. Typical load profile for the study case

In our example, the user has two controllable loads that it uses frequently between 7:00 and 18:00 hours and between 1:00 and 24:00 hours, consuming 400W during 4 hours and 100W during 6 hours, respectively. The system is composed of a wind turbine of 3500W, a diesel generator of 1kW, an inverter of 1kW, and a battery bank of 1000Ah. Figures 22 and 23 show that, in applying the proposed idea, the load shifts to the wind power peak, reducing the requirements of the diesel generator and the battery bank.

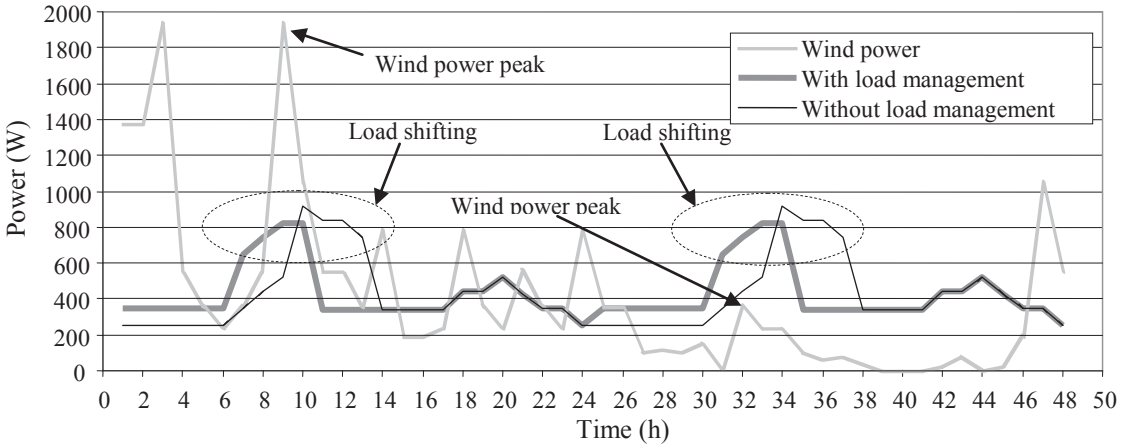

Figure 22. Wind power and load profiles for the 5th and 6th of August 2005

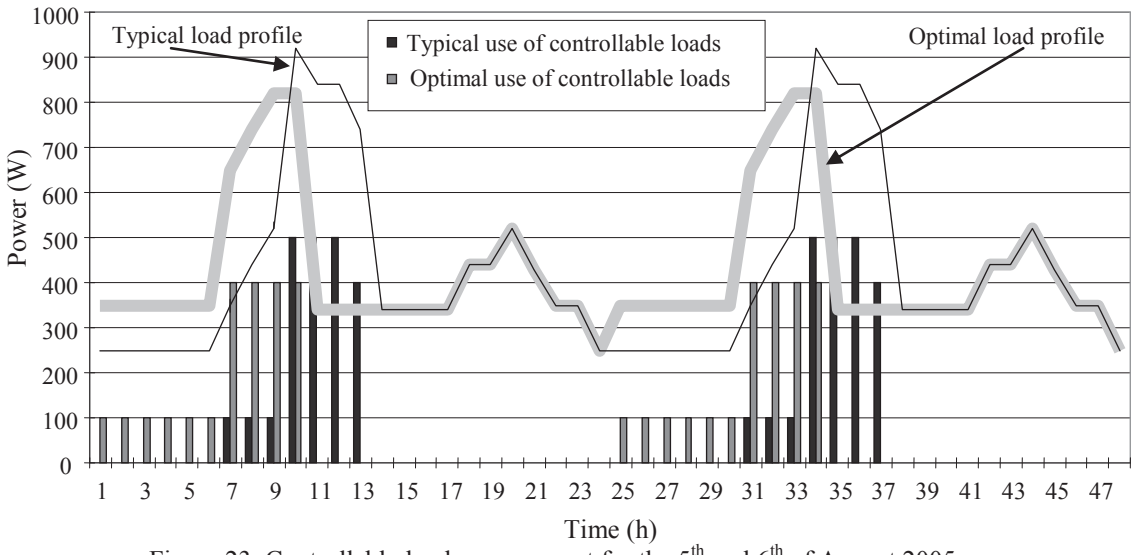

Figure 23. Controllable load management for the 5th and 6th of August 2005

Figures 24 and 25 show the effect of the load shifting in the state of charge of the battery bank and the reduction in the operating hours of the diesel generator. This strategy allows the improvement of the performance of the system, increasing the state of charge of the battery bank and reducing the number of operating hours of the diesel generator compared with a situation in which the load management is not implemented.

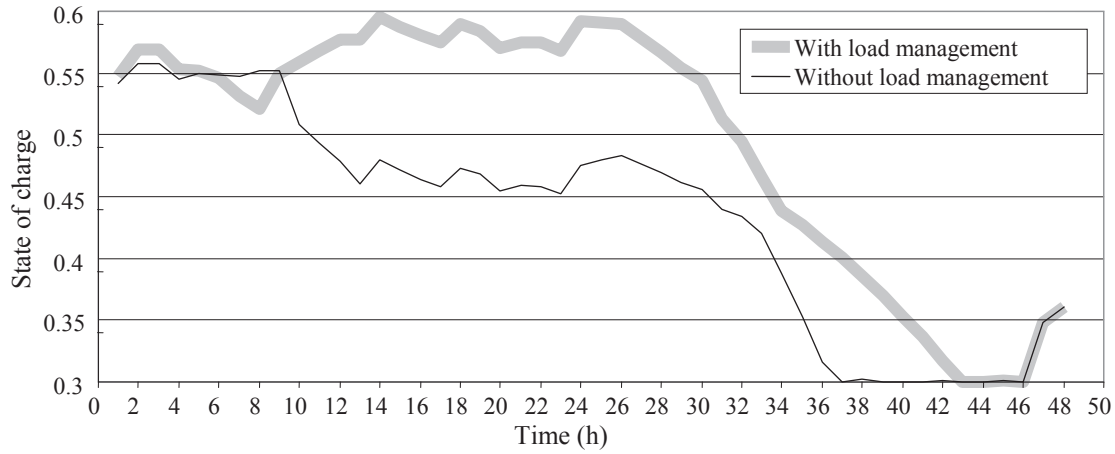

Figure 24. State of charge for the 5th and 6th of August 2005

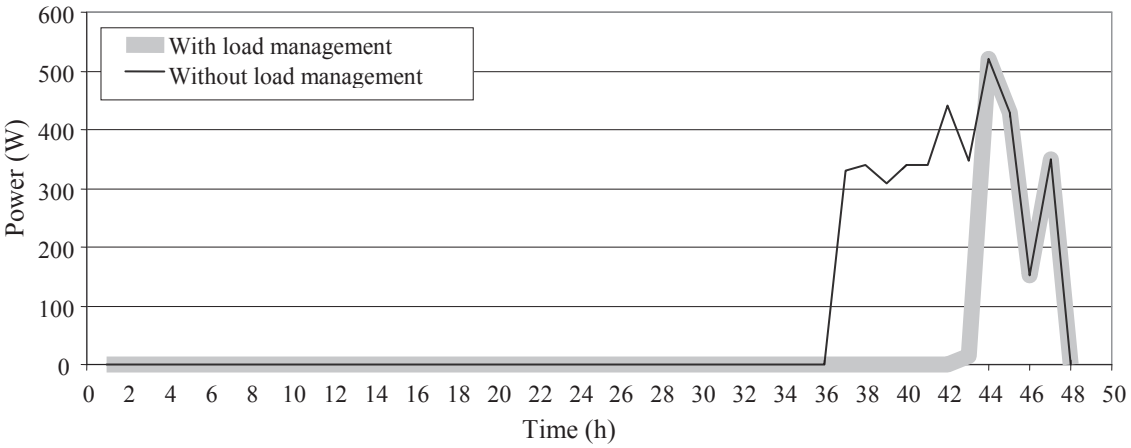

Figure 25. Diesel generator output power for the 5th and 6th of August 2005

Optimum load management strategies for grid-connected residential consumers

Recently, the concept of the smart grid has been discussed by many authors in the specialized literature. Possibly, in the near future, residential consumers will buy electricity according to hourly dynamic prices; i.e., the implementation of the smart grid will allow the marginal cost of power generation to be reflected in the price at which residential consumers buy the energy. To meet this objective, the smart grid requires a communication infrastructure between the retailer and the consumers. This communication could be carried out using computer networks. An energy services interface (ESI) is a secure, two-way communication interface between the utility and the consumers. Using this interface, consumers could receive information about the hourly prices from the utility, and then, using a Web-based energy management system (EMS) connected to the energy services interface, the consumers can respond to the pricing signal previously received. For a typical house that had a smart meter, wind turbine,

several photovoltaic panels, household appliances, and a electric vehicle, [57] developed a demand response strategy for residential consumers that, using forecasting of electricity prices, power production from the renewable generators and energy demand, and information on the power purchase of the consumers, allowed the determination of the optimal use of the household appliances for the next day.

Figure 26 describes the strategy proposed, where, using an energy services interface, consumers are informed about the electricity prices and other important variables 24 hours ahead. Then, using the activity scheduling of the user, the energy management system can determine, optimizing the negotiation between the retailer and the consumer, the optimal use of the household appliances for the next day. Finally, using the energy services interface, the energy management system informs the user about the savings that are available if the household appliances are used in the proposed way.

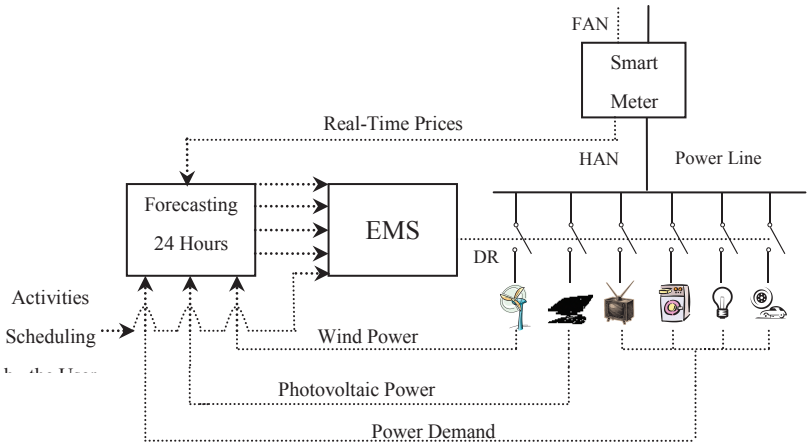

Figure 26. Description of the proposed load management strategy

The analysis of this residential demand response model was carried out considering a residential consumer of Zaragoza during a typical summer day. It assumes that the house of this consumer is equipped with a television, an air conditioning system, a computer, several bulbs, other appliances, and an electric vehicle. In our analysis, two situations are considered. In the first situation, the day before of our analysis, the user was inform that he or she could pay 1c€/kWh to use the television between 14:00 and 23:00 hours, 10 c€/kWh to use the air conditioner between 13:00 and 22:00 hours (5 hours), 10 c€/kWh to use the computer between 9:00 and 20:00 hours, 10 c€/kWh to use the bulbs between 21:00 and 23:00 hours, 10 c€/kWh to use other appliances during the next 24 hours, and 5 c€/kWh to use the electric vehicle for 5 hours at any time the next day.

Figure 27 shows the forecasted and actual values of the electricity prices and ambient temperature for the typical day under study.

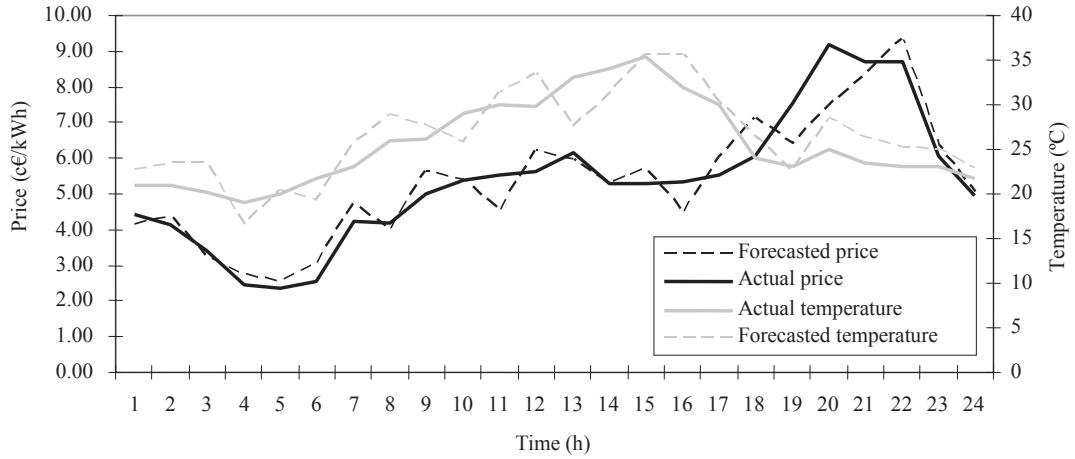

Figure 27. Forecasted electricity prices and temperature for a typical summer day

Typically, the resident of this house uses the air conditioner between 18:00 and 22:00 hours; assuming that this house has good thermal insulation, the air conditioner could be used when the electricity prices will be low. Figure 28 shows the suggested use of the air conditioner.

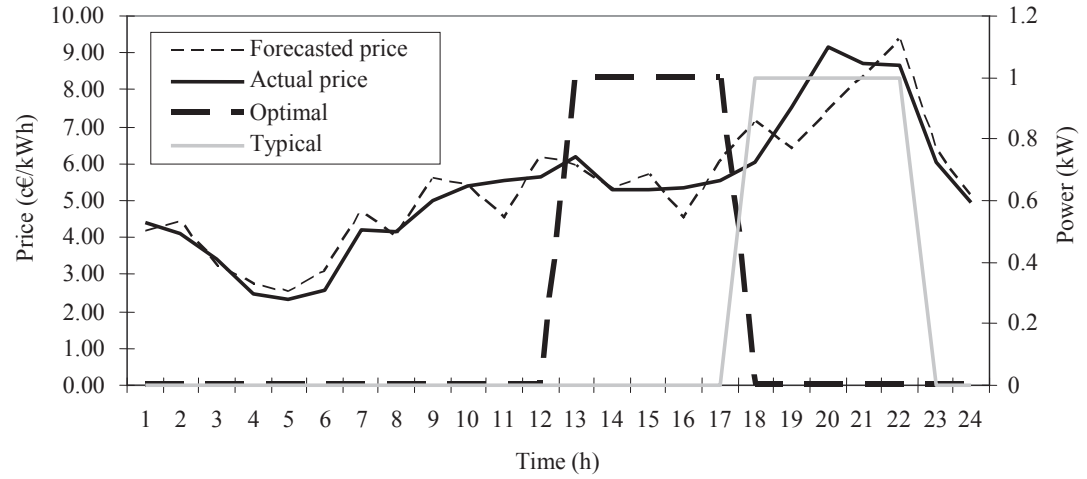

Figure 28. Typical and optimal use of air conditioner

The residents of this house typically use the electric vehicle between 8:00 and 13:00 hours. However, in planning, the consumer has indicated flexibility in the use of the electric vehicle for the next day, requiring travel autonomy at a level equivalent to the state of charge (SOC) of 60%. Figure 29 shows the suggestions from the optimal load management strategy regarding the use of the electric vehicle. Note that if the residents travel using the electric vehicle at 8:00 hours (SOC=61.7%) and return at 13:00 hours

(SOC=50%), the energy to recharge the battery bank will be bought when the energy prices will be high. However, if the residents travel using the electric vehicle at 19:00 hours (SOC=77.7%) and return at 23:00 hours, the autonomy of the electric vehicle is increased and its battery bank is charged when electricity prices are low.

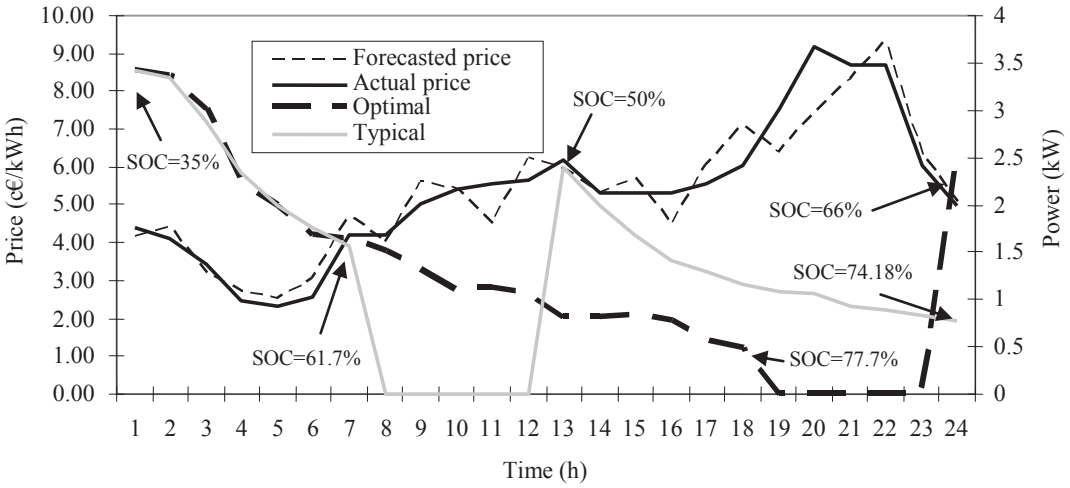

Figure 29. Optimal use of the electric vehicle for the first situation

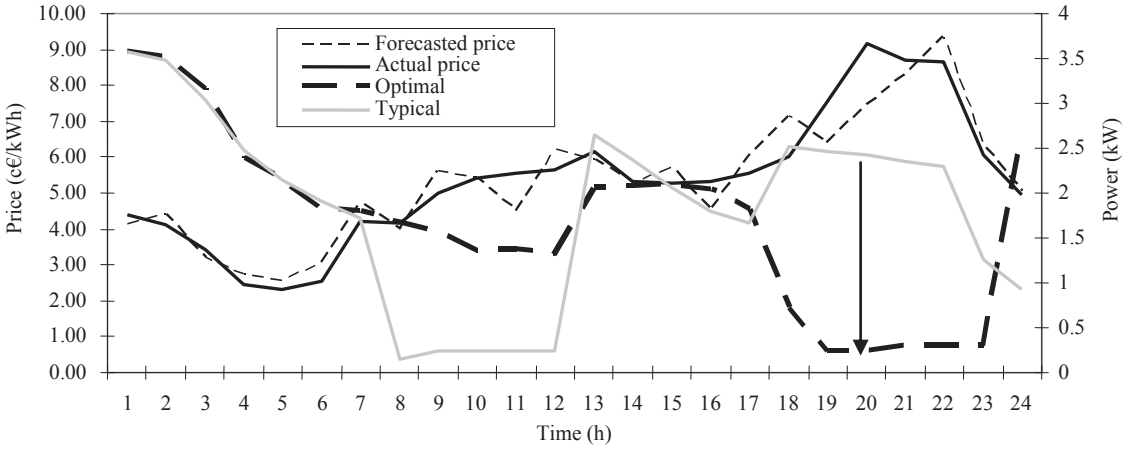

Figure 30. Typical and optimal load profiles for the first situation

According to Figure 27, 1c€/kWh to use the television between 14:00 and 23:00 hours is a very low value, so the load management strategy suggests turning off the television. Figure 30 shows the comparison of the typical load profile and the optimal load profile obtained by the optimal load management strategy, which allows savings of about 22% on the electricity bill.

In the second situation, the residents need to travel using the electric vehicle between 8:00 and 13:00 hours, paying 5 c€/kWh (in this situation, there is no flexibility in using

the electric vehicle) for the energy required to charge the vehicle's battery bank. The specifications for the other appliances are the same as in the previous situation. Figure 31 shows how the residents could use the electric vehicle. Because the users can pay enough money to buy the energy required from the grid, the optimal negotiation coincides with the use required by the residents.

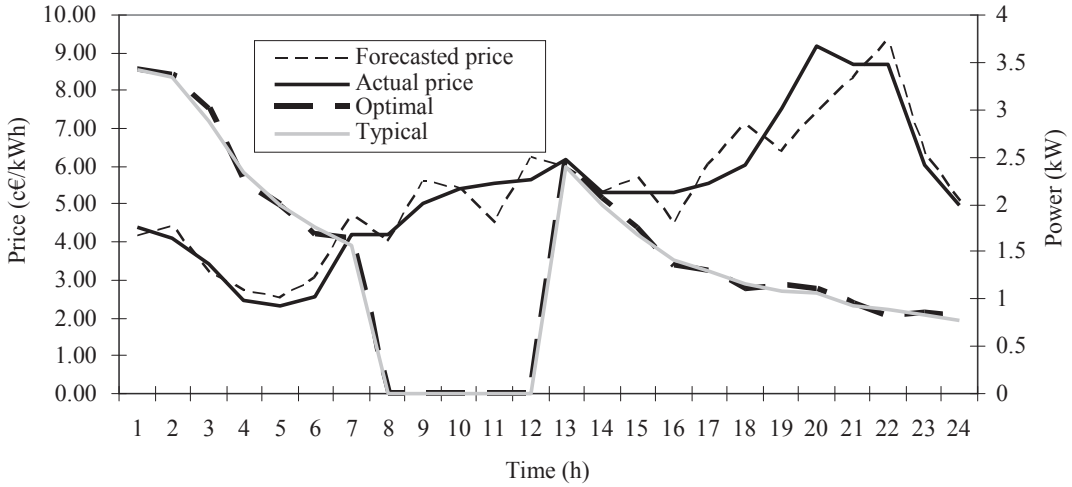

Figure 31. Optimal use of electric vehicle for the second situation

Figure 32 shows the comparison of the typical load profile and the optimal load profile for this situation, which offers about 8% savings on the electricity bill.

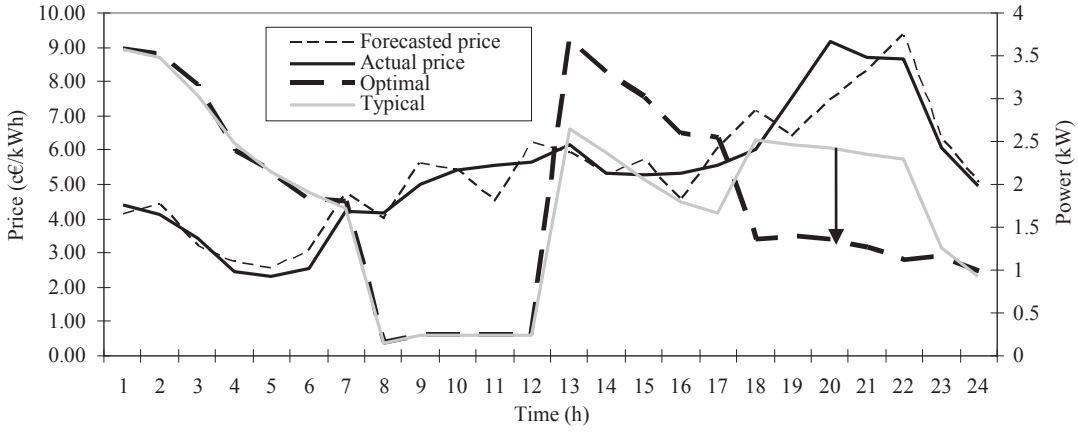

Figure 32. Typical and optimal load profiles for the second situation

Conclusions

This doctoral thesis has analyzed the main factors related to the performance of standalone hybrid power systems and residential systems connected to the future smart grid with renewable energy sources. It has analyzed the effects of a charge controller and the coulombic efficiency of the battery bank on the reliability of small wind energy systems and the estimation of operating hours, fuel consumption, and net present cost in systems with conventional generation as backup. The thesis has developed a probabilistic model that is able to consider the uncertainties in the battery bank lifetime, fuel prices, photovoltaic production, load profile, and variability of wind and solar resources. Recently, the rational use of energy sources has been analyzed by many authors, and this thesis has developed a novel technique to manage the energy demand in hybrid power systems. This strategy suggests to the users the best times to use the controllable loads in the system, reducing fuel consumption and improving the use of the energy stored in the battery bank. In addition, it has developed an optimal load management strategy for residential systems connected to the future smart grid. In this strategy, using bidirectional communication between the retailer and the consumers, the optimal use of the different household appliances and electric vehicles is obtained, optimizing the negotiation between the retailer and the consumers; this approach allows consideration of the power purchase of the consumers and their preferences in the optimal load management problem.

The results obtained by this doctoral thesis suggest important improvements in many computational tools used frequently for the simulation and optimization of hybrid systems, specifically regarding subjects related to the charge controller operation and uncertainty in battery bank lifetime estimation. The load management strategies presented in this research work are an important tool to support residential users in improving the use of local renewable resources and adapting consumption patterns to actual economic situations.

Referencias

[1] International Energy Outlook 2011. US Energy Information Administration; 2011.

[2] Leung DYC, Yang Y. Wind energy development and its environmental impact: A review. Renewable and Sustainable Energy Reviews 2012;16(1):1031-1039.

[3] The Wind Power Report. ABS Energy Research; 2010.

[4] Timilsina GR, Kurdgelashvili L, Narbel PA. Solar energy: Markets, economics and policies. Renewable and Sustainable Energy Reviews 2012;16(1):449-465.

[5] Renewables 2011. Global status report. Renewable Energy Policy Network for the 21st Century (REN21); 2011.

[6] Albadi MH, El-Saadany EF. Overview of wind power intermittency impacts on power systems. Electric Power Systems Research 2010;80(6):627-632.

[7] Kim JH, Shcherbakova A. Common failures of demand response. Energy 2011;36(2):873-880.

[8] Anagnostopoulos JS, Papantonis DE. Simulation and size optimization of a pumped-storage power plant for the recovery of wind-farms rejected energy. Renewable Energy 2008;33(7):1685-1694.

[9] Varkani AK, Daraeepour A, Monsef H. A new self-scheduling strategy for integrated operation of wind and pumped-storage power plants in power markets. Applied Energy 2011;88(12):5002-5012.

[10] Fertig E, Apt J. Economics of compressed air energy storage to integrate wind power: A case study in ERCOT. Energy Policy 2011;39(5):2330-2342.

[11] Bernal-Agustín JL, Dufo-López R. Hourly energy management for grid-connected wind-hydrogen systems. International Journal of Hydrogen Energy 2008;33(22):6401-6413.

[12] Dufo-López R, Bernal-Agustín JL, Domínguez-Navarro JA. Generation management using batteries in wind farms: Economical and technical analysis for Spain. Energy Policy 2009;37(1):126-139.

[13] Palit D, Chaurey A. Off-grid rural electrification experiences from South Asia: Status and best practices. Energy for Sustainable Development 2011;15(3):266-276.

[14] Díaz P, Arias CA Peña R, Sandoval D. FAR from the grid: A rural electrification field study. Renewable Energy 2010;35(12):2829-2834.

[15] Zhang X, Kumar A. Evaluating renewable energy-based rural electrification program in western China: Emerging problems and possible scenarios. Renewable and Sustainable Energy Reviews 2011;15(1):773-779.

[16] Fleck B, Huot M. Comparative life-cycle assessment of a small wind turbine for residential off-grid use. Renewable Energy 2009;34(12):2688-2696.

[17] Lambert T, Gilman P, Lilienthal P. Micropower system modeling with HOMER. In: Farret FA, Simões MG. Integration of Alternative Sources of Energy, John Wiley & Sons, Inc; 2006, p. 379-418.

[18] Belfkira R, Zhang L, Barakat G. Optimal sizing study of hybrid wind/PV/diesel power generation unit. Solar Energy 2011;85(1):100-110.

[19] Boonbumroong U, Pratinthong N, Thepa S, Jivacate C, Pridasawas W. Particle swarm optimization for AC-coupling stand alone hybrid power systems. Solar Energy 2011;85(3):560-569.

[20] Hakimi SM, Moghaddas-Tafreshi SM. Optimal sizing of a stand-alone hybrid power system via particle swarm optimization for Kahnouj area south-east of Iran. Renewable Energy 2009;34(7):1855-1862.

[21] Dufo-López R. Dimensionado y control óptimos de sistemas híbridos aplicando algoritmos evolutivos. PhD Thesis. University of Zaragoza; 2007.

[22] Ekren O, Ekren BY. Size optimization of a PV/wind hybrid energy conversion system with battery storage using simulated annealing. Applied Energy 2010;87(2):592-598.

[23] Bagul AD, Salameh M, Borowy B. Sizing of a stand-alone hybrid wind photovoltaic system using a three-event probability density approximation. Solar Energy 1996;56(4):323-335.

[24] Karaki SH, Chedid RB, Ramadan R. Probabilistic performance assessment of wind energy conversion systems. IEEE Transactions on Energy Conversion 1999;14(2):217-224.

[25] Karaki SH, Chedid RB, Ramadan R. Probabilistic performance assessment of autonomous solar-wind energy conversion systems. IEEE Transactions on Energy Conversion 1999;14(3):766-772.

[26] Roy A, Kedare SB, Bandyopadhyay S. Optimum sizing of wind-battery systems incorporating resource uncertainty. Applied Energy 2010;87(8):2712-2727.

[27] Távora CCV, Oliveira FD, Alves CDAS, Martins JH, Toledo OM, Machado NLV. A stochastic method for stand-alone photovoltaic system sizing. Solar Energy 2010;84(9):1628-36.

[28] Giannakoudis G, Papadopoulos AI, Seferlis P, Voutetakis S. Optimum design and operation under uncertainty of power systems using renewable energy sources and hydrogen storage. International Journal of Hydrogen Energy 2010;35(3):872-91.

[29] Tan CW, Green TC, Hernandez-Aramburo CA. A stochastic method for battery sizing with uninterruptible-power and demand shift capabilities in PV (photovoltaic) systems. Energy 2010;35(12):5082-92.

[30] Barley CD, Winn B. Optimal dispatch strategy in remote hybrid power systems. Solar Energy 1996;58(4-6):165-179.

[31] Ashari M, Nayar CV. An optimum dispatch strategy using set points for a photovoltaic (PV)-Diesel-Battery hybrid power system. Solar Energy 1999;66(1):1-9.

[32] Dufo-López R, Bernal-Agustín JL. Design and control strategies of PV-Diesel systems using genetic algorithms. Solar Energy 2005;79(1):33-46.

[33] Yamamoto S, Park JS, Takata M, Sasaki K, Hashimoto T. Basic study on the prediction of solar irradiation and its application to photovoltaic-diesel hybrid generation system. Solar Energy Materials and Solar Cells 2003;75(3-4):577-584.

[34] Groumps PP, Cull RC, Ratajczak AF. An overview of control aspects of a village stand-alone photovoltaic power system. IEEE Transaction on Power Apparatus and Systems 1984; PAS-103(10):2845-2853.

[35] Groumps PP, Papegeorgiou G. An optimum load management strategy for stand-alone photovoltaic power systems. Solar Energy 1991;46(2):121-128.

[36] Khouzam K, Khouzam L. Load prioritization and shedding in photovoltaic power systems. Solar Cells 1991;31(6):505-511.

[37] Moreno A, Julve J, Silvestre S, Castañer L. A fuzzy logic controller for stand alone PV systems. IEEE Photovoltaic Specialists Conference 2000; 1618-1621

[38] Salah CB, Chaabene M, Ammar MB. Multi-criteria fuzzy algorithm for energy management of a domestic photovoltaic panel. Renewable Energy 2008;33(5):993-1001.

[39] Ammar CB, Chaabene M, Elhajjaji A. Daily energy planning of a household photovoltaic panel. Applied Energy 2010;87(7):2340-2351.

[40] Thiaux Y, Seigneurbieux J, Multon B, Ahmed HB. Load profile impact on the gross energy requirement of stand-alone photovoltaic systems. Renewable Energy 2010;35(3):602-613.

[41] Albadi MH, El-Saadany EF. A summary of demand response in electricity markets. Electric Power Systems Research 2008;78(11):1989-1996.

[42] Eissa MM. Demand side management program evaluation based in industrial and commercial field data. Energy Policy 2011;39(10):5961-5969.

[43] Walawalkar R, Fernands S, Thakur N, Chevva KR. Evolution and current status of demand response (DR) in electricity markets: Insights from PJM and NYISO. Energy 2010;35(4):1553-1560.

[44] Torriti J, Hassan GH, Leach M. Demand response experience in Europe: Policies, programmes and implementation. Energy 2010;35(4):1575-1583.

[45] Wang J, Bloyd CN, Hu Z, Tan Z. Demand response in China. Energy 2010;35(4):1592-1597.

[46] Molderink A, Bakker V, Bosman MGC, Hurink JL, Smit GJM. Management and control of domestic smart grid technology. IEEE Transactions on Smart Grid 2010;1(2):109-119.

[47] Mohsenian-Rad AH, Leon-Garcia A. Optimal residential load control with price prediction in real-time electricity pricing environments. IEEE Transactions on Smart Grid 2010;1(2):120-133.

[48] Mohsenian-Rad AH, Wong VWS, Jatkevich J, Schober R, Leon-Garcia A. Autonomous demand-side management based on game-theoretic energy consumption scheduling for the future smart grid. IEEE Transactions on Smart Grid 2010;1(3):320-331.

[49] Conejo AJ, Morales JM, Baringo L. Real-time demand response model. IEEE Transactions on Smart Grid 2010;1(3):236-242.

[50] Sianaki OA, Hussain O, Tabesh AR. A knapsack problem approach for achieving efficient energy consumption in smart grid for end-users' life style. IEEE Conference on Innovative Technologies for an Efficient and Reliable Electricity Supply (CITRES) 2010; 159-164.

[51] Lujano-Rojas JM, Dufo-López R, Bernal-Agustín JL. Optimal sizing of small wind/battery systems considering the DC bus voltage stability effect on energy capture, wind speed variability, and load uncertainty. Applied Energy 2012;93:404-412.

[52] Lujano-Rojas JM, Dufo-López R, Bernal-Agustín JL. Optimal design of PV/Wind/Battery systems by genetic algorithms considering the effect of charge regulation. International Conference on Mechanical and Electronic Engineering (ICMEE 2012).

[53] Lujano-Rojas JM, Dufo-López R, Bernal-Agustín JL. A qualitative evaluation of operational conditions in PV/Wind/Battery systems. Asia-Pacific Power and Energy Engineering Conference (APPEEC 2012).

[54] Lujano-Rojas JM, Dufo-López R, Bernal-Agustín JL. Probabilistic modeling and analysis of PV/Wind/Diesel/Battery systems. Applied Energy (*En revisión*).

[55] Lujano-Rojas JM, Bernal-Agustín JL, Dufo-López R, Domínguez-Navarro JA. Forecast of hourly average wind speed using ARMA model with discrete probability transformation. Lecture Notes in Electrical Engineering 98. Springer-Verlag; 2011. p. 1003-1010.

[56] Lujano-Rojas JM, Monteiro C, Dufo-López R, Bernal-Agustín JL. Optimum load management strategy for wind/diesel/battery hybrid power systems. Renewable Energy 2012;44:288-295.

[57] Lujano-Rojas JM, Monteiro C, Dufo-López R, Bernal-Agustín JL. Optimum residential load management strategy for real time pricing (RTP) demand response programs. Energy Policy 2012;45:671-679.

[58] Baring-Gould EI, Newcomb C, Corbus D, Kalidas R. Field performance of hybrid power systems. US National Renewable Energy Laboratory; 2001.

[59] Corbus D, Newcomb C, Baring-Gould EI, Friedly S. Battery voltage stability effects on small wind turbine energy capture. US National Renewable Energy Laboratory; 2002.

[60] Sexton ED, Olson JB. Coulombic efficiency of a sealed, thin plate spiral lead-acid battery. In: IEEE battery conference on applications and advances; 1998.

[61] Stevens JW, Corey GP. A study of lead-acid battery efficiency near top-of-charge and the impact on PV system design. IEEE Photovoltaic Specialists Conference 1996; 1485-1488.

[62] Copetti JB, Chenlo F. Lead/acid batteries for photovoltaic applications. Test results and modeling. Journal of power sources 1994;47(1-2):109-118.

[63] Copetti JB, Lorenzo E, Chenlo F. A general battery model for PV system simulation. Progress in Photovoltaics: Research and Applications 1993;1(4):283-292.

[64] Sauer DU, Wenzl H. Comparison of different approaches for lifetime prediction of electrochemical systems-Using lead-acid batteries as example. Journal of Power Sources 2008;176(2):534-546.

[65] Svoboda V, Wenzl H, Kaiser R, Jossen A, Baring-Gould I, Manwell J, Lundsager P, Bindner H, Cronin T, Nøgard P, Ruddell A, Perujo A, Douglas K, Rodrigues C, Joyce A, Tselepis S, van der Borg N, Nieuwenhout F, Wilmot N, Mattera F, Sauer DU. Operating conditions of batteries in off-grid renewable energy systems. Solar Energy 2007;81(11):1409-1425.

[66] Bindner H, Cronin T, Lundsager P, Manwell JF, Abdulwahid U, Baring-Gould I. Lifetime modelling of lead acid batteries. Denmark National Laboratory Risø; 2005.

Apéndice

A continuación se incluyen:

- Cartas de aceptación de los trabajos pendientes de publicación.
- El factor de impacto de las revistas y áreas temáticas correspondientes a las publicaciones que se recogen en la tesis.

Cartas de aceptación de los trabajos pendientes de publicación.

- Documento justificativo de haber presentado la publicación correspondiente al congreso APPEEC 2012, requisito indispensable para que IEEE ponga en IEEE Xplore el artículo.

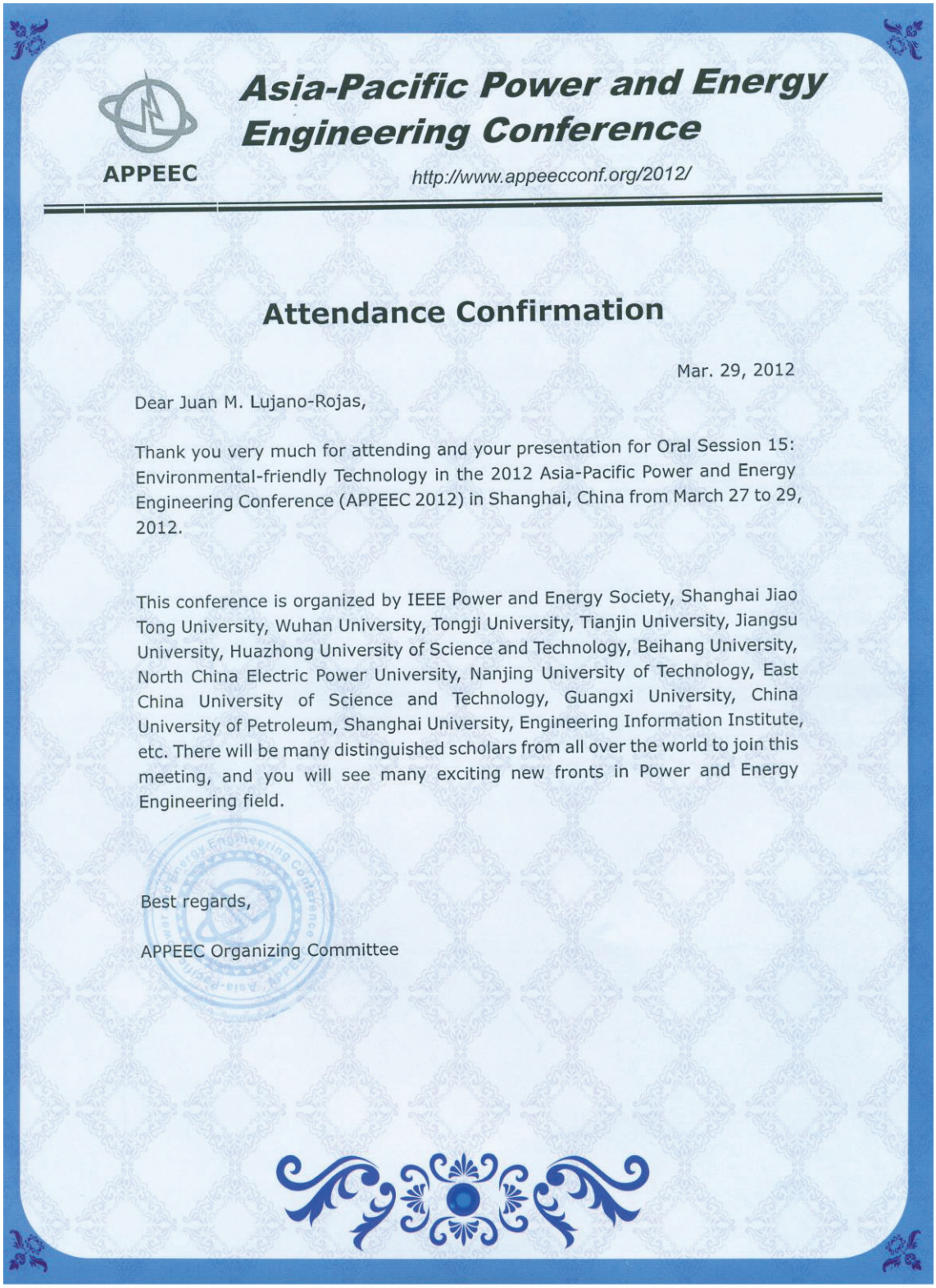

APPEEC

Asia-Pacific Power and Energy Engineering Conference

http://www.appeecconf.org/2012/

Attendance Confirmation

Mar. 29, 2012

Dear Juan M. Lujano-Rojas,

Thank you very much for attending and your presentation for Oral Session 15: Environmental-friendly Technology in the 2012 Asia-Pacific Power and Energy Engineering Conference (APPEEC 2012) in Shanghai, China from March 27 to 29, 2012.

This conference is organized by IEEE Power and Energy Society, Shanghai Jiao Tong University, Wuhan University, Tongji University, Tianjin University, Jiangsu University, Huazhong University of Science and Technology, Beihang University, North China Electric Power University, Nanjing University of Technology, East China University of Science and Technology, Guangxi University, China University of Petroleum, Shanghai University, Engineering Information Institute, etc. There will be many distinguished scholars from all over the world to join this meeting, and you will see many exciting new fronts in Power and Energy Engineering field.

Best regards,

APPEEC Organizing Committee

- Carta de aceptación del artículo *Optimal design of PV/Wind/Battery systems by genetic algorithms considering the effect of charge regulation*

2012 International Conference on Mechanical and Electronic Engineering(ICMEE2012)
June 23-24,2012, Hefei

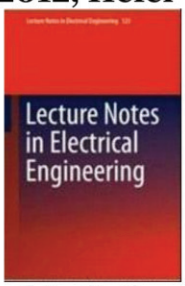

Official Acceptance and Invitation Letter

Dear author(s),

Congratulations to you! We are pleased to inform you that your paper
Paper id: 495
Title: Optimal Design of PV/Wind/Battery Systems by Genetic Algorithms Considering the Effect of Charge Regulation
Authors: Juan M. Lujano-Rojas, Rodolfo Dufo-López, José L. Bernal-Agustín

After the reviewing course of the reviewers of ICMEE2012 Committees, has been accepted as a regular selected paper in ICMEE2012 **, which will be** published by **Springer (ISSN: 1876-1100)** , which **will be indexed in ISI Proceedings(ISTP),Scopus and DBLP and submitted for EI Compendex.** Please revise your paper again to meet the English quality of **Springer (ISSN: 1876-1100) ,LNEE**. The length of the paper should be in 4-7 pages **(the registration fee can be seen in the registration form)**. The whole topic of the selected volumes proceeding is " **Mechanical and Electronic Engineering", please pay attention to.**

In order to meet high standard of selected volumes of ICMEE2012 proceedings, the camera-ready version of authors should follow **Springer** format strictly. If you do not follow **Springer (ISSN: 1876-1100)** format strictly, your paper will be not indexed by ISTP and submitted for EI indexing. Kindly send your Final paper to **ICMEE2012@163.com within the registration time.**
All authors for being accepted papers should submit the paper with formal format, copyright, scanned bank receipt,registration form to **ICMEE2012@163.com within the registration time in your notification** . If all of the items can not be submitted within the registration time,your paper will not be included in **Springer,LNEE** and Indexed by EI and ISTP.
Registration Fees: The registration fee can be seen in the registration form. Please pay attention to it. We hope to see you in June 23-24,2012, Hefei, China.

International Science & Education Researcher Association
ISER Association
ICMEE2012 Committee
2012-3-05

Factor de impacto de las revistas y áreas temáticas correspondientes a las publicaciones que se recogen en la tesis.

El factor de impacto se ha obtenido de la base de datos "ISI Web of Knowledge"

Applied Energy:

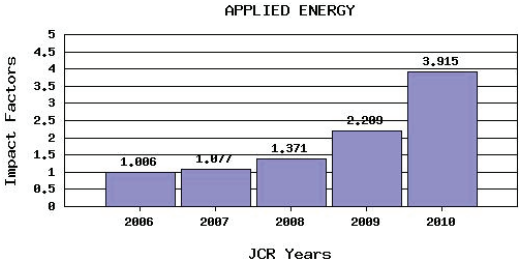

Category Name	Total Journals in Category	Journal Rank in Category	Quartile in Category
ENERGY & FUELS	79	14	Q1
ENGINEERING, CHEMICAL	135	7	Q1

Renewable Energy:

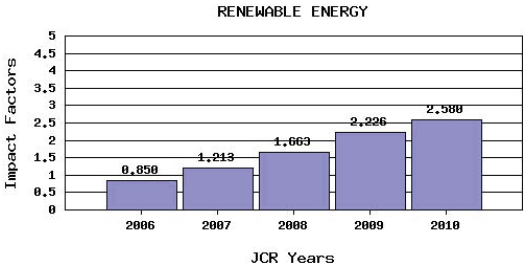

Category Name	Total Journals in Category	Journal Rank in Category	Quartile in Category
ENERGY & FUELS	79	22	Q2

Energy Policy:

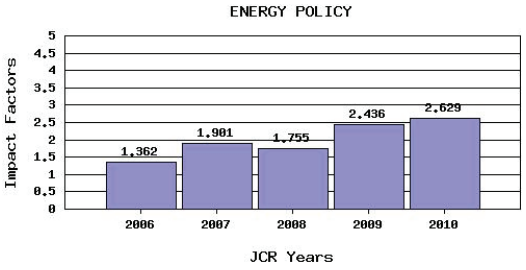

Category Name	Total Journals in Category	Journal Rank in Category	Quartile in Category
ENERGY & FUELS	79	21	Q2
ENVIRONMENTAL SCIENCES	193	46	Q1

Indexación de las publicaciones relacionadas con los artículos de congresos internacionales que forman parte del compendio:

- *Lecture Notes in Electrical Engineering* (ISSN: 1876-1100) es una publicación de Springer, y está indexada por ISI Proceedings, EI-Compendex, SCOPUS, EI Compendex, MetaPress, Springerlink.

  Los artículos que publica corresponden al área temática de la Ingeniería Eléctrica

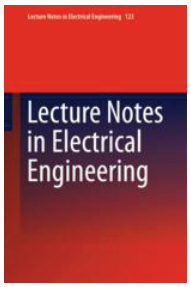

  http://www.springer.com/series/7818

- Los artículos presentados en la Asia-Pacific Power and Energy Engineering Conference (APPEEC 2012) se indexarán en las bases de datos más relevantes (ISI Proceedings, SCOPUS, etc.). Además, estarán disponibles en IEEE Xplore (http://ieeexplore.ieee.org).

  Las publicaciones que se encuentran en IEEE Xplore corresponden a las áreas temáticas relacionadas con la asociación IEEE (Institute of Electrical and Electronics Engineers).